4. RESULTS AND DISCUSSION

The work carried out has been discussed under the following two main heads:

4.1. Triazinoindole-based multifunctional anti-AD agents and,

4.2. Carbazole-based multifunctional anti-AD agents.

4.1. Triazinoindole-based multifunctional anti-AD agents

Two types of compounds have been synthesized under this category:

4.1.1. 3-/5-substituted [1,2,4]triazino[5,6-*b*]indole derivatives and

4.1.2. 3- And 6-/7-/8-/9-disubstituted [1,2,4]triazino[5,6-*b*]indole derivatives.

4.1.1. 3-/5-Substituted [1,2,4]triazino[5,6-*b*]indole derivatives

The work carried out under this heading has been further divided into 4 subheadings i.e. designing aspect, chemical studies, biological studies, and computational studies as mentioned below:

4.1.1.1. Designing aspect of 3-/5-substituted-[1,2,4]triazino[5,6-*b*] indole derivatives as anti-AD agents,

4.1.1.2. Synthesis and characterization of the designed compounds,

4.1.1.3. Biological evaluation of the synthesized compounds and

4.1.1.4. Computational studies of the promising compounds.

4.1.1.1. Designing aspect of 3-/5-substituted [1,2,4]triazino[5,6-*b*]indole derivatives as anti-AD agents

To combat the diseases like AD having complex etiology, development of MTDLs is recognized as one of the most assuring drug discovery approaches. In spite of considerable research on new targets available for AD treatment, the cholinesterase inhibitors still remain the drugs of choice, although they provide symptomatic and transient benefits to the patients. Oxidative stress plays an important role in pathogenesis of AD. However, antioxidant molecules all alone might not be enough to treat such highly complex pathologies like AD.[96] So, dual cholinesterase inhibitors endowed with additional anti-oxidant and neuroprotective properties could increase the chances of success to combat AD.

Indole ring is prodigiously present in many natural compounds displaying invaluable medicinal and biological properties.[63,97] Melatonin is an indole ring containing pineal neurohormone whose levels decrease during aging, especially in AD patients.[64,98] It is endowed with strong free radical scavenging properties. High reactivity of melatonin with ROS is apparently due to the presence of electron-rich indole ring present in its structure, allowing it to act readily as an electron donor. Recent studies have also shown that melatonin offers protective effects against Aβ-induced apoptosis,[99] nitric oxide toxicity,[100] glutamate-induced excitotoxicity,[67] and decreases neurofilament hyperphosphorylation and augments learning and memory in rats. In recent years, many indole-based hybrids e.g. tacrine-melatonin,[68] donepezil-chromone-melatonin,[101] melatonin-*N,N*-dibenzyl(*N*-methyl)amine[102] and carbamate derivatives of indolines[69] and have been designed to act as multifunctional agents for the treatment of AD. Furthermore, the indole moiety is present in several CNS-active drugs like rizatriptan, oxypertine etc. Hence, the indole moiety manifests a privileged profile for CNS-active drugs which could prove to be useful in the search for new therapeutics for AD.

1,2,4-Triazine nucleus is another important structural system present in several biologically active compounds.[103] The significance of triazines in neuropharmacology is explored progressively for their potential anti-AD,[104,105] antianxiety,[106] antiepileptic[107] and anti-depressant[108] activities. Some triazine derivatives have been reported to be potent neuroprotective agents against H_2O_2-induced cell death in PC12 cell line.[109] Recently our research group has also reported substituted diaryltriazines as potential entities for the treatment of AD.[89] Abundant remarkable biological activities associated with the indole ring and the 1,2,4-triazine nucleus prompted us to fuse these two privileged scaffolds into a single scaffold which could offer multiple favorable activities for the treatment of AD.

Different 5*H*-[1,2,4]triazino[5,6-*b*]indole-3-thiol and 5*H*-[1,2,4] triazino[5,6-*b*]indol-3-amine derivatives were designed by following a rational hybridization approach (**Figure 4.1**). Molecular interactions of the designed derivatives were evaluated by means of docking the designed compounds within

the active site of AChE and BuChE. Both the scaffolds showed promising binding affinities within the active sites of AChE as well as BuChE.

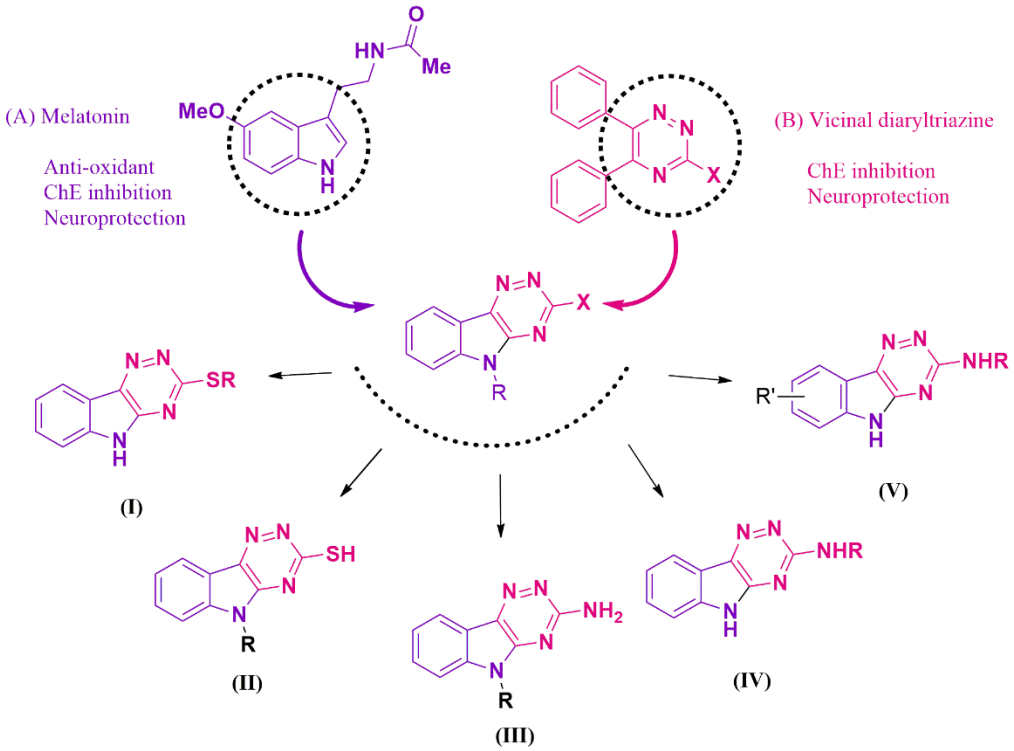

Figure 4.1. Molecular hybridization approach to design triazinoindole derivatives.

In molecular modeling studies performed in the lab prior to this work 5*H*-[1,2,4]triazino[5,6-*b*]indole-3-thiol scaffold showed stability within the CAS of AChE (docking score: -7.96) by forming π-π interactions with Trp84 and Phe330 and hydrogen bonding with His440. While, the same scaffold in the active site of BuChE (docking score: -7.21) exhibited π-π interactions with Trp82, Trp430 and His438 along with hydrogen bonding with His438 (**Figure 4.2**). Another designed scaffold 5*H*-[1,2,4]triazino[5,6-*b*]indol-3-amine showed similar π-π interactions but offering higher binding affinities with AChE (docking score: -8.89) and BuChE (docking score: -7.22) enzymes due to additional strong hydrogen bonding imparted by the 3-amino group (**Figure 4.2**). In the *in vitro* enzyme inhibition study, 5*H*-[1,2,4]triazino[5,6-*b*]indole-3-thiol showed 11.26 µM and 55.81 µM inhibitory activity (IC_{50}) against AChE and BuChE respectively, whereas 5*H*-[1,2,4]triazino [5,6-*b*]indol-3-amine was found to possess IC_{50} values of 9.76 µM and 51.25 µM against AChE and BuChE, respectively. On the basis of these moderately promising activities of these designed scaffolds, compounds of the five different series (I-IV) were

designed (**Figure 4.1**). Series I and II were reported by Kanhed *et. al.* from this laboratory. The remaining three series (III, IV and V) have been synthesized and discussed here in this thesis.

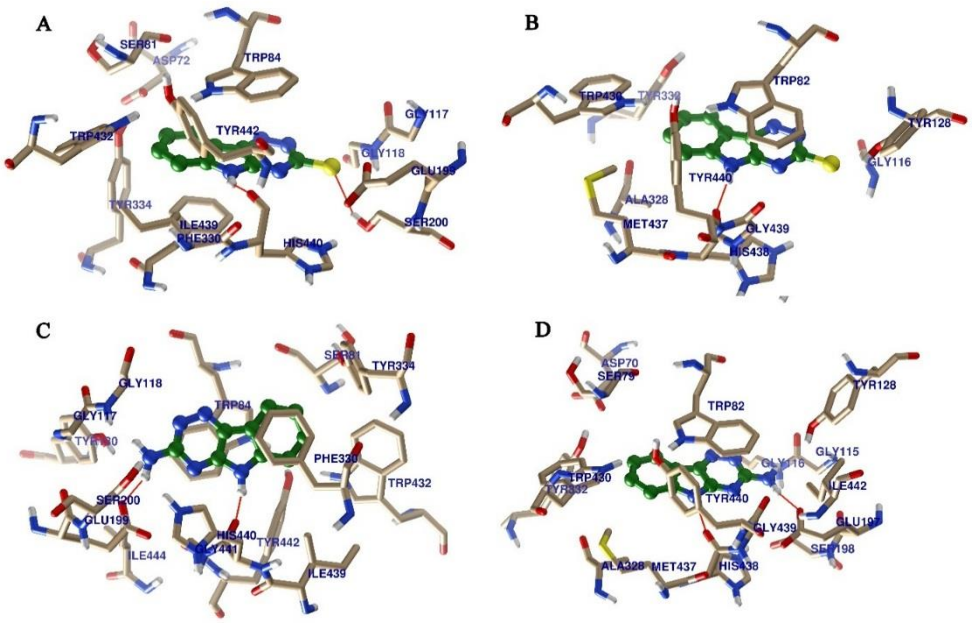

Figure 4.2. Interaction of 5*H*-[1,2,4]triazino[5,6-*b*]indole-3-thiol with (**A**) AChE, (**B**) BuChE, and 5*H*-[1,2,4]triazino[5,6-*b*]indol-3-amine with (**C**) AChE and (**D**) BuChE.

4.1.1.2. Synthesis of the designed triazinoindole derivatives

The synthetic methodologies for the preparation of the designed series of triazinoindole derivatives have been discussed under three subheads as mentioned below:

4.1.1.2.1. Synthesis of *N*-substituted 5*H*-[1,2,4]triazino[5,6-*b*]indol-3-amine derivatives (**71-80**),

4.1.1.2.2. Synthesis of 5-substituted 5*H*-[1,2,4]triazino[5,6-*b*]indol-3-amine derivatives (**117-126**) and

4.1.1.2.3. Synthesis of *N*-(aminoalkyl)-5*H*-[1,2,4]triazino[5,6-b]indol-3-amine derivatives (**179-202**).

4.1.1.2.1. Synthesis of *N*-substituted 5*H*-[1,2,4]triazino[5,6-*b*]indol-3-amine derivatives (71-80)

When the isatin/substituted isatins were subjected to cyclization reaction with aminoguanidine, uncyclized isatin/*N*-substituted isatin-3-guanyl hydrazones were obtained instead of the 5*H*/substituted-[1,2,4]triazino[5,6-*b*]

indol-3-amine derivatives (**III**) (**Scheme. 4.1**). All efforts made to cyclize these isatin-3-guanylhydrazones (**II**) to get substituted [1,2,4]triazino[5,6-*b*]indol-3-amine derivatives (**III**) failed and the uncyclized starting compounds only were obtained back.

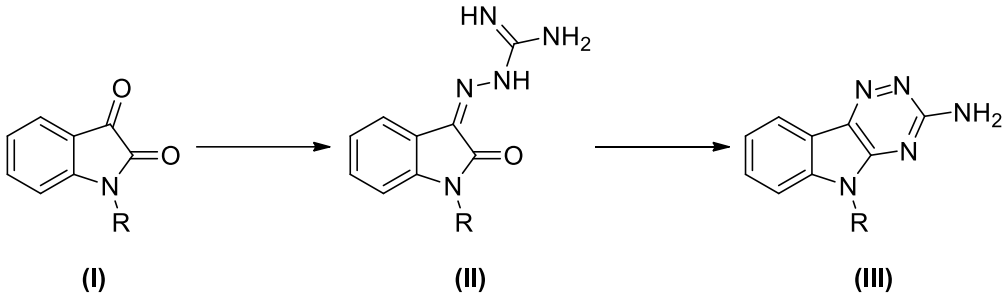

Scheme 4.1. Attempted synthetic path for the synthesis of *N*-substituted 5*H*-[1,2,4]triazino[5,6-*b*]indol-3-amine derivative from isatin and aminoguanidine.

In an effort to obtain the desired product (**III**), compound (**II**) was subjected to a drastic condition. Cyclization of N_1-benzylisatin-3-guanyl hydrazone (**II**, R = benzyl) in the presence of potassium hydroxide as a strong base and diethylene glycol as a polar protic solvent led to isolation of the hydrolyzed product, i.e. 2-(benzylamino)benzoic acid (**IV**).

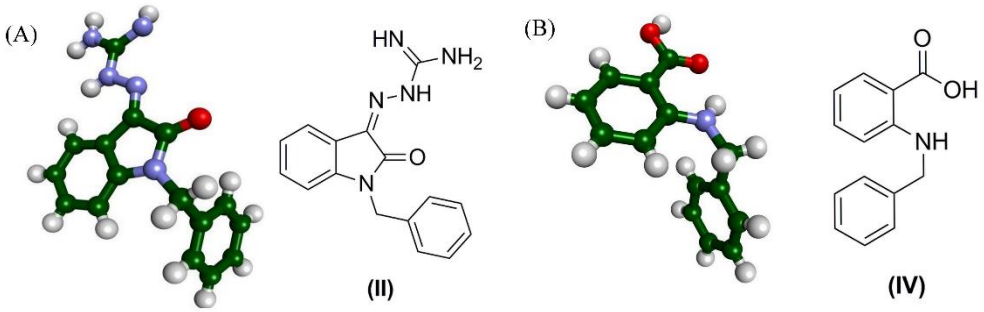

Figure. 4.3. Single crystal X-ray diffraction of (**A**) N_1-benzylisatin-3-guanyl hydrazone (**II**) and (**B**) 2-(benzylamino)benzoic acid (**IV**).

In an alternative approach (**Scheme 4.2**), we planned to synthesize the desired amino derivatives from the thiol derivatives. The thiol derivatives were synthesized by condensation of isatins with thiosemicarbazide. These thiol derivatives were methylated and the methylthio derivatives were treated with various amines.[110] Unfortunately, the thiomethyl derivatives failed to react with the amines. So, the thiomethyl group at the C-3 position was converted to sulfone, as it has more electron withdrawing ability compared to the parent

thiomethyl group. This was achieved by oxidizing the thiomethyl group by *meta*-chloroperbenzoic acid (*m*CPBA) to sulfone. When these sulfone derivatives were reacted with amines in THF at refluxing conditions, the sulfone group was substituted by the amino group offering the desired substituted [1,2,4]triazino[5,6-*b*]indol-3-amine derivatives (**71-80**) as depicted in **Scheme 4.2**.

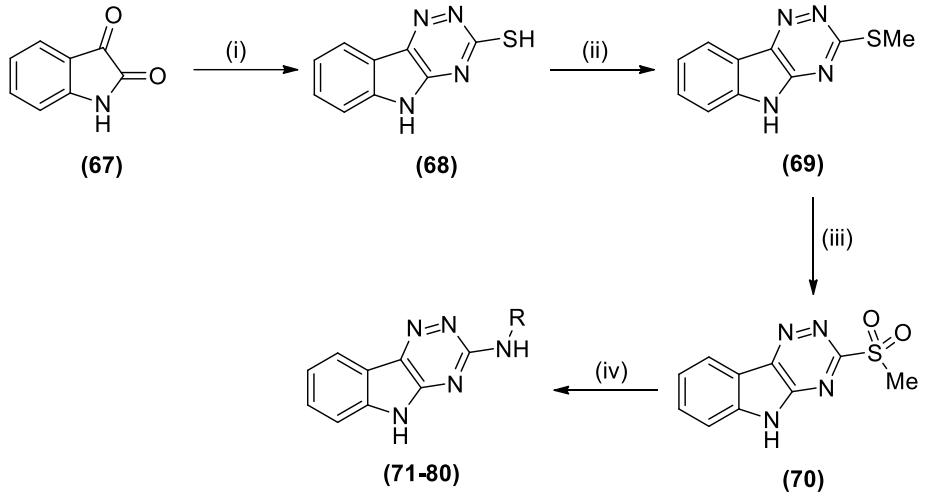

Scheme 4.2. General synthetic route for the synthesis of compounds (**71-80**); Reagents and conditions: (i) Thiosemicarbazide, K_2CO_3, H_2O, reflux, overnight; (ii) MeI, K_2CO_3, DMF. (iii) *m*CPBA, DCM, 0 °C to RT; (iv) amine, THF, reflux.

Isatin (**67**) was reacted with thiosemicarbazide in presence of aqueous potassium carbonate solution to offer the uncyclized intermediate which was cyclized by acetic acid to give 5*H*-[1,2,4]triazino[5,6-*b*]indole-3-thiol (**68**).[111] IR spectrum of the cyclized compound (**68**) showed peaks at 3410 cm^{-1} (N-H stretching), at 3038 cm^{-1} (aromatic C-H stretching), at 1609 cm^{-1} (C=N stretching) and absence of C=O stretching vibration peak. The ^{1}H-NMR spectrum of compound (**68**) showed two broad singlets at δ 14.58 for one proton (-SH_f) and at δ 12.35 for one proton (-NH_e). A doublet at δ 7.98 for one proton (ArH_a), a multiplet at δ 7.58-7.62 for one proton (ArH_c), a doublet at δ 7.43 for one proton (ArH_d) and a multiplet at δ 7.31-7.34 for one proton (ArH_b) confirmed a total of four aromatic protons in the structure. Its mass spectrum showed $[M+H]^+$ ion peak at 203 m/z.

3-(Methylthio)-5*H*-[1,2,4]triazino[5,6-*b*]indole (**69**) was obtained by methylation of 5*H*-[1,2,4]triazino[5,6-*b*]indole-3-thiol (**68**) by methyl iodide.[112]

The IR spectrum of compound (**69**) showed peaks at 3056 cm^{-1} (aromatic C-H stretching), at 2801 cm^{-1} (aliphatic C-H stretching) and at 1604 cm^{-1} (C=N stretching). The ^{1}H-NMR spectrum of compound (**69**) showed a broad singlet at δ 12.62 for one NH proton (-NH_e) of the indole ring. A doublet at δ 8.28 for one proton (ArH_a), a multiplet at δ 7.64-7.67 for one proton (ArH_c), a doublet at δ 7.55 for one proton (ArH_d) and a multiplet at δ 7.39-7.42 for one proton (ArH_b) confirmed a total of four aromatic protons in the structure. A singlet appeared at δ 2.66 accounting for methyl protons (-SC$H_{3/f}$). In ^{13}C-NMR spectrum, the aromatic carbons appeared at δ 168.1, 147.2, 141.3, 140.8, 131.3, 122.9, 121.9, 118.2 and 113.2 whereas the thiomethyl carbon appeared at δ 13.9. Its mass spectrum showed $[M+H]^+$ ion peak at 216 m/z.

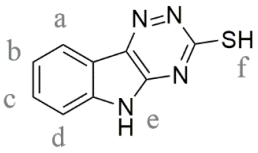

(68)

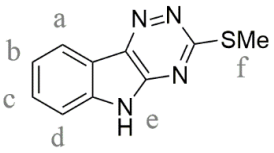

(69)

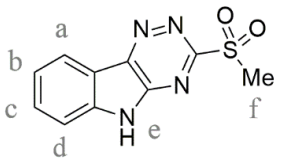

(70)

3-(Methylsulfonyl)-5*H*-[1,2,4]triazino[5,6-*b*]indole (**70**) was obtained by oxidation of thiomethyl group in compound (**69**) to methylsulfone by *m*CPBA.[113] The IR spectrum of compound (**70**) showed characteristic peaks at 1297 cm^{-1} (asymmetric S=O stretching) and at 1138 cm^{-1} for (symmetric S=O stretching). The ^{1}H-NMR spectrum of compound (**70**) showed a broad singlet at δ 13.25 for one NH proton (-NH_e) of the indole ring. A doublet at δ 8.45 for one proton (ArH_d), a multiplet at δ 7.77-7.81 for one proton (ArH_c), a doublet at δ 7.68 for one proton (ArH_a) and a multiplet at δ 7.49-7.53 for one proton (ArH_b) were present for aromatic protons in the structure. A singlet appeared at δ 3.50 accounting for three protons (-SO_2C$H_{3/f}$) of the methyl group, which were previously observed at δ 2.66 in compound (**69**). This down field shift was observed in compound (**70**), due to presence of two oxygen atoms directly attached to the sulfur atom. Its mass spectrum showed $[M+H]^+$ ion peak at 249 m/z.

Synthesis of the *N*-substituted 5*H*-[1,2,4]triazino[5,6-*b*]indol-3-amine derivatives (**71-80**) was carried out by reacting 3-(methylsulfonyl)-5*H*-[1,2,4] triazino[5,6-*b*]indole with the respective amines as depicted in **Scheme 4.2**.[113]

The IR spectra of the synthesized compounds showed characteristic peaks for amine N-H stretching (~3440 cm^{-1}), aromatic C-H stretching (~3060 cm^{-1}), aliphatic C-H stretching (~2963 cm^{-1}), C=N stretching (~1615 cm^{-1}) and C=C stretching (~1530 cm^{-1}) as well as disappearance of S=O stretching peaks. The analytical data i.e. melting points, characteristic IR peaks and HPLC data for compounds (**71-80**) have been summarized in **Table 4.1**.

Table 4.1. Analytical data for *N*-substituted 5*H*-[1,2,4]triazino[5,6-*b*]indol-3-amine derivatives (71-80)

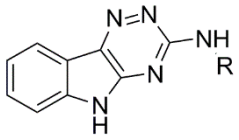

(71-80)

Compd	R	M.P.	IR characteristic peaks (cm^{-1})	HPLC data
71	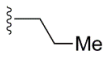	252-253 °C	3447, 3060, 2963, 1614, 1533, 1459, 1393, 749	Purity: 96.1 %, t_R = 4.65 min
72	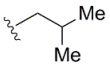	243-245 °C	3429, 3069, 2960, 1609, 1524, 1467, 750	Purity: 96.7 %, t_R = 3.39 min
73	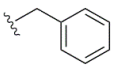	> 250 °C	3440, 3076, 2966, 1606, 1528, 694	Purity: 96.9 %, t_R = 7.32 min
74	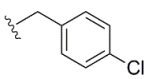	218-220 °C	3414, 3062, 2921, 1620, 1592, 1092, 758	Purity: 96.4 %, t_R = 5.94 min
75	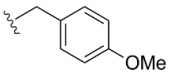	241-243 °C	3371, 3058, 2961, 1610, 1517,756	Purity: 97.3 %, t_R = 4.11 min
76	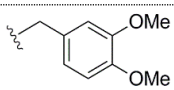	201-203 °C	3374, 3063, 2928, 1615, 1518, 806	Purity: 97.7 %, t_R = 3.63 min
77	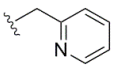	242-244 °C	3396, 3069, 2972, 1615, 1562, 750	Purity: 98.3 %, t_R = 3.36 min
78	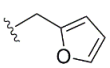	234-236 °C	3406, 3118, 2967, 1615, 1559, 751	Purity: 98.0 %, t_R = 3.55 min
79	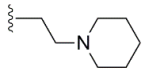	217-219 °C	3399, 3231, 3113, 1618, 1524, 1126, 1092, 754	Purity: 98.5 %, t_R = 5.33 min
80	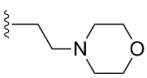	> 270 °C	3337, 3070, 2967, 1607, 1526, 1132, 757	Purity: 99.1 %, t_R = 4.55 min

The ^{1}H-NMR spectrum of compound (**71**) showed a broad singlet at δ 11.73 for one NH proton (-N*H*$_e$) of the indole ring. A doublet at δ 8.07 for one

proton (ArH_a), multiplets at δ 7.22-7.44 for three protons (Ar$H_{b,c,d}$) confirmed a total of four aromatic protons in the structure and one NH proton (-NH_f) peak got merged in the peak for the aromatic protons at δ 7.22-7.44. A multiplet appeared at δ 3.37-3.40 for two protons (-NHC$H_{2/g}$), a multiplet appeared at δ 1.63-1.69 for two protons (-NHCH$_2$C$H_{2/h}$) and a triplet appeared at δ 0.97 for three protons (-C$H_{3/i}$) of the aliphatic side chain. In ^{13}C-NMR spectrum, the aromatic carbons appeared at δ 161.7, 149.0, 139.5, 128.5, 121.9, 119.9, 119.7, 116.2 and 112.3 while the aliphatic carbons appeared at δ 43.0, 22.6 and 11.9. Its mass spectrum showed $[M+H]^+$ ion peak at 228.1 m/z.

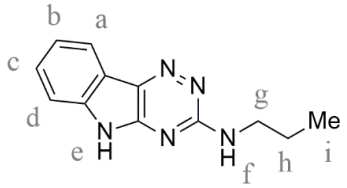

(**71**)

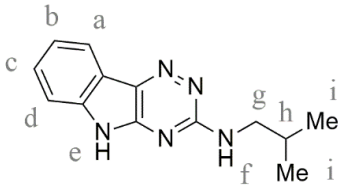

(**72**)

The ^{1}H-NMR spectrum of compound (**72**) showed a broad singlet at δ 11.81 for one NH proton (-NH_e) of the indole ring. A doublet at δ 8.08 for one proton (ArH_a), multiplets at δ 7.25-7.45 for three protons (Ar$H_{b,c,d}$) confirmed a total of four aromatic protons in the structure. It showed a multiplet at δ 3.21-3.28 accounting for two protons (-NHC$H_{2/g}$), a multiplet at δ 1.95-2.02 accounting for one proton (-CH_h) and a doublet at δ 0.94 accounting for six protons (-C$H_{3/i}$) of the aliphatic chain. In ^{13}C-NMR spectrum, the aromatic carbons appeared at δ 161.7, 149.0, 139.5, 128.5, 121.9, 119.9, 119.7, 116.2 and 112.3 whereas the aliphatic carbons appeared at δ 49.4, 28.1 and 20.8. Its mass spectrum showed $[M+H]^+$ ion peak at 242.1 m/z.

The ^{1}H-NMR spectrum of compound (**73**) showed a broad singlet at δ 11.79 for one NH proton (-NH_e) of the indole ring. A doublet at δ 8.07 for one proton (ArH_a) and multiplet at δ 7.18-7.45 for eight protons (Ar$H_{b-d,h-j}$) conformed a total of nine aromatic protons in the structure. A doublet appeared at δ 4.67 accounting for two benzylic protons (-C$H_{2/g}$). In ^{13}C-NMR spectrum, the aromatic carbons appeared at δ 161.7, 148.9, 140.5, 139.6, 128.9, 128.7, 127.5, 127.2, 122.0, 120.0, 119.6, 116.2 and 112.3 while the benzylic carbon appeared at δ 44.4. Its mass spectrum showed $[M+H]^+$ ion peak at 276.1 m/z.

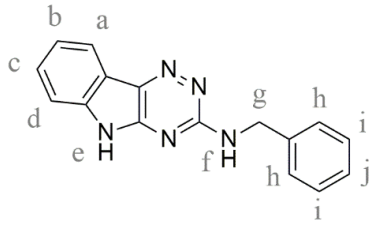

(**73**)

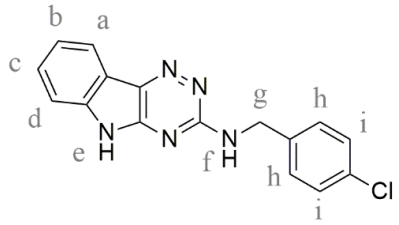

(**74**)

The ^{1}H-NMR spectrum of compound (**74**) showed a broad singlet at δ 11.82 for one NH proton (-N*H*$_{e}$) of the indole ring. A doublet at δ 8.07 for one proton (Ar*H*$_{a}$), multiplet at δ 7.24-7.46 for seven aromatic protons (Ar*H*$_{b\text{-}d,h,i}$) and one NH proton (-N*H*$_{f}$) and a doublet at δ 4.62 for two benzylic protons ($CH_{2/g}$) were also observed. In ^{13}C-NMR spectrum, the aromatic carbons appeared at δ 161.5, 149.0, 139.6, 139.0, 131.6, 129.3, 128.8, 128.7, 122.4, 120.1, 119.5, 116.0 and 112.4 whereas the benzylic carbon appeared at δ 43.9. Its mass spectrum showed $[M+H]^{+}$ ion peak at 310.1 m/z.

The ^{1}H-NMR spectrum of compound (**75**) showed a broad singlet at δ 11.83 for one NH proton (-N*H*$_{e}$) of the indole ring. A doublet at δ 8.07 for one proton (Ar*H*$_{a}$), multiplets at δ 7.24-7.46 for five protons (Ar*H*$_{b\text{-}h}$), multiplets at δ 6.82-6.86 for two protons (Ar*H*$_{i}$) were seen conforming a total of eight aromatic protons in the structure. A broad singlet appeared at δ 7.96 accounting for one NH proton (-N*H*$_{f}$). A doublet appeared at δ 4.57 for two benzylic protons ($-CH_{2/g}$) and a singlet appeared at δ 3.73 for three protons ($-OCH_{3/j}$) of the methoxyl group. Its mass spectrum showed $[M+H]^{+}$ ion peak at 306.1 m/z.

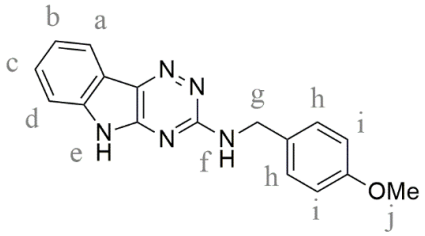

(**75**)

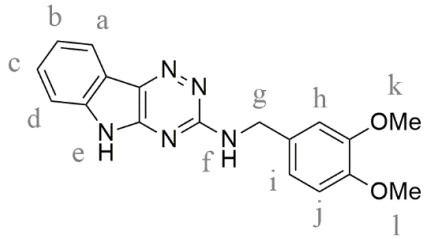

(**76**)

The ^{1}H-NMR spectrum of compound (**76**) showed a doublet at δ 8.07 for one proton (Ar*H*$_{a}$) and multiplet at δ 6.82-7.46 for six protons (Ar*H*$_{b\text{-}d,h\text{-}j}$) confirming a total of seven aromatic protons in the structure. The NH proton (-N*H*$_{f}$) peak merged with the aromatic protons appearing at δ 6.82-7.46. A doublet appeared at δ 4.56-4.58 accounting for two benzylic protons ($CH_{2/g}$). Two singlets appeared at δ 3.76 for three protons ($-OCH_{3/k}$) and at δ 3.74 for

three protons (-$OCH_{3/l}$) confirming a total of six protons of the methoxy groups in the structure. In ^{13}C-NMR spectrum, the aromatic carbons appeared at δ 161.2, 149.1, 148.9, 148.2, 139.7, 132.9, 128.7, 122.0, 120.1, 119.7, 116.0, 112.4, 112.5 and 111.9. The methoxy group carbons appeared at δ 56.0 and 55.9 whereas the benzylic carbon appeared at δ 44.3. Its mass spectrum showed $[M+H]^+$ ion peak at 336.1 m/z.

The ^{1}H-NMR spectrum of compound (**77**) showed a broad singlet at δ 11.79 for one NH proton (-NH_e) of the indole ring. A doublet at δ 8.52 for one proton (ArH_a), multiplet at δ 7.18-8.13 for seven protons (Ar$H_{b\text{-}d,h\text{-}k}$) were observed confirming a total of eight aromatic protons in the structure. A doublet appeared at δ 4.71-4.78 accounting for two benzylic protons (-$CH_{2/g}$). In ^{13}C-NMR spectrum, the aromatic carbons appeared at δ 159.8, 149.3, 148.9, 139.6, 137.2, 137.1, 128.8, 122.5, 121.1, 120.9, 120.2, 119.5, 116.0 and 112.4, whereas the benzylic carbon appeared at δ 46.5. Its mass spectrum showed $[M+H]^+$ ion peak at 277.1 m/z.

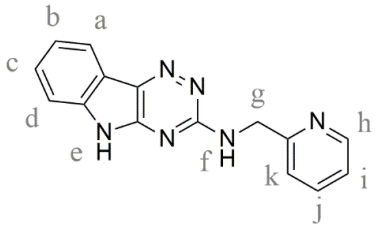

(**77**)

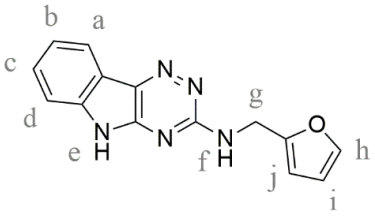

(**78**)

The ^{1}H-NMR spectrum of compound (**78**) showed a broad singlet at δ 11.83 for one NH proton (-NH_e) of the indole ring, a multiplet at δ 8.06-8.12 for one proton (ArH_a), a multiplet at δ 6.26-7.92 for six aromatic protons (Ar$H_{b\text{-}d,h\text{-}j}$) and one NH proton (-N$H_f$) and a doublet at δ 4.64 for two benzylic protons (C$H_{2/g}$). In ^{13}C-NMR spectrum, the aromatic carbons appeared at δ 155.8, 153.5, 148.9, 142.5, 139.7, 128.8, 122.1, 120.9, 120.2, 119.5, 116.0 , 110.9 and 107.3 whereas the benzylic carbon appeared at δ 38.3. Its mass spectrum showed $[M+H]^+$ ion peak at 266.1 m/z.

The ^{1}H-NMR spectrum of compound (**79**) showed a broad singlet at δ 11.84 for one NH proton (-NH_e) of the indole ring. A doublet at δ 8.07 (ArH_a) for one proton, a multiplet at δ 7.24-7.46 for three protons (Ar$H_{b\text{-}d}$) were seen confirming a total of four aromatic protons in the structure. A broad singlet

appeared at δ 7.2 accounting for one NH proton (-NH_f). A multiplet appeared at δ 3.50-3.52 for two protons (-NHC$H_{2/g}$) and a multiplet appeared at δ 2.52-2.55 for two protons (-NC$H_{2/h}$) confirming a total of four protons of methylene group in the aliphatic chain of the structure. A multiplet at δ 2.43 for four protons (-NC$H_{2/i}$), a multiplet at δ 1.51-1.55 for four protons (-NCH$_2$C$H_{2/j}$) and a multiplet at δ 1.41-1.42 for two protons (-C$H_{2/k}$) confirmed a total of ten protons of the piperidine ring. In ^{13}C-NMR spectrum, the aromatic carbons appeared at δ 155.8, 149.0, 139.5, 128.4, 122.0, 120.0, 119.7, 116.0 and 112.3 whereas the aliphatic carbons appeared at δ 57.9, 54.6, 41.4, 26.0 and 24.5. Its mass spectrum offered $[M+H]^+$ ion peak at 297.1 m/z.

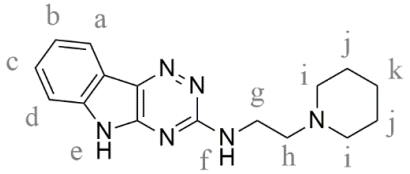

(**79**)

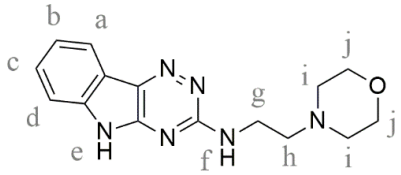

(**80**)

The ^{1}H-NMR spectrum of compound (**80**) showed a broad singlet at δ 11.74 for one NH proton (-NH_e) of the indole ring. A doublet at δ 8.08 for one proton (ArH_a) and a multiplet at δ 7.03-7.45 for three protons (ArH_{b-d}) were seen confirming a total of four aromatic protons in the structure. A multiplet at δ 3.62-3.64 for four protons (-OC$H_{2/j}$) and a multiplet at δ 2.47-2.49 for four protons (-NC$H_{2/i}$) confirmed a total of eight protons of the morpholine ring. A multiplet at δ 3.55-3.57 for two protons (-NHC$H_{2/g}$) and a multiplet at δ 2.59-2.62 for two protons (-NC$H_{2/h}$) confirmed a total of four protons of methylene group in the aliphatic chain in the structure. In ^{13}C-NMR spectrum, the aromatic carbons appeared at δ 161.7, 149.0, 139.5, 128.6, 122.0, 120.0, 119.6, 116.2 and 112.4, while the aliphatic carbons appeared at δ 66.7, 57.7, 53.8 and 38.3. Its mass spectrum showed $[M+H]^+$ ion peak at 299.1 m/z.

4.1.1.2.2. Synthesis of 5-substituted 5*H*-[1,2,4]triazino[5,6-*b*]indol-3-amine derivatives (117-126)

The designed 5-substituted 5*H*-[1,2,4]triazino[5,6-*b*]indol-3-amine derivatives (**117-126**) were synthesized from *N*-substituted isatins as depicted in **Scheme 4.3.** *N*-Alkylation or *N*-benzylation of the isatin was achieved with the corresponding alkyl/benzyl halides in the presence of potassium carbonate in DMF.[111] Condensation of these *N*-substituted isatins (**81-89**) with

thiosemicarbazide gave *N*-substituted [1,2,4]triazino-[5,6-*b*]indole-3-thiol derivatives (**90-98**). These thiol derivatives were methylated and further oxidized to the corresponding sulfone derivatives (**108-116**). These sulfone derivatives were reacted with ammonia to obtain the desired 5-substituted [1,2,4]triazino[5,6-*b*]indol-3- amine derivatives (**117-127**).

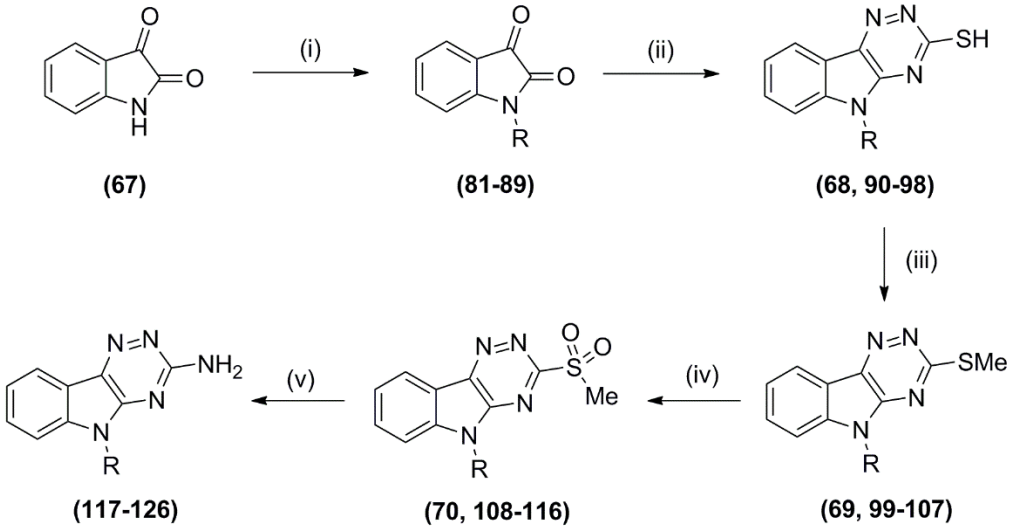

Scheme 4.3. Synthesis of 5-substituted 5*H*-[1,2,4]triazino[5,6-*b*]indol-3-amine derivatives (**117-126**). Reagents and conditions: (i) Alkyl/substituted benzyl halides, K_2CO_3, DMF; (ii) thiosemicarbazide, K_2CO_3, H_2O, reflux, overnight; (iii) MeI, K_2CO_3, DMF; (iv) *m*CPBA, DCM, 0 °C to RT; (v) ammonia, THF, reflux.

The work carried out for the synthesis of 5-substituted 5*H*-[1,2,4]triazino[5,6-*b*]indol-3-amine derivatives (**117-126**) from commercially available isatin has been discussed under the following headings:

4.1.1.2.2.1. Synthesis of *N*-substituted isatins (**81-89**),

4.1.1.2.2.2. Synthesis of 5-substituted 5*H*-[1,2,4]triazino[5,6-*b*]indol-3-thiol derivatives (**90-98**),

4.1.1.2.2.3. Synthesis of 5-substituted 3-(methylthio)-5*H*-[1,2,4] triazino[5,6-*b*]indole derivatives (**99-107**),

4.1.1.2.2.4. Synthesis of 5-substituted 3-(methylsulfonyl)-5*H*-[1,2,4] triazino[5,6-*b*]indole derivatives (**108-116**) and

4.1.1.2.2.5. Synthesis of 5-substituted 5*H*-[1,2,4]triazino[5,6-*b*]indol-3-amine derivatives (**117-126**).

4.1.2.2.1. Synthesis of *N*-substituted isatins (81-89)

Commercially available isatin (**67**) was *N*-alkylated/benzylated by the corresponding alkyl/benzyl halides in the presence of potassium carbonate as a base in DMF solvent (**Scheme 4.3**).[111] The IR spectra of *N*-substituted isatins (**81-89**) showed disappearance of NH stretching peaks whereas the two C=O stretching vibration peaks remained intact. The analytical data for *N*-substituted isatins (**81-89**) have been summarized in **Table 4.2**.

Table 4.2. Analytical data for *N*-substituted isatin derivatives (81-89)

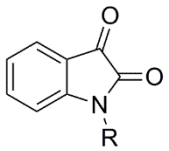

(81-89)

Compd	R	M.P.	R*f*[a]	IR characteristic peaks (cm^{-1})
81		130-131 °C	0.49	1724, 1607, 1467, 1366, 1325, 1116, 1089, 759, 699
82	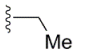	132-134 °C	0.52	1731, 1609, 1465, 1352, 1289, 1126, 1092, 758, 699
83	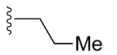	80-82 °C	0.56	1718, 1601, 1465, 1386, 1348, 1180, 1116, 1088, 754
84	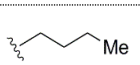	40-42 °C	0.60	1727, 1611, 1469, 1354, 1294, 1131, 1094, 750, 706
85	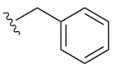	132-134 °C	0.67	1733, 1611, 1469, 1348, 1177, 756 ,697
86	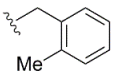	128-130 °C	0.63	1732, 1610, 1469, 1347, 1175, 1092, 757
87	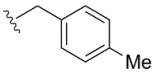	136-138 °C	0.65	1733, 1611, 1468, 1347, 1177, 1093, 757
88	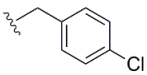	138-140 °C	0.48	1732, 1610, 1467, 1340, 1168, 756
89	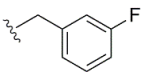	168-169 °C	0.69	1727, 1614, 1471, 1356, 1249, 1142, 1096, 755, 688

[a]Mobile phase: *n*-Hexane: Ethyl acetate 50%

4.1.1.2.2.2. Synthesis of 5-substituted 5*H*-[1,2,4]triazino[5,6-*b*]indol-3-thiol derivatives (90-98)

5-Substituted [1,2,4]triazino[5,6-*b*]indol-3-thiol derivatives (**90-98**) were synthesized by condensation of thiosemicarbazide and *N*-substituted isatins (**81-89**) in presence of potassium carbonate (**Scheme 4.3**). This reaction

was carried out at reflux conditions using water as polar protic solvent. After completion of the reaction, the reaction mixture was acidified with glacial acetic acid to precipitate the thiol compounds.[111,112] IR spectra of the compounds showed disappearance of C=O stretching vibrational peaks. The mass spectra confirmed that the molecular weights of the compounds were in accordance with the calculated molecular weights of the synthesized thiol derivatives. The analytical data for 5-substituted [1,2,4]triazino[5,6-*b*]indol-3-thiol derivatives (**90-98**) have been summarized in **Table 4.2.**

Table 4.3. Analytical data for 5-substituted 5*H*-[1,2,4]triazino[5,6-*b*]indol-3-thiol derivatives (90-98)

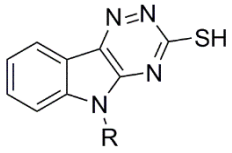

(90-98)

Compd	R	M.P. (DSC)	IR characteristic peaks (cm^{-1})	MS (m/z)
90		290.34 °C	2975, 1601, 1566, 1362, 1139, 750	217.20 $(M+H)^+$
91		304.17 °C	2855, 1574, 1347, 1143, 743	231.10 $(M+H)^+$
92		307.01 °C	2941, 1602, 1559, 1349, 1146, 742	245.20 $(M+H)^+$
93	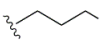	274.32 °C	2925, 1603, 1561, 1330, 1137, 757	259.20 $(M+H)^+$
94	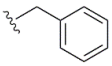	293.24 °C	2841, 1599, 1569, 1163, 744	291.68 $(M+H)^+$
95	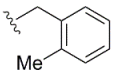	301.22 °C	2980, 1608, 1346, 1246, 759	307.20 $(M+H)^+$
96	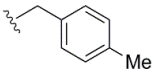	292.88 °C	2924, 1599, 1572, 1347, 1145, 752	307.20 $(M+H)^+$
97	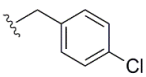	300.43 °C	2980, 2885, 1571, 1377, 1141, 754	325.99 $(M)^+$, 328 $(M+2)^+$
98	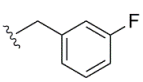	282.15 °C	2925, 1597, 1571, 1349, 1146, 745	311.20 $(M+H)^+$

4.1.1.2.2.3. Synthesis of 5-substituted 3-(methylthio)-5*H*-[1,2,4]triazino [5,6-*b*]indole derivatives (99-107)

Syntheses of 5-substituted 3-(methylthio)-5*H*-[1,2,4]triazino[5,6-*b*] indole derivatives (**99-107**) were carried out by methylation of the respective thiol derivatives (**90-98**) with methyl iodide as depicted in **Scheme 4.3**.[112] The mass spectra of the derivatives were in accordance with the calculated molecular weights of the synthesized thiomethyl derivatives. The analytical data for 5-substituted 3-(methylthio)-5*H*-[1,2,4]triazino[5,6-*b*]indole derivatives (**99-107**) have been summarized in **Table 4.4.**

Table 4.4. Analytical data for 5-substituted 3-(methylthio)-5*H*-[1,2,4] triazino[5,6-*b*]indole derivatives (99-107)

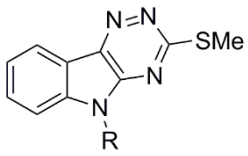

(99-107)

Compd	R	M.P.	IR characteristic peaks (cm^{-1})	MS (m/z)
99		160-162 °C	3052, 3022, 2968, 2925, 1578, 1179, 1072, 762	231 $(M+H)^+$
100		148-150 °C	3054, 2970, 2928, 2872, 1580, 1188, 1078, 749	245 $(M+H)^+$
101	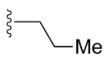	128-130 °C	3053, 3026, 2966, 2924, 1575, 1190, 1073, 746	259 $(M+H)^+$
102	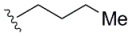	140-142 °C	3054, 2953, 2925, 1578, 1187, 1075, 742	273 $(M+H)^+$
103	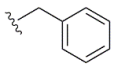	168-170 °C	3058, 2955, 2923, 1578, 1186, 1074, 745, 694;	307 $(M+H)^+$
104	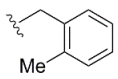	161-163 °C	3059, 3029, 2974, 2924, 1574, 1181, 1073, 748	321 $(M+H)^+$
105	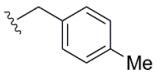	195-197 °C	3056, 2922, 1581, 1182, 1083, 749	321 $(M+H)^+$
106	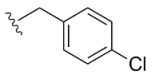	181-183 °C	3059, 3026, 2927, 1583, 1184, 1088, 748	341 $(M+H)^+$
107	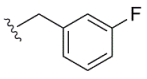	176-178 °C	3055, 2924, 1581, 1185, 1078, 751	325 $(M+H)^+$

4.1.1.2.2.4. Synthesis of 5-substituted 3-(methylsulfonyl)-5*H*-[1,2,4] triazino[5,6-*b*]indole derivatives (108-116)

As depicted in **Scheme 4.3**, 5-substituted 3-(methylsulfonyl)-5*H*-[1,2,4]triazino[5,6-*b*]indole derivatives (**108-116**) were synthesized by the oxidation of the respective thiomethyl derivatives (**99-107**) with *m*CPBA.[113] The obtained products were used in the next step without further purification.

4.1.1.2.2.5. Synthesis of 5-substituted-5*H*-[1,2,4]triazino[5,6-*b*]indol-3-amine derivatives (117-126)

5-substituted 5*H*-[1,2,4]triazino[5,6-*b*]indol-3-amine derivatives (**117-126**) were synthesized by reaction of the respective sulfone derivatives (**70** and **108-116**) with ammonia.[113] The obtained solids were purified by flash chromatography to yield the titled compounds (**117-126**).

Table 4.5. Analytical data for 5-substituted 5*H*-[1,2,4]triazino[5,6-*b*]indol-3-amine derivatives (117-126)

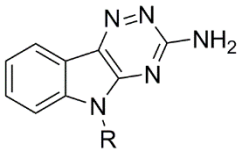

(117-126)

Compd	R	M.P.	IR characteristic peaks (cm^{-1})	HPLC data
117		>270 °C	3383, 3307, 3212, 1549, 1106, 770	Purity: 95.2 %, t_R = 4.32 min
118		> 270 °C	3384, 3308, 3211, 2937, 1549, 1019, 755	Purity: 99 %, t_R = 4.68 min
119		265-267 °C	3384, 3308, 3212, 2938, 1588, 1105, 755	Purity: 99.1 %, t_R = 4.88 min
120		208-210 °C	3377, 3298, 3210, 2961, 1525, 1035, 741	Purity: 98.0 %, t_R = 5.65 min
121	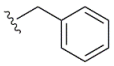	265-267 °C	3396, 3329, 3029, 2929, 1542, 1030, 746	Purity: 99.1 %, t_R = 8.92 min
122	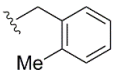	253-254 °C	3462, 3334, 3009, 2922, 1553, 1107, 744	Purity: 95.9 %, t_R = 5.54 min
123	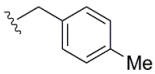	245-247 °C	3471, 3271, 3057, 2963, 1536, 1098, 743	Purity: 96.6 %, t_R = 5.73 min
124	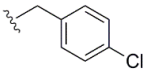	215-217 °C	3417, 3298, 2925, 1540, 1039, 746	Purity: 97.4 %, t_R = 5.99 min
125	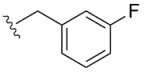	230-232 °C	3418,3299, 2924, 1550, 1039, 748	Purity: 97.4 %, t_R = 6.93 min
126	-H	> 270 °C	3383, 3307, 3212, 1558, 1021, 755	Purity: 98.7 %, t_R = 3.45 min

The IR spectra of the synthesized compounds showed characteristic peaks for primary amine N-H stretching (two bands at ~3440-3250 cm^{-1}) as well as disappearance of S=O stretching peaks. The mass spectra of the derivatives were in accordance with the calculated molecular weights of the synthesized derivatives. The analytical data for the 5-substituted 5*H*-[1,2,4]triazino [5,6-*b*]indol-3-amine derivatives (**117-126**) have been summarized in **Table 4.5.**

The ^{1}H-NMR spectrum of compound (**117**) showed a doublet at δ 8.09 for one proton (ArH_a), a doublet at δ 7.60 for one proton (ArH_d), a multiplet at δ 7.54-7.50 for one proton (ArH_b) and a multiplet at δ 7.35-7.31 for one proton (ArH_c) confirming a total of four aromatic protons in the structure. A broad singlet appeared at δ 7.26 accounting for two protons (-NH_e) of the amino group whereas a singlet appeared at δ 3.72 accounting for three protons (-NC$H_{3/f}$). Its mass spectrum showed $[M+H]^+$ ion peak at 200 m/z.

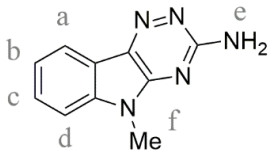

(117)

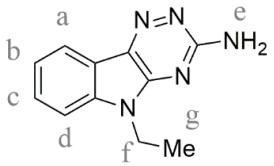

(118)

The ^{1}H-NMR spectrum of compound (**118**) showed a doublet at δ 8.02 for one proton (ArH_a), multiplet at δ 7.71-7.62 for two protons (Ar$H_{b,c}$), a multiplet at δ 7.41-7.37 for one proton (ArH_d) confirming a total of four aromatic protons in the structure. A broad singlet appeared at δ 6.84 accounting for two protons (-NH_e) of amino group. A multiplet appeared at δ 4.24-4.30 accounting for two protons (-NC$H_{2/f}$) and a multiplet at δ 1.76-1.82 accounting for three protons (-$NCH_2CH_{3/g}$) confirming ethyl group attached to the nitrogen of the indole ring. Its mass spectrum showed $[M+H]^+$ ion peak at 214.2 m/z.

The ^{1}H-NMR spectrum of compound (**119**) showed a doublet at δ 8.11 for one proton (ArH_a), a doublet at δ 7.65 for one proton (ArH_d), a multiplet at δ 7.52-7.48 for one proton (ArH_b) and a multiplet at δ 7.34-7.30 for one proton (ArH_c) confirming a total of four aromatic protons in the structure. A broad singlet appeared at δ 7.27 accounting for two protons (-NH_e) of the amino group. A triplet appeared at δ 4.21 accounting for two protons (-$NCH_{2/f}$), a multiplet at δ 1.78-1.85 accounting for two protons (-C$H_{2/g}$) and a triplet at δ 0.90

accounting for three protons (C$H_{3/h}$) confirming the propyl group attached to the nitrogen of the indole ring. Its mass spectrum showed $[M]^+$ ion peak at 227 m/z.

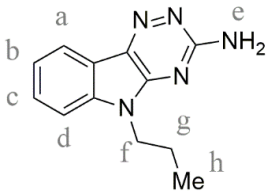

(119)

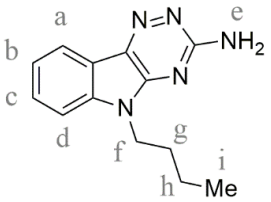

(120)

The ^{1}H-NMR spectrum of compound (**120**) showed a doublet at δ 8.10 for one proton (ArH_a), a multiplet at δ 7.51-7.52 for two protons (Ar$H_{b/c}$) and a multiplet at δ 7.27-7.31 for one proton (ArH_d) confirming a total of four aromatic protons. A broad singlet appeared at δ 6.90 accounting for two protons (-NH_e) of amino group. A multiplet at δ 4.19-4.22 for two protons (-NC$H_{2/f}$), a multiplet at δ 1.74-1.81 for two protons (-C$H_{2/g}$), a multiplet at δ 1.30-1.36 for two protons (-C$H_{2/h}$) and a triplet at δ 0.92 for three protons (-C$H_{3/i}$) confirmed the butyl group attached to the nitrogen of the indole ring. Its mass spectrum showed molecular ion peak $[M+H]^+$ at 242.3 m/z.

The ^{1}H-NMR spectrum of compound (**121**) showed a multiplet at δ 8.14-7.93 for one proton (ArH_a) and multiplet at δ 7.49-7.22 for eight protons (ArH_{b-i}) confirmed a total of nine aromatic protons. A singlet appeared at δ 5.45 accounting for two methylene protons (-NC$H_{2/e}$). Its mass spectrum showed $[M+H]^+$ ion peak at 276.2 m/z.

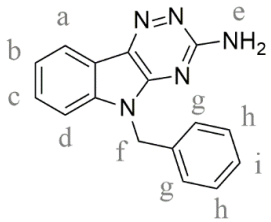

(121)

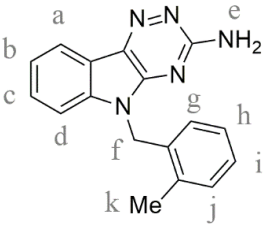

(122)

The ^{1}H-NMR spectrum of compound (**122**) showed a doublet at δ 8.40 for one proton (Ar*H*), multiplets at δ 7.35-7.44 for two protons (Ar*H*) and at δ 7.20-7.28 for two protons (Ar*H*), a doublet at δ 7.13 for one proton (Ar*H*), a multiplet at δ 7.09-7.06 for one proton (Ar*H*) and a doublet at δ 6.72 for one proton (Ar*H*) confirming a total of eight aromatic protons in the structure. A

broad singlet appeared at δ 5.44 accounting for two protons (-NH_e) of amino group. A singlet appeared at δ 5.21 accounting for two protons (-NC$H_{2/e}$), whereas a singlet appeared at δ 2.44 accounting for three protons (ArC$H_{3/k}$) of the methyl group attached to the phenyl ring. Its mass spectrum displayed $[M+H]^+$ ion peak at 290 m/z.

The ^{1}H-NMR spectrum of compound (**123**) showed a multiplet at δ 7.93-7.95 for one proton, multiplet at δ 7.14-7.55 for five protons and a multiplet at δ 6.88-6.90 for two protons confirming a total of eight aromatic protons in the structure. A singlet appeared at δ 5.27 accounting for two protons (-NC$H_{2/e}$) and a singlet at δ 3.72, accounting for three protons (ArC$H_{3/i}$) of methyl group attached to the phenyl ring. Its mass spectrum showed $[M+H]^+$ ion peak at 290.2 m/z.

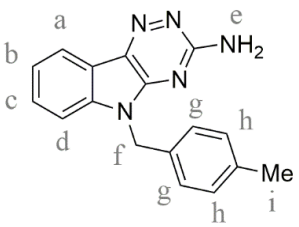

(123)

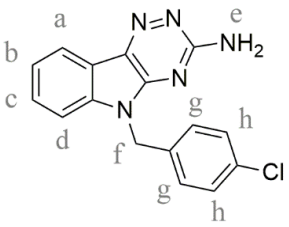

(124)

The ^{1}H-NMR spectrum of compound (**124**) showed a doublet at δ 8.39 for one proton (ArH_a), a multiplet at δ 7.43-7.47 for one proton (Ar*H*) and at δ 7.26-7.39 for six protons (Ar*H*) confirming a total of eight aromatic protons in the structure. A singlet appeared at δ 5.47 accounting for two protons (-NC$H_{2/e}$). A broad singlet appeared at δ 5.16 accounting for two protons (-NH_e) of the amino group. Its mass spectrum showed $[M+H]^+$ ion peak at 310 m/z.

The ^{1}H-NMR spectrum of compound (**125**) showed a multiplet at δ 7.94-7.96 for one proton, multiplets at δ 7.46-7.55 for four protons, at δ 7.30-7.32 for one proton and at δ 7.16-7.18 for two protons confirming a total of eight aromatic protons in the structure. A singlet appeared at δ 5.33 accounting for two protons (-NC$H_{2/e}$). Its mass spectrum displayed $[M+H]^+$ ion peak at 294 m/z.

The ^{1}H-NMR spectrum of compound (**126**) showed a doublet at δ 8.30 for one proton (ArH_a), a multiplet at δ 7.63-7.67 for one proton (ArH_b), a doublet at δ 7.56 for one proton (ArH_d) and a multiplet at δ 7.93-7.43 for one proton

(ArH_c) confirming a total of four aromatic protons in the structure. A broad singlet appeared at δ 6.90 accounting for two protons (-NH_e) of the amino group. Its mass spectrum showed $[M+H]^+$ ion peak at 186.09 m/z.

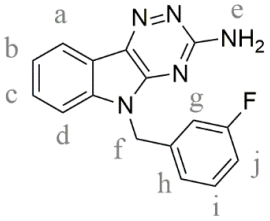

(125)

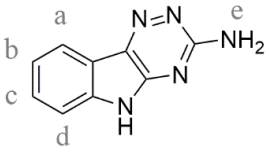

(126)

4.1.2.3. Synthesis of *N*-(aminoalkyl)-5*H*-[1,2,4]triazino[5,6-b]indol-3-amine derivatives (179-202)

As depicted in **Scheme 4.4**, *N*-(aminoalkyl)-5*H*-[1,2,4]triazino[5,6-*b*] indol-3-amine derivatives (**179-202**) were synthesized by the reaction of 3-(methylsulfonyl)-5*H*-[1,2,4]triazino-[5,6-*b*]indole (**70**) with the respective *N*,*N*-(disubstituted-amino)alkylamines.

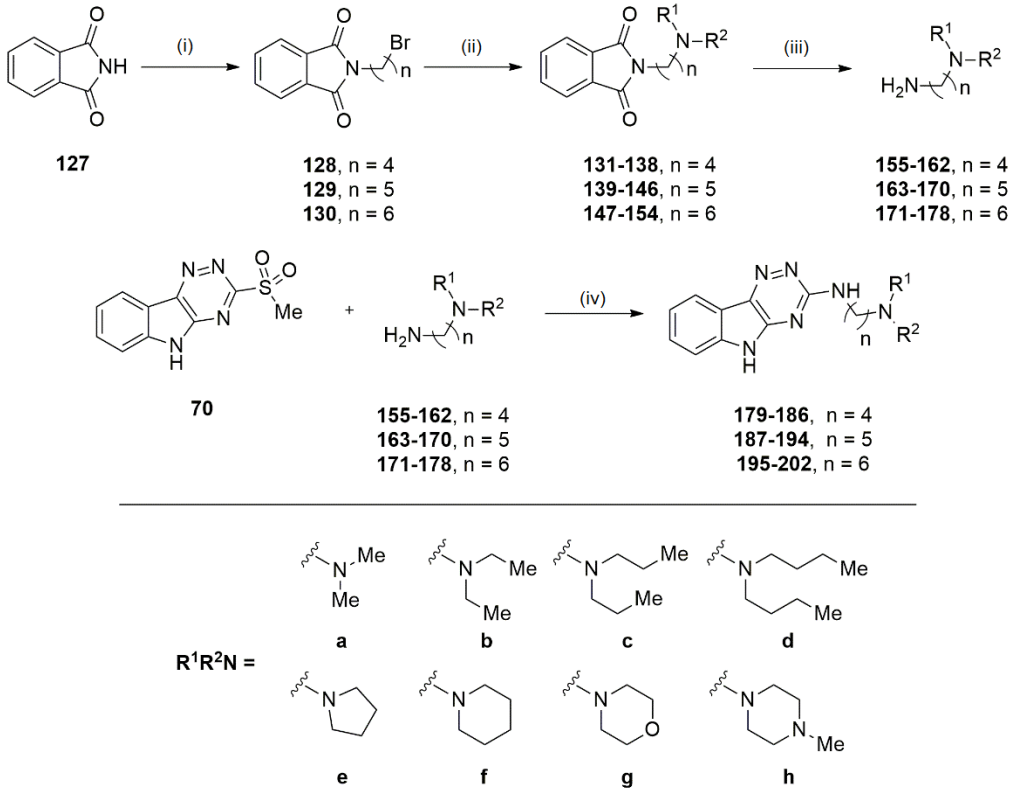

Scheme 4.4. Synthetic route for the synthesis of *N*-(aminoalkyl)-5*H*-[1,2,4]triazino [5,6-*b*]indol-3-amine derivatives (**179-202**). Reagents and conditions: (i) $Br(CH_2)_nBr$, K_2CO_3, TEBAC, acetone, RT; (ii) HNR^1R^2, TEA, MeOH, reflux; (iii) $NH_2NH_2.H_2O$, MeOH, reflux; (iv) THF, reflux.

The work carried out to synthesize *N*-(aminoalkyl)-5*H*-[1,2,4]triazino [5,6-*b*]indol-3-amine derivatives (**179-202**) has been discussed in three subheads as mentioned below:

4.1.1.2.3.1. Synthesis of *N*-(bromoalkyl)phthalimides (**128-130**),

4.1.1.2.3.2. Synthesis of *N, N*-(disubstituted-amino)alkylamines (**155-178**) and

4.1.1.2.3.3. Synthesis of *N*-(aminoalkyl)-5*H*-[1,2,4]triazino[5,6-*b*] indol-3-amine derivatives (**179-202**).

4.1.1.2.3.1. Synthesis of *N*-(bromoalkyl)phthalimides (128-130)

Phthalimide (**127**) was reacted with dibromoalkanes in presence of potassium carbonate and benzyltriethylammonium chloride (TEBAC) in acetone to form *N*-(bromoalkyl)phthalimides (**128-130**).[114] Analytical data for *N*-(bromoalkyl)-phthalimides (**128-130**) have been summarized in **Table 4.6.**

Table 4.6. Analytical data for *N*-(bromoalkyl)phthalimides (128-130)

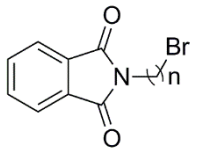

(128-130)

Compd	n	M.P.	R_f[a]	Characteristic IR peaks (cm^{-1})
128	4	75-78 °C	0.44	2988, 2862, 1768, 1712, 1610, 717
129	5	61-63 °C	0.45	2932, 2862, 1769, 1710, 1613, 717
130	6	57-59 °C	0.45	2983, 2860, 1764, 1704, 1610, 720

[a]Mobile phase: *n*-Hexane: Ethyl acetate 3:2

4.1.1.2.3.2. Synthesis of *N,N*-(disubstituted-amino)alkylamines (155-178)

The aminoalkylamines (**155-178**) required for the synthesis of compounds (**179-202**) were prepared through Gabriel synthesis.[114] The desired basic amines (a-h; R^1R^2NH) were reacted with *N*-(bromoalkyl)phthalimides (**128-130**) to yield compounds (**131-154**). Hydrazinolysis of compounds (**131-154**) offered the desired aminoalkylamines (**155-178**) as viscous yellowish oil in 67-87 % yields which were used as such without further purification.

4.1.1.2.3.3. Synthesis of *N*-(aminoalkyl)-5*H*-[1,2,4]triazino[5,6-b]indol-3-amine derivatives (179-202)

Syntheses of *N*-(aminoalkyl)-5*H*-[1,2,4]triazino[5,6-b]indol-3-amine derivatives (**179-202**) were carried out by the reaction of 3-(methylsulfonyl)-5*H*-[1,2,4]triazino[5,6-*b*]indole (**70**) with aminoalkylamines (**155-178**).[113] The obtained crude products were purified by flash chromatography to yield the titled compounds (**179-202**). The IR spectra of the synthesized compounds showed characteristic peaks for amine N-H stretching (~3440 cm^{-1}), aromatic C-H stretching (~3060 cm^{-1}), aliphatic C-H stretching (~2950 cm^{-1}), C=N stretching (~1615 cm^{-1}) and C=C stretching (~1530 cm^{-1}) as well as disappearance of S=O stretching peaks. The mass spectra of the derivatives were in accordance with the calculated molecular weights of the synthesized compounds. The analytical data for *N*-(aminoalkyl)-5*H*-[1,2,4]triazino[5,6-*b*] indol-3-amine derivatives (**179-202**) have been summarized in **Table 4.7.**

Table 4.7. Analytical data for *N*-(aminoalkyl)-5*H*-[1,2,4]triazino[5,6-b] indol-3-amine derivatives (179-202)

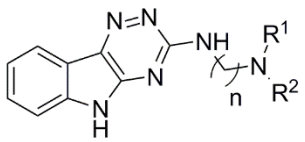

(179-202)

Compd	n	NR^1R^2	M.P.	IR characteristic peaks (cm^{-1})	HPLC data
179	4		161-163 °C	3443, 3327, 3048, 2944, 1615, 1556, 1393, 742	Purity: 98.1 %, t_R = 3.45 min
180	4	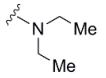	190-192 °C	3442, 3336, 2966, 1616, 1560, 1391, 748	Purity: 97.4 %, t_R = 3.43 min
181	4	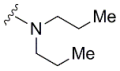	198-200 °C	3444, 3333, 3003, 2956, 1615, 1531, 1390, 746	Purity: 97.6 %, t_R = 3.72 min
182	4	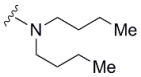	180-182 °C	3442, 3222, 3003, 2955, 1614, 1523, 1388, 743	Purity: 96.2 %, t_R = 3.51 min
183	4		220-222 °C	3434, 3219, 3000, 2934, 1617, 1522, 1382, 745	Purity: 97.6 %, t_R = 3.42 min
184	4		199-201 °C	3445, 3326, 3061, 2933, 1613, 1558, 1393, 748	Purity: 98.2 %, t_R = 3.43 min
185	4		191-193 °C	3430, 3222, 3007, 2944, 1612, 1526, 1387, 747	Purity: 97.2 %, t_R = 3.49 min

Compd	n	NR^1R^2	M.P.	IR characteristic peaks (cm^{-1})	HPLC data
186	4	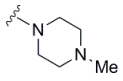	175-177 °C	3425, 3222, 3052, 2935, 1615, 1581, 741	Purity: 99.5 %, t_R = 3.45 min
187	5		198-200 °C	3222, 3111, 3007, 2945, 1612, 1527, 1388, 748	Purity: 97.8 %, t_R = 3.25 min
188	5	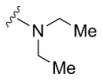	191-193 °C	3442, 3333, 3059, 2967, 1615, 1554, 1370, 745	Purity: 98.4 %, t_R = 4.18 min
189	5	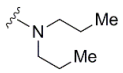	200-202 °C	3443, 3329, 3057, 2956, 1614, 1532, 1390, 747	Purity: 99.2 %, t_R = 5.0 min
190	5	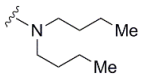	184-186 °C	3444, 3332, 3059, 2931, 1614, 1535, 1390, 746	Purity: 98.8 %, t_R = 3.07 min
191	5		191-193 °C	3459, 3306, 3059, 2937, 1615, 1526, 1383, 743	Purity: 98.3 %, t_R = 2.84 min
192	5		196-198 °C	3423, 3223, 3007, 2935, 1614, 1526, 1383, 741	Purity: 96.8 %, t_R = 5.43 min
193	5		199-201 °C	3426, 3222, 3050, 2925, 1613, 1524, 1384, 749	Purity: 98.5 %, t_R = 3.20 min
194	5	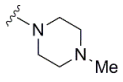	162-164 °C	3439, 3234, 3061, 2931, 1614, 1530, 1389, 745	Purity: 98.4 %, t_R = 3.13 min
195	6		180-182 °C	3321, 3223, 3058, 2937, 1615, 1523, 1386, 744	Purity: 99.8 %, t_R = 3.52 min
196	6	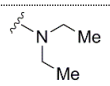	170-172 °C	3443, 3333, 3060, 2929, 1614, 1557, 1374, 747	Purity: 99.5 %, t_R = 4.70 min
197	6	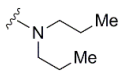	195-197 °C	3445, 3332, 3060, 2929, 1614, 1533, 1374, 747	Purity: 99.1 %, t_R = 9.72 min
198	6	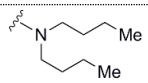	192-194 °C	3445, 3322, 3058, 2955, 1615, 1533, 1391, 747	Purity: 98.6 %, t_R = 8.67 min
199	6		177-179 °C	3442, 3330, 3058, 2930, 1614, 1527, 1390, 743	Purity: 97.5 %, t_R = 4.35 min
200	6		178-180 °C	3445, 3322, 3058, 2955, 1615, 1534, 1391, 747	Purity: 97.1 %, t_R = 4.66 min
201	6		163-165 °C	3460, 3334, 3057, 2931, 1614, 1535, 1392, 748	Purity: 98.9 %, t_R = 3.70 min
202	6	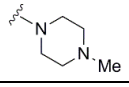	160-162 °C	3460, 3336, 3056, 2928, 1614, 1534, 1391,747	Purity: 99.1 %, t_R = 3.26 min

The ^{1}H-NMR spectrum of compound (**179**) showed a broad singlet at δ 11.75 for one NH proton (-NH_e) of the indole ring. A doublet at δ 8.08 for one proton (ArH_a), multiplet at δ 7.39-7.46 for two protons (Ar$H_{c,d}$), a multiplet at δ 7.23-7.27 for one proton (ArH_b) were observed confirming a total of four

aromatic protons in the structure. The protons at (-NHC$H_{2/g}$) and (-NC$H_{2/j}$) appeared as multiplets at δ 3.49-3.50 and 2.78-2.80, respectively. A singlet appeared at δ 2.56 accounting for six protons (-NC$H_{3/k}$). The protons at (-C$H_{2/h}$) and (-C$H_{2/i}$) of the aliphatic chain appeared as multiplets at δ 1.80-1.82 and 1.68-1.75, respectively. In ^{13}C-NMR spectrum, the aromatic carbons appeared at δ 155.9, 149.0, 139.6, 128.6, 122.1, 120.03, 119.6, 116.1 and 112.4 whereas the aliphatic carbons appeared at δ 56.9, 46.1, 42.6, 26.3 and 26.2. Its mass spectrum showed $[M+H]^+$ ion peak at 285.1 m/z.

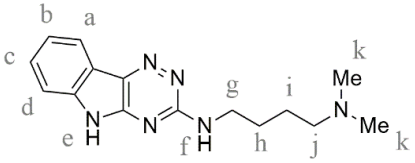

(**179**)

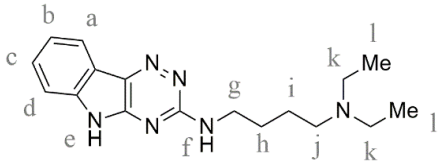

(**180**)

The ^{1}H-NMR spectrum of compound (**180**) showed a doublet at δ 8.24 for one proton (ArH_a), a multiplet at δ 7.44-7.48 for one proton (ArH_c), a doublet at δ 7.36 for one proton (ArH_d) and a multiplet at δ 7.29-7.33 for one proton (ArH_b) confirming a total of four aromatic protons in the structure. A broad singlet appeared at δ 6.04 accounting for one NH proton (-NH_f). It showed a multiplet at δ 3.50-3.55 for two protons (-NHC$H_{2/g}$), a multiplet at δ 2.42-2.51 for six protons (-NC$H_{2/j,k}$), a multiplet at δ 1.54-1.74 for four protons (-C$H_{2/h,i}$) whereas a triplet at δ 1.04 accounting for six protons (-NCH$_2$C$H_{3/l}$) for the methyl group. Its mass spectrum exhibited $[M+H]^+$ ion peak at 313.3 m/z.

The ^{1}H-NMR spectrum of compound (**181**) showed a broad singlet at δ 11.72 for one NH proton (-NH_e) of the indole ring. A doublet at δ 8.06 for one proton (ArH_a), multiplets at δ 7.36-7.44 for two protons (Ar$H_{c,d}$) and a multiplet at δ 7.22-7.26 for one proton (ArH_b) confirmed a total of four aromatic protons in the structure. Multiplets appeared at δ 3.36-3.38 accounting for two protons (-NHC$H_{2/g}$), at δ 2.38-2.41 accounting for two protons (-NC$H_{2/j}$) and at δ 2.30-2.33 accounting for four protons (-NC$H_{2/k}$). The methylene protons (-C$H_{2/h}$), (-C$H_{2/i}$) and (-C$H_{2/l}$) appeared as multiplets at δ 1.62-1.66, δ 1.48-1.51 and δ 1.37-1.42, respectively. A triplet was observed at δ 0.84 for six protons (-C$H3/_m$). In ^{13}C-NMR spectrum, the aromatic carbons appeared at δ 155.8, 149.1, 139.5, 128.5, 121.9, 119.9, 119.7, 116.2 and 112.3 whereas the aliphatic

carbons appeared at δ 56.0, 53.8, 41.1, 27.3, 24.8, 20.0 and 12.3. Its mass spectrum showed $[M+H]^+$ ion peak at 341.1 m/z.

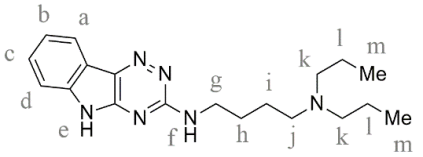

(**181**)

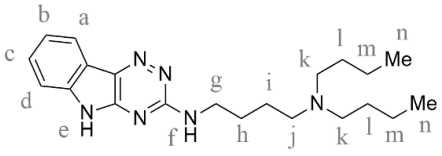

(**182**)

The ^{1}H-NMR spectrum of compound (**182**) showed a broad singlet at δ 9.53 for one NH proton (-NH_e) of the indole ring. A doublet at δ 8.25 for one proton (ArH_a), a multiplet at δ 7.44-7.48 for one proton (ArH_c), a doublet at 7.38 for one proton (ArH_d) and a multiplet at 7.29-7.33 for one proton (ArH_b) confirmed a total of four aromatic protons in the structures. A broad singlet appeared at δ 5.89 for one NH proton (-NH_f). Multiplets appeared at δ 3.50-3.55 for two protons (-NHC$H_{2/g}$), at δ 2.50-2.54 accounting for two protons (-NC$H_{2/j}$) and at δ 2.40-2.48 accounting for four protons (-NC$H_{2/k}$). It showed multiplet at δ 1.66-1.73 for two protons (-NHCH$_2$C$H_{2/h}$), multiplet at δ1.56-1.63 for two protons (-C$H_{2/i}$), multiplet at δ 1.39-1.47 for four protons (-NCH$_2$C$H_{2/l}$) and multiplet at δ 1.23-1.32 for four protons (-C$H_{2/m}$CH$_3$) of the aliphatic chain. A triplet appeared at δ 0.89 for six protons (-C$H_{3/m}$). In ^{13}C-NMR spectrum, the aromatic carbons appeared at δ 155.9, 149.1, 139.5, 128.4, 121.9, 119.9, 119.7, 116.2 and 112.3 whereas the aliphatic carbons appeared at δ 53.6, 53.8, 41.1, 29.4, 27.3, 24.8, 20.5 and 14.3. Its mass spectrum showed $[M+H]^+$ ion peak at 369.2 m/z.

The ^{1}H-NMR spectrum of compound (**183**) showed a doublet at δ 8.06 for one proton (ArH_d), multiplet at δ 7.36-7.44 for two protons (Ar$H_{c,d}$) and a multiplet at δ 7.22-7.26 for one proton (ArH_b) confirming a total of four aromatic protons in the structure. It showed multiplets at δ 3.34-3.41 for two protons (-NHC$H_{2/g}$), at δ 2.43-2.47 for six protons (-NC$H_{2/j,k}$), at δ 1.64-1.71 for six protons (-NCH$_2$C$H_{2/i,l}$) and at δ 1.54-1.59 for two protons (-C$H_{2/h}$). Its mass spectrum showed $[M+H]^+$ ion peak at 311.1 m/z.

The ^{1}H-NMR spectrum of compound (**184**) showed a broad singlet at δ 11.74 for one NH proton (-NH_e) of the indole ring. A doublet at δ 8.06 for one proton (ArH_d), multiplet at 7.35-7.44 for two protons (Ar$H_{c,d}$) and a multiplet at δ 7.22-7.26 for one proton (ArH_b) confirmed a total of four aromatic protons in

the structure. It showed multiplets at δ 3.40-3.41 for two protons (-NHC$H_{2/g}$), at δ 2.25-2.32 for six protons (-NC$H_{2/j,k}$), at δ 1.59-1.66 for two protons (-C$H_{2/h}$), at δ 1.49-1.58 for six protons (-NCH$_2$C$H_{2/i,l}$) and at δ 1.39-1.40 for two protons (-C$H_{2/m}$). In ^{13}C-NMR spectrum, the aromatic carbons appeared at δ 155.78, 149.05, 139.54, 128.44, 121.9, 119.9, 119.7, 116.1 and 112.3 whereas the aliphatic carbons appeared at δ 58.8, 54.5, 41.2, 27.4, 26.0, 24.7 and 24.4. Its mass spectrum showed $[M+H]^+$ ion peak at 325.5 m/z.

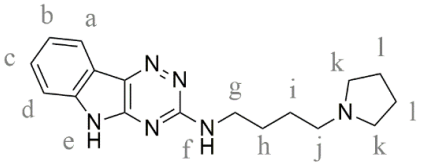

(**183**)

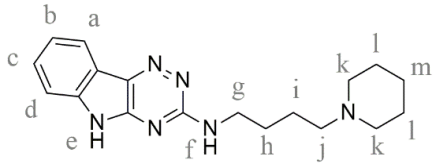

(**184**)

The ^{1}H-NMR spectrum of compound (**185**) showed a broad singlet at δ 11.63 for one NH proton (-NH_e) of the indole ring. A doublet at δ 8.07 for one proton (ArH_a), multiplet at δ 7.36-7.44 for two protons (Ar$H_{c,d}$) and a multiplet at δ 7.22-7.26 for one proton (ArH_b) confirmed a total of four aromatic protons in the structure. It showed multiplets at δ 3.62-3.64 for four protons (-OC$H_{2/l}$), at δ 3.44-3.46 for two protons (-NHC$H_{2/g}$), at δ 2.32-2.39 for six protons (-NC$H_{2/j,k}$), at δ 1.62-1.71 for two protons (-C$H_{2/h}$), at δ 1.54-1.60 for two protons (-NCH$_2$C$H_{2/i}$). In ^{13}C-NMR spectrum, the aromatic carbons appeared at δ 155.8, 149.1, 139.5, 128.5, 121.9, 119.9, 119.7, 116.2 and 112.3 whereas the aliphatic carbons appeared at δ 66.7, 58.5, 53.8, 41.1, 27.2 and 24.0. Its mass spectrum showed $[M+H]^+$ ion peak at 327.3 m/z.

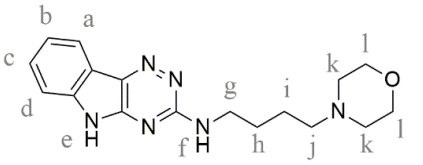

(**185**)

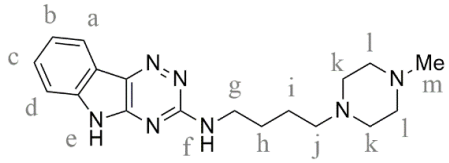

(**186**)

The ^{1}H-NMR spectrum of compound (**186**) showed a broad singlet at δ 11.68 for NH proton (NH_e) of the indole ring. A doublet at δ 8.03 for one proton (ArH_a), multiplet at δ 7.32-7.41 for two protons (Ar$H_{c,d}$) and a multiplet at δ 7.19-7.23 for one proton (ArH_b) confirmed a total of four aromatic protons in the structure. It showed multiplets at δ 3.38-3.39 for two protons (-NHC$H_{2/g}$), at δ 2.27-2.31 for ten protons (-NC$H_{2/j,k,l}$), at δ 1.59-1.64 for two protons

(-C$H_{2/h}$), at δ 1.48-1.55 for two protons (-NCH$_2$C$H_{2/i}$). A singlet appeared at δ 2.15 for three protons (-NC$H_{3/m}$) of the methyl group. In ^{13}C-NMR spectrum, aromatic carbons appeared at δ 155.9, 149.1, 139.6, 128.5, 121.9, 119.9, 119.7, 116.2 and 112.3 whereas the aliphatic carbons appeared at δ 58.0, 55.2, 53.2, 46.2, 41.2, 27.2 and 24.4. Its mass spectrum showed $[M+H]^+$ ion peak at 340.3 m/z.

The ^{1}H-NMR spectrum of compound (**187**) showed a multiplet at δ 8.05-8.10 for one proton (ArH_a), multiplet at δ 7.35-7.44 for two protons (Ar$H_{c,d}$) and a multiplet at δ 7.21-7.26 for one proton (ArH_b) confirming a total of four aromatic protons in the structure. It showed multiplet at δ 3.30-3.35 for two protons (-NHC$H_{2/g}$), triplet at δ 2.20 for two protons (-NC$H_{2/k}$), multiplet at δ 1.60-1.68 for two protons (-C$H_{2/h}$), multiplet at δ 1.34-1.46 for four protons (-C$H_{2/i,j}$). A singlet appeared at δ 2.14 for six protons (-NC$H_{3/l}$). In ^{13}C-NMR spectrum, the aromatic carbons appeared at δ 155.9, 149.0, 139.5, 128.4, 121.9, 119.9, 119.7, 116.2 and 112.3 whereas the aliphatic carbons appeared at δ 59.6, 45.7, 41.2, 29.2, 27.4 and 24.9. Its mass spectrum showed $[M+H]^+$ ion peak at 299.3 m/z.

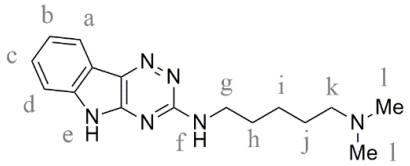

(**187**)

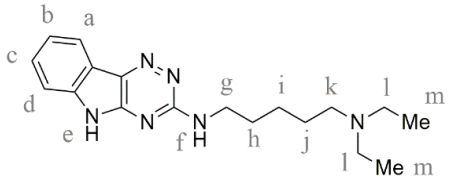

(**188**)

The ^{1}H-NMR spectrum of compound (**188**) showed a broad singlet at δ 11.62 for NH proton (-NH_e) of the indole ring. A multiplet at δ 8.03-8.06 for one proton (ArH_a), multiplet at δ 7.32-7.37 for two proton (Ar$H_{c,d}$) and a multiplet at δ 7.19-7.23 for one proton (ArH_b) confirmed a total of four aromatic protons in the structure. It showed a multiplet at δ 3.29-3.36 for two protons (-NHC$H_{2/g}$), a multiplet at δ 2.39-2.44 for four protons (-NC$H_{2/l}$), a triplet at δ 2.34 for two protons (-NC$H_{2/k}$), a multiplet at δ 1.57-1.63 for two protons (-C$H_{2/h}$), a multiplet at δ 1.30-1.41 for four protons (-C$H_{2/i,j}$). A triplet appeared at δ 0.92 for six protons (-C$H_{3/m}$). In ^{13}C-NMR spectrum, the aromatic carbons appeared at δ 155.9, 149.0, 139.5, 128.4, 121.9, 119.9, 119.7, 116.2 and 112.3 whereas the aliphatic carbons appeared at δ 52.7, 46.7, 41.2, 29.3, 26.9, 24.9 and 12.2. Its mass spectrum showed $[M+H]^+$ ion peak at 327.1 m/z.

The ^{1}H-NMR spectrum of compound (**189**) showed a doublet at δ 8.25 for one proton (ArH_a), a multiplet at δ 7.45-7.49 for one proton (ArH_c), a doublet at δ 7.37 for one proton (ArH_d) and a multiplet at δ 7.30-7.33 for one proton (ArH_b) confirming a total of four aromatic protons. A broad singlet appeared at δ 5.54 accounting for NH proton (-NH_f). It showed multiplets at δ 3.49-3.54 for two protons (-NHC$H_{2/g}$), at δ 2.38-2.47 for six protons (-NC$H_{2/k,l}$), at δ 1.66-1.71 for two protons (-C$H_{2/h}$), at δ 1.39-1.55 for eight protons (-NCH$_2$C$H_{2/i,j,m}$). A triplet appeared at δ 0.86 for six protons (-C$H_{3/n}$). In ^{13}C-NMR spectrum, the aromatic carbons appeared at δ 155.9, 149.1, 139.6, 128.4, 121.9, 119.9, 119.7, 116.2 and 112.3 whereas the aliphatic carbons appeared at δ 56.1, 53.9, 41.1, 29.2, 27.1, 24.9, 20.4 and 12.2. Its mass spectrum showed $[M+H]^+$ ion peak at 355.1 m/z.

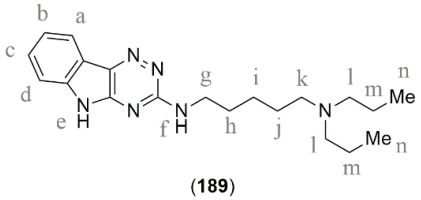

(**189**)

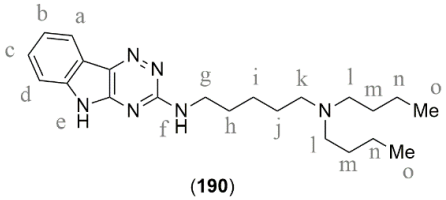

(**190**)

^{1}H-NMR spectrum of compound (**190**) showed a doublet at δ 8.18 for one proton (ArH_a), a multiplet at δ 7.37-7.41 for one proton (ArH_c), a doublet at δ 7.30 for one proton (ArH_d) and a multiplet at δ 7.22-7.25 for one proton (ArH_b) confirming a total of four aromatic protons in the structure. A broad singlet appeared at δ 5.54 for one NH proton (-NH_f). It showed multiplets at δ 3.36-3.40 for two protons (-NHC$H_{2/g}$), at δ 2.36-2.42 for six protons (-NC$H_{2/k,l}$), at δ 1.54-1.65 for two protons (-C$H_{2/h}$), at δ 1.42-1.50 for two protons (-C$H_{2/i}$), at δ 1.31-1.39 for six protons (-NCH$_2$C$H_{2/j,m}$) and at δ 1.16-1.25 for four protons (-C$H_{2/n}$). A triplet appeared at δ 0.82 for six protons (-C$H_{3/o}$). In ^{13}C-NMR spectrum, the aromatic carbons appeared at δ 155.8, 149.0, 139.5, 128.4, 121.9, 119.9, 119.7, 116.1 and 112.3 whereas the aliphatic carbons appeared at δ 53.9, 53.6, 41.2, 29.4, 29.2, 27.0, 24.9, 20.5 and 14.4. Its mass spectrum showed $[M+H]^+$ ion peak at 383.2 m/z.

The ^{1}H-NMR spectrum of compound (**191**) showed a broad singlet at δ 11.66 for amine proton (-NH_e) of the indole ring. A multiplet at δ 8.02-8.06 for one proton (ArH_a), multiplet at δ 7.32-7.40 for two protons (Ar$H_{c,d}$) and a multiplet at δ 7.18-7.22 for one proton (ArH_b) confirmed a total of four aromatic

protons in the structure. It showed multiplets at δ 3.37-3.38 for two protons (-NHC$H_{2/g}$), at δ 2.34-2.40 for six protons (-NC$H_{2/k,l}$), at δ 1.57-1.68 for six protons (-NCH$_2$C$H_{2/j,m}$), at δ 1.45-1.52 for two protons (-C$H_{2/h}$) and at 1.33-1.41 for two protons (-C$H_{2/i}$). In ^{13}C-NMR spectrum, the aromatic carbons appeared at δ 155.8, 149.1, 139.5, 128.5, 121.9, 119.7, 119.6, 116.2 and 112.2 whereas the aliphatic carbons appeared at δ 55.2, 54.1, 41.1, 29.3, 28.7, 25.0 and 23.5. Its mass spectrum showed $[M+H]^+$ ion peak at 325.4 m/z.

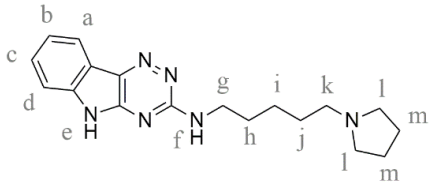

(**191**)

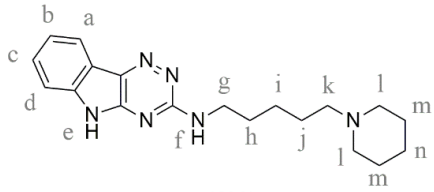

(**192**)

The ^{1}H-NMR spectrum of compound (**192**) showed a broad singlet at δ 11.58 for one NH proton (-NH_e) of the indole ring. A doublet at δ 8.04 for one proton (ArH_a), a multiplet at δ 7.39-7.43 for one proton (ArH_c), a doublet at δ 7.41 for one proton (ArH_d) and a multiplet at δ 7.21-7.24 for one proton (ArH_b) confirmed a total of four aromatic protons. It showed multiplets at δ 3.40-3.41 for two protons (-NHC$H_{2/g}$), at δ 2.18-2.27 for six protons (-NC$H_{2/k,l}$), at δ 1.59-1.64 for two protons (-C$H_{2/h}$), at δ 1.41-1.49 for six protons (-NCH$_2$C$H_{2/j,m}$) and at δ 1.34-1.37 for four protons (-C$H_{2/i,n}$). In ^{13}C-NMR spectrum, the aromatic carbons appeared at δ 155.9, 149.1, 139.6, 128.5, 121.9, 119.9, 119.7, 116.2 and 112.3 whereas aliphatic carbons appeared at δ 59.2, 54.6, 41.2, 29.3, 26.7, 26.1, 25.0 and 24.7. Its mass spectrum showed $[M+H]^+$ ion peak at 339.3 m/z.

The ^{1}H-NMR spectrum of compound (**193**) showed a broad singlet at δ 11.41 for NH proton (NH_e) of the indole ring. A doublet at δ 8.03 for one proton (ArH_a), multiplet at δ 7.32-7.40 for two protons (Ar$H_{c,d}$) and a multiplet at δ 7.18-7.22 for one proton (ArH_b) confirming a total of four aromatic protons. It showed multiplets at δ 3.54-3.56 for two protons (-OC$H_{2/m}$), at δ 3.37-3.39 for two protons (-NHC$H_{2/g}$), at δ 2.29-2.33 for four protons (-NC$H_{2/l}$), at δ 2.23-2.27 for two protons (-NC$H_{2/k}$), at δ 1.58-1.65 for two protons (-C$H_{2/h}$), at δ 1.43-1.50 for two protons (-NCH$_2$C$H_{2/i}$) and δ 1.32-1.40 for two protons (-C$H_{2/j}$). In ^{13}C-NMR spectrum, the aromatic carbons appeared at δ 155.8, 149.1, 139.5, 128.4, 122.0, 119.9, 119.7, 116.1 and 112.3 whereas the aliphatic

carbons appeared at δ 66.7, 58.8, 53.9, 41.1, 29.2, 26.2 and 24.9. Its mass spectrum showed $[M+H]^+$ ion peak at 341.1 m/z.

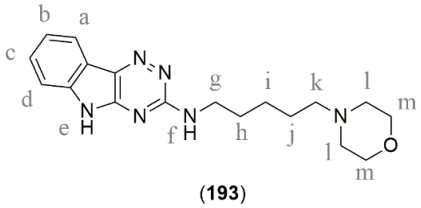

(**193**)

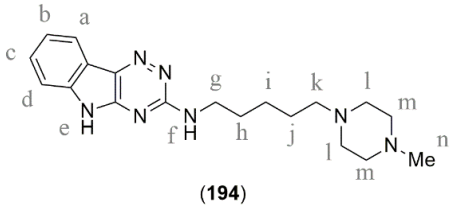

(**194**)

The ^{1}H-NMR spectrum of compound (**194**) showed a broad singlet at δ 9.76 for one NH proton (-NH_e) of the indole ring. A doublet at δ 8.25 for one proton (ArH_a), multiplet at δ 7.44-7.49 for two protons (Ar$H_{c,d}$) and a multiplet at δ 7.31-7.37 for one proton (ArH_b) confirmed a total of four aromatic protons in the structure. A broad singlet appeared at δ 5.57 for one NH proton (-NH_f). It showed multiplets at δ 3.47-3.53 for two protons (-NHC$H_{2/g}$), at δ 2.42-2.60 for six protons (-NC$H_{2/k,l}$), a triplet at δ 2.37 for two protons (-NC$H_{2/m}$), multiplets at δ 1.65-1.72 for two protons (-C$H_{2/h}$), at δ 1.53-1.62 for two protons (-NCH$_2$C$H_{2/i}$) and δ 1.37-1.46 for two protons (-C$H_{2/j}$). A singlet appeared at δ 2.29 for three protons (-NC$H_{3/n}$) of the methyl group. In ^{13}C-NMR spectrum, the aromatic carbons appeared at δ 155.6, 149.1, 139.7, 128.5, 121.9, 119.9, 119.3, 116.2 and 112.3 whereas aliphatic carbons appeared at δ 58.4, 55.2, 53.2, 46.2, 41.1, 29.2, 26.6 and 24.9. Its mass spectrum showed $[M+H]^+$ ion peak at 354.3 m/z.

The ^{1}H-NMR spectrum of compound (**195**) showed a broad singlet at δ 11.76 for one NH proton (-NH_e) of the indole ring. A doublet at δ 8.06 for one proton (ArH_a), multiplet at δ 7.36-7.43 for two protons (Ar$H_{c,d}$) and a multiplet at δ 7.25-7.27 for one proton (ArH_b) confirming a total of four aromatic protons. It showed a multiplet at δ 3.32-3.39 for two protons (-NHC$H_{2/g}$), a triplet at δ 2.19 for two protons (-NC$H_{2/l}$), a multiplet at δ 1.61-1.63 for two protons (-C$H_{2/h}$), a multiplet at δ 1.32-1.44 for six protons (-C$H_{2/i,j,k}$). A singlet appeared at δ 2.12 for six protons (-NC$H_{3/m}$). In ^{13}C-NMR spectrum, the aromatic carbons appeared at δ 155.7, 149.1, 139.5, 128.4, 121.9, 119.9, 119.7, 116.1 and 112.3 whereas the aliphatic carbons appeared at δ 59.6, 45.6, 41.1, 29.3, 27.5, 27.1 and 26.9. Its mass spectrum showed $[M+H]^+$ ion peak at 313.1 m/z.

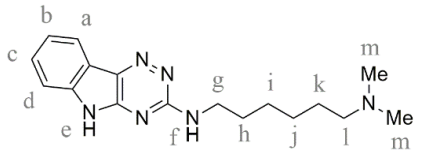

(**195**)

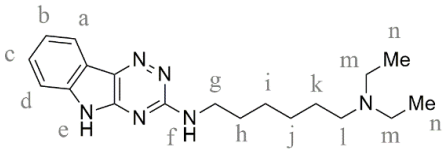

(**196**)

The ^{1}H-NMR spectrum of compound (**196**) showed a doublet at δ 8.25 for one proton (ArH_a), a multiplet at δ 7.44-7.47 for one proton (ArH_c), a doublet at δ 7.41 for one proton (ArH_d) and a multiplet at δ 7.35-7.37 for one proton (ArH_b) confirming a total of four aromatic protons in the structure. A broad singlet appeared at δ 5.75 for one NH proton (-NH_f). It showed a multiplet at δ 3.43-3.50 for two protons (-NHC$H_{2/g}$), a multiplet at δ 2.59-2.65 four protons (-NC$H_{2/m}$), a multiplet at δ 2.48-2.52 for two protons (-NC$H_{2/l}$), a multiplet at δ 1.60-1.71 for four protons (-C$H_{2/h,i}$), a multiplet at δ 1.37-1.46 for four protons (-C$H_{2/j,k}$). A triplet appeared at δ 1.06 for six protons (-C$H_{3/n}$). In ^{13}C-NMR spectrum, the aromatic carbons appeared at δ 155.9, 149.1, 139.6, 128.4, 121.9, 119.9, 119.7, 116.2 and 112.3 whereas the aliphatic carbons appeared at δ 52.6, 46.7, 41.2, 29.3, 27.3, 27.2, 26.9 and 12.0. Its mass spectrum showed $[M+H]^+$ ion peak at 341.1 m/z.

The ^{1}H-NMR spectrum of compound (**197**) showed a broad singlet at δ 11.67 for one NH proton (-NH_e) of the indole ring. A doublet at δ 8.03 for one proton (ArH_a), a multiplet at δ 7.38-7.40 for one proton (ArH_c), a multiplet at δ 7.33-7.35 for one proton (ArH_d) and a multiplet at δ 7.20-7.24 for one proton (ArH_b) confirmed a total of four aromatic protons in the structure. It showed multiplets at δ 3.31-3.33 for two protons (-NHC$H_{2/g}$), at δ 2.24-2.32 for six protons (-NC$H_{2/l,m}$), at δ 1.58-1.62 for two protons (-C$H_{2/h}$), at δ 1.29-1.39 for ten protons (-NCH$_2$C$H_{2/i,j,k,n}$). A triplet appeared at δ 0.80 for six protons (-C$H_{3/n}$). In ^{13}C-NMR spectrum, the aromatic carbons appeared at δ 155.8, 149.1, 139.6, 128.5, 121.9, 119.9, 119.7, 116.2 and 112.3 whereas the aliphatic carbons appeared at δ 56.1, 53.9, 41.1, 29.3, 27.2, 27.1, 26.9, 20.4 and 12.3. Its mass spectrum showed $[M+H]^+$ ion peak at 369.1 m/z.

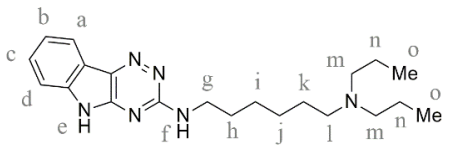

(**197**)

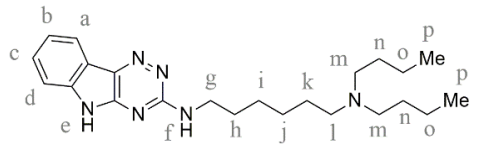

(**198**)

The ^{1}H-NMR spectrum of compound (**198**) showed a broad singlet at δ 11.74 for one NH proton (-NH_e) of the indole ring. A multiplet at δ 8.07-8.09 for one proton (ArH_a), multiplet at δ 7.24-7.40 for three protons (Ar$H_{b,c,d}$) confirmed a total of four aromatic protons. A broad singlet appeared at δ 5.54 for NH proton (-NH_f). It showed multiplets at δ 3.40-3.42 for two protons (-NHC$H_{2/g}$), at δ 2.33-2.54 for six protons (-NC$H_{2/l,m}$), at δ 1.58-1.68 for two protons (-C$H_{2/h}$), at δ 1.24-1.44 for fourteen protons (-C$H_{2/i,j,k,n,o}$). A triplet appeared at δ 0.87 for six protons (-C$H_{3/p}$). In ^{13}C-NMR spectrum, the aromatic carbons appeared at δ 155.8, 149.1, 139.6, 128.4, 121.9, 119.9, 119.7, 116.1 and 112.3 whereas the aliphatic carbons appeared at δ 53.9, 53.6, 41.2, 29.4, 29.3, 27.2, 26.9, 26.0, 20.5 and 14.4. Its mass spectrum showed $[M+H]^+$ ion peak at 397.2 m/z.

The ^{1}H-NMR spectrum of compound (**199**) showed a broad singlet at δ 11.66 for one NH proton (-NH_e) of the indole ring. A doublet at δ 8.02 for one proton (ArH_a), multiplet at δ 7.31-7.39 for two protons (Ar$H_{c,d}$) and a multiplet at δ 7.17-7.21 for one proton (ArH_b) confirmed a total of four aromatic protons. It showed multiplets at δ 3.35-3.37 for two protons (-NHC$H_{2/g}$), at δ 2.32-2.38 for six protons (-NC$H_{2/l,m}$), at δ 1.57-1.66 for six protons (-NCH$_2$C$H_{2/k,n}$), at δ 1.40-1.45 for two protons (-C$H_{2/h}$) and at δ 1.33-1.41 for four protons (-C$H_{2/i,j}$). In ^{13}C-NMR spectrum, the aromatic carbons appeared at δ 155.8, 149.0, 139.6, 128.5, 121.9, 119.9, 119.7, 116.1 and 112.3 whereas the aliphatic carbons appeared at δ 56.2, 54.1, 41.2, 29.3, 28.9, 27.4, 26.9 and 23.5. Its mass spectrum showed $[M+H]^+$ ion peak at 339.1 m/z.

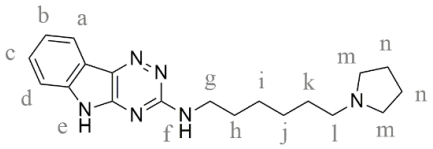

(**199**)

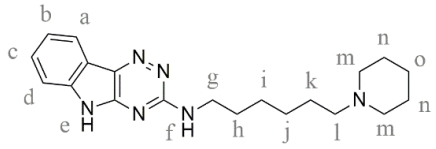

(**200**)

The ^{1}H-NMR spectrum of compound (**200**) showed a broad singlet at δ 11.68 for one NH proton (-NH_e) of the indole ring. A doublet at δ 8.07 for one proton (ArH_a), multiplet at δ 7.35-7.44 for two protons (Ar$H_{c,d}$) and a multiplet at δ 7.22-7.26 for one proton (ArH_b) confirmed a total of four aromatic protons. It showed multiplets at δ 3.32-3.42 for two protons (-NHC$H_{2/g}$), at δ 2.21-2.31 for six protons (-NC$H_{2/l,m}$), at δ 1.61-1.68 for two protons (-C$H_{2/h}$), at δ 1.48-

1.52 for six protons (-NCH$_2$C$H_{2/k,n}$) and at δ 1.34-1.37 for six protons (-C$H_{2/i,j,o}$). In ^{13}C-NMR spectrum, the aromatic carbons appeared at δ 155.8, 149.0, 139.5, 128.4, 121.9, 119.9, 119.7, 116.1 and 112.3, whereas the aliphatic carbons appeared at δ 59.1, 54.6, 41.1, 29.3, 27.3, 26.9, 26.8, 26.1 and 24.7. Its mass spectrum showed $[M+H]^+$ ion peak at 353.1 m/z.

The ^{1}H-NMR spectrum of compound (**201**) showed a broad singlet at δ 9.20 for NH proton (-NH_e) of the indole ring. A doublet at δ 8.26 for one proton (ArH_a), a multiplet at δ 7.46-7.50 for one proton (ArH_c), a multiplet at δ 7.38-7.41 for one proton (ArH_d), and a multiplet at δ 7.30-7.34 for one proton (ArH_b) confirmed a total of four aromatic protons in the structure. It showed multiplets at δ 3.72-3.74 for four protons (-OC$H_{2/n}$), at δ 3.48-3.53 for two protons (-NHC$H_{2/g}$), at δ 2.44-2.48 for four protons (-NC$H_{2/m}$), at δ 2.33-2.36 for two protons (-NC$H_{2/l}$), at δ 1.64-1.70 for two protons (-C$H_{2/h}$), at δ 1.49-1.54 for two protons (-C$H_{2/i}$) and δ 1.36-1.45 for four protons (C$H_{2/j,k}$). In ^{13}C-NMR spectrum, the aromatic carbons appeared at δ 155.9, 149.1, 139.6, 128.5, 121.9, 119.9, 119.7, 116.2 and 112.3 whereas the aliphatic carbons appeared at δ 66.6, 58.7, 53.8, 41.1, 29.3, 27.1, 26.9 and 26.8. Its mass spectrum showed $[M+H]^+$ ion peak at 355.5 m/z.

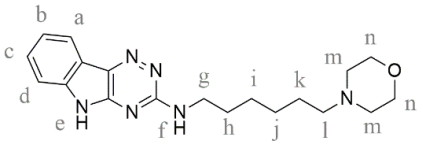

(**201**)

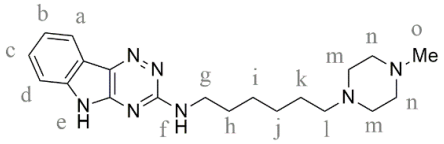

(**202**)

The ^{1}H-NMR spectrum of compound (**202**) showed a broad singlet at δ 11.71 for one NH proton (-N*H*e) of the indole ring. A doublet at δ 8.03 for one proton (ArH_a), multiplet at δ 7.33-7.41 for two protons (Ar$H_{c,d}$) and a multiplet at δ 7.19-7.23 for one proton (ArH_b) confirmed a total of four aromatic protons in the structure. It showed multiplets at δ 3.34-3.36 for two protons (-NHC$H_{2/g}$), at δ 2.28-2.32 for six protons (-NC$H_{2/l,m}$), at δ 2.20-2.24 for two protons (-NC$H_{2/n}$), at δ 1.56-1.62 for two protons (-C$H_{2/h}$), at δ 1.29-1.42 for six protons (-C$H_{2/i,j,k}$). A singlet appeared at δ 2.13 for three protons (-NC$H_{3/n}$) of the methyl group. In ^{13}C-NMR spectrum, the aromatic carbons appeared at δ 155.1, 149.1, 139.6, 128.5, 121.9, 119.9, 119.7, 116.4 and 112.3 whereas the aliphatic carbons

appeared at δ 58.3, 55.2, 53.2, 46.2, 41.1, 29.3, 27.2, 26.9 and 26.8. Its mass spectrum showed $[M+H]^+$ ion peak at 368.1 m/z.

4.1.1.3. Biological evaluation of the synthesized compounds

The synthesized triazinoindole derivatives (**71-80, 117-126** and **179-202**) (Series III and IV in **Figure 4.1**) were evaluated for their multifactorial anti-AD activities, including cholinesterase inhibitory activity, antioxidant activity, cytoprotective effect against H_2O_2/Aβ-induced cell injury, cognition improving activity and acute toxicity in animal models detailed under the following subheadings:

4.1.1.3.1. Inhibition studies on cholinesterase enzymes,

4.1.1.3.2. Antioxidant activity [1,1-diphenyl-2-picrylhydrazyl (DPPH) radical scavenging activity],

4.1.1.3.3. Assessment of cytotoxicity and neuroprotection offered by the synthesized compounds,

4.1.1.3.4. *In vitro* blood-brain barrier permeation assay,

4.1.1.3.5. Assessment of cognitive improvement in animal model of AD, using:

4.1.1.3.5.1. Morris Water Maze test,

4.1.1.3.5.2. Neurochemical analysis,

4.1.1.3.5.3. Y-Maze test,

4.1.1.3.6. Acute toxicity study.

4.1.1.3.1. Inhibition studies on cholinesterase enzymes

The potential of the synthesized compounds to inhibit cholinesterases (ChEs) was evaluated *in vitro* using a spectrophotometric method of Ellman *et. al.* using donepezil and tacrine as reference drugs.[115-117] The obtained IC_{50} values of the compounds for the two enzymes and their selectivity over each other were summarized in **Tables 4.8-4.10**. All the tested compounds showed IC_{50} values for both the enzymes in micromolar to submicromolar ranges. Amongst them, compounds (**199** and **200**) exhibited the highest AChE (IC_{50} values of 0.56 μM and 0.67 μM, respectively) and BuChE (IC_{50} values of 1.17 μM and 0.84 μM, respectively) inhibitory activities.

To validate our design rationale, initially compound (**68**) was prepared and evaluated for its cholinesterase inhibitory potential. To our delight, compound (**68**) exhibited good inhibitory activity (AChE, IC_{50} value of 11.26 µM; BuChE, IC_{50} value of 55.81 µM). This encouraging result of the lead scaffold prompted us to explore various substituents on thiol sulphur and on the nitrogen of the indole ring to frame a structure-activity relationship.

Table 4.8. *In vitro* inhibition of AChE, BuChE and selectivity index (SI) of compounds (71-80)

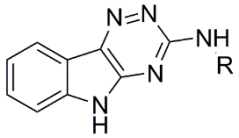

(71-80)

Compd	R	IC_{50} ± SEM (µM)		S.I.
		AChE[a]	BuChE[b]	
71	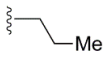	11.07 ± 0.86	52.19 ± 2.01	4.71
72	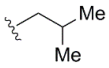	9.21 ± 0.54	61.23 ± 1.12	6.64
73	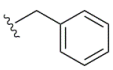	8.06 ± 0.75	56.41 ± 1.65	6.99
74	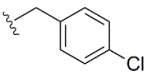	41.22 ± 1.83	9.09 ± 0.65	0.22
75	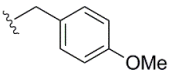	36.63 ± 1.22	67.32 ± 1.32	1.84
76	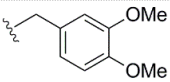	10.75 ± 0.62	13.12 ± 1.02	1.22
77	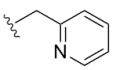	14.71 ± 1.37	26.08 ± 1.21	1.77
78	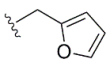	20.22 ± 1.21	33.02 ± 1.65	1.63
79	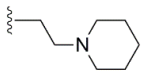	6.16 ± 0.53	20.53 ± 2.01	3.33
80	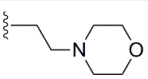	6.61 ± 0.69	9.14 ± 0.54	1.38

[a]AChE from human erythrocytes; IC_{50}, 50% inhibitory concentration (means ± SEM of three experiments), [b]BuChE from equine serum, [c]Selectivity Index = IC_{50} (BuChE)/IC_{50} (AChE).

The 3-substituted thio-5*H*-[1,2,4]triazino[5,6-*b*]indole derivatives (Series I, **Figure 4.1**) were reported to have IC_{50} values in the range of 9-16 µM for AChE. The inhibitory activity was retained as such when thiol group was replaced with amino group in compounds (**71-80**) as shown in **Table 4.8**.

When the *N*-propyl moiety in compound (**71**) was replaced with 2-(1-piperidinyl)ethyl (compound **79**) and 2-(4-morpholinyl)ethyl (compound **80**) moieties, inhibitory activities against both the enzymes got increased notably. Compounds (**79** and **80**) showed inhibitory activities (AChE; IC_{50}values of 6.16 µM and 6.61 µM, respectively) and (BuChE; IC_{50} values of 20.53 µM and 9.14 µM, respectively).

The 5-substituted 5*H*-[1,2,4]triazino[5,6-*b*]indole-3-thiol derivatives (Series II, **Figure 4.1**) were reported to have IC_{50} values in the range of 5-15 µM for AChE.[118] The inhibitory activity was moderately reduced when thiol group was replaced with amino group in compounds (**117-126**) as shown in **Table 4.9**.

Table 4.9. *In vitro* inhibition of AChE, BuChE and selectivity index (SI) of compounds (117-126)

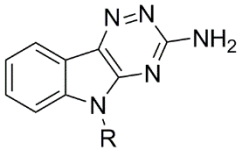

(117-126)

Compd	R	IC_{50} ± SEM (µM)		SI
		AChE[a]	BuChE[b]	
117		7.81 ± 1.01	52.23 ± 1.76	6.69
118		8.13 ± 1.32	29.42 ± 1.21	3.62
119	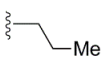	10.12 ± 1.16	32.78 ± 1.47	3.24
120	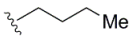	9.26 ± 0.82	16.02 ± 1.10	1.73
121	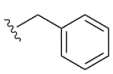	20.57 ± 1.34	24.87 ± 1.38	1.21
122	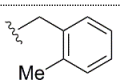	17.23 ± 1.22	32.72 ± 1.32	1.90

Compd	R	IC_{50}± SEM (µM)		SI
		AChE[a]	BuChE[b]	
123	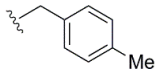	22.09 ± 1.78	22.64 ± 1.49	1.02
124	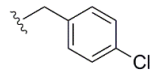	24.63 ± 2.01	29.45 ± 1.62	1.20
125	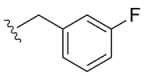	20.22 ± 1.25	25.32 ± 1.23	1.25
126		9.76 ± 1.25	51.25 ± 1.32	5.25

[a]AChE from human erythrocytes; IC_{50}, 50% inhibitory concentration (means ± SEM of three experiments), [b]BuChE from equine serum, [c] Selectivity Index = IC_{50} (BuChE)/IC_{50} (AChE).

Joining of the tricyclic triazinoindole moiety with cyclic amines like piperidine and morpholine through two carbon atom spacers improved AChE inhibition dramatically compared to the simple alkyl/benzyl substituted triazinoindole derivatives. Based on this observation, we planned to study the effect of the attached basic amines and the length of the linker on the cholinesterase inhibitory activity of the resulting compounds (**Table 4.10**).

Table 4.10. *In vitro* inhibition of AChE, BuChE and selectivity index (SI) of compounds (179-202)

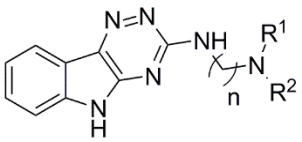

(179-202)

Compd	n	NR^1R^2	IC_{50} ± SEM (µM)		SI[c]
			AChE[a]	BuChE[b]	
179	4		33.70 ± 1.12	6.39 ± 0.22	0.19
180	4	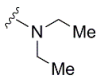	6.31 ± 0.43	11.09 ± 0.27	1.75
181	4	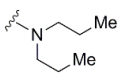	2.47 ± 0.11	8.05 ± 0.51	3.26
182	4	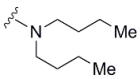	20.70 ± 0.76	0.47 ± 0.03	0.02
183	4		2.69 ± 0.08	5.89 ± 0.70	2.19

Compd	n	NR^1R^2	IC_{50}± SEM (µM)		SI[c]
			AChE[a]	BuChE[b]	
184	4		3.17 ± 0.10	18.01± 1.31	5.68
185	4		15.01 ± 0.54	1.92 ± 0.15	0.13
186	4	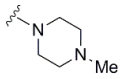	2.61 ± 0.07	32.19 ± 1.02	12.3
187	5		3.58 ± 0.28	23.24 ± 0.67	6.49
188	5	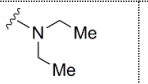	6.79 ± 0.22	0.34 ± 0.03	0.05
189	5	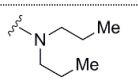	2.77 ± 0.07	0.48 ± 0.03	0.17
190	5	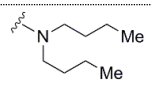	2.76 ± 0.18	0.38 ± 0.05	0.14
191	5		0.85 ± 0.05	17.01 ± 0.40	20.0
192	5		0.96 ± 0.04	2.77 ± 0.05	2.89
193	5		18.58 ± 0.41	6.74 ± 0.21	0.36
194	5	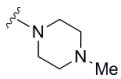	1.65 ± 0.11	29.19 ± 1.10	17.7
195	6		1.25 ± 0.09	4.43 ± 0.27	3.54
196	6	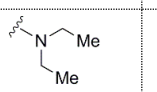	2.40 ± 0.11	12.70 ± 0.42	5.29
197	6	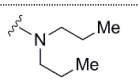	1.48 ± 0.08	3.43 ± 0.24	2.32
198	6	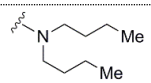	1.43 ± 0.07	4.01 ± 0.32	2.80
199	6		**0.56 ± 0.02**	**1.17 ± 0.09**	**2.09**
200	6		0.67 ± 0.02	0.84 ± 0.03	1.25
201	6		4.16 ± 0.15	23.65 ± 1.38	5.69
202	6	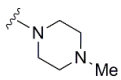	0.79 ± 0.04	3.92 ± 0.21	4.96

[a]AChE from human erythrocytes; IC_{50}, 50% inhibitory concentration (means ± SEM of three experiments), [b]BuChE from equine serum, [c] Selectivity Index = IC_{50} (BuChE)/IC_{50} (AChE).

As depicted in **Table 4.10**, all the compounds (**179-202**) exhibited good inhibitory activity against both the enzymes ranging from IC_{50}values of 0.564 to 36.7 μM for AChE and from 0.341 to 32.19 μM for BuChE. These results suggested that the presence of heterocyclic amines is particularly important for the ChE inhibitory activity as all the compounds bearing pyrrolidino, piperidino, morpholino and *N*-methylpiperazino moieties exhibited strong ChE inhibition. Pyrrolidino moiety appeared to be a better choice over other amines, as compounds (**183**, **191** and **199**) bearing pyrrolidino moiety exhibited higher activity than the rest of the compounds having other amines as attachments.

It has been observed that changing the length of the carbon chain also potentially affected the inhibitory activity. A comparative analysis of the inhibitory potential of compounds (**183**, **191** and **199)** having a pyrrolidine ring as heterocyclic amine revealed that compound (**199**, n = 6) exhibited the highest AChE inhibitory activity (IC_{50} value of 0.564 μM) while compound (**183**, n = 4) and compound (**191**, n = 5) showed 5-fold and 1.5-fold decrease in AChE inhibitory activities (IC_{50} values of 2.690 μM and 0.853 μM, respectively) in comparison to compound (**199**). However, their inhibitory activity against BuChE was slightly lower than that against AChE, which might be due to the conformational differences between the structures of these two enzymes.[119] Compound (**199**) exhibited an acceptable level of BuChE inhibitory activity (IC_{50} value of 1.178 μM) while compound (**183**) and compound (**191)** showed 5-fold and 14-fold decrease in BuChE inhibitory activities (IC_{50} values of 5.893 μM and 17.01 μM, respectively). Compounds (**199** and **200**) have more balanced activity on both the cholinesterase enzymes (SI values of 2.09 and 1.25, respectively) than donepezil (SI value of 81.3) and tacrine (SI value of 0.14).

4.1.1.3.2. Antioxidant activity [1,1-diphenyl-2-picrylhydrazyl (DPPH) radical scavenging activity]

The DPPH radical scavenging assay is commonly used as a rapid and reliable method to assess the antioxidant/free radical scavenging potential of compounds.[120] DPPH is a stable free radical that can accept a hydrogen radical or an electron to become a stable molecule. The antioxidant activity of the selected compounds was estimated by their ability to reduce $DPPH^{\cdot}$ radical

(purple color) to DPPHH (yellow) and the corresponding radical-scavenging potential was evaluated by the decrease in the absorbance at 517 nm.[121] Only those compounds having IC_{50} values (AChE) less than 5 μM were selected for this study. Ascorbic acid was used as the positive control in this assay. All the test compounds exhibited notable free radical scavenging activity ranging from 40-55 % and 56-70 % at 10 μM and 20 μM concentrations respectively (**Table 4.11**).

Compound (**199**) showed better free radical scavenging activity (54.9 %, 64.3 % at 10 μM and 20 μM concentrations, respectively) compared to ascorbic acid (36.5 %, 61.8 % at 10 μM and 20 μM concentrations, respectively) whereas tacrine and donepezil were found to be devoid of significant free radical scavenging activity at these concentrations.

Table 4.11. DPPH radical scavenging activity of the compounds[a]

Compd	RP of DPPH (%)[b]		Compd	RP of DPPH (%)[b]	
	10 μM	20 μM		10 μM	20 μM
181	45.5 ± 3.1	57.3 ± 2.9	**196**	43.7 ± 2.5	60.3 ± 3.4
183	52.1 ± 2.4	63.1 ± 2.3	**197**	42.7 ± 3.7	58.4 ± 3.1
184	51.5 ± 1.6	62.7 ± 1.7	**198**	47.3 ± 2.0	59.6 ± 2.2
186	53.7 ± 2.7	65.4 ± 1.3	**199**	**54.9 ± 1.8**	**64.3 ± 2.8**
187	43.2 ± 3.3	60.2 ± 2.7	**200**	54.3 ± 2.1	66.4 ± 2.4
189	44.3 ± 2.4	59.4 ± 3.1	**201**	56.7 ± 1.6	67.3 ± 1.7
190	46.7 ± 1.9	60.7 ± 3.3	**202**	55.1 ± 3.4	64.2 ± 1.9
191	53.2 ± 2.4	62.4 ± 2.5	**Tacrine**	3.4 ± 0.4	6.4 ± 0.3
192	52.8 ± 2.9	60.7 ± 2.9	**Done.**	4.5 ± 0.6	4.9 ± 1.2
194	54.1 ± 1.7	65.1 ± 2.1	**Asc. acid**	36.5 ± 2.9	61.8 ± 3.2
195	44.1 ± 3.4	61.3 ± 2.3			

[a]Data are expressed as Mean ± SE (three independent experiments), [b]RP of DPPH (%) = reduction percentage of DPPH.

4.1.1.3.3. Assessment of cytotoxicity and neuroprotection offered by the synthesized compounds

To ascertain the therapeutic potential of the synthesized compounds, their effect on cell viability and neuroprotective ability against oxidative stress were assessed using the human neuroblastoma SH-SY5Y cell line.[115] Only those compounds having IC_{50} values (AChE) less than 5 μM were selected for these studies. For the assessment of cytotoxicity of the test compounds, cells were exposed to significantly high concentrations of the test compounds (40 μM and 80 μM) for 24 hours, followed by determination of the cell viability using MTT assay. Even at such high concentrations, all the test compounds caused negligible cell death (**Table 4.12**).

The neuroprotective potential of the selected compounds against the oxidative stress induced by exogenous toxins (H_2O_2 or $A\beta_{1-42}$) was evaluated. H_2O_2-induced toxicity is due to the oxidative damage to the neuronal cells[122] while the Aβ-induced toxicity is more complex, involving generation of reactive oxygen species, interleukin-1, interleukin-6, TNF-α like damaging cytokines' release, and mitochondrial dysfunction.[123,124]

In this study, when the cells were exposed to H_2O_2 (100 μM) and $A\beta_{1-42}$ (25 μM) separately, notable toxicities to cells were observed and the cell viability got declined to nearly 55 % and 52 %, respectively. To assess the neuroprotective potential of the test compounds against these toxic insults, the cells were pretreated with the test compounds (10 μM, and 20 μM) for 2 h followed by treatment with the insults for 24 h. The selected derivatives exhibited a significant neuroprotective effect at 10 μM and 20 μM concentrations. For comparison, the cells were co-incubated with compounds (**199**, **200**), donepezil and tacrine at different concentrations. Compound (**199**) offered significant protection to the cells against the toxic insults (**Figure 4.12**). The results suggested that these compounds possessed the ability to protect neuronal cells against oxidative-stress-associated cell death.

Table 4.12. Cell viability, and neuroprotective action of the selected test compounds against H_2O_2 and $A\beta_{1-42}$ induced toxicity in the human neuroblastoma SH-SY5Y cell line[a]

Compd	Cell viability (%)		Neuroprotection (%) (against H_2O_2)		Neuroprotection (%) (against $A\beta_{1-42}$)	
	40 µM	80 µM	10 µM	20 µM	10 µM	20 µM
181	92.4 ± 2.2	90.3 ± 1.8	34.4 ± 2.7	48.9 ± 2.3	37.5 ± 2.1	56.2 ± 1.9
183	93.0 ± 1.5	91.2 ± 2.1	39.8 ± 1.9	53.2 ± 3.2	40.3 ± 2.5	57.5 ± 2.2
184	91.9 ± 2.4	87.1 ± 3.3	41.7 ± 1.3	55.4 ± 1.9	42.1 ± 1.9	60.7 ± 1.4
186	91.3 ± 3.2	85.7 ± 2.4	37.2 ± 2.8	50.3 ± 2.9	41.5 ± 2.7	59.0 ± 1.5
187	92.2 ± 3.1	90.5 ± 1.9	30.4 ± 3.6	46.5 ± 2.3	39.4 ± 3.1	57.3 ± 2.2
189	92.4 ± 2.5	89.8 ± 3.1	31.8 ± 3.5	48.4 ± 2.2	38.1 ± 2.8	56.2 ± 2.9
190	90.4 ± 3.3	87.1 ± 2.2	33.5 ± 2.9.	48.7 ± 3.1	38.5 ± 2.5	59.5 ± 2.3
191	93.1 ± 2.7	90.6 ± 1.5	41.8 ± 3.5	54.3 ± 1.7	43.7 ± 3.1	60.1 ± 3.4
192	93.9 ± 3.2	92.2 ± 1.9	43.4 ± 2.2	55.6 ± 2.1	41.4 ± 2.4	62.4 ± 1.9
194	90.5 ± 3.7	86.4 ± 2.9	41.2 ± 2.7.	50.2 ± 2.8	40.3 ± 1.9	58.7 ± 2.1
195	92.4 ± 3.2	89.3 ± 2.5	32.7 ± 3.4	43.5 ± 2.6	37.1 ± 2.3	59.3 ± 3.3
196	93.2 ± 2.1	91.7 ± 1.9	31.2 ± 2.5	40.4 ± 3.6	37.7 ± 3.1	57.2 ± 3.4
197	94.3 ± 2.2	91.1 ± 3.2	35.3 ± 1.4	46.1 ± 2.0	39.1 ± 2.6	57.5 ± 2.3
198	91.4 ± 2.8	87.4 ± 2.3	34.2 ± 3.5	49.5 ± 2.7	38.8 ± 1.9	58.3 ± 2.9
199	**94.9 ± 3.2**	**92.3 ± 1.5**	**42.5 ± 2.1**	**53.7 ± 1.3**	**44.5 ± 2.1**	**62.6 ± 1.9**
200	94.5 ± 2.1	91.8 ± 2.8	44.8 ± 1.7	54.5 ± 2.4	43.2 ± 2.5	63.6 ± 2.2
201	92.1 ± 2.7	89.7 ± 1.9	40.3 ± 1.8	52.3 ± 2.2	45.3 ± 2.2	61.4 ± 3.3
202	91.4 ± 3.2	85.4 ± 2.7	41.2 ± 1.4	51.6 ± 2.5	42.7 ± 3.1	62.5 ± 2.5
Tacrine	90.1 ± 1.8	88.1 ± 2.4	51.0 ± 3.4	70.4 ± 3.2	40.5 ± 2.3	58.7 ± 2.7
Donep.	92.4 ± 2.5	90.7 ± 1.2	53.4 ± 3.1	72.1 ± 2.7	47.2 ± 2.1	65.1 ± 1.8

[a]Data are expressed as Mean ± SE (three independent experiments)

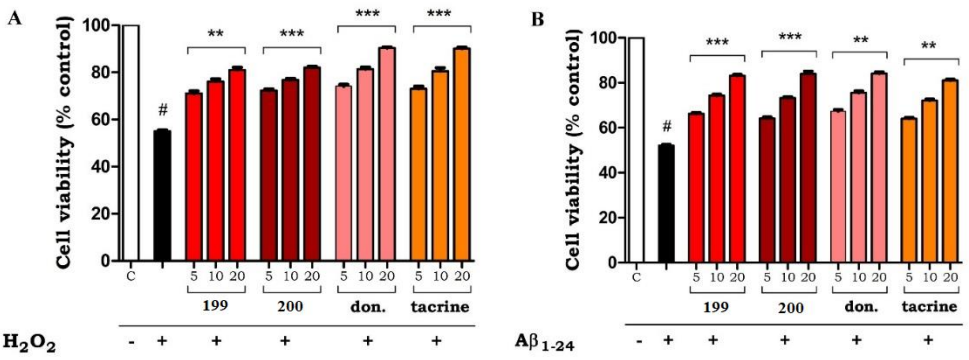

Figure 4.4. Protective effects of compounds (**199**, **200**), donepezil and tacrine against H_2O_2 and $A\beta_{1-42}$-induced cytotoxicity in SH-SY5Y cells. Determination of the viability of SH-SY5Y cells by the MTT assay after treatment with (**A**) H_2O_2 (100 μM) and (**B**) $A\beta_{1-42}$ (25 μM) in the absence or presence of the indicated concentrations of compounds (**199**, **200**) and the standard drugs. All the data were expressed as mean ± SD of three experiments and each included triplicate sets. #$p < 0.05$ vs control; **$p < 0.01$, ***$p < 0.001$ vs $H_2O_2/A\beta_{1-42}$ alone.

4.1.1.3.4. *In vitro* blood-brain barrier permeation assay

The BBB permeability is a primary criterion for the development of novel CNS active agents. The ability of triazinoindole derivatives to penetrate into the brain was assessed using a parallel artificial membrane permeation assay (PAMPA), in a similar manner as described by Di *et. al*.[125,126] This assay is used to predict the passive diffusion of a molecule through the BBB. The BBB permeability (P_e) of the most active compounds (**199** and **200**) was determined through a porcine brain lipid.

Table 4.13. **Permeability (P_e 10^{-6} cm s^{-1}) of selected commercial drugs for the validation of the PAMPA-BBB permeation assay**

Sr. No.	Commercial drugs	(P_e 10^{-6} cm s^{-1})	
		Reference value	Experimental value
i	Dopamine	0.2	0.3 ± 0.1
ii	Atenolol	0.8	1.1 ± 0.3
iii	Ofloxacin	0.8	1.7 ± 0.5
iv	Lomefloxacin	1.1	1.9 ± 0.3
v	Corticosterone	5.1	4.3 ± 0.6
vi	Progesterone	9.3	11.5 ± 1.2
vii	Donepezil	12.0	14.3 ± 1.7

Data are expressed as mean ± SEM of three independent experiments.

The assay was validated by comparing the experimental permeability values [P_e(exp)] of seven commercial drugs with the reported permeability values [P_e(ref)] (**Table 4.13**), offering a linear relationship i.e., P_e(exp.) = 1.16 P_e(ref.) + 0.1668 (R^2 = 0.9781) (**Figure 4.5**).

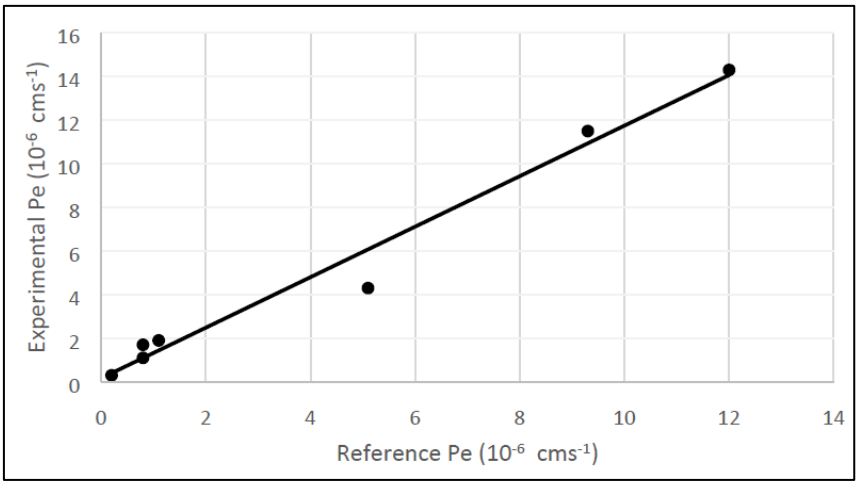

Figure 4.5. Linear correlation between experimental and reference permeabilities of selected commercial drugs using PAMPA-BBB assay. P_e (exp.) = 1.16P_e (ref.) + 0.1668 (R^2 = 0.9781)

From this equation and considering the limits for BBB permeation established by Di *et. al.*,[125] it was concluded that compounds with P_e(exp) greater than 4.8 × 10^{-6} cm/s (**Table 4.14**) were capable of crossing the BBB. Both the compounds (**199** and **200)** showed permeability values above this limit (**Table 4.15**). Therefore, P_e(exp) suggested a high potential of the compounds to cross the BBB by passive diffusion.

Table 4.14. Permeability range (P_e 10^{-6} cm s^{-1}) of PAMPA-BBB assay

	PBS:ethanol (70:30)
Compounds of low BBB permeation (CNS-)	2.5>P_e
Compounds of uncertain BBB permeation (CNS+/-)	4.8 >P_e> 2.5
Compounds of high BBB permeation (CNS+)	P_e> 4.8

Table 4.15. Permeability (P_e 10^{-6} cm s^{-1}) of compounds (199, 200) and donepezil in the PAMPA-BBB permeation assay with their predicted penetration into the CNS

Compd.	(P_e 10^{-6} cm s^{-1})	Prediction
199	11.3 ± 1.8	CNS+
200	12.5 ± 1.2	CNS+
Donepezil	14.3 ± 1.7	CNS+

Data are expressed as mean ± SEM of three independent experiments.

4.1.1.3.5. Assessment of cognitive improvement in animal model of AD

The work carried out to assess the cognitive improvement induced by the test compounds in animal model of AD is described under three subheading:

4.1.1.3.5.1. Morris Water Maze test,

4.1.1.3.5.2. Neurochemical analysis, and

4.1.1.3.5.3. Y-Maze test.

4.1.1.3.5.1. Morris Water Maze test

To determine the effect of compound (**199**) on cognitive improvement, an animal model of scopolamine-induced amnesia in the rodents was adopted.[127-129] Scopolamine blocks the cholinergic pathway distinctly by antagonizing the muscarinic receptors, offering a typical AD model to explore the role of cholinergic system in cognition.

Morris water maze learning test was utilized to assess the hippocampal-dependent spatial learning ability of the animals. This test assesses the reference or long-term memory by observing the escape latency.[130] During the last 5 days of the treatment period, escape latency time (ELT) was recorded for the animals of the experimental groups. The ELT was significantly prolonged (**Figure 4.6-A**) by scopolamine treatment (1.4 mg/kg, ip). In donepezil (5 mg/kg, po) treated group, ELT was considerably shortened as compared to the scopolamine-treated control group. Compound (**199**) (5 mg/kg and 10 mg/kg, po) significantly reduced ELT as compared to the scopolamine-treated control group. This result revealed that the animals retained the previous memory in the Morris water maze test, showing spatial memory improvement.

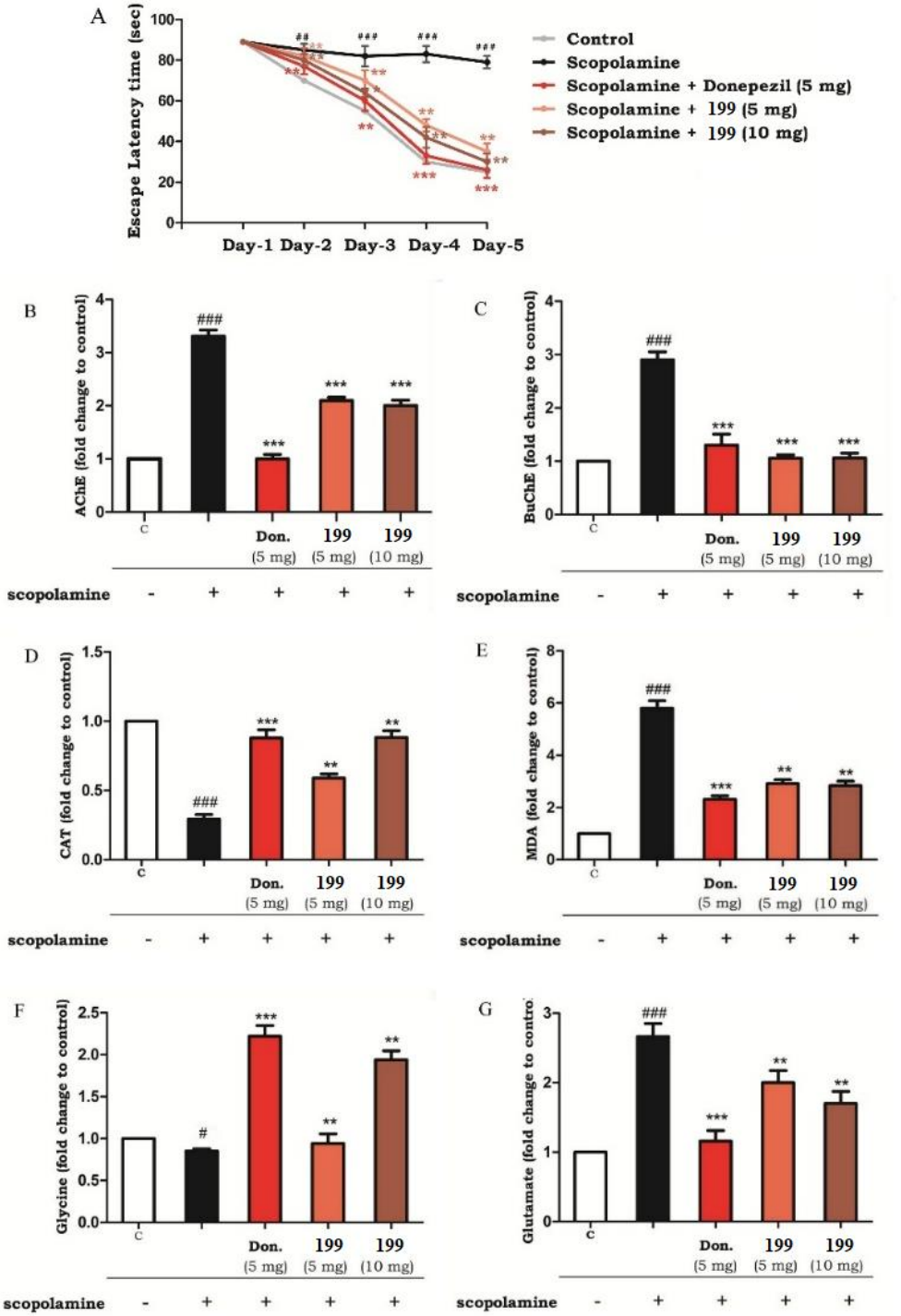

Figure 4.6. MWM test, ex vivo anticholinesterase and antioxidant activities, neurotransmitters' level in scopolamine- induced amnesic brain. Data are expressed as mean ± SEM (n = 7): (###) $p < 0.001$, (#) $p < 0.05$ vs vehicle-treated control group; (***) $p < 0.001$, (**) $p < 0.01$, vs scopolamine-treated control group. C = vehicle-treated control group.

4.1.1.3.5.2. Neurochemical analysis

After completion of the MWM test, the effects of scopolamine and compound (**199**) on cholinesterase levels and oxidant stress parameters in brain were assessed. Scopolamine treatment significantly increases the cholinesterase levels in the brain. The effect of compound (**199**) on the brain cholinesterase levels was assessed in mice using Ellman's method. The inflated levels of AChE (**Figure 4.6-B**) and BuChE (**Figure 4.6-C**) were significantly attenuated by compound (**199**) at a dose equivalent to donepezil. Malondialdehyde (MDA), catalase (CAT), glutamate and glycine levels in the brain were assessed in order to further perceive the anti-amnesic effects of compound (**199**). Estimation of the lipid peroxidation products in the brain homogenate samples was carried out by thiobarbituric acid reactive substances (TBARS) assay, which estimates the MDA, a byproduct of lipid peroxidation by measuring the absorbance at 532 nm. Scopolamine-treated group showed elevated MDA levels (**Figure 4.6-C**) in comparison to the vehicle-treated control group. Treatment of compound (**199**) to the amnesic mice appreciably attenuated the increase in MDA levels in the brain (**Figure 4.6-C**) as compared to the scopolamine-treated group. CAT is an important antioxidant defense system responsible for the decomposition of hydrogen peroxide to water and oxygen. Scopolamine treatment significantly reduced the CAT levels (**Figure 4.6-D**) in the brains of the treated animals compared to the vehicle-treated control group animals. However, treatment of the amnesic mice with compound (**199**) elevated the CAT levels considerably (**Figure 4.6-D**). These results revealed the anti-oxidant potential of the test compound (**199**).

Disturbances in the balance between glutamate (excitatory neurotransmitter) and glycine (inhibitory neurotransmitter) system leads to the development of pathological features observed in AD.[84] Apart from the role in signal transmission and plasticity, glutamate also takes part in the regulation of survival or apoptosis induction of brain cells. This system is counter balanced by glycine signaling to assure normal brain functioning by maintaining equilibrium between these inhibitory and excitatory activities. Scopolamine-treated group showed reduced levels of glycine (**Figure 4.6-F**) compared to the vehicle-treated control group. The reduced level of glycine is also associated with impairment in the cognitive functions. Treatment of the

amnesic mice with compound (**199**) increased the glycine levels (**Figure 4.6-F**) as compared to the scopolamine-treated group. The elevated levels of glycine could improve the NMDA receptor hypofunction which is helpful in reviving the cognitive function and memory. Furthermore, the scopolamine-treated group showed elevated levels of glutamate (**Figure 4.6-G**) compared to the vehicle-treated control group. The elevated level of glutamate is alarming to the neuronal cells. It causes the triggering of calcium-dependent intracellular pathways, generating highly reactive free radical species, surging the oxidative stress which ultimately leads to cell death. Treatment of the amnesic mice with compound (**199**) decreased the glutamate levels (**Figure 4.6-G**) as compared to the scopolamine-treated group. This might provide protection against excitotoxicity induced by elevated levels of glutamate.

4.1.1.3.5.3. Y-Maze test

The animal model of $A\beta_{1\text{-}42}$-induced AD in rodents was used to assess the effect of compound (**199**) on learning and memory. In this model, animals were subjected to intracerebroventricular (icv) injection of $A\beta_{1\text{-}42}$ in the hippocampal region of the brain. Impairment of the working memory in the animals was assessed using Y-maze test.[89] The spontaneous alteration in the behavior of the animals was considered to reflect short-term or spatial working memory.

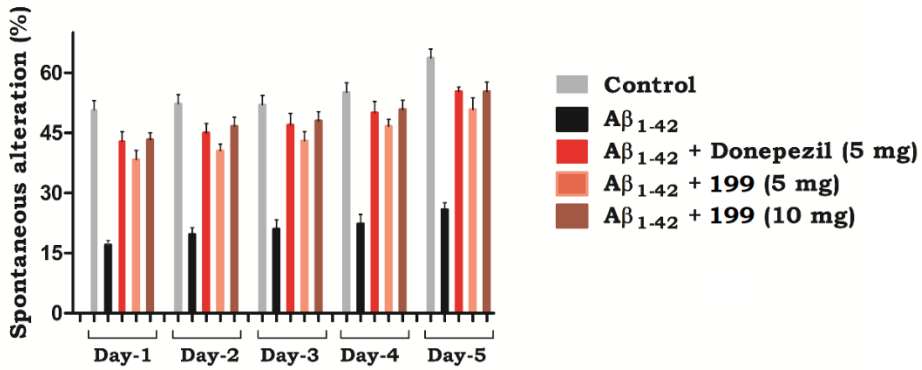

Figure 4.7. Compound (**199**) improved immediate working memory in rats which received icv injection of $A\beta_{1\text{-}42}$ in the Y-maze test.

As shown in **Figure 4.7**, spontaneous alternations in $A\beta_{1\text{-}42}$-treated mice were significantly lowered over the vehicle treated control mice. Donepezil, used as a reference standard, could considerably increase spontaneous

alternation behavior compared to the $A\beta_{1-42}$-treated group. Further, the lowered spontaneous alternations induced by $A\beta_{1-42}$ were significantly reversed by compound (**199**) at both 5 mg/kg and 10 mg/kg dose levels (**Figure 4.7**).

Results of these behavioral studies and neurochemical analysis in scopolamine-induced amnesia and Aβ-induced AD models revealed that compound (**199**) possessed the ability to reverse the reference and working memory-deficit as well as manage the oxidative stress-induced dementia.

4.1.1.3.6. Acute toxicity study

For the development of a NCE as a drug, determination of its acute toxicity is considered to be an important criterion. Acute toxicity of compound (**199**), the most promising candidate of the current study, was determined according to OECD 423 guidelines.[131] Wistar female rats were dosed with compound (**199**) at a dose of 2000 mg/kg (n = 3 per group) by oral administration. After administration of the compound, the animals were monitored continuously for the first 4 hrs for any abnormal behavior and mortality. Later on, the animals were intermittently observed for the next 24 hrs and occasionally for 14 days for any sign of delayed effects. All the animals survived in the duration of the study period and appeared healthy in terms of fur sleekness, water and food consumption, and body weight. On the 15^{th} day, all the animals were sacrificed for macroscopic examination of the heart, liver, and kidneys for any damage. No damage was observed in these organs. The results from the study showed that mice treated with compound (**199**) did not produce any acute toxicity or mortality immediately or during the post-treatment period. Therefore, compound (**199**) can be considered to be nontoxic and well tolerated at doses up to 2000 mg/kg.

4.1.1.4. Computational studies of the most promising compounds

Computational studies of the most promising compounds were performed to offer an insight into the binding mode of the compounds with the target proteins, to understand the time dependent stability of the ligand-receptor complex of the most active ligand by molecular dynamic simulation and to predict the *in silico* ADMET properties of the promising compounds. The work carried out under this head is described into the following three subheadings:

4.1.1.4.1. Docking studies of compound (**199**) with target proteins,

4.1.1.4.2. Molecular dynamics simulation and

4.1.1.4.3. Prediction of virtual physicochemical and pharmacokinetics parameters of the promising compounds.

4.1.1.4.1. Docking studies of compound (199) with target proteins

To have an idea of the binding mode of compound (**199**) with the cholinesterase enzymes, docking studies were performed within the active sites of Torpedo Californica AChE (*Tc*AChE) and Human BuChE (*h*BuChE). To validate the generated grids for docking studies, the co-crystallized molecules in the 3D structures of *Tc*AChE and *h*BuChE (PDB Code: **2CKM** and **4BDS** respectively)[132] were initially knocked out of the binding sites. The knocked-out molecules were constructed afresh, energy minimized and re-docked into the active sites of the grids. Very similar interactions were observed between the re-docked molecules and the enzymes as was the case with the original co-crystallized ligands. The RMSD values of the re-docked ligands with those of the original orientations in co-crystallized forms in 2CKM and 4BDS were observed to be 0.40 Å and 0.26 Å, respectively.

It is well known that AChE has a dumbbell shaped active site gorge composed of two active sites: the CAS at the bottom and the PAS at the lip. The CAS pocket looks like a vessel, on its bottom lies Trp84 which is crucial for binding of both the substrates to the inhibitors. Moreover, halfway up the gorge is a narrow tunnel where some crucial amino acid residues such as Phe330 and Tyr-334 stabilize the enzyme-inhibitor complex. At the entrance of the gorge exists the PAS, which is mainly built up by Trp279 and Tyr70 residues. The docking interactions of compound (**199**) were studied in the active site of the AChE of *Tc*AChE, and then *Tc*AChE was humanized with *h*AChE to know the human sequence interacting with compound (**199**).

The interaction view of compound (**199**) with AChE is represented in **Figure 4.8-A**. As presented, compound (**199**) was stacked well in the groove formed by Trp84, Trp279 and Phe330 (*h*AChE: Trp86, Trp284 and Tyr337) amino acid residues. It has orientation along the active site gorge similar to the reference compound donepezil, extending from the active site amino acid residue Trp84 to the peripheral site amino acid residue Trp279. Ligand

interactions with these two amino acids are important to elicit a strong inhibitory effect by the dual binding site inhibitors. Hydrophobic planar nature of the tricyclic scaffold allows making of a more favorable sandwich type π-π stacking with Trp84 and Phe330 (*h*AChE: Trp86 and Tyr337). The -NH group of the indole ring exhibited hydrogen bonding with Gly80 (*h*AChE: Gly82). The -NH group at the 3rd position of the triazine ring showed hydrogen bonding with Ser122 (*h*AChE: Ser125). The nitrogen atom of pyrrolidine ring could be protonated at physiological *p*H. The protonated nitrogen showed strong cation-π interaction with Trp279 (*h*AChE Trp284). This interaction is particularly important as Trp279 plays a prominent role in deposition of beta-amyloid plaques.[23]

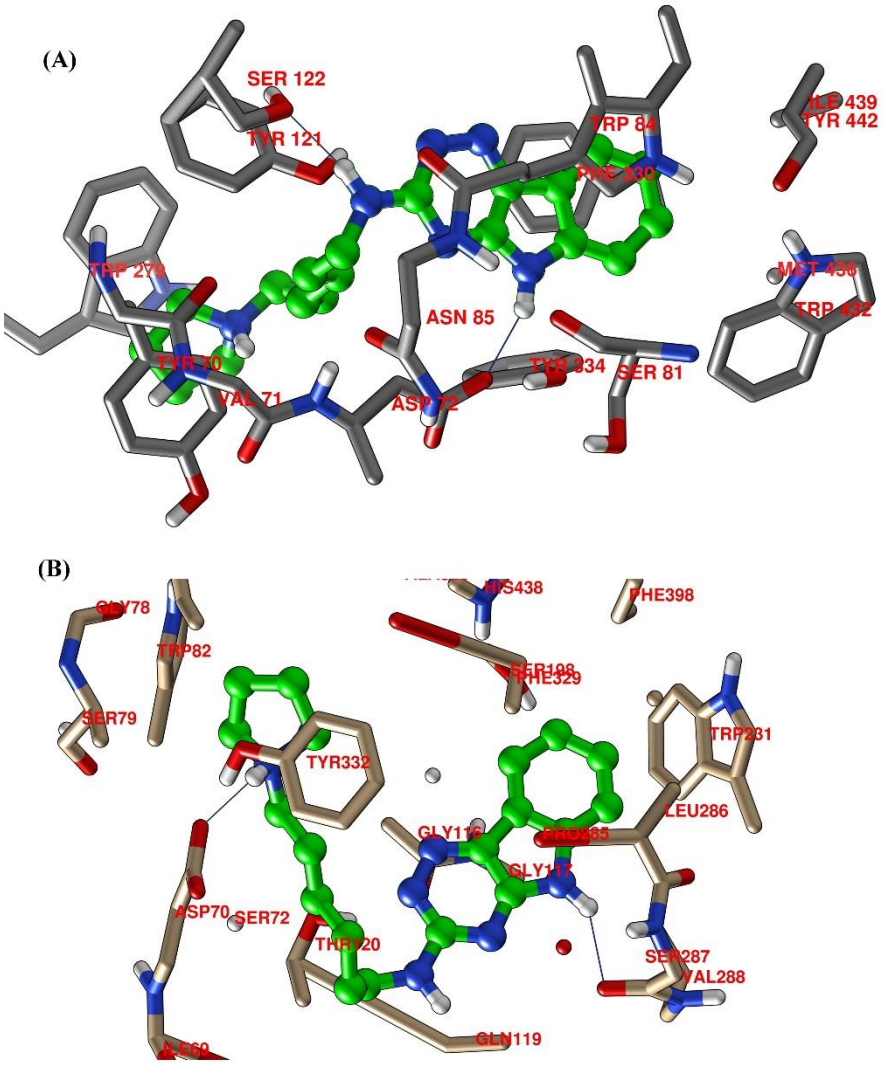

Figure 4.8. Docking interactions of compound (**199**) in the active sites of (**A**) AChE and (**B**) BuChE.

The binding mode of the compound (**199**) with BuChE revealed that it also occupied the large catalytic cavity of BuChE (**Figure 4.8-B**). The aromatic ring of the tricyclic moiety was observed to be interacting with Trp231 and Phe329 residues by π-π stacking. π-Alkyl interaction was observed between the aromatic ring of the scaffold and Leu286. Further, the -NH group on 3rd position added stability to the ligand-receptor complex by forming hydrogen bond with Ser287. Additionally, salt bridge between -NH of the pyrrolidine and Asp70, and cation-π interaction between the nitrogen of pyrrolidine and Trp82 provided stability to the ligand-receptor complex.

4.1.1.4.2. Molecular dynamics simulation

In the molecular docking studies, compound (**199**) exhibited very strong interactions within the active sites of the AChE and BuChE enzymes. Thus, to confirm, validate and understand the time dependent interactions of the active compound (**199**) with AChE and BuChE enzymes and stability of the ligand-receptor complex, molecular dynamics study was performed.[133,134] The binding stability of the ligand-receptor complex was studied for a period of 20 ns duration to check its time dependent stability. In order to observe the binding stability of the complex over a period of time, certain parameters like RMSD-P, RMSF-P and RMSD-L (P = Protein; L = Ligand) were scrutinized to support the results of the docking study. Initial pose of the ligand-receptor complex was considered as the reference frame to calculate these values. The RMSD-P is essentially studied to understand the level of movements of various atoms/groups in the enzyme when the ligand is present in the active site of the receptor. This provides insight into the changes in structural conformations of the enzyme over a given period of simulation. The RMSD-P for AChE in the ligand -receptor complex was found to be in the range of 0.7 to 2.0 Å. This finding explained that the presence of **199** in the active site of the AChE has not prejudiced the stability of the protein backbone all the way throughout the simulation period. To recognize the stability of the ligand with respect to the receptor and its active binding site, the RMSD-L of **199** was determined. The 'Lig fit' on Prot RMSD-L for ligand was observed in the range of 0.8 to 3.2 Å. The 'Lig fit Prot' is the RMSD of a ligand when the protein-ligand complex is first aligned on the reference protein backbone and then the RMSD of the ligand

heavy atoms is determined. Here, despite having a large number of rotatable bonds in the ligand, the RMSD value is not observed to be significantly higher than the protein RMSD, suggesting that the compound (**199**) is stable within the binding site and it does not diffuse away from the active site during the entire course of simulation period. Additionally, the Lig fit on Lig RMSD was calculated to comprehend the internal fluctuation of the ligand atoms, and it was observed in the acceptable range of 0.4 to 2.4 Å (**Figure 4.9-A**).

The structural integrity of the receptor and the residual mobility of the ligand were quantified in terms of RMSF-P (**Figure 4.9-B**). For all the residues, including the loop as well as the terminal residues of the protein, with the compound (**199**) in the active site, the RMSF-P was below 3.2 Å. The protein-ligand stability interaction study was also performed over a period of time to evaluate the interaction stability. In the docking studies, the H-bond was observed between -NH of indole and -NH of 3-amino group of compound (**199**) with Gly80 and Ser122 (*h*AChE: Gly82 and Ser125) residues respectively. From the MD simulation study, it was established that the two -NH groups of the compound (**199**) formed H-bonds with Gly80 and Ser122. These were observed to be stable over 54 % and 91 % of the simulation time with Gly80 and Ser122 respectively. Further, the salt bridge between the protonated pyrrolidine and Asp72 (*h*AChE: Asp74) was observed to be stable for around 24 % of the simulation time. All these H-bond strengths were with H-bond distance of 2.5 Å or less and donor angle of ≥ 120° and acceptor angle of ≥ 90°. The cation-π interactions between the protonated pyrrolidine and Trp279 and Tyr334 (*h*AChE: Trp284 and Tyr341) were also found to be stable over 76 % and 29 % of entire simulation time respectively. Further, strong hydrophobic interactions of the compound (**199**) with Trp-84, Trp-279 and Phe-330 played a vital role in providing stability to the ligand-receptor complex where all these hydrophobic interactions were observed for more than 60 % of a total of simulation time (**Figure 4.9-C**). The other ligand parameters like rGyr, MolSA, SASA and PSA were observed in the acceptable range as shown in **Figure 4.9-D.**

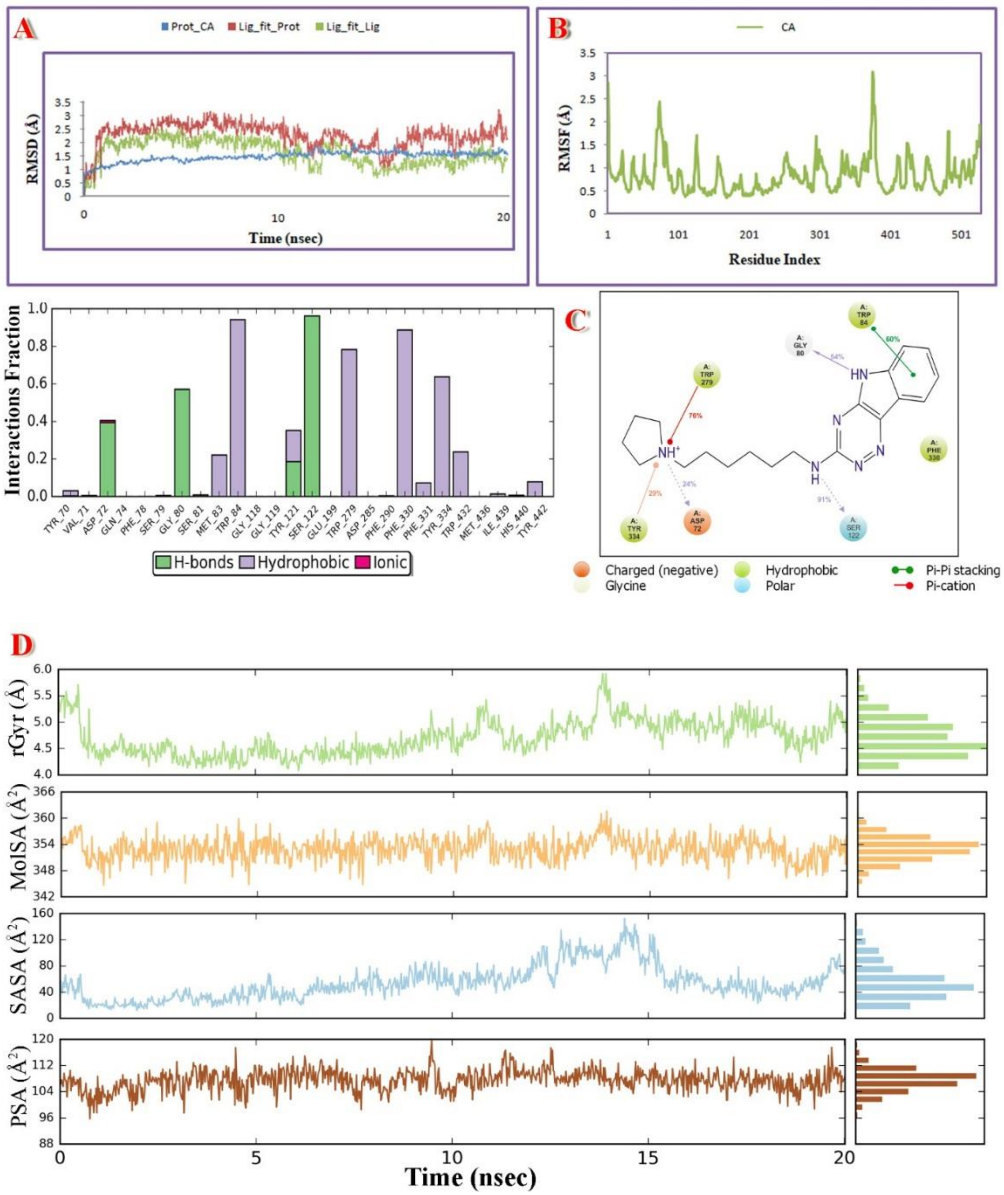

Figure 4.9. (**A**) RMSD-P and RMSD-L plots for AChE with compound (**199**); (**B**) RMSF-P plot for AChE with compound (**199**); (**C**) Ligand and receptor residue contact diagram for AChE with compound (**199**); (**D**) rGyr; MolSA; SASA and PSA for compound (**199**) with AChE.

Similarly, the molecular dynamics study of compound (**199**) with BuChE was also performed and this also indicated good stability of the ligand-receptor complex. The RMSD-P was in the range of 0.8 to 1.9 Å. Whereas the RMSD-L 'Lig fit' on Prot was observed in between 1.2 to 3.2 Å which was not alarmingly higher than the RMSD-P. The 'Lig fit' on the ligand was observed in 0.4 to 1.8 Å range (**Figure 4.10-A**). The protein fluctuation value RMSF-P was observed below 3.6 Å (**Figure 4.10-B**).

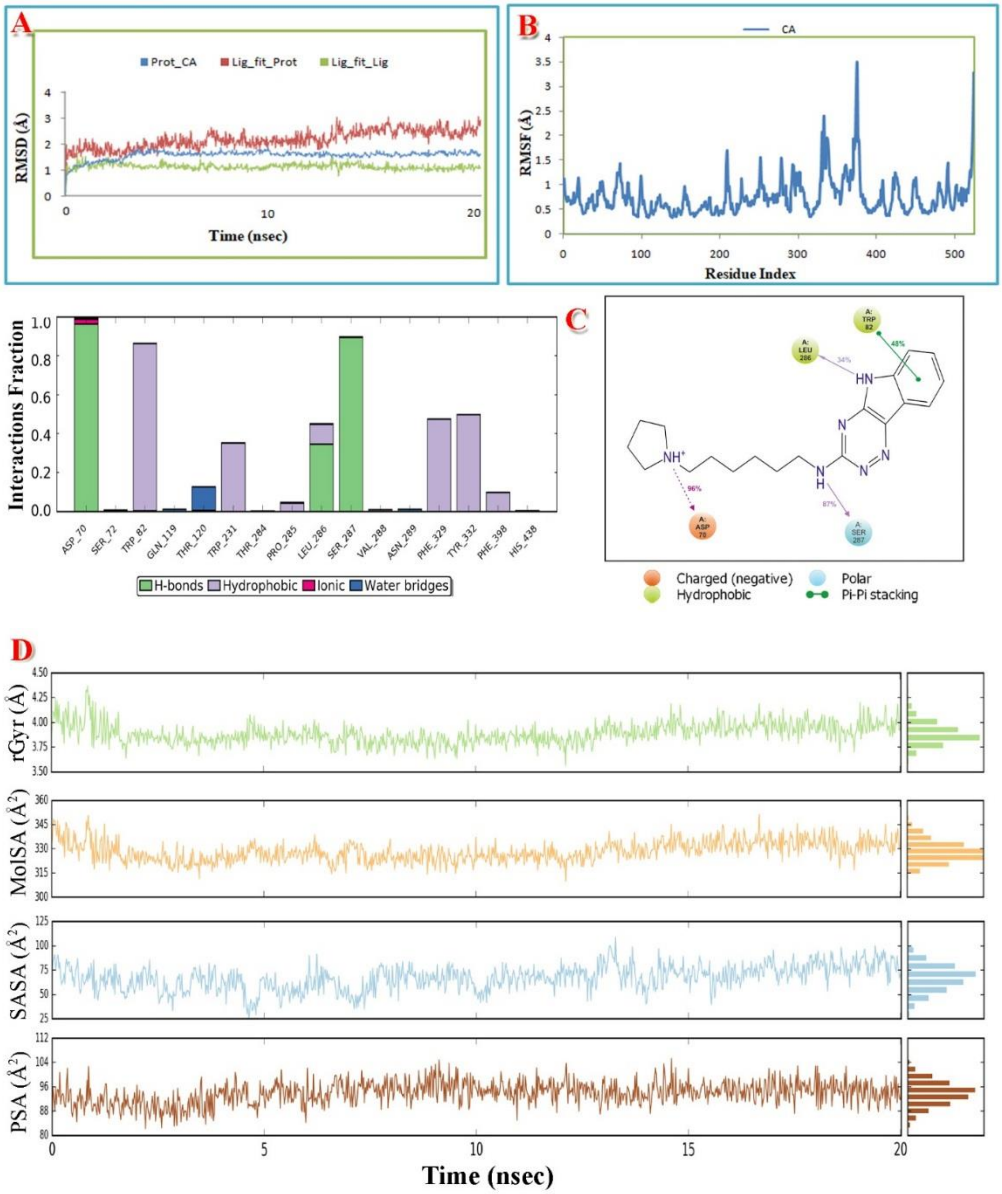

Figure 4.10. (**A**) RMSD-P and RMSD-L plots for BuChE with compound (**199**); (**B**) RMSF-P plot for BuChE with compound (**199**); (**C**) Ligand and receptor residue contact diagram for BuChE with compound (**199**); (**D**) rGyr; MolSA; SASA and PSA for compound (**199**) with BuChE.

The ligand-receptor interaction analysis elucidated the stability of ligand-receptor complex by supporting the H-bonding between -NH of indole and -NH at 3rd position of the compound (**199**) with protein residues Leu286 and Ser287, respectively. These were observed to be stable over 34 % and 87 % of simulation time respectively. The protonated pyrrolidine formed a stable salt bridge with Asp70 over 96 % of the simulation time period. The residues Trp82, Trp231, Leu286, Phe329 and Tyr332 were positively contributing towards the

stability of the complex by hydrophobic interactions (**Figure 4.10-C**). The other ligand parameters like rGyr, MolSA, SASA and PSA were also observed in the acceptable range (**Figure 4.10-D**). These observations from the molecular dynamics study strongly supported the observations made in the docking studies.

4.1.1.4.3. Prediction of virtual physicochemical and pharmacokinetics parameters of the promising compounds

On account of poor ADME (absorption, distribution, metabolism, and excretion) properties, approximately four drug candidates out of ten flunk in clinical trials. These late-stage failures significantly contribute to the enhancement of development cost for the new drugs. Hence, we need to resort to ADME predictions as a part of the drug development process to have an idea of the ADME properties during clinical trials.[135] Due to significant developments in the field of computational chemistry in recent times, virtual prediction of ADME properties becomes relatively easy and also reliable. For the most active compounds (**199** and **200**) along with donepezil and tacrine as reference drugs, pharmacokinetics profile indicators like Lipinski's parameters, QPlog$P_{o/w}$, PSA, QDCK, QPlogBB, QPPCaco, QPlogKhSa, etc. were predicted with QikProp module (**Table 4.16**).[136]

According to Lipinski's rule-of-five,[137] most "drug-like" molecules have LogP ≤ 5, molecular weight ≤ 500, number of hydrogen bond acceptors ≤ 10, and number of hydrogen bond donors ≤ 5. According to this rule, poor absorption or permeation is more likely when molecules violate more than one of these rules. Compounds (**199** and **200**) do not break Lipinski's rule of five at all, predicting them to be promising drug candidates. Number of rotatable bonds and topological Polar Surface Area (TPSA) are the two other important parameters introduced by Veber and co-workers.[138] Number of rotatable bonds is the simple topological parameter for molecular flexibility. It has been shown to be a very good descriptor for oral bioavailability of drugs. For oral bioavailability, a molecule should have less than 7 atoms in linear chains outside the rings or 8 rotatable bonds. TPSA value is another key descriptor that was shown to equate well with passive molecular diffusion through membranes and therefore, allows prediction of drug absorption, including intestinal absorption,

Table 4.16. Predicted ADMET indicators of compounds (199 and 200), donepezil and tacrine

Parameter	Limit	Compd (199)	Compd (200)	Donepezil	Tacrine
MW	130-725	338.455	352.481	379.498	198.267
HBA	2-20	5.5	5.5	5.5	2
HBD	0-6	2	2	0	1.5
NRB	0-8	8	8	6	1
QPlogP$_{o/w}$	-2 to 6.5	3.196	3.455	4.242	2.536
PSA	7 to 200	69.799	71.149	46.234	33.825
Volume	500-2000	1180.047	1225.635	1248.451	701.299
ReFG	0-2	0	0	0	0
SASA	300 to 1000	679.568	701.805	681.675	425.06
Rule of Five (violation)	0-1	0	0	0	0
CNS	-	1	1	1	1
QDCK	-	122.099	111.307	589.289	1602.036
QPlogBB	-3 to 1.2	-0.628	-0.686	0.223	0.047
QPPCaco	-	249.594	229.114	1070.771	2965.755
QPlogKhSa	-1.5 to 1.5	0.36	0.476	0.516	0.049
QPlogS	-6.5 to 0.5	-4.034	-4.419	-4.059	-3.036
% HOA	0-100	88.567	89.416	100	100
#star	0-5	0	0	0	0

MW: molecular weight, HBA: hydrogen-bond acceptor atoms, HBD: hydrogen-bond donor atoms, QPlogPo/w: predicted octanol/water partition coefficient, PSA: polar surface area, ReFG: number of reactive functional groups, SASA: a total of solvent accessible surface area, CNS: predicted central nervous system activity on a -2 (inactive) to +2 (active) scale, QDCK: predicted apparent MDCK cell permeability in nm/s, QPPCaco: caco-2 cell permeability in nm/s, QPlogBB: brain/blood partition coefficient, QPlogKhsa: binding to human serum albumin, QPlogS: predicted aqueous solubility, % HOA: human oral absorption on 0–100% scale, #star: number of parameters' values that fall outside the 95 % range of similar values for known drugs.

bioavailability and blood-brain barrier (BBB) penetration.[139] The mean TPSA value for the marketed CNS drugs is 40.5 $Å^2$ with a range of 4.63-108 $Å^2$.[140] Compounds (**199** and **200**) possess 8 rotatable bonds each and TPSA values of 69.8 $Å^2$ and 71.2 $Å^2$ respectively.

The QPCaco-2 is indicative of the oral absorption of a drug. It assesses the apparent gut-blood barrier permeability. Values above 500 predict high oral absorption which is obtained for both the compounds (**199** and **200**). Similarly, human oral absorption percent (% HOA) values also support prediction of good oral bioavailability of the test compounds. Brain/blood partition coefficient (QPlogBB), *n*-octanol–water partition coefficient ($QPlogP_{o/w}$), apparent MDCK cell permeability (QDCK), and CNS predict the ability of a compound to cross the blood–brain barrier (BBB), a mandatory criterion for CNS active drugs. Typically, drugs which penetrate the BBB through passive diffusion should have *n*-octanol–water partition coefficient ($logP_{o/w}$) values of ~3.[141] The QDCK predicts the apparent MDCK cell permeability in nm/s. MDCK (Madin-Darby canine kidney) cell permeability is considered to be a good mimic for the blood-brain barrier.[142] A value of QDCK above 25 is considered as good and almost all the test ligands have shown considerably high values. The test ligands are predicted to be CNS active as they have a value of CNS as 1. The QPlogKhsa value predicts the binding of CNS active drug with human serum albumin. Compounds (**199** and **200**) showed compliance with the recommended values, indicating that these compounds would have low serum albumin binding and the unbound fraction would have access to the putative receptor drug target. #Star denotes the number of parameters' values that fall outside the 95 % range of similar values for known drugs. A large number of #stars indicates that the molecule is less drug-like than the molecule with few #stars. Values of #star for compounds (**199** and **200**) indicate their drug-likeness. Additionally, a compound possessing tertiary nitrogen containing moiety which is a common feature in many CNS acting drugs, shows a higher degree of brain permeation.[140] Thus, it can be claimed that compounds (**199** and **200**) are predicted to possess good pharmacokinetics profile, which would enhance their biological significance.

4.1.2. 3- And 6-/7-/8-/9-disubstituted [1,2,4]triazino[5,6-*b*]indole derivatives

The work carried out under this heading has been further divided into 4 subheadings i.e. designing aspect, chemical studies, biological studies, and computational studies as mentioned below:

4.1.2.1. Designing aspect of 3- and 6-/7-/8-/9-disubstituted [1,2,4] triazino[5,6-*b*]indole derivatives,

4.1.2.2. Synthesis of the C_6-C_9-substituted *N*-(aminoalkyl)-5*H*-[1,2,4] triazino[5,6-*b*]indole derivatives (**249-257, 261**),

4.1.2.3. Biological evaluation of the synthesized compounds;

4.1.2.4. Computational studies of the most promising compound.

4.1.2.1. Designing aspect of 3- and 6-/7-/8-/9-disubstituted [1,2,4]triazino [5,6-*b*]indole derivatives

Among the all above described triazinoindole derivatives, compound (**199**) was found to be the most potent compound with an IC_{50} value of 0.56 μM for AChE and an IC_{50} value of 1.17 μM for BuChE. The salient structural features of the compound have been represented in **Figure 4.11.** To further improve the biological activity of compound (**199**) we thought to carry out some modifications in the structure of compound (**199**).

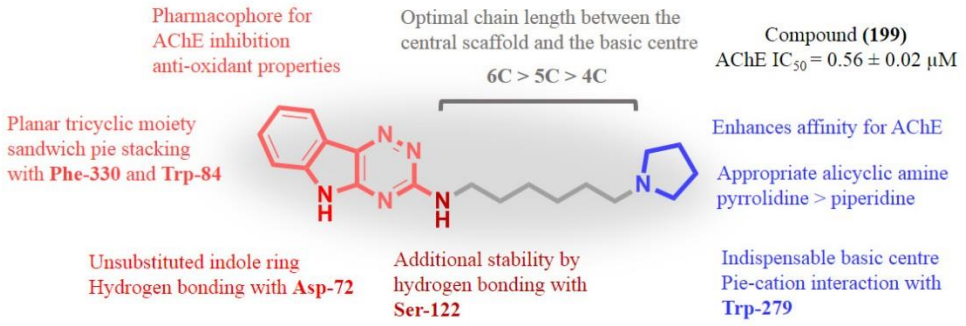

Figure 4.11. Salient structural features of compound (**199**).

It is reported that metabolism of triazinoindole derivative preferentially occurs at 7 and/or 8-position of the triazinoindole scaffold resulting in compounds that might be less active or subject to rapid elimination.[143] Further, to understand the metabolically active sites, *in silico* prediction for the common sites of metabolism (SOM) was carried out for compound (**199**) by SMARTCyp[144,145] and XenoSite[146] tools. The phenyl ring and alicyclic amine

ring appeared to be the two main SOM in the compound (**199**) as shown in **Figure 4.12**.

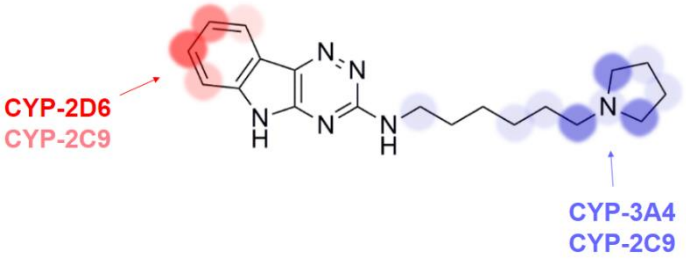

Figure 4.12. Common predicted metabolically active sites of compound (**199**) by SMARTCyp and XenoSite tools.

The alicyclic amine ring is an indispensable pharmacophore for the cholinesterase inhibitory activity as alteration or removal of it was detrimental to the ChE inhibitory activity. So, we thought to introduce some substituents on the phenyl ring of the triazinoindole scaffold keeping in mind that at least one substituent in this ring could lower the tendency of metabolism at this position. We planned to introduce various substituents i.e. chloro, bromo, fluoro, methyl, ethyl and piperidinyl at different positions of the phenyl ring of the triazinoindole scaffold which might not only hinder the metabolism but could also improve the interaction of the designed compounds with the ChEs.

4.1.2.2. Synthesis of the C_6-C_9-substituted *N*-(aminoalkyl)-5*H*-[1,2,4] triazino[5,6-*b*]indole derivatives (249-257, 261)

The designed C_6-C_9-substituted 5*H*-[1,2,4]triazino[5,6-*b*]indol-3-amine derivatives (**249-257, 261**) were synthesized from substituted isatins as depicted in **Scheme 4.5** and **Scheme 4.6.** Substituted isatin derivatives were synthesized by Sandmeyer process of isatin synthesis.[147] Condensation of these substituted isatins (**212-220**) with thiosemicarbazide gave substituted-*N*-(aminoalkyl)-5*H*-[1,2,4]triazino-[5,6-*b*]indole-3-thiol derivatives (**222-230**). These thiol derivatives were methylated and further oxidized to the corresponding sulfone derivatives (**240-248**). These sulfone derivatives were then reacted with the desired amines to obtain the C_6-C_9-substituted *N*-(aminoalkyl)-5*H*-[1,2,4]triazino[5,6-*b*]indol-3-amine derivatives (**249-257**).

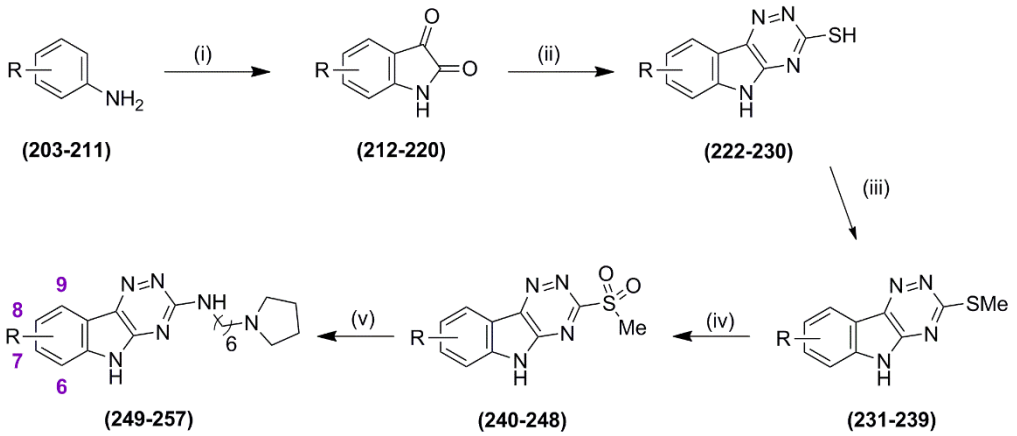

Scheme 4.5. General synthetic route for the **s**ynthesis of C_6-C_9-substituted-*N*-(aminoalkyl)-5*H*-[1,2,4]triazino[5,6-*b*]indol-3-amine derivatives (**249-257**). Reagents and conditions: (i) (a) Chloral hydrate, sodium sulfate, hydroxylamine HCl, (b) sulphuric acid, 80 ºC; (ii) thiosemicarbazide, K_2CO_3, H_2O, reflux, overnight; (iii) MeI, K_2CO_3, DMF. (iv) *m*CPBA, DCM, 0 ºC to RT; (v) 6-(pyrrolidin-1-yl)hexan-1-amine, THF, reflux.

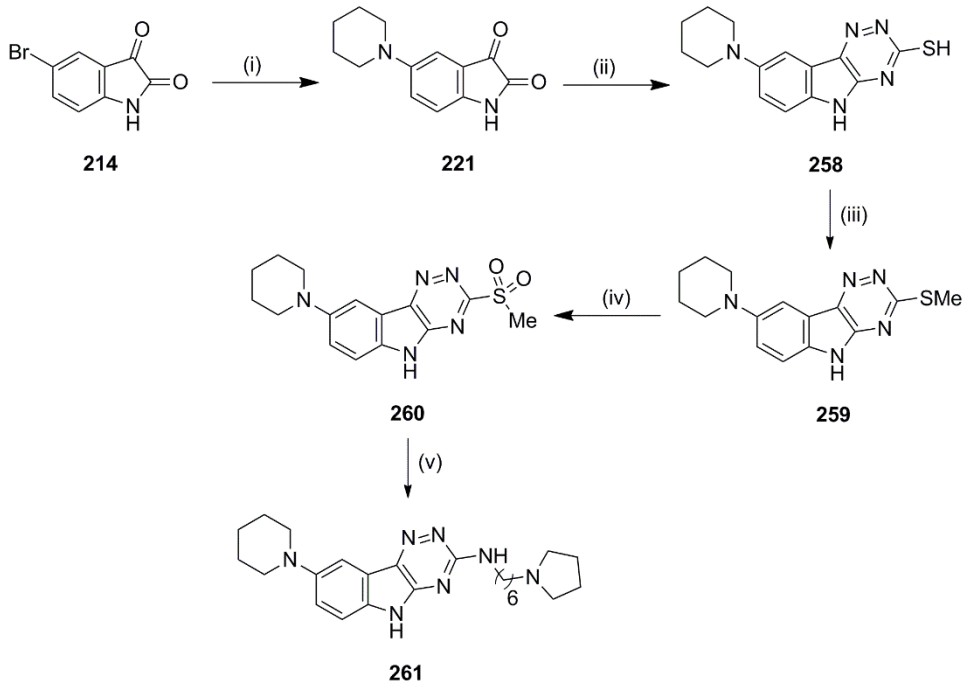

Scheme 4.6. Synthetic route for the **s**ynthesis of the compound (**261**). Reagents and conditions: (i) Piperidine, K_2CO_3, DMF, 80 ºC; (ii) thiosemicarbazide, K_2CO_3, H_2O, reflux, overnight; (iii) MeI, K_2CO_3, DMF. (iv) *m*CPBA, DCM, 0 ºC to RT; (v) 6-(pyrrolidin-1-yl)hexan-1-amine, THF, reflux.

The work carried out for the synthesis of C_6-C_9-substituted *N*-(amino alkyl)-5*H*-[1,2,4]triazino[5,6-*b*]indol-3-amine derivatives (**249-257, 261**) has been discussed in detail under the following subheadings:

4.1.2.2.1. Synthesis of substituted isatins (**212-221**),

4.1.2.2.2. Synthesis of substituted-5*H*-[1,2,4]triazino[5,6-*b*]indol-3-thiol derivatives (**222-230, 258**),

4.1.2.2.3. Synthesis of substituted-3-(methylthio)-5*H*-[1,2,4]triazino [5,6-*b*]indole derivatives (**231-239, 259**),

4.1.2.2.4. Synthesis of substituted-3-(methylsulfonyl)-5*H*-[1,2,4] triazino[5,6-*b*]indole derivatives (**240-248, 260**) and

4.1.2.2.5. Synthesis of C_6-C_9-substituted *N*-(aminoalkyl)-5*H*-[1,2,4] triazino[5,6-*b*]indol-3-amine derivatives (**249-257, 261**, **262**).

4.1.2.2.1. Synthesis of substituted isatins (212-221)

Substituted isatins (**212-220**) were synthesized by Sandmeyer process of isatin synthesis. Condensation of substituted anilines with chloral hydrate and hydroxylamine to α-isonitrosoacetanilide, and subsequent cyclization of the latter in the presence of concentrated sulfuric acid resulted into substituted isatins.[148]

5-(Piperidin-1-yl)isatin (**221**) was synthesized by reaction of piperidine with 5-bromoisatin (**214**) in presence of potassium carbonate in DMF.[149] The IR spectra of the substituted isatins exhibited characteristic peaks for amide NH stretching (~3100 cm^{-1}), and C=O stretching (~1750 cm^{-1} and ~1700 cm^{-1}). The analytical data for the substituted isatins (**212-221**) have been summarized in **Table 4.17**.

Table 4.17. Analytical data for substituted isatins (212-221)

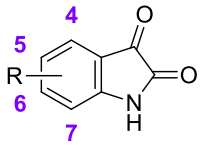

(212-221)

Compd	R	M.P.	IR characteristic peaks (cm^{-1})	MS (*m/z*)
212	5-Cl	255-257 °C	3094, 1751, 1704, 1616, 1310, 846	182 $[M+H]^+$
213	5,7-diCl	221-223 °C	3068, 1751, 1704, 1615, 1309, 846, 747	217 $[M+H]^+$
214	5-Br	247-249 °C	3180, 3104, 1743, 1613, 1318, 688;	224 $[M-2]^+$.
215	7-F	192-194 °C	3169, 3031, 1736, 1638, 1260, 1037	166 $[M+H]^+$
216	5-F	226-228 °C	3095, 1753, 1705, 1616, 1309	166 $[M+H]^+$
217	5-Me	184-187 °C	3288, 1749, 1704, 1625, 1301, 737	162 $[M+H]^+$
218	4,6-diMe	228-231 °C	3201, 1756, 1722, 1626, 1269, 747	176 $[M+H]^+$
219	4,7-diMe	190-192 °C	3207, 3107, 1730, 1594, 1320, 957, 809, 712	176 $[M+H]^+$
220	5-Et	131-133 °C	3284, 3037, 1746, 1709, 1619, 1488, 1317, 694	176 $[M+H]^+$
221	5–N⟨⟩	150-152 °C	3419, 1623, 1541, 1240, 825, 748	231 $[M+H]^+$

4.1.2.2.2. Synthesis of substituted 5*H*-[1,2,4]triazino[5,6-*b*]indol-3-thiol derivatives (222-230, 258)

Substituted [1,2,4]triazino[5,6-*b*]indol-3-thiols (**222-230**, **258**) were synthesized by condensation of substituted isatins (**212-221**) with thiosemicarbazide as discussed previously. The IR spectra of these thiol derivatives showed disappearance of C=O stretching vibration peaks. Mass spectra confirmed that the molecular weights of the compounds were in accordance with the calculated molecular weights of the synthesized thiol derivatives. The analytical data for the substituted [1,2,4]triazino[5,6-*b*]indol-3-thiol derivatives (**222-230**, **258**) have been summarized in **Table 4.18**.

Table 4.18. Analytical data for substituted [1,2,4]triazino[5,6-*b*]indol-3-thiol derivatives (222-230, 258)

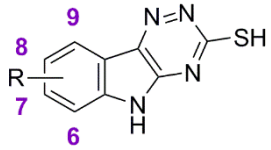

29a-29i

Compd	R	M.P.	IR characteristic peaks (cm^{-1})	MS (*m/z*)
222	8-Cl	>250 °C	3095, 2992, 1617, 1458, 1310, 1166, 847	237 $[M]^+$
223	6,8-diCl	>250 °C	3289, 3061, 1605, 1433, 1318, 1146, 841	271 $[M]^+$, 273 $[M+2]^+$
224	8-Br	>250 °C	3359, 3091, 1600, 1449, 1313, 1167, 813	281 $[M]^+$
225	6-F	>250 °C	3424, 3063, 1621, 1480, 1320, 1141, 1015	221 $[M+H]^+$
226	8-F	>250 °C	3425, 3014, 1620, 1477, 1320, 1140, 1015	221 $[M+H]^+$
227	8-Me	>250 °C	3438, 3030, 2884, 1609, 1477, 1323, 1190, 1142	217 $[M+H]^+$
228	7,9-diMe	>250 °C	3021, 2871, 1611, 1432, 1303, 1163	231 $[M+H]^+$
229	6,9-diMe	>250 °C	3391, 3034, 2935, 1586, 1439, 1325, 1149	231 $[M+H]^+$
230	8-Et	>250 °C	3433, 3029, 2877, 1604, 1478, 1320, 1186, 1141	231 $[M+H]^+$
258	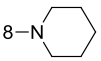	>250 °C	3361, 3089, 1599, 1449, 1312, 1239, 1167	286 $[M+H]^+$

4.1.2.2.3. Synthesis of substituted 3-(methylthio)-5*H*-[1,2,4]triazino[5,6-*b*] indole derivatives (231-239, 259)

Substituted [1,2,4]triazino[5,6-*b*]indol-3-thiol derivatives (**222-230, 258**) were methylated by methyl iodide in presence of potassium carbonate and DMF to obtain the substituted-3-(methylthio)-5*H*-[1,2,4]triazino[5,6-*b*] indole derivatives (**231-239**, **259**). The mass spectra of the thiomethyl derivatives (**231-239, 259**) confirmed that the molecular weights of the compounds were in accordance with the calculated molecular weights of synthesized derivatives. The analytical data for 3-(methylthio)-5*H*-[1,2,4]triazino[5,6-*b*]indole derivatives (**231-239, 259**) have been summarized in **Table 4.19**.

Table 4.19. Analytical data for substituted-3-(methylthio)-5*H*-[1,2,4] triazino[5,6-*b*]indole derivatives (231-239, 259)

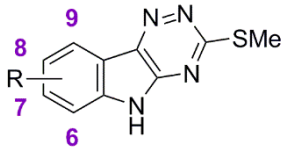

(231-239, 259)

Compd	R	M.P.	IR characteristic peaks (cm^{-1})	MS (*m/z*)
231	8-Cl	> 250 °C	3446, 3048, 2933, 1606, 1454, 1186, 825, 780	251 $[M+H]^+$, 253 $[M+2]^+$
232	6,8-diCl	> 250 °C	3047, 2962, 2860, 1606, 1452, 1183, 820, 775	285 $[M]^+$, 287 $[M+2]^+$
233	8-Br	>250 °C	3047, 2961, 1607, 1316, 1183,1091, 820, 776	295 $[M]^+$, 297 $[M+2]^+$
234	6-F	>250 °C	3106, 3054, 2955,1611, 1495, 1321, 1155	235 $[M+H]^+$
235	8-F	> 250 °C	3054, 2954, 1609, 1323, 1156, and 820	235 $[M+H]^+$
236	8-Me	> 250 °C	3061, 2976, 1603, 1471, 1319, 1208, 977, 814	231 $[M+H]^+$
237	7,9-diMe	> 250 °C	3049, 2966, 2919, 1589, 1426, 1313, 1179, 844, 752	245 $[M+H]^+$
238	6,9-diMe	> 250 °C	3093, 2965, 2920, 1588, 1334, 1180, 809, 752	245 $[M+H]^+$
239	8-Et	> 250 °C	3062, 2961, 1599, 1480, 1318, 1204, 972, 806, 739	245 $[M+H]^+$.
259		> 250 °C	3087, 2966, 1607, 1453, 1317, 1183, 1092, 976, 819, 778	300 $[M+H]^+$

4.1.2.2.4. Synthesis of substituted 3-(methylsulfonyl)-5*H*-[1,2,4]triazino [5,6-*b*]indole derivatives (240-248, 260)

As depicted in **Scheme 4.3**, substituted 3-(methylsulfonyl)-5*H*-[1,2,4] triazino[5,6-*b*]indole derivatives (**240-248, 260**) were synthesized by oxidation of the respective thiomethyl derivatives (**231-239, 259**) with *m*CPBA.[113] The obtained products were used in the next step without further purification.

4.1.2.5. Synthesis of C_6-C_9-substituted *N*-(aminoalkyl)-5*H*-[1,2,4]triazino [5,6-*b*]indol-3-amine derivatives (249-257, 261, 262)

C_6-C_9-Substituted *N*-(aminoalkyl)-5*H*-[1,2,4]triazino[5,6-*b*]indol-3-amine derivatives (**249-257, 261**) were synthesized by reaction of the respective

sulfone derivatives **(240-248, 260)** with 1-(6-aminohexyl) pyrrolidine.[113] The obtained solids were purified by flash chromatography to yield the titled compounds (**249-257**). The analytical data for C_6-C_9-substituted *N*-(aminoalkyl)-5*H*-[1,2,4]triazino[5,6-*b*]indol-3-amine derivatives (**249-257, 261**) have been summarized in **Table 4.19**.

Table 4.20. Analytical data for C(6)-C(9)-substituted-*N*-(aminoalkyl)-5*H*-[1,2,4]triazino[5,6-*b*]indol-3-amine derivatives (249-257, 261)

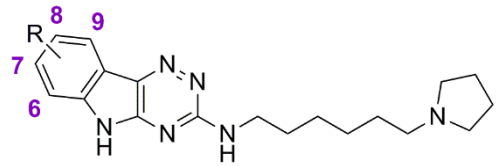

(249-257, 261)

Compd	R	IR characteristic peaks (cm^{-1})	HPLC data
249	8-Cl	3421, 3075, 2930, 1618, 1547, 1365, 1142, 1107, 816	Purity: 96.7 %, t_R = 4.08 min
250	6,8-diCl	3405, 3062, 2931, 1608, 1528, 1376, 1312, 1076, 834, 724	Purity: 97.6 %, t_R = 6.883 min
251	8-Br	3415, 3073, 2929, 1615, 1524, 1453, 1142, 1106, 738	Purity: 99.1 %, t_R = 4.787 min
252	6-F	3235, 3108, 2935, 1584, 1526, 1361, 1128, 1026	Purity: 98.5 %, t_R = 3.617 min
253	8-F	3233, 3106, 2935, 1528, 1360, 1293, 1128, 1025, 798, 735	Purity: 98.4 %, t_R = 3.653 min
254	8-Me	3225, 3104, 2931, 1613, 1523, 1282, 1209, 1100, 801, 737	Purity: 98.7 %, t_R = 3.813 min
255	7,9-diMe	3372, 2931, 1619, 1312, 1136, 841, 769	Purity: 98.9 %, t_R = 4.060 min
256	6,9-diMe	3228, 3010, 2930, 1599, 1518, 1264, 1121, 1032, 799, 751	Purity: 97.5 %, t_R = 4.050 min
257	8-Et	3226, 3012, 2933, 1613, 1525, 1379, 1100, 877, 742	Purity: 97.0 %, t_R = 4.383 min
261	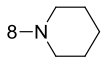	3416, 2930, 1617, 1538, 1363, 1143, 1107, 813, 737	Purity: 98.9 %, t_R = 4.827 min

The ^{1}H-NMR spectrum of compound (**249**) showed a broad singlet at δ 11.84 for one NH proton (-NH_d) of the indole ring. A doublet at δ 8.02 for one proton (ArH_a), a doublet of doublet at δ 7.43 for one proton (ArH_b) and a doublet at δ 7.36 for one proton (ArH_c) confirmed a total of three aromatic protons in the structure. It showed multiplets at δ 3.34-3.42 for two protons (-NHC$H_{2/f}$), multiplets at δ 2.42-2.54 for six protons (-NC$H_{2/k,l}$), at δ 1.59-1.71 for four

protons (-NCH$_2$C$H_{2/m}$), at δ 1.52-1.57 for two protons (-NCH$_2$C$H_{2/j}$), at δ 1.39-1.45 for two methylene protons (-NHCH$_2$C$H_{2/g}$) and at δ 1.25-1.34 for four protons (-C$H_{2/h,i}$). Its mass spectrum showed $[M]^+$ and $[M+2]^+$ ion peaks at 373 m/z and 375 m/z, respectively.

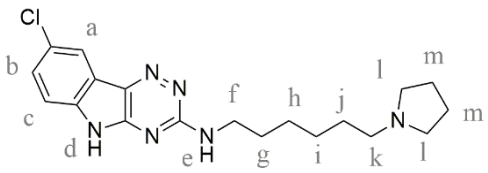

(**249**)

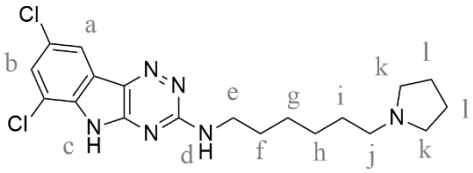

(**250**)

The ^{1}H-NMR spectrum of compound (**250**) showed a doublet at δ 7.43 for one proton (ArH_a) and a doublet at δ 7.39 for one proton (ArH_b) confirmed a total of two aromatic protons in the structure. It showed multiplets at δ 3.35-3.45 for two protons (-NHC$H_{2/e}$), at δ 2.36-2.51 for six protons (-NC$H_{2/j,k}$), at δ 1.56-1.71 for six protons (-NCH$_2$C$H_{2/i,l}$), at δ 1.42-1.49 for two protons (-NHCH$_2$C$H_{2/f}$) and at δ 1.31-1.40 for four protons (-C$H_{2/g,h}$). Its mass spectrum showed $[M]^+$ and $[M+2]^+$ ion peaks at 407 m/z and 409 m/z, respectively.

The ^{1}H-NMR spectrum of compound (**251**) showed a doublet at δ 8.18 for one proton (ArH_a), a doublet of doublet at δ 7.58 for one proton (ArH_b) and a doublet at δ 7.34 for one proton (ArH_c) confirmed a total of three aromatic protons in the structure. It showed a multiplet at δ 3.35-3.40 for two protons (-NHC$H_{2/f}$), a multiplet at δ 2.30-2.38 for six protons (NC$H_{2/k,l}$), a multiplet at δ 1.55-1.66 for six protons (-C$H_{2/j,m}$) and a multiplet at δ 1.28-1.46 for six protons (-C$H_{2/g-h}$). Its mass spectrum showed $[M]^+$ and $[M+2]^+$ ion peaks at 417 m/z and 419 m/z, respectively.

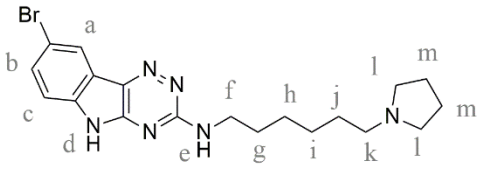

(**251**)

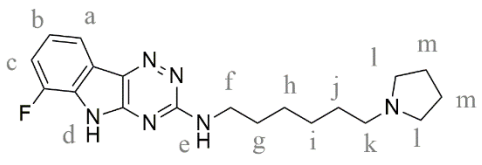

(**252**)

The ^{1}H-NMR spectrum of compound (**252**) showed a broad singlet at δ 11.82 for one NH proton (-NH_d) of the indole ring. A multiplet at δ 7.82-7.87 for one proton (ArH_a), a multiplet at δ 7.34-7.41 for one proton (ArH_c) and a multiplet at δ 7.25-7.33 for one proton (ArH_b) confirmed a total of three aromatic protons in the structure. It showed multiplets at δ 3.32-3.37 for two

protons (-NHC$H_{2/e}$), at 2.30-2.38 for six protons (-NC$H_{2/k,l}$), at δ 1.55-1.67 for six protons (-NCH$_2$C$H_{2/j,m}$), at δ 1.26-1.46 for six protons (-C$H_{2/g-i}$). Its mass spectrum showed $[M]^+$ and $[M+2]^+$ ion peaks at 356 m/z and 358 m/z, respectively.

The ^{1}H-NMR spectrum of compound (**253**) showed a broad singlet at δ 11.87 for one NH proton (NH_d) of the indole ring. A multiplet at δ 7.83-7.86 for one proton (ArH_a), a multiplet at δ 7.36-7.39 for one proton (ArH_b) and a multiplet at δ 7.26-7.31 for one proton (ArH_c) confirmed a total of three aromatic protons in the structure. It showed multiplets at δ 3.34-3.36 for two protons (-NHC$H_{2/e}$), δ 2.28-2.41 for six protons (-NC$H_{2/k,l}$), at δ 1.53-1.67 for six protons (-NCH$_2$C$H_{2/j,m}$) and at δ 1.25-1.46 for six protons (-C$H_{2/g-i}$). Its mass spectrum showed $[M]^+$ and $[M+2]^+$ ion peaks at 356 m/z and 358 m/z, respectively.

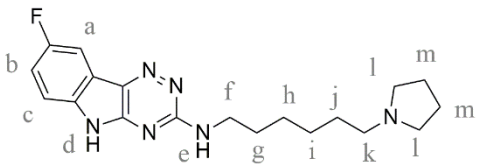

(**253**)

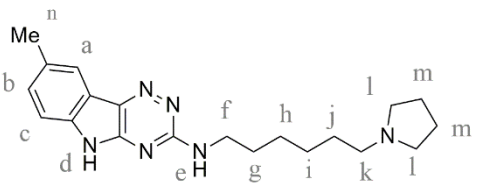

(**254**)

The ^{1}H-NMR spectrum of compound (**254**) showed a broad singlet at δ 11.61 for one amine proton (-NH_d) of the indole ring. A multiplet at δ 7.80-7.91 for one proton (ArH_a) and multiplets at δ 7.15-7.36 for two protons (Ar$H_{b,c}$) confirmed a total of three aromatic protons. It showed a multiplet at δ 3.29-3.40 for two protons (-NHC$H_{2/e}$), a singlet at δ 2.43 for three protons (ArC$H_{3/n}$), a multiplet at δ 2.30-2.41 for six protons (-NC$H_{2/k,l}$), a multiplet at δ 1.54-1.74 for six protons (-C$H_{2/j,m}$) and a multiplet at δ 1.10-1.49 for six protons (-C$H_{2/g-i}$). Its mass spectrum showed $[M]^+$ ion peak at 353 m/z.

The ^{1}H-NMR spectrum of compound (**255**) showed a broad singlet at δ 11.72 ppm for NH proton (-NH_c) of the indole ring. A singlet at δ 7.00 for one proton (ArH_a) and a singlet at δ 6.90 for one proton (ArH_b) confirmed total two aromatic protons. It showed a multiplet at δ 3.36-3.40 for two protons (-NHC$H_{2/e}$), a singlet at δ 2.78 for three protons (ArC$H_{3/n}$), multiplets at 2.37-2.49 for nine protons (-NC$H_{2/j,k}$, ArC$H_{3/m}$), a multiplet at δ 1.55-1.71 for six

protons (-NCH$_2$C$H_{2/i,l}$), a multiplet at δ 1.42-1.49 for two protons (-NHCH$_2$C$H_{2/f}$) and a multiplet at δ 1.30-1.40 for four protons (-C$H_{2/g,h}$). Its mass spectrum showed $[M+H]^+$ ion peak at 367 m/z.

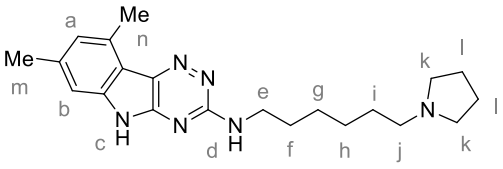

(255)

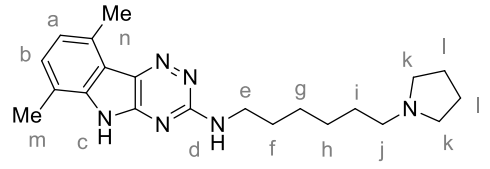

(256)

The ^{1}H-NMR spectrum of compound (**256**) showed a broad singlet at δ 11.44 for NH proton (NH_c) of the indole ring. A doublet at δ 7.14 for one proton (ArH_a) and a doublet at δ 6.95 for one proton (ArH_b) confirmed total two aromatic protons in the structure. It showed a multiplet at δ 3.32-3.34 for two protons (-NHC$H_{2/e}$), a singlet at δ 2.77 for three protons (ArC$H_{3/n}$), a singlet at δ 2.41 for methyl protons (ArC$H_{3/m}$), a multiplet at δ 2.29-2.38 for six protons (-NC$H_{2/j,k}$), a multiplet at δ 1.56-1.66 for six protons (-NCH$_2$C$H_{2/i,l}$) and a multiplet at δ 1.26-1.46 for six protons (-C$H_{2/f-h}$). Its mass spectrum showed $[M+H]^+$ ion peak at 367 m/z.

The ^{1}H-NMR spectrum of compound (**257**) showed a broad singlet at δ 13.21 for one NH proton (-NH_d) of the indole ring. A doublet at δ 8.31 for one proton (ArH_a), a doublet of doublet at δ 7.71 for one proton (ArH_c) and a doublet at δ 7.64 for one proton (ArH_c) confirmed a total of three aromatic protons in the structure. It showed a multiplet at δ 3.36-3.37 for two protons (-NHC$H_{2/e}$), a multiplet at δ 2.82-2.87 for two protons (ArC$H_{2/n}$), a multiplet at δ 2.31-2.38 for six protons (-NC$H_{2/k,l}$), a multiplet at δ 1.54-1.66 for six protons (-NCH$_2$C$H_{2/j,m}$) and multiplets at δ 1.28-1.44 for nine protons (-C$H_{2/g-i}$, -C$H_{3/o}$). Its mass spectrum showed $[M+H]^+$ ion peak at 367 m/z.

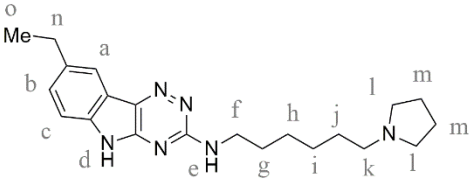

(257)

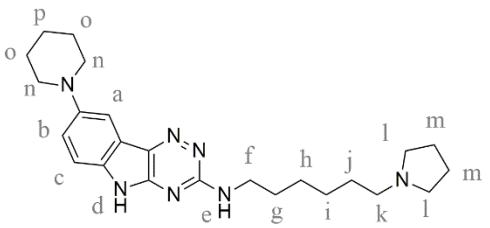

(261)

The ^{1}H-NMR spectrum of compound (**261**) showed a broad singlet at δ 11.98 for NH proton (NH_d) of the indole ring. A doublet at δ 8.18 for one proton

(ArH_a), a doublet of doublet at δ 7.58 for one proton (ArH_b) and a doublet at δ 7.34 for one proton (ArH_c) confirmed a total of three aromatic protons in the structure. It showed multiplets at δ 3.10-3.53 for six protons (-NHC$H_{2/f}$, -NC$H_{2/n}$), a multiplet at δ 2.27-2.40 for six (-NC$H_{2/k,l}$), a multiplet at δ 1.50-1.66 for six protons (-C$H_{2/j,m}$) and multiplet at δ 1.25-1.48 for nine protons (-C$H_{2/g-i}$, -C$H_{2/o}$C$H_{2/p}$). Its mass spectrum showed $[M+H]^+$ ion peak at 422 m/z.

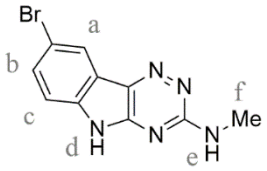

(**262**)

Synthesis of 8-bromo-*N*-methyl-5*H*-[1,2,4]triazino[5,6-*b*]indol-3-amine (**262**) was carried out by reaction of 8-bromo-3-(methylsulfonyl)-5*H*-[1,2,4]triazino[5,6-*b*]indole (**260**) with methylamine. The crude product was purified by flash chromatography. The IR spectrum of compound showed peaks at 3426 cm^{-1}(N-H stretching), 3076 cm^{-1}(aromatic C-H stretching), 2972 cm^{-1} (aliphatic C-H stretching), 1632 cm^{-1}(C=N stretching), 1552 cm^{-1} (C=C stretching) and 1193 cm^{-1} (C-N stretching). The ^{1}H-NMR spectrum of compound **(262)** showed a doublet at δ 8.16 for one proton (ArH_a), a doublet of doublet at δ 7.56 for one proton (ArH_b) and a doublet at δ 7.33 for one proton (ArH_c) confirmed a total of three aromatic protons in the structure. It showed singlet at δ 2.87 for three protons (-NHC$H_{3/e}$). Its mass spectrum showed $[M]^+$ and $[M+2]^+$ ion peaks at 278 and 280 m/z, respectively.

4.1.2.3. Biological evaluation of the synthesized compounds

The synthesized triazinoindole derivatives (**249-257, 261, 262**) (Series V in **Figure 4.1**) were evaluated for their multifactorial anti-AD activities, including cholinesterase inhibitory, antioxidant, cognition improving activities and acute toxicity in animal models detailed under the following subheadings:

4.1.2.3.1. Inhibition studies on cholinesterase enzymes,

4.1.2.3.2. Antioxidant activity [1,1-diphenyl-2-picrylhydrazyl (DPPH) radical scavenging activity],

4.1.2.3.3. *In vitro* blood-brain barrier permeation assay,

4.1.2.3.4. Assessment of cognitive improvement in animal model of AD which is subdivided into two parts:

4.1.2.3.4.1. Morris Water Maze test,

4.1.2.3.4.2. Neurochemical analysis,

4.1.2.3.5. Acute toxicity study.

4.1.2.3.1. Inhibition studies on cholinesterase enzymes

The potential of the synthesized compounds to inhibit cholinesterases (ChEs) was evaluated *in vitro* using a spectrophotometric method of Ellman *et. al.* as discussed previously.[115,117] The obtained IC_{50} values of the compounds for the two enzymes and their selectivity over each other are summarized in **Table 4.21**. All the tested compounds showed IC_{50} values for both the enzymes comparable to the parent compound (**199**). Amongst them, compounds (**261**) exhibited the highest AChE (IC_{50} value of 0.32 μM) and BuChE (IC_{50} value of 0.21 μM) inhibitory activity.

Insertion of halo-substituent in the indole ring of the parent compound (**199**) showed moderate decline in cholinesterase inhibitory activity as observed in compounds (**249-253**). Similarly, mono alkyl substituents i.e. methyl group at C_8 position in compound (**254**) and ethyl group at C_8 position in compound (**257**) were also detrimental to the ChE inhibitory activity, whereas di-alkyl substitutions i.e. 6, 9-dimethyl and 7, 9-dimethyl substituents in compound (**255**) and compound (**256**), respectively improved the BuChE inhibitory activity. Compound (**255**) showed improvement in AChE and BuChE inhibitory activity (IC_{50} values of 0.41 μM and 0.23 μM, respectively). Compound (**261**) with piperidine ring at C_8 substituent showed significant improvement in the AChE and BuChE inhibitory activities in comparison to the parent compound (**199**). Compound (**261**) showed 1.75-fold and 3.2-fold increase in AChE and BuChE inhibitory activities, respectively in comparison to compound (**199**). Removal of pyrrolidine ring from the compound (**251**) led to compound (**262**) which showed moderate ChE inhibition, suggesting that this basic centre is an indispensable pharmacophore for cholinesterase inhibition.

Table 4.21. *In vitro* inhibition of AChE and BuChE, and selectivity index (SI) of compounds (249-257, 261, 262)

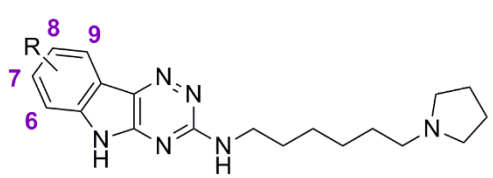

(249-257, 261)

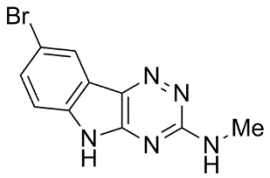

(262)

Compd	R	IC_{50} ± SEM (µM)		SI[c]	RP of DPPH % inhibition at 20 µM
		AChE[a]	BuChE[b]		
249	8-Cl	0.98 ± 0.09	1.18 ± 0.13	1.20	55.3 ± 2.4
250	6,8-diCl	1.06 ± 0.12	0.94 ± 0.07	0.89	58.6 ± 2.1
251	8-Br	1.45 ± 0.23	1.14 ± 0.15	0.78	55.1 ± 3.7
252	6-F	0.91 ± 0.04	1.42 ± 0.21	1.56	54.3 ± 2.8
253	8-F	0.94 ± 0.03	1.53 ± 0.10	1.62	52.7 ± 2.4
254	8-Me	1.16 ± 0.09	1.84 ± 0.17	1.58	51.4 ± 3.3
255	6,9-diMe	0.41 ± 0.12	0.23 ± 0.08	0.56	49.5 ± 2.7
256	7,9-diMe	0.54 ± 0.15	0.79 ± 0.12	1.46	48.4 ± 3.2
257	8-Et	1.54 ± 0.18	1.70 ± 0.25	1.10	52.6 ± 1.8
261	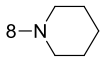	0.32 ± 0.04	0.21 ± 0.05	0.65	55.8 ± 2.1
262	-	15.2 ± 0.15	8.37 ± 1.02	0.55	54.7 ± 2.7
Tacrine		0.056 ± 0.01	0.008 ± 0.00	0.14	6.4 ± 0.3
Donepezil		0.023 ± 0.01	1.87 ± 0.08	81.3	4.9 ± 1.2
Ascorbic acid		nd	nd	-	IC_{50} = 13.9 ± 1.8 µM

[a]AChE from human erythrocytes; IC_{50}, 50% inhibitory concentration (means ± SEM of three experiments), [b]BuChE from equine serum, [c]Selectivity index = IC_{50} (BuChE)/IC_{50} (AChE), [d]RP of DPPH (%) = reduction percentage of DPPH.

4.1.2.3.2. Antioxidant activity [1,1-diphenyl-2-picrylhydrazyl (DPPH) radical scavenging activity]

As previously discussed, the DPPH radical scavenging assay was used to assess the antioxidant/free radical scavenging potential of the compounds. Antioxidant activity of the selected compounds was estimated by their ability to

reduce DPPH· radical (purple color) to DPPHH (yellow) and the corresponding radical-scavenging potential was evaluated by the decrease in the absorbance at 517 nm.[120] All the test compounds exhibited notable free radical scavenging activity ranging from 48-56 % at 20 μM concentrations (**Table 4.21**). Compound (**250**) showed better free radical scavenging activity (58.6 % at 20 μM concentrations) whereas tacrine and donepezil were found to be devoid of significant free radical scavenging activity at these concentrations.

4.1.2.3.3. *In vitro* blood-brain barrier permeation assay

The ability of compound (**261**) to penetrate into the brain was assessed using a parallel artificial membrane permeation assay (PAMPA) as mentioned earlier.[125,126] As shown in **Table 4.22**, compound (**261**) showed P_e value of 7.46 which was above the limit (**Table 4.14**). Therefore, P_e(exp) suggested a potential of the compounds to cross the BBB by passive diffusion.

Table 4.22. Permeability (P_e 10^{-6} cm s^{-1}) of compound (261) and donepezil in the PAMPA-BBB permeation assay with their predicted penetration into the CNS

Compd	(P_e 10^{-6} cm s^{-1})	Prediction
261	7.46± 2.1	CNS+
Donepezil	14.3 ± 1.7	CNS+

Data are expressed as mean ± SEM of three independent experiments.

4.1.2.3.4. Assessment of cognitive improvement in animal model of AD

The work carried out to assess the cognitive improvement induced by the test compounds in animal model of AD is described under two subheadings:

4.1.2.3.4.1. Morris Water Maze test and

4.1.2.3.4.2. Neurochemical analysis

4.1.2.3.4.1. Morris Water Maze test

To determine the effect of compound (**261**) on cognitive improvement, an animal model of scopolamine-induced amnesia in the rodents was adopted.[127-129]

Morris water maze learning test was utilized to assess the hippocampal-dependent spatial learning ability of the animals. This test assesses the reference

or long-term memory by observing the escape latency. During the last 5 days of the treatment period, escape latency time (ELT)[130] was recorded for the animals of the experimental groups. The ELT was significantly prolonged (**Figure 4.13-A**) by scopolamine treatment (1.4 mg/kg, ip). In donepezil (5 mg/kg, po) treated group, ELT was considerably shortened as compared to the scopolamine-treated control group. Compound (**261)** (5 mg/kg and 10 mg/kg, po) significantly reduced ELT as compared to the scopolamine-treated control group. This result revealed that the animals retained the previous memory in the Morris water maze test, showing spatial memory improvement.

4.1.2.3.4.2. Neurochemical analysis

After completion of the MWM test, the effects of scopolamine and compound (**261**) on cholinesterase levels and oxidant stress parameters in brain were assessed. Scopolamine treatment significantly increases the cholinesterase levels in the brain. The effect of compound (**261**) on the brain cholinesterase levels was assessed in mice using Ellman's method. The inflated levels of AChE (**Figure 4.13-B**) and BuChE (**Figure 4.13-C**) were significantly attenuated by compound (**261**) at a dose equivalent to donepezil. Malondialdehyde (MDA), catalase (CAT), dopamine and glycine levels in the brain were also assessed in order to further perceive the anti-amnesic effects of compound (**261**) as shown in **Figure 4.13**.

Scopolamine-treated group showed elevated MDA levels (**Figure 4.13-C**) in comparison to the vehicle-treated control group. Treatment of compound (**261**) to the amnesic mice appreciably attenuated the increase in MDA levels in the brain (**Figure 4.13-C**) as compared to the scopolamine-treated group. Scopolamine treatment significantly reduced the CAT levels (**Figure 4.13-D**) in the brains of the treated animals compared to the vehicle-treated control group animals. However, treatment of the amnesic mice with compound (**261**) elevated the CAT levels considerably (**Figure 4.13-D**). These results revealed the anti-oxidant potential of the test compound (**261**).

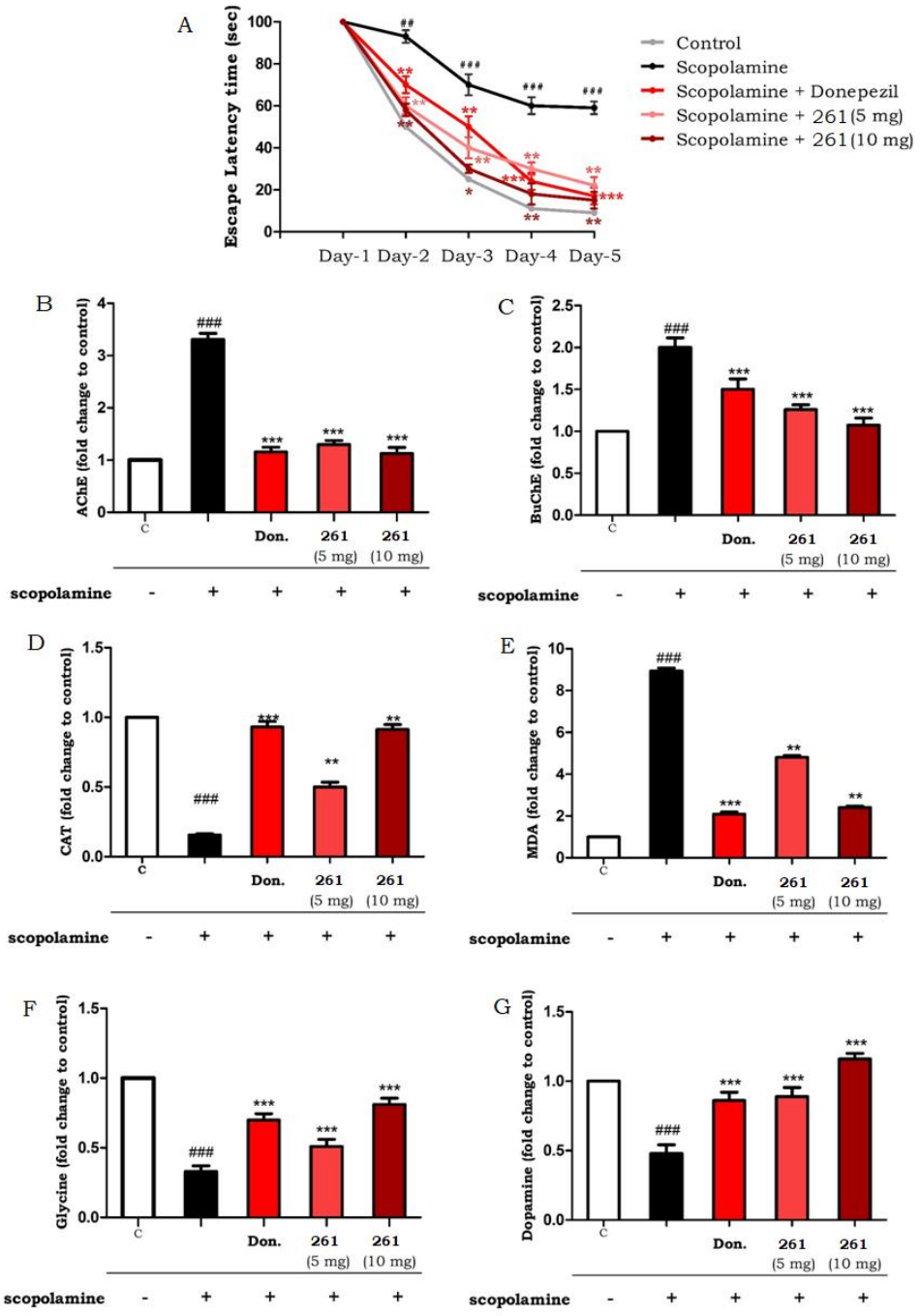

Figure 4.13. MWM test, *ex vivo* anticholinesterase and antioxidant activities, neurotransmitters' level in scopolamine- induced amnesic brain. Data are expressed as mean ± SEM (n = 7): (###) $p < 0.001$, (#) $p < 0.05$ vs vehicle-treated control group; (***) $p < 0.001$, (**) $p < 0.01$, vs scopolamine-treated control group. C = vehicle-treated control group.

Scopolamine-treated group showed reduced levels of glycine (**Figure 4.13-E**) compared to the vehicle-treated control group. Treatment of the amnesic mice with compound (**261**) increased the glycine levels (**Figure 4.13-**

E) as compared to the scopolamine-treated group. The elevated levels of glycine could improve the NMDA receptor hypofunction which is helpful in reviving the cognitive function and memory. Furthermore, the scopolamine-treated group showed reduced levels of dopamine (**Figure 4.13-F**) compared to the vehicle-treated control group. Treatment of the amnesic mice with compound (**261)** increased the dopamine levels (**Figure 4.13-F**) as compared to the scopolamine-treated group.

Results of these behavioral studies and neurochemical analysis in scopolamine-induced amnesia models revealed that compound (**261)** possessed the ability to reverse the memory-deficit as well as manage the oxidative stress-induced dementia.

4.1.2.3.5. Acute toxicity study

Acute toxicity of compound (**261**), the most promising candidate of the series, was determined according to OECD 423 guidelines.[131] Wistar female rats were dosed with compound (**261**) at a dose of 2000 mg/kg (n = 3 per group) by oral administration. After administration of the compound, the animals were monitored continuously for the first 4 hrs for any abnormal behavior and mortality. Later on the animals were intermittently observed for the next 24 hrs and occasionally for 14 days for any sign of delayed effects. All the animals survived in the duration of the study period and appeared healthy in terms of fur sleekness, water and food consumption, and body weight. On the 15th day, all the animals were sacrificed for macroscopic examination of the heart, liver, and kidneys for any damage. No damage was observed in these organs. The results from the study showed that mice treated with compound (**261**) did not produce any acute toxicity or mortality immediately or during the post-treatment period. Therefore, compound (**261**) can be considered to be nontoxic and well tolerated at doses up to 2000 mg/kg.

4.1.2.4. Computational studies of the most promising compound

Computational studies of the most promising compound (**261**) were performed to offer an insight into the binding mode of the compound with the target proteins and to predict its *in silico* ADMET properties. The work carried out under this head is described into the following two subheadings:

4.1.2.4.1. Docking studies of compound (**261**) with target proteins and

4.1.2.4.2. Prediction of virtual physicochemical and pharmacokinetics parameters of the most promising compound (**261**).

4.1.2.4.1. Docking studies of compound (261) with target proteins

To have a view of the binding mode of the most active compound (**261**) with the ChEs, docking studies were performed with the active sites of *Tc*AChE (PDB code: 2CKM)[132] (**Figure 4.14**) and *h*BuChE (PDB code: 4BDS)[132] (**Figure 4.15**).

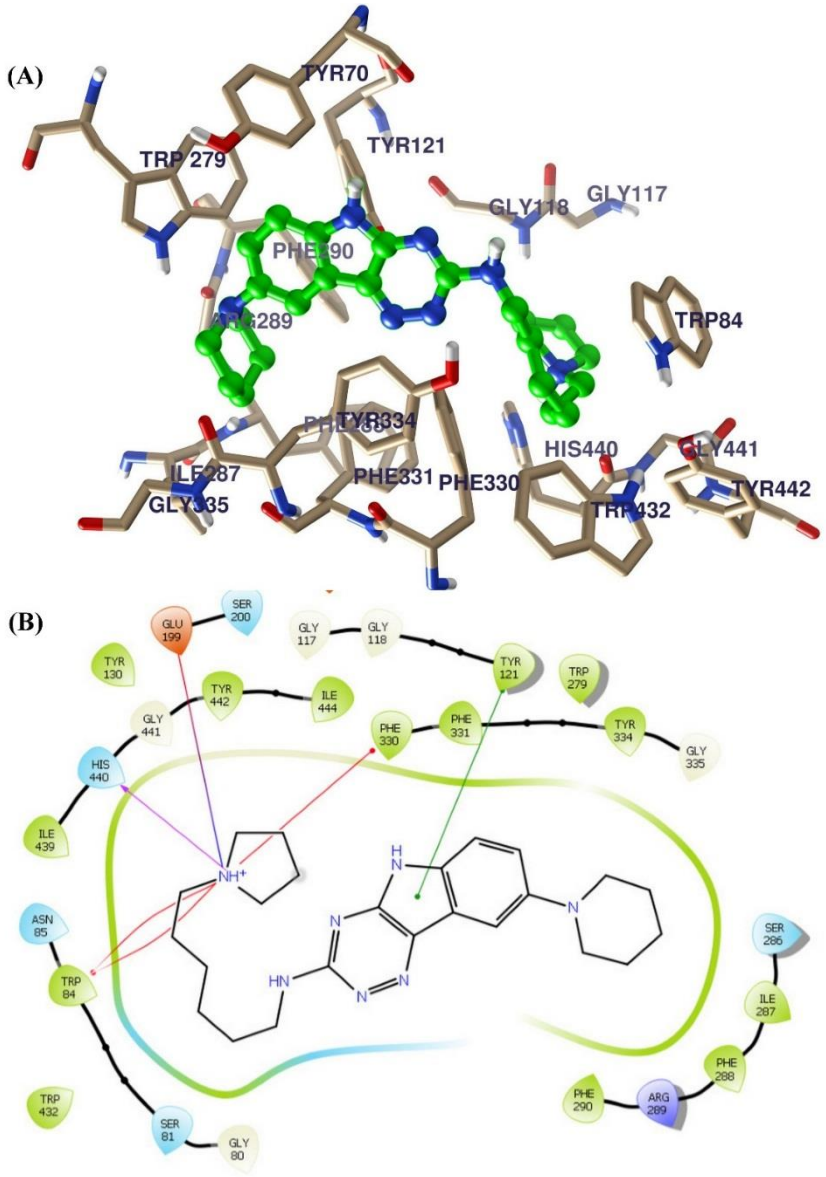

Figure 4.14. Docking model of compound (**261**) with *Tc*AChE (PDB ID: 2CKM). (A) Binding mode of **261** in the active site of *Tc*AChE. (B) Ligand interaction diagram of **261** with *Tc*AChE.

In the docking study of **261** with AChE, the planar tricyclic scaffold was observed interacting with the PAS of the active site gorge and the pyrrolidine ring of compound (**261**) was observed to be oriented well towards the CAS (**Figure 4.14**). At PAS, the tricyclic scaffold exhibited very strong π-π interaction with Tyr121 (*h*AChE: Tyr124). At physiological *p*H, the nitrogen of the pyrrolidine ring could be protonated and showed highly stable cation-π interactions with Trp84 and Phe330 (*h*AChE: Trp86, Phe337) along with a hydrogen bonding and salt bridge interaction with Glu199 (*h*AChE: Glu202).

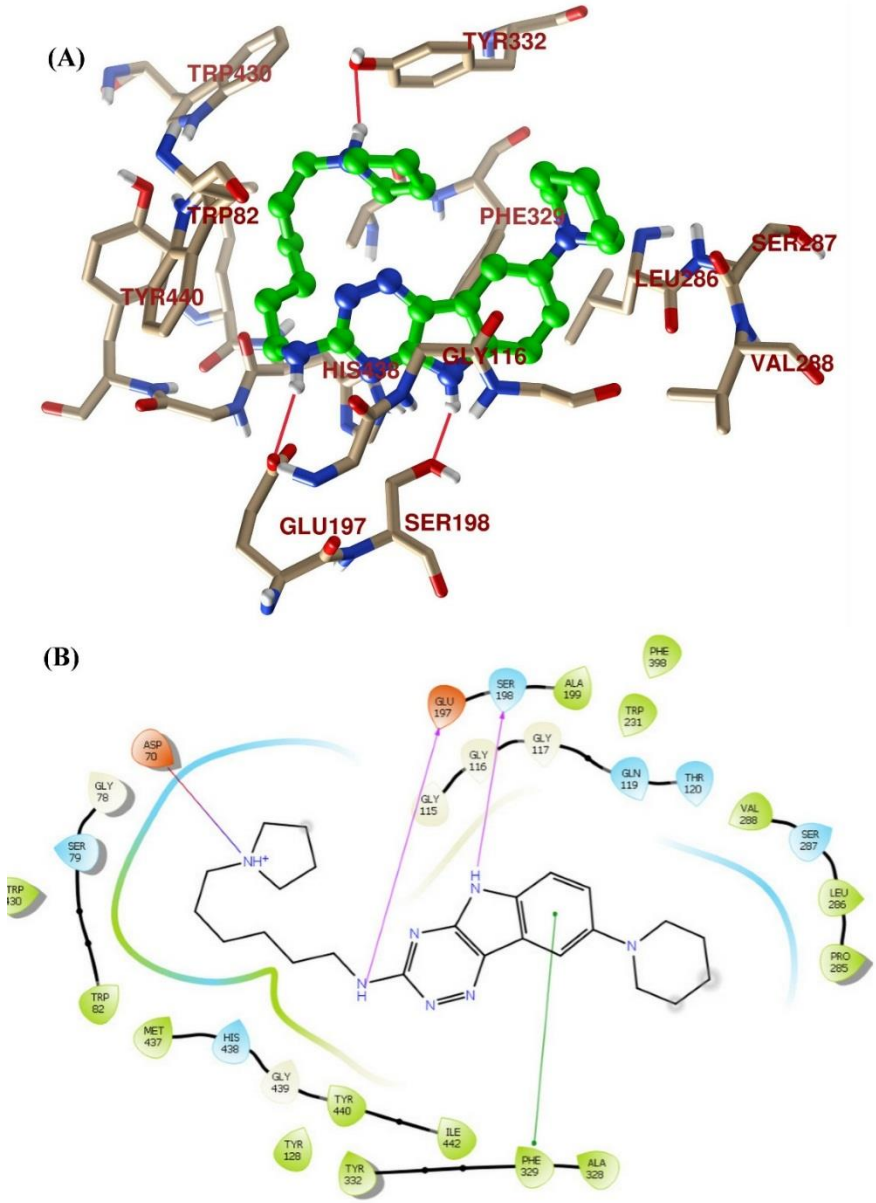

Figure 4.15. Docking model of compound (**261**) with *h*BuChE (PDB ID: 4BDS). (A) Binding mode of **261** in the active site of *h*BuChE. (B) Ligand interaction diagram of **261** with *h*BuChE.

The binding mode of **261** with the active sites of BuChE is represented in **Figure 4.15**. The terminal aromatic ring of the triazinoindole scaffold exhibited π–π interactions with the Phe329. The hydrogen bonding between the -NH of the indole ring and Ser198 imparted stability to the ligand-receptor complex. The -NH group at the third position of the triazine ring also showed hydrogen bonding with Glu197. Further stability to this complex was also provided by the protonated nitrogen of the pyrrolidine by forming cation-π interaction with Asp70 along with a hydrogen bonding interaction with Tyr332.

4.1.2.4.2. Prediction of virtual physicochemical and pharmacokinetics parameters of the most promising compound (261)

For the most active compound (**261**) along with donepezil and tacrine as reference drugs, pharmacokinetics profile indicators like Lipinski's parameters, QPlog$P_{o/w}$, PSA, QDCK, QPlogBB, QPPCaco, QPlogKhSa, etc. were predicted with QikProp module **(Table 4.23)**.[136]

Compound (**261**) does not break Lipinski's rule of five[137] at all, predicting it to be a promising drug candidate. Compound (**261**) possesses 8 rotatable bonds and TPSA values of 75.37 $Å^2$. QPCaco-2 value below 500 predicts moderate to good oral absorption. Similarly, human oral absorption percent (% HOA) value also supports the prediction of oral bioavailability of the test compounds. The test ligand is predicted to have a borderline CNS penetration as it has a value of CNS as 1 and a value of logBB as -0.8. Compound (**261**) showed compliance with the recommended values for QPlogKhsa, indicating that the compound would have low serum albumin binding and the unbound fraction would have access to the putative receptor drug target. Value of #star for compound (**261**) indicates its drug-likeness. Additionally, a compound possessing tertiary nitrogen-containing moiety which is a common feature in many CNS acting drugs, shows a higher degree of brain permeation.[140] Thus, it can be stated that compound (**261**) is predicted to possess a good pharmacokinetics profile, which would enhance its biological significance.

Table 4.23. Predicted ADMET indicators of compound (261), donepezil and tacrine

Parameter	Limit	Comp (261)	Donepezil	Tacrine
MW	130-725	421.587	379.498	198.267
HBA	2-20	6.5	5.5	2
HBD	0-6	2	0	1.5
NRB	0-8	8	6	1
QPlogP$_{o/w}$	-2 to 6.5	4.5	4.242	2.536
PSA	7 to 200	75.37	46.234	33.825
Volume	500-2000	1474.544	1248.451	701.299
ReFG	0-2	0	0	0
SASA	300-1000	833.996	681.675	425.06
Rule of Five (violation)	0-1	0	0	0
CNS	-	0	1	1
QPMDCK	-	112.817	589.289	1602.036
QPlogBB	-3 to 1.2	-0.8	0.223	0.047
QPPCaco	-	231.988	1070.771	2965.755
QPlogKhSa	-1.5 to 1.5	0.929	0.516	0.049
QPlogS	-6.5 to 0.5	-6.395	-4.059	-3.036
% HOA	0-100	95.663	100	100
#star	0-5	0	0	0

MW: molecular weight, HBA: hydrogen-bond acceptor atoms, HBD: hydrogen-bond donor atoms, QPlogPo/w: predicted octanol/water partition coefficient, PSA: polar surface area, ReFG: number of reactive functional groups, SASA: total solvent accessible surface area, CNS: predicted central nervous system activity on a -2 (inactive) to +2 (active) scale, QDCK: predicted apparent MDCK cell permeability in nm/s, QPPCaco: caco-2 cell permeability in nm/s, QPlogBB: brain/blood partition coefficient, QPlogKhsa: binding to human serum albumin, QPlogS: predicted aqueous solubility, % HOA: human oral absorption on 0–100% scale, #star: number of parameters' values that fall outside the 95 % range of similar values for known drugs.

4.2. Carbazole-based multifunctional anti-AD agents

The work carried out has been discussed under the following two main heads:

4.2.1. Carbazole-based stilbene derivatives and

4.2.2. Carbazole-based azahelicene derivatives.

4.2.1. Carbazole-based stilbene derivatives

The work carried out under this heading has been further divided into 4 subheadings i.e. designing aspect, chemical studies, biological studies, and computational studies as mentioned below:

4.2.1.1. Designing of novel carbazole based stilbene derivatives as anti-AD agents,

4.2.1.2. Synthesis and characterization of the designed carbazole based stilbene compounds,

4.2.1.3. Biological evaluation of the synthesized compounds, and

4.2.1.4. Computational studies of the most promising compound.

4.2.1.1. Designing of novel carbazole-based stilbene derivatives as anti-AD agents

The multifactorial nature of AD demands treatment with MTDLs to assault the key pathological hallmarks. Although ChEIs provide only symptomatic and transient benefits to the patients, they still remain the drugs of choice. Neurotoxic Aβ plaques, metal ion dyshomeostasis and oxidative stress play a crucial role in the pathogenesis of AD. However, targeting these factors all alone might not be enough to combat such a highly complex pathological disease like AD. So, cholinesterase inhibitors endowed with additional Aβ aggregation inhibitory, metal chelating and antioxidant activities might be the competent candidates to confront this multifaceted disease.

Carbazole is an important nitrogen containing heterocycle widely present in many phytochemicals with a large array of biological activities associated with AD.[150] It has been reported that the carbazole derivatives possess cholinesterase inhibitory,[71] Aβ aggregation inhibitory,[151] ROS scavenging, and protect neurons against oxidative damage.[152] Recently, various hybrid molecules having carbazole moiety incorporated with other biological

active moieties like carbazole-ferulic acid hybrid (**14**),[71] carbazole-tacrine hybrid (**25**)[76] and carbazole-thiazole hybrid (**263**)[153] were developed as potential MTDLs for AD (**Figure 4.16**). Plethora of biological activities associated with carbazole make it an interesting building block in the search for new anti-AD agents.

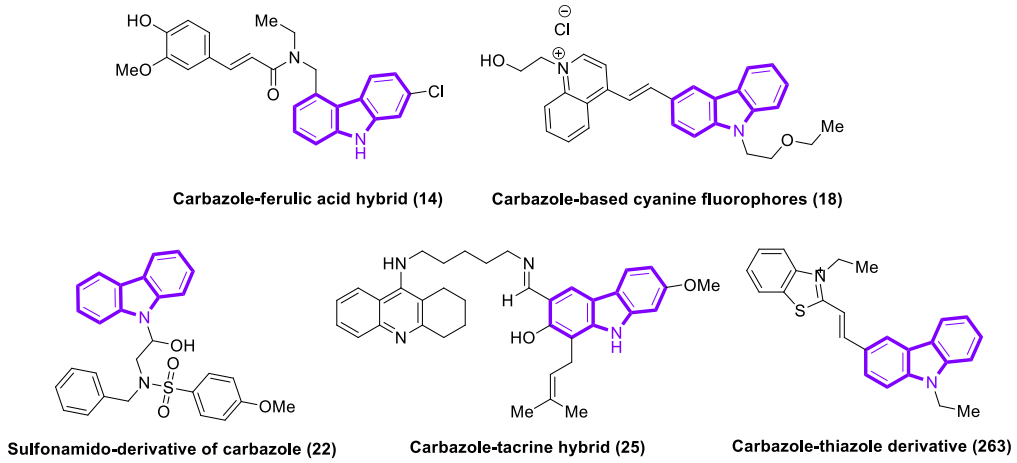

Figure 4.16. Chemical structures of reported carbazole-based anti-AD agents.

Resveratrol (3,5,4'-trihydroxy-*trans*-stilbene) (**39**) is a naturally occurring stilbene derivative possessing multiple anti-AD properties i.e. Aβ aggregation inhibitory,[154] neuroprotective[155] and antioxidant activities.[156] Several stilbene derivatives with encouraging Aβ binding abilities have been developed as Aβ imaging probes and Aβ aggregation inhibitors during the last two decades (**Figure 4.17**).[81]

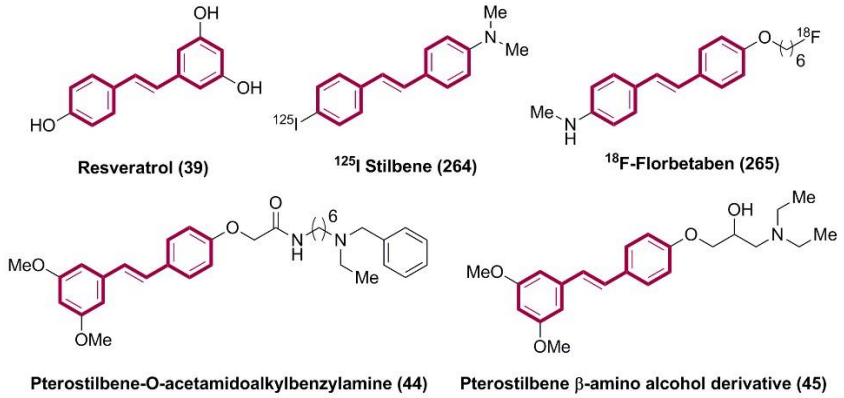

Figure 4.17. Chemical structures of some reported stilbene derivatives.

In combination with other bioactive moieties, these stilbene hybrids showed cholinesterase inhibitory, metal chelating, Aβ aggregation inhibitory, and free radical scavenging activities.[78,83,87] The central lipophilic scaffold with

the terminal amine group is the salient feature of most of the reported stilbene derivatives which might have an impact on their anti-AD properties.

A combination of the pharmacophoric moieties having different activities offering some novel hybrids brought new hope for the treatment of AD. By molecular hybridization approach, fusion of one pharmacophore to other results into a highly integrated scaffold with lower molecular weight. Here, the carbazole based stilbene scaffold was generated by the fusion of carbazole ring with stilbene scaffold. We have previously reported substituted triazinoindole derivatives as anti-AD agents, in which pyrrolidine and piperidine moieties played an indispensable role in offering cholinesterase inhibitory activity. Here, we have designed two series of carbazole based stilbene derivatives in which the heterocyclic amines were linked with the designed scaffold using linkers endowed with additional anti-AD property (**Figure 4.18**).

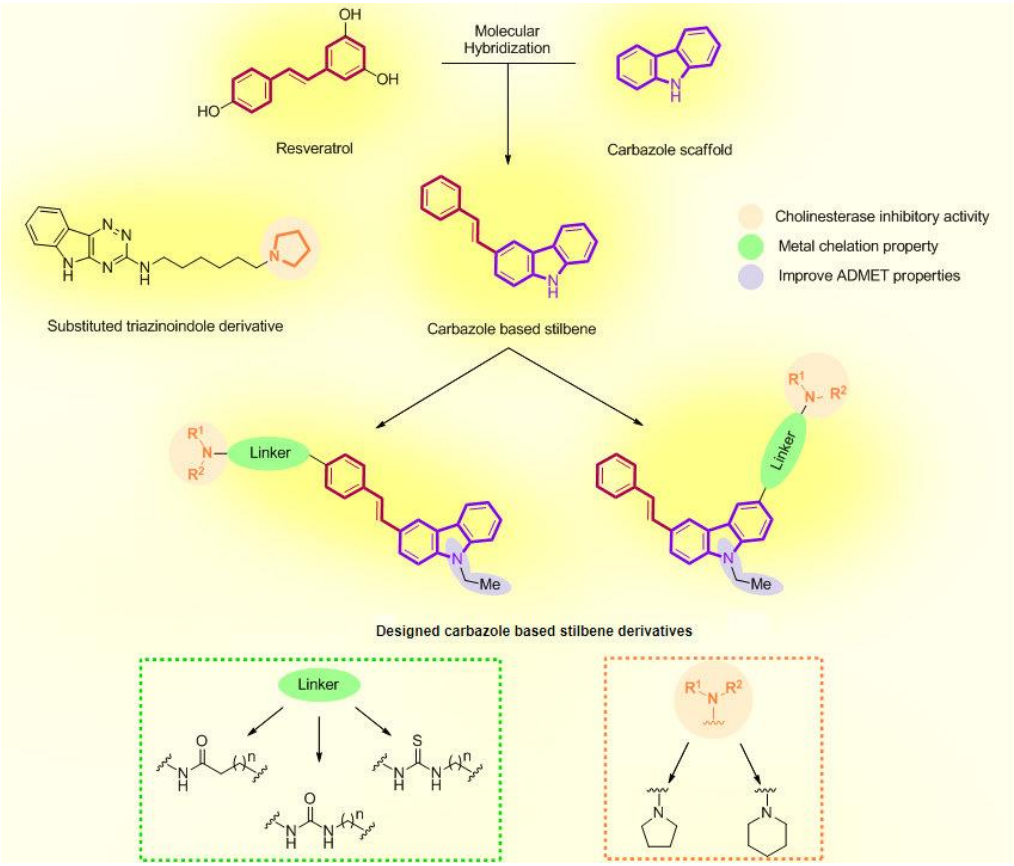

Figure 4.18. Molecular hybridization approach to design carbazole-based stilbene derivatives.

4.2.1.2. Synthesis of the designed carbazole-based stilbene derivatives

Based on the attachment of heterocyclic amine with proper linkers to designed scaffold's either site, these carbazole-based stilbene derivatives have been divided into two series i.e. Series-1 where the attachment was at carbazole ring and Series-2 where the attachment was at phenyl ring (**Figure 4.18**).

The synthetic work has been divided into two subheadings as mentioned below:

4.2.1.2.1. Synthesis of carbazole-based stilbene derivatives (**Series-1**),

4.2.1.2.2. Synthesis of carbazole-based stilbene derivatives (**Series-2**).

4.2.1.2.1. Synthesis of carbazole-based stilbene derivative (Series-1)

Synthesis of novel carbazole-based stilbene derivatives (Series-1) was carried out from commercially available carbazole. The synthetic procedures and characterization of the synthesized derivatives have been discussed under the following subheadings:

4.2.1.2.1.1. Synthesis of a key amine intermediate (*E*)-9-ethyl-6-styryl-9*H*-carbazol-3-amine (**271**),

4.2.1.2.1.2. Synthesis of (*E*)-*N*-(9-ethyl-6-styryl-9*H*-carbazol-3-yl) aminoalkylamines (**275-280**),

4.2.1.2.1.3. Synthesis of (*E*)-1-(9-ethyl-6-styryl-9*H*-carbazol-3-yl) aminoalkylureas (**281-286**).

4.2.1.2.1.1. Synthesis of a key amine intermediate (*E*)-9-ethyl-6-styryl-9*H*-carbazol-3-amine (271)

Synthesis of a key intermediate (*E*)-9-ethyl-6-styryl-9*H*-carbazol-3-amine (**271**) was carried out from carbazole as depicted in **Scheme.4.7**.

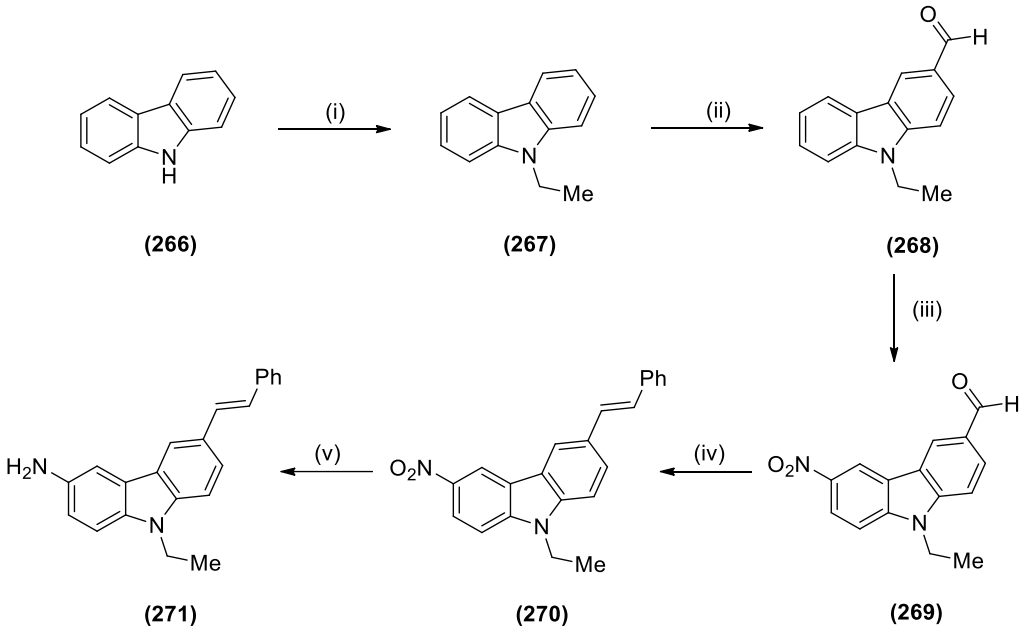

Scheme 4.7. Synthesis of a key intermediate (*E*)-9-ethyl-6-styryl-9*H*-carbazol-3-amine (**271**)**.** Reagents and conditions: (i) EtBr, NaOH, DMSO, rt; (ii) $POCl_3$, DMF; (iii) conc. HNO_3, AcOH; (iv) (a) benzyltriphenylphosphonium bromide, LiOH, IPA, reflux, (b) I_2, toluene, reflux; (v) $SnCl_2$, THF, MeOH, reflux.

Commercially available carbazole (**266**) was reacted with ethyl bromide in the presence of aqueous sodium hydroxide solution in DMSO to obtain *N*-ethylcarbazole (**267**).[157] The IR spectrum of compound (**267**) showed peaks at 3049 cm^{-1} (aromatic C-H stretching), at 2869 cm^{-1} (aliphatic C-H stretching), at 1596 cm^{-1} (C=C stretching) and disappearance of N-H stretching peak.

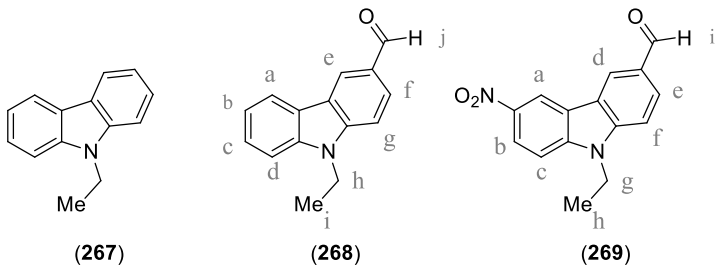

Mono-formylation of compound (**267**) by Vilsmeier-Haack formylation method using *N,N*-dimethylformamide (DMF) and phosphorus oxychloride gave 9-ethyl-3-formylcarbazole (**268**).[158] The IR spectrum of compound (**268**)

showed peaks at 3049 cm^{-1} (aromatic C-H stretching), 2971 cm^{-1} (aliphatic C-H stretching), 2822 cm^{-1} and at 2743 cm^{-1} (aldehyde C-H stretching), 1679 cm^{-1} (aldehyde C=O stretching) and at 1588 cm^{-1} (C=C stretching). The ^{1}H-NMR spectrum of compound (**268**) showed a singlet at δ 10.12 for one aldehyde proton (-CH_jO). A singlet at δ 8.64 for one proton (ArH_e), a doublet at δ 8.18 for one proton (ArH_f), a doublet at δ 8.04 for one proton (ArH_g) and multiplet at δ 7.37-7.58 for four protons (ArH_{a-d}) confirmed a total of seven aromatic protons in the structure. The aliphatic protons appeared as a quartet at δ 4.44 for two protons (-NC$H_{2/h}$$CH_3$) and a triplet at δ 1.49 for three protons (-NCH_2C$H_{3/i}$). Its mass spectrum showed $[M+H]^+$ ion peak at 224 m/z.

Nitration of compound (**268**) by nitric acid in presence of acetic acid gave 9-ethyl-6-nitro-9*H*-carbazole-3-carbaldehyde (**269**).[159] Its IR spectrum showed peaks at 2821 cm^{-1} and 2729 cm^{-1} (aldehyde C-H stretching), 1686 cm^{-1} (C=O stretching), 1595 cm^{-1} (asymmetrical N-O stretching) and at 1315 cm^{-1} (symmetrical N-O stretching). The ^{1}H-NMR spectrum of compound (**269**) showed a singlet at δ 10.16 for one aldehyde proton (-CH_iO). It showed a singlet at δ 9.09 for one proton (ArH_a), a singlet at δ 8.69 for one proton (ArH_d), a doublet at δ 8.47 for one proton (ArH_b), a doublet at δ 8.15 for one proton (ArH_e), a doublet at δ 7.61 for one proton (ArH_c), a doublet at δ 7.53 for one proton (ArH_f) confirming a total of six aromatic protons in the structure. The aliphatic protons appeared as a quartet at δ 4.68 for two protons (-NC$H_{2/g}$$CH_3$) and a triplet at δ 1.54 for three protons (-NCH_2C$H_{3/h}$). Its mass spectrum showed $[M+H]^+$ ion peak at 269 m/z.

Wittig reaction of 9-ethyl-6-nitro-9*H*-carbazole-3-carbaldehyde (**269**) with benzyltriphenylphosphonium bromide in the presence of lithium hydroxide in *iso*propyl alcohol (IPA) gave a mixture of *cis* and *trans* 9-ethyl-3-nitro-6-styryl-9*H*-carbazole. This isomeric mixture was converted to a single *trans* isomer (**270**) by refluxing it in toluene in presence of catalytical amount of iodine.[160] Its IR spectrum showed peaks at 2986 cm^{-1} and 2939 cm^{-1} (aliphatic C-H stretching), 1592 cm^{-1} (asymmetrical N–O stretching) and at 1315 cm^{-1} (symmetrical N–O stretching)**.** It also showed disappearance of characteristic IR peaks for aldehyde group. The ^{1}H-NMR spectrum of compound (**270**) showed a doublet at δ 9.00 for one proton (ArH_a), a doublet of doublet at δ 8.38 for one proton (ArH_b), a singlet at δ 8.23 for one proton (ArH_d), a doublet at δ

7.76 for one proton (ArH_c), multiplet at δ 7.57-7.59 for two protons (Ar$H_{e,f}$), multiplet at δ 7.16-7.45 for seven protons (Ar$H_{g\text{-}i,}$ vinylic-$H_{j,k}$). The aliphatic protons appeared as a quartet at δ 4.40 for two protons (–NC$H_{2/h}$$CH_3$) and a triplet at δ 1.48 for three protons (–$NCH_2C$$H_{3/i}$). Its mass spectrum showed $[M+H]^+$ ion peak at 343 m/z.

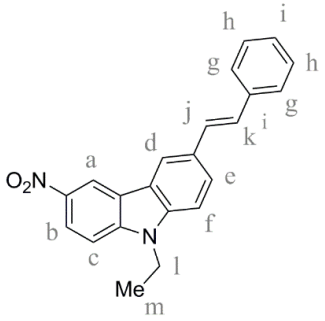

(**270**)

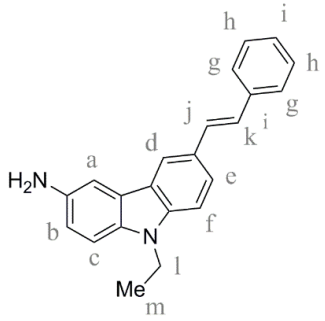

(**271**)

9-Ethyl-6-styryl-9*H*-carbazole-3-amine (**271**) was synthesized by reduction of the nitro group in compound (**270**) by stannous chloride. This key amine intermediate was purified by recrystallization in methanol. Its IR spectrum showed peaks at 3401 cm^{-1} and 3304 cm^{-1} (primary N-H stretching), at 3053 cm^{-1} (aromatic C-H stretching), at 2971 cm^{-1} (aliphatic C-H stretching), 1331 cm^{-1} (C-N stretching) and 1600 cm^{-1} (N-H bending). It also showed disappearance of characteristic peaks (N-O stretching) for nitro group. The NMR spectrum of compound (**271**) showed a singlet at δ 8.15 for one proton (Ar*H*), a multiplet at δ 7.65-7.67 for one proton (Ar*H*), multiplet at δ 7.57-7.59 for two protons (Ar*H*), multiplet at δ 7.23-7.48 for seven protons (Ar*H*, vinylic-*H*), a multiplet at δ 7.12-7.17 for one proton (Ar*H*) and a multiplet at δ 6.94-6.96 for one proton (Ar*H*) confirming a total of eleven aromatic protons and two vinylic protons in the structure. The aliphatic protons appeared as a quartet at δ 4.32 for two protons (-NC$H_{2/h}$$CH_3$) and triplet at δ 1.42 for three protons (-$NCH_2C$$H_{3/i}$). Its mass spectrum showed $[M+H]^+$ ion peak at 313.5 m/z.

4.2.1.2.1.2. Synthesis of (*E*)-*N*-(9-ethyl-6-styryl-9*H*-carbazol-3-yl)amino alkylamides (275-280)

Synthesis of (*E*)-*N*-(9-ethyl-6-styryl-9*H*-carbazol-3-yl)aminoalkyl amide derivatives (**275-280**) were carried out from the amine intermediate (**271**) in two steps as depicted in **Scheme 4.8**. In the first step, acylation of compound (**271**) was carried out by reacting it with respective acid chlorides to obtain

compounds (**272-274**). These amide intermediates (**272-274**) in the second step, were reacted with respective alicyclic amines to obtain the titled compounds (**275-280**) which were purified by crystallization.

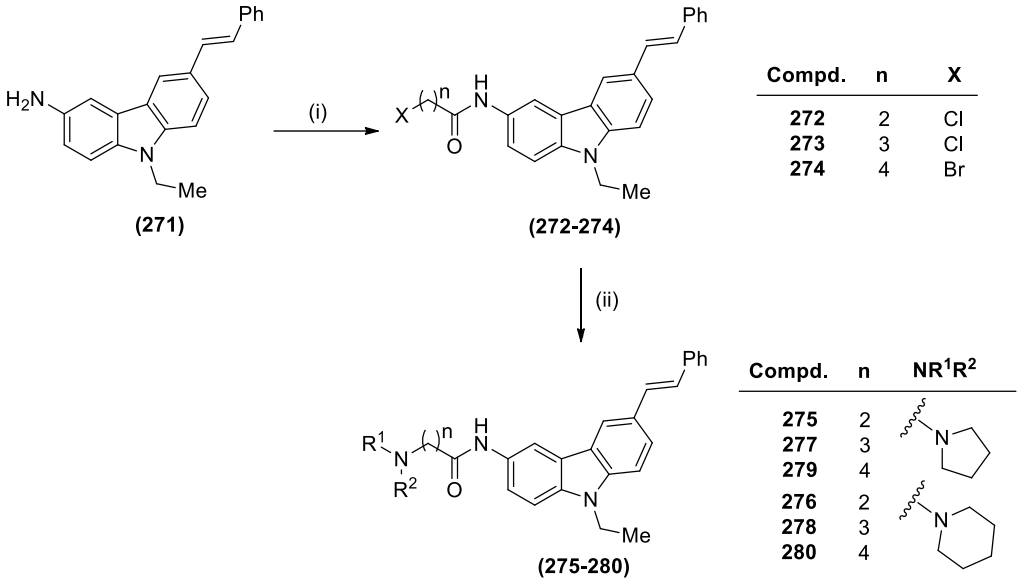

Scheme 4.8. Synthetic route for the synthesis of compounds (**275-280**): Reagents and conditions: (i) acid chloride, K_2CO_3, acetone; (ii) NHR^1R^2, THF, reflux.

The IR spectra of compounds (**272-274**) showed peaks at ~1650 cm^{-1} (amide C=O stretching), and ~3295cm^{-1} (amide N-H stretching), whereas the amine N-H stretching peaks got disappeared. The analytical data of the compounds (**272-274**) are mentioned in **Table 4.24**.

Table 4.24. Analytical data of amide intermediates (272-274)

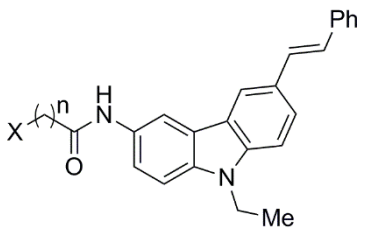

(272-274)

Compd	n	X	M.P.	MS	Characteristic IR peaks (cm^{-1})
272	4	-Cl	154-157 °C	403.6 $[M]^+$, 405.6 $[M+2]^+$	3297, 3024, 2972, 1652, 1595, 1554, 1231, 799, 699
273	5	-Cl	161-164 °C	417.3 $[M]^+$, 419.3 $[M+2]^+$	3291, 3118, 2969, 1648, 1542, 1486, 1229, 956, 799, 692
274	6	-Br	147-150 °C	476.4 $[M+H]^+$, 477.4 $[M+2]^+$	3288, 3025, 2967, 1647, 1593, 1540, 1486, 793

The IR spectra of compounds (**275-280**) showed peaks at ~3300 cm^{-1} (amide N-H stretching), 3053 cm^{-1} (aromatic C-H stretching), 2971 cm^{-1} (aliphatic C-H stretching) and ~1650 cm^{-1} (amide C=O stretching). The analytical data for (*E*)-*N*-(9-ethyl-6-styryl-9*H*-carbazol-3-yl)aminoalkylamide derivatives (**275-280**) have been shown in **Table 4.25.**

Table 4.25. Analytical data for (*E*)-*N*-(9-ethyl-6-styryl-9*H*-carbazol-3-yl) aminoalkylamide (275-280)

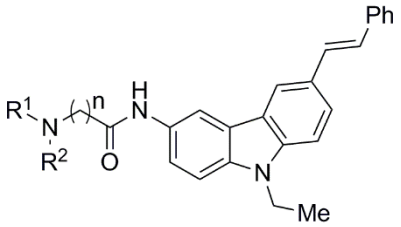

(275-280)

Compd	N	NR^1R^2	M.P.	IR characteristic peaks (cm^{-1})	LCMS data
275	2		129-131 °C	3366, 3056, 3018, 2966, 1596, 1488, 1229, 806,791	438.26 $[M+H]^+$ Purity: ~100 %
276	2	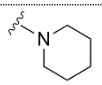	148-151 °C	3309, 3023, 2967, 1690, 1587, 1520, 1478, 1233, 749	452.16 $[M+H]^+$ Purity: 98.58 %
277	3		127-130 °C	3292, 3027, 2961, 1651, 1596, 1532, 1486, 1305, 797	452.26 $[M+H]^+$ Purity: ~100 %
278	3		114-118 °C.	3286, 3025, 2928, 1644, 1594, 1536, 1486, 1152, 791	466.4 $[M+H]^+$ Purity: ~100 %
279	4		161-164 °C	3289, 3026, 2962, 2933, 1648, 1596, 1484, 1082, 796	466.26 $[M+H]^+$; Purity: ~100 %.
280	4	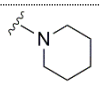	159-161 °C	3290, 3025, 2929, 1647, 1540, 1487, 1228, 799	480.17 $[M+H]^+$ Purity: 98.79 %

The ^{1}H-NMR spectrum of compound (**275**) showed a singlet at δ 10.11 for one amide proton (-NH_eCO). A doublet at δ 8.53 for one proton (ArH_a), a doublet at δ 8.31 for one proton (ArH_d), a doublet of doublet at δ 7.73 for one proton (ArH_b) and multiplet at δ 7.22-7.63 for ten protons (Ar$H_{c,f,g-i,}$ vinylic-$H_{j,k}$) confirmed a total of eleven aromatic protons and two vinylic protons in the structure. It showed a triplet at δ 2.76 for two protons (-COC$H_{2/o}$), a multiplet at δ 2.45-2.54 for six protons (-NC$H_{2/p,q}$) and a multiplet at δ 1.68-1.71 for four protons (-NCH$_2$C$H_{2/r}$). A quartet appeared at δ 4.41 for two protons

(-NC$H_{2/l}$CH$_3$) and a triplet appeared at δ 1.30 for three protons (-NCH$_2$C$H_{3/m}$) confirming the presence of *N*-ethyl group.

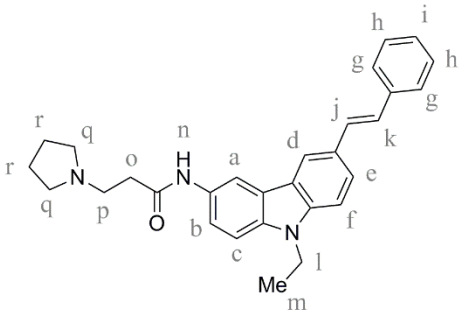

(**275**)

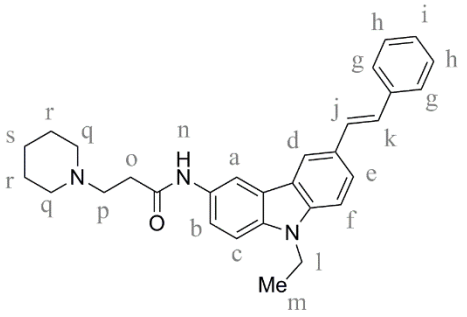

(**276**)

The ^{1}H-NMR spectrum of compound (**276**) showed a singlet at δ 10.20 for one amide proton (-NH_eCO). A doublet at δ 8.53 for one proton (ArH_a), a doublet at δ 8.30 for one proton (ArH_d), a doublet of doublet at δ 7.73 for one proton (ArH_b), multiplet at δ 7.24-7.63 for ten protons (Ar$H_{c,f,g-i,}$ vinylic-$H_{j,k}$) confirmed a total of eleven aromatic protons and two vinylic protons in the structure. It showed a triplet at δ 2.64 for two protons (-COCH$_{2/o}$), a multiplet at δ 2.48-2.52 for four protons (-NC$H_{2/q}$), a multiplet at δ 2.35-2.42 for two protons (-NC$H_{2/p}$), a multiplet at δ 1.49-1.55 for four protons (-NCH$_2$C$H_{2/r}$) and a multiplet at δ 1.39-1.40 for two protons (-C$H_{2/s}$). A quartet appeared at δ 4.40 for two protons (-NC$H_{2/l}$CH$_3$) and triplet appeared at δ 1.30 for three protons (-NCH$_2$C$H_{3/m}$) confirming the presence of *N*-ethyl group.

The ^{1}H-NMR spectrum of compound (**277**) showed a singlet at δ 9.94 for one amide proton (-NH_eCO). A doublet at δ 8.53 for one proton (ArH_a), a singlet at δ 8.30 for one proton (ArH_d), a doublet of doublet at δ 7.73 for one proton (ArH_b), multiplet at δ 7.24-7.63 for ten protons (Ar$H_{c,f,g-i,}$ vinylic-$H_{j,k}$), confirmed a total of eleven aromatic protons and two vinylic protons in the structure. It showed multiplet at δ 2.37-2.46 for eight protons (-NC$H_{2/q,r}$, -COCH$_{2/o}$), a multiplet at δ 1.78-1.82 for two protons (-NCH$_2$C$H_{2/p}$) and a multiplet at δ 1.66-1.69 for four protons (-NCH$_2$C$H_{2/s}$). A quartet appeared at δ 4.41 for two protons (-NC$H_{2/l}$CH$_3$) and a triplet appeared at δ 1.30 for three protons (-NCH$_2$C$H_{3/m}$) confirming the presence of *N*-ethyl group.

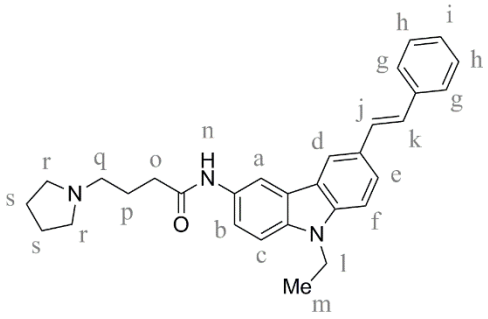

(277)

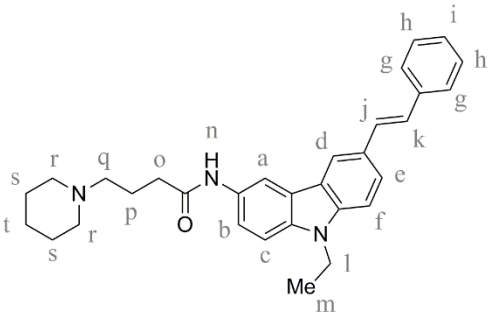

(278)

The ^{1}H-NMR spectrum of compound (**278**) showed a singlet at δ 9.89 for one amide proton (-N*H*$_{e}$CO). A doublet at δ 8.35 for one proton (Ar*H*$_{a}$), a doublet at δ 8.16 for one proton (Ar*H*$_{d}$), a doublet of doublet at δ 7.70 for one proton (Ar*H*$_{b}$) and multiplet at δ 7.17-7.62 for ten protons (Ar*H*$_{c,f,g-i,}$ vinylic-*H*$_{j,k}$) confirmed a total of eleven aromatic protons and two vinylic protons in the structure. It showed multiplet at δ 2.24-2.34 for eight protons (-NC*H*$_{2/q,r}$, -COCH$_{2/o}$), a multiplet at δ 1.69-1.77 for two protons (-NCH$_2$C*H*$_{2/p}$), a multiplet at δ 1.44-1.50 for four protons (-NCH$_2$C*H*$_{2/s}$) and a multiplet at δ 1.35-1.38 for two protons (-C*H*$_{2/t}$). A quartet appeared at δ 4.44 for two protons (-NC*H*$_{2/l}$CH$_3$) and a triplet appeared at δ 1.32 for three protons (-NCH$_2$C*H*$_{3/m}$) confirming the presence of *N*-ethyl group.

The ^{1}H-NMR spectrum of compound (**279**) showed a singlet at δ 9.91 for amide proton (-N*H*$_{e}$CO). A doublet at δ 8.52 for one proton (Ar*H*$_{a}$), a singlet at δ 8.30 for one proton (Ar*H*$_{d}$), a doublet of doublet at δ 7.73 for one proton (Ar*H*$_{b}$) and multiplet at δ 7.24-7.63 for ten protons (Ar*H*$_{c,f,g-i,}$ vinylic-*H*$_{j,k}$), confirmed a total of eleven aromatic protons and two vinylic protons in the structure. It showed multiplet at δ 2.42-2.34 for eight protons (-NC*H*$_{2/r,s}$, -COCH$_{2/o}$), a multiplet at δ 1.65-1.69 for six protons (-NCH$_2$C*H*$_{2/q,t}$) and a multiplet at δ 1.49-1.52 for two protons (-C*H*$_{2/p}$). A quartet appeared at δ 4.40 for two protons (-NC*H*$_{2/l}$CH$_3$) and a triplet appeared at δ 1.30 for three protons (-NCH$_2$C*H*$_{3/m}$) confirming the presence of *N*-ethyl group.

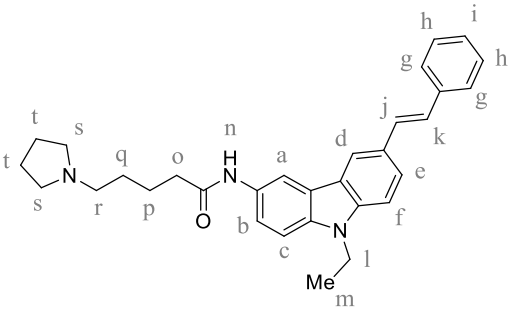

(279)

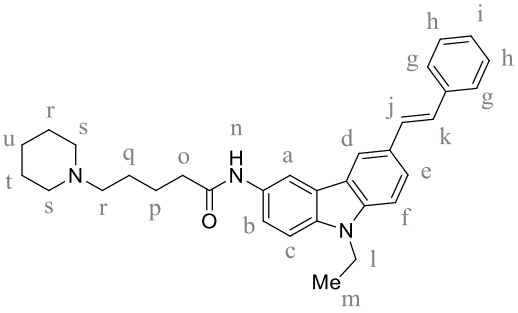

(280)

The ^{1}H-NMR spectrum of compound (**280**) showed a singlet at δ 9.91 for amide proton (-N*H*$_{n}$CO). A doublet at δ 8.52 for one proton (Ar*H*$_{a}$), a doublet at δ 8.30 for one proton (Ar*H*$_{d}$), a doublet of doublet at δ 7.73 for one proton (Ar*H*$_{b}$), multiplet at δ 7.22-7.63 for ten protons (Ar*H*$_{c,f,g-i,}$ vinylic-*H*$_{j,k}$), confirmed a total of eleven aromatic protons and two vinylic protons in the structure. It showed multiplets at δ 2.23-2.37 for eight protons (-NC*H*$_{2/r,s}$, -COCH$_{2/o}$), a multiplet at δ 1.61-1.65 for two protons (-NHCOCH$_2$C*H*$_{2/p}$), a multiplet at δ 1.45-1.49 for six protons (-NCH$_2$C*H*$_{2/q,t}$) and a multiplet at δ 1.35-1.37 for two protons (-C*H*$_{2/u}$). A quartet appeared at δ 4.41 for two protons (-NC*H*$_{2/l}$CH$_3$) and a triplet appeared at δ 1.30 for three protons (-NCH$_2$C*H*$_{3/m}$) confirming the presence of *N*-ethyl group.

4.2.1.2.1.3. Synthesis of (*E*)-1-(9-ethyl-6-styryl-9*H*-carbazol-3-yl)amino alkylureas (281-286)

Synthesis of (*E*)-1-(9-ethyl-6-styryl-9*H*-carbazol-3-yl)aminoalkylurea derivatives (**281-286**) was carried out as presented in **Scheme 4.9**. The (*E*)-9-ethyl-6-styryl-9*H*-carbazol-3-amine (**271**) was reacted with *p*-nitrophenyl chloroformate in the presence of triethylamine in DCM:THF (1:1), followed by reaction with the respective aminoalkylamines to get the titled (*E*)-1-(9-ethyl-6-styryl-9*H*-carbazol-3-yl)aminoalkylurea derivatives (**281-286**).[161]

The IR spectra of compounds (**281-286**) showed peaks at ~3300 cm^{-1} (amide N-H stretching), 3025 cm^{-1} (aromatic C-H stretching), 2950 cm^{-1} (aliphatic C-H stretching) and ~1630 cm^{-1} (amide C=O stretching). The analytical data for (*E*)-*N*-(9-ethyl-6-styryl-9*H*-carbazol-3-yl)aminoalkylamide derivatives (**281-286**) have been shown in **Table 4.26**.

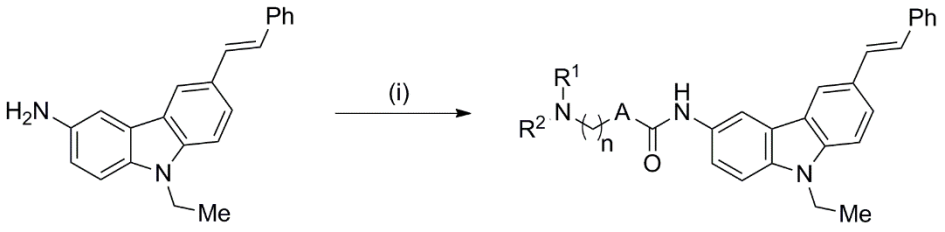

(271) (281-286)

Compd.	A	n	NR^1R^2	Compd.	A	n	NR^1R^2
281	--	0	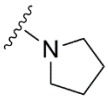	**282**	--	0	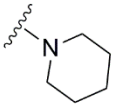
283	NH	2		**284**	NH	2	
285	NH	3		**286**	NH	3	

Scheme 4.9. Synthetic route for the synthesis of the compounds (**281-286**). Reagents and conditions: (i) (a) *p*-Nitrophenyl chloroformate, TEA, DCM:THF (1:1), 0 °C to RT; (b) pyrrolidine/piperidine/aminoalkylamines, RT.

Table 4.26. Analytical data for (*E*)-1-(9-ethyl-6-styryl-9*H*-carbazol-3-yl) aminoalkylurea derivatives (281-286)

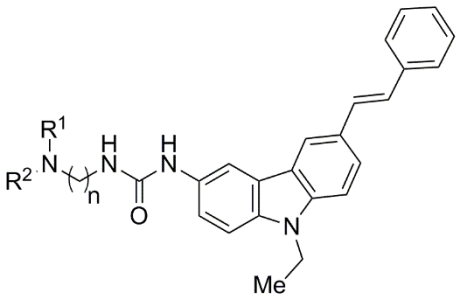

(281-286)

Compd	n	NHR^1R^2	M.P.	IR characteristic peaks (cm^{-1})	LCMS data
281	0		193-195 °C	3313, 3058, 3023, 2960, 2868, 1635, 1551, 1481, 1151, 956, 801, 691	410.30 $[M+H]^+$ Purity: ~100 %
282	0		217-219 °C	3346, 3026, 2929, 2847, 1627, 1532, 1486, 1232, 1140, 860, 750	424.25 $[M+H]^+$ Purity: ~100 %
283	2		176-178 °C	3322, 3022, 2961, 2872, 1630, 1562, 1486, 1132, 952, 799, 691	453.3 $[M+H]^+$ Purity: ~100 %
284	2		187-189 °C	3325, 3024, 2932, 2777, 1635, 1561, 1484, 1137, 952, 796, 748	467.26 $[M+H]^+$ Purity: 99.59 %
285	3		164-166 °C	3304, 3024, 2962, 2873, 1628, 1590, 1486, 1150, 957, 800, 692	467.4 $[M+H]^+$ Purity: ~100 %
286	3		168-170°C	3289, 3024, 2927, 1645, 1595, 1485, 1285, 1083, 951, 798, 688	481.4 $[M+H]^+$ Purity: ~100 %

The ^{1}H-NMR spectrum of compound (**281**) showed a multiplet at δ 8.27-8.29 for two protons (ArH_a, -NH_nCO), a singlet at δ 8.14 for one proton (ArH_d), a multiplet at δ 7.70-7.72 for one proton (ArH_b), multiplet at δ 7.21-7.63 for ten protons (Ar$H_{c,f,g-i}$, vinylic-$H_{j,k}$) confirming a total of eleven aromatic protons and two vinylic protons in structure. It showed a multiplet at δ 3.39-3.43 for four protons (-NC$H_{2/o}$) and a multiplet at δ 1.86-1.90 for two protons (-NCH$_2$C$H_{2/p}$). A quartet appeared at δ 4.40 for two protons (-NC$H_{2/l}$CH$_3$) and a triplet appeared at δ 1.31 for three protons (-NCH$_2$C$H_{3/m}$) confirming the presence of *N*-ethyl group.

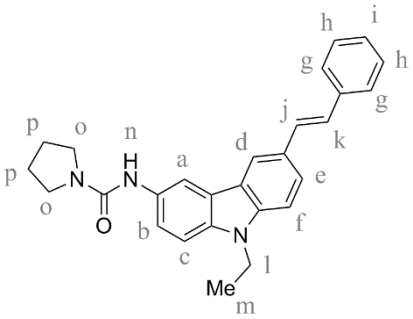

(281)

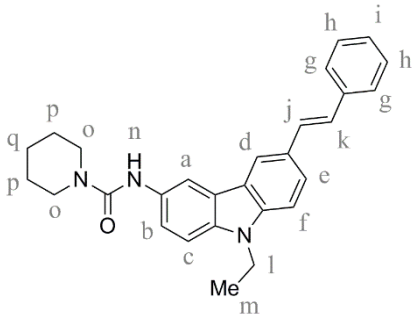

(282)

The ^{1}H-NMR spectrum of compound (**282**) showed a multiplet at δ 8.26-8.29 for two protons (Ar$H_{a,b}$), multiplet at δ 7.22-7.72 for eleven protons (Ar$H_{c,f,g-i}$,vinylic-$H_{j,k}$) confirming a total of eleven aromatic protons and two vinylic protons in the structure. It showed a multiplet at δ 3.45-3.48 for four protons (-NC$H_{2/o}$), a multiplet at δ 1.52-1.60 for six protons (-C$H_{2/p,q}$). A quartet appeared at δ 4.40 for two protons (-NC$H_{2/l}$CH$_3$) and a triplet appeared at δ 1.30 for three protons (-NCH$_2$C$H_{3/m}$) confirming the presence of *N*-ethyl group.

The ^{1}H-NMR spectrum of compound (**283**) showed a singlet at δ 10.23 for one proton (-NH_nCONH), and a broad singlet at δ 8.52 for one proton (-NHCONH_o). A singlet at δ 8.31 for one proton (ArH_a) and multiplet at δ 7.24-7.75 for twelve protons (Ar$H_{b-i,}$ vinylic-$H_{j,k}$) confirmed a total of eleven aromatic protons and two vinylic protons in the structure. It showed a multiplet at δ 2.62-2.67 for two protons (-NHC$H_{2/p}$), a multiplet at δ 2.35-2.45 for six protons (-NC$H_{2/q,r}$) and a multiplet at δ 1.50-1.52 for four protons (-NCH$_2$C$H_{2/s}$). A quartet appeared at δ 4.41 for two protons (-NC$H_{2/l}$CH$_3$) and a triplet appeared at δ 1.31 for three protons (-NCH$_2$C$H_{3/m}$) confirming the presence of *N*-ethyl group.

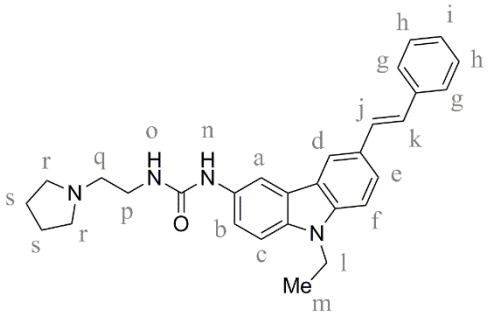

(283)

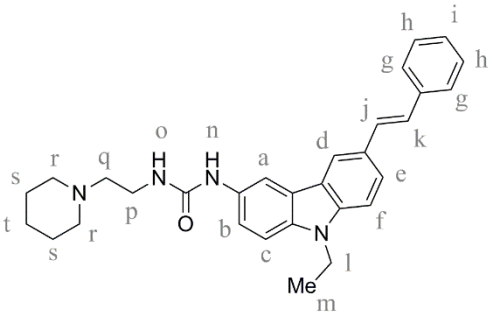

(284)

The ^{1}H-NMR spectrum of compound (**284**) showed a singlet at δ 8.61 for one proton (-N*H*$_{n}$CONH), and a broad singlet at δ 6.01 for one proton (-NHCON*H*$_{o}$). A singlet at δ 8.29 for one proton (Ar*H*$_{a}$) and multiplet at δ 7.21-7.71 for eleven protons (Ar*H*$_{b\text{-}i,}$ vinylic-*H*$_{j,k}$) confirmed a total of eleven aromatic protons and two vinylic protons in the structure. It showed a multiplet at δ 3.22-3.24 for two protons (-NHC*H*$_{2/p}$), a multiplet at δ 2.35-2.39 for six protons (-NC*H*$_{2/q,r}$), a multiplet at δ 1.50-1.52 for four protons (-NCH$_2$C*H*$_{2/s}$) and a multiplet at δ 1.39-1.40 for two protons (-C*H*$_{2/t}$). A quartet appeared at δ 4.39 for two protons (-NC*H*$_{2/l}$CH$_3$) and a triplet appeared at δ 1.29 for three protons (-NCH$_2$C*H*$_{3/m}$) confirming the presence of *N*-ethyl group.

The ^{1}H-NMR spectrum of compound (**285**) showed a singlet at δ 8.43 for one proton (-N*H*$_{n}$CONH) and a triplet at δ 6.18 for one proton (-NHCON*H*$_{o}$). Multiplets appeared at δ 8.26-8.28 for one proton (Ar*H*$_{a}$) and at δ 7.21-7.71 for eleven protons (Ar*H*$_{b\text{-}i,}$ vinylic-*H*$_{j,k}$) confirming a total of eleven aromatic protons and two vinylic protons in the structure. It showed a multiplet at δ 3.14-3.19 for two protons (-NHC*H*$_{2/p}$), a multiplet at δ 2.52-2.55 for six protons (-NC*H*$_{2/r,s}$), a multiplet at δ 1.62-1.74 for six protons (-NCH$_2$C*H*$_{2/t,q}$). A quartet appeared at δ 4.39 for two protons (-NC*H*$_{2/l}$CH$_3$) and a triplet appeared at δ 1.29 for three protons (-NCH$_2$C*H*$_{3/m}$) confirming the presence of *N*-ethyl group.

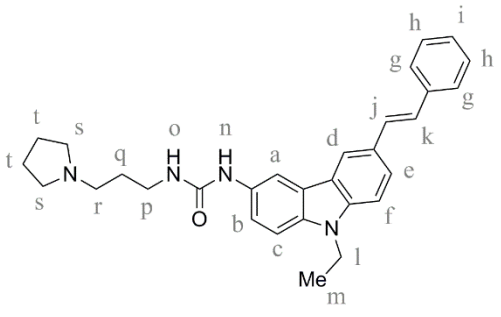

(285)

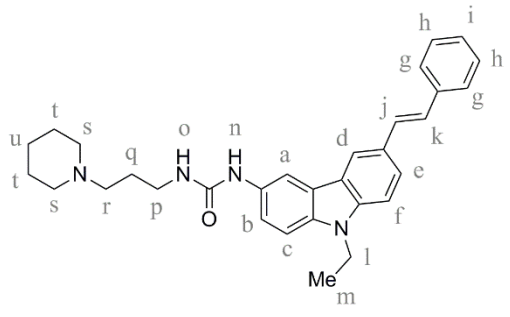

(286)

The ^{1}H-NMR spectrum of compound (**286**) showed a singlet at δ 8.36 for one proton (-N*H*$_n$CONH) and a triplet at δ 6.01 for one proton (-NHCON*H*$_o$). Multiplets appeared at δ 8.26-8.29 for two protons (Ar*H*$_{a,d}$) and at δ 7.21-7.71 for eleven protons (Ar*H*$_{b\text{-}i,}$ vinylic-*H*$_{j,k}$) confirming a total of eleven aromatic protons and two vinylic protons in the structure. It showed a multiplet at δ 3.11-3.16 for two protons (-NHC*H*$_{2/p}$), a multiplet at δ 2.27-2.33 for six protons (-NC*H*$_{2/r,s}$), a multiplet at δ 1.57-1.64 for two protons (-NCH$_2$C*H*$_{2/q}$), a multiplet at δ 1.46-1.51 for four protons (-NCH$_2$C*H*$_{2/t}$) and a multiplet at δ 1.34-1.39 for two protons (-C*H*$_{2/u}$). A quartet appeared at δ 4.39 for two protons (-NC*H*$_{2/l}$CH$_3$) and a triplet appeared at δ 1.30 for three protons (-NCH$_2$C*H*$_{3/m}$) confirming the presence of *N*-ethyl group.

4.2.1.2.2. Synthesis of carbazole-based stilbene derivative (Series-2)

Carbazole-based stilbene derivatives (Series-2) were prepared from commercially available carbazole. The synthetic procedures and characterization of the synthesized derivatives have been discussed under the following subheadings:

- **4.2.1.2.2.1.** Synthesis of (*E*)-4-(2-(9-ethyl-9*H*-carbazol-3-yl)vinyl) aniline (**289**),
- **4.2.1.2.2.2.** Synthesis of (*E*)-*N*-(4-(2-(9-ethyl-9*H*-carbazol-3-yl)vinyl) phenyl)aminoalkylamide (**293-298**),
- **4.2.1.2.2.3.** Synthesis of (*E*)-*N*-(4-(2-(9-ethyl-9*H*-carbazol-3-yl)vinyl) phenyl)aminoalkylureas (**299-304**) and
- **4.2.1.2.2.4.** Synthesis of (*E*)-1-(9-ethyl-6-styryl-9*H*-carbazol-3-yl)-3-(aminoalkyl)thioureas (**305-307**).

4.2.1.2.2.1 Synthesis of a key intermediate (*E*)-4-(2-(9-ethyl-9*H*-carbazol-3-yl)vinyl)aniline (289)

A key amine intermediate (*E*)-9-ethyl-6-styryl-9*H*-carbazole-3-amine (**289**) for the synthesis of compounds (**293-307**) was synthesized as depicted in **Scheme 4.10**. 2-(4-Nitrophenyl)acetic acid (**287**) was synthesized from 2-phenylacetonitrile by a reported two steps procedure.[162] Commercially available 2-phenylacetonitrile was nitrated by nitric acid under cold condition to 2-(4-nitrophenyl)acetonitrile as the sole product. Acidic hydrolysis of the

cyano group present in 2-(4-nitrophenyl)acetonitrile by 50 % sulfuric acid gave 2-(4-nitrophenyl)acetic acid (**287**). The analytical data for 2-(4-nitro phenyl)acetic acid (**287**) was in accordance with the literature values.[162]

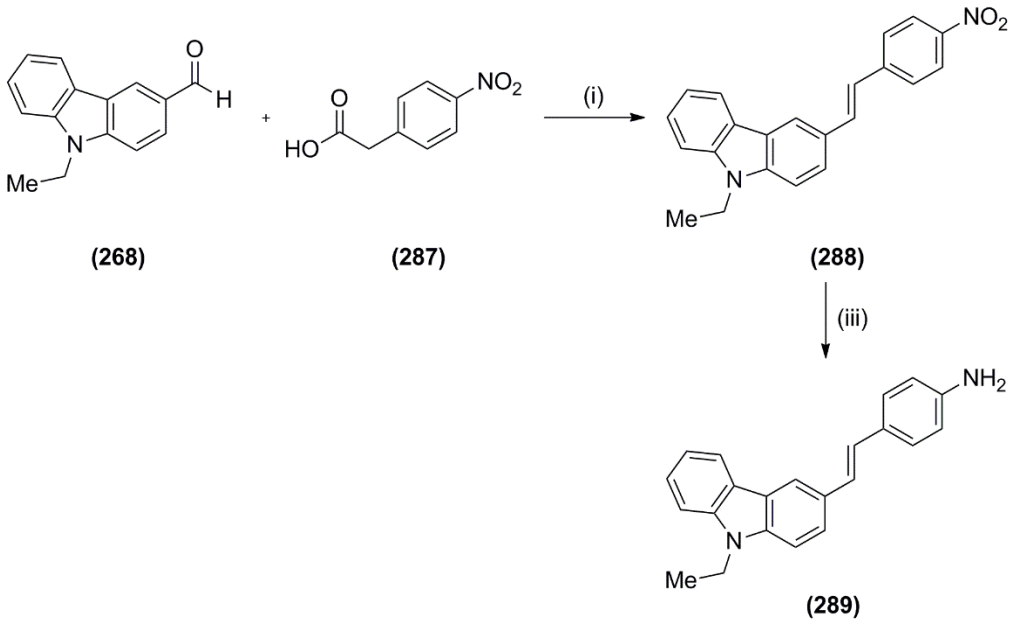

Scheme 4.10. Synthetic route for the synthesis of a key amine intermediate (**289**). Reagents and conditions: (i) Piperidine, MW; (ii) $SnCl_2$, THF, MeOH, reflux.

4-Nitrophenylacetic acid (**287**) was reacted with 9-ethyl-9*H*-carbazole-3-carbaldehyde (**268**) in presence of piperidine under microwave conditions to obtain (*E*)-9-ethyl-3-(4-nitrostyryl)-9*H*-carbazole (**288**).[163] Its IR spectrum showed characteristic peaks at ~3048 cm^{-1} (aromatic C-H stretching), ~2976 cm^{-1} (aliphatic C-H stretching), ~1593 cm^{-1} (aromatic C=C stretching), 1505 cm^{-1} (asymmetrical N–O stretching) and at 1333 cm^{-1} (symmetrical N–O stretching). It also showed disappearance of characteristic IR peaks for the aldehyde group. The ^{1}H NMR spectrum of compound (**288**) showed a singlet at δ 8.49 for one proton (ArH_e), a doublet at δ8.24 for two protons (ArH_i), a doublet at δ8.18 for one proton (ArH_a), a doublet at δ 7.86 for two proton (ArH_h) and multiplet at δ 7.83-7.22 for seven protons (Ar$H_{b\text{-}d,f,g,j,k}$) confirming a total of eleven aromatic protons and two vinylic protons in the structure. A quartet appeared at δ 4.46 for two protons (-NC$H_{2/l}$CH$_3$) and a triplet appeared at δ 1.32 for three protons (-NCH$_2$C$H_{3/m}$) confirming the presence of *N*-ethyl group. Its mass spectrum showed $[M+H]^+$ ion peak at 343 m/z.

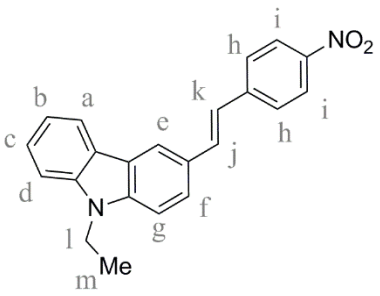

(288)

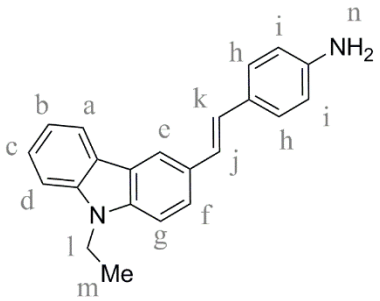

(289)

(*E*)-9-Ethyl-3-(4-nitrostyryl)-9*H*-carbazole (**288**) was reduced to (*E*)-4-(2-(9-ethyl-9*H*-carbazol-3-yl)vinyl)aniline (**289**) by stannous chloride. The amine was purified by recrystallization with methanol. Its IR spectrum showed characteristic peaks at 3417 $cm^{-1}$and 3368 cm^{-1} (primary N-H stretching), at 3028 cm^{-1} (aromatic C-H stretching), 2966 cm^{-1} (aliphatic C-H stretching), 1513 cm^{-1} (C=C stretching). It also showed disappearance of characteristic peaks (N-O stretching) for nitro group. The ^{1}H NMR spectrum of compound (**289**) showed a singlet at δ 8.26 for one proton (ArH_e), and multiplet at δ 8.14-8.16 for one proton (ArH_a), and at δ 6.56-7.65 for eleven protons (Ar$H_{b\text{-}d,f\text{-}k}$) accounting for the presence of total thirteen aromatic protons in the structure. A broad singlet appeared at δ 5.20 for two protons (ArNH_{2n}). A quartet appeared at δ 4.42 for two protons (-NC$H_{2/l}$$CH_3$) and a triplet appeared at δ 1.31 for three protons (-$NCH_2CH_{3/m}$) confirming the presence of *N*-ethyl group. The mass spectrum of compound showed $(M+H)^+$ peak at 313.5 m/z.

Single crystal X-ray diffraction analysis confirmed the *trans* configuration of the compound (**288**) (**Figure 4.19**).

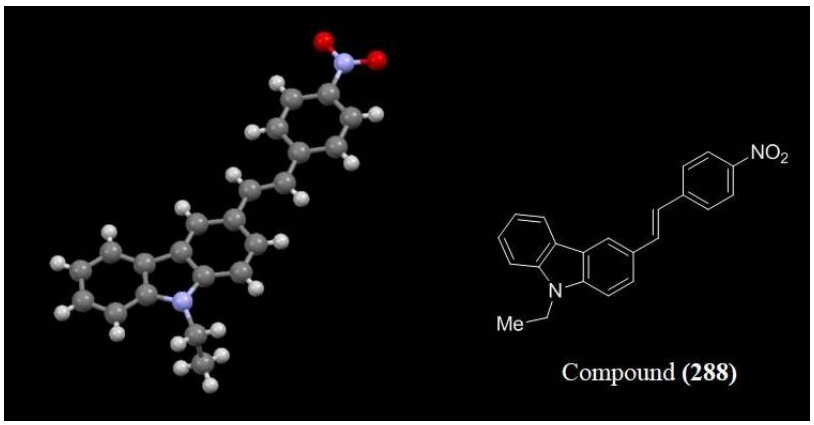

Figure 4.19. Single crystal X-ray diffraction of compound (**288**).

4.2.1.2.2.2. Synthesis of (*E*)-*N*-(4-(2-(9-ethyl-9*H*-carbazol-3-yl)vinyl) phenyl)aminoalkylamides (293-298)

Synthesis of (*E*)-*N*-(4-(2-(9-ethyl-9*H*-carbazol-3-yl)vinyl)phenyl) aminoalkylamide derivatives (**293-298**) were carried out from amine intermediate (**289**) in two steps as depicted in **Scheme 4.11**. In the first step, acylation of compound (**289**) was carried out by reacting it with the respective acid chlorides to obtain intermediates (**290-292**). These amide intermediates (**290-292**) in second step, were reacted with respective alicyclic amines to obtain the titled compounds (**293-298**) which were further purified by crystallization.

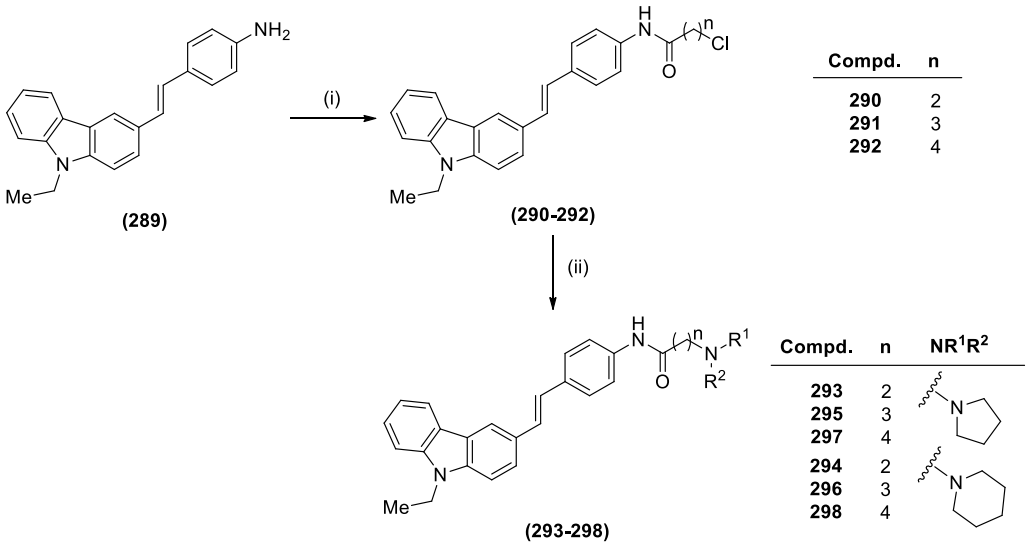

Scheme 4.11. Synthetic route for the synthesis of (*E*)-*N*-(4-(2-(9-ethyl-9*H*-carbazol-3-yl)vinyl)phenyl)aminoalkylamide (**293-298**). Reagents and conditions: (i) acid chloride, K_2CO_3, acetone; (ii) NHR^1R^2, THF, reflux.

IR spectra of the amide intermediates (**290-292**) showed peaks at ~1650 cm^{-1} (amide C=O stretching) and ~3275 cm^{-1} (amide N-H stretching), whereas the amine N-H stretching peaks disappeared. The analytical data of the amide intermediates (**290-292**) are mentioned in **Table.4.27**.

Table 4.27. Analytical data of amide intermediates (290-292)

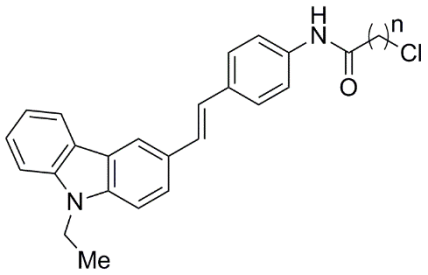

(290-292)

Compd	n	M.P.	IR characteristic peaks (cm^{-1})	MS
290	1	207-209 °C	3249, 3038, 2974, 1664, 1593, 738	388.2 $[M]^+$, 390.2 $[M+2]^+$
291	2	219-222 °C	3273, 3036, 2970, 1644, 1594, 744	403.3 $[M]^+$, 405.3 $[M+2]^+$
292	3	193-195 °C	3295, 3028, 2968, 1653, 1589, 746	417.32 $[M]^+$, 419.30 $[M+2]^+$

IR spectra of the compounds (**293-298**) showed peaks at ~3300 cm^{-1} (amide N-H stretching), 3020 cm^{-1} (aromatic C-H stretching), 2950 cm^{-1} (aliphatic C-H stretching) and ~1680 cm^{-1} (amide C=O stretching). The analytical data for (*E*)-*N*-(9-ethyl-6-styryl-9*H*-carbazol-3-yl)aminoalkylamide derivatives (**293-298**) have been shown in **Table 4.28**.

Table 4.28. Analytical data of (*E*)-*N*-(9-ethyl-6-styryl-9*H*-carbazol-3-yl) aminoalkylamide derivatives (293-298)

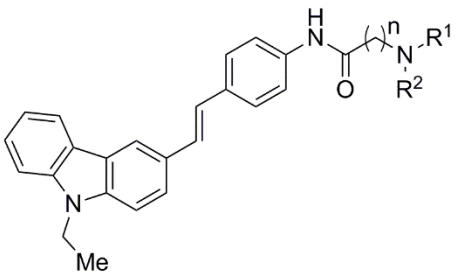

(293-298)

Compd	n	NHR^1R^2	M.P.	IR characteristic peaks (cm^{-1})	LCMS data
293	1		120-122 °C	3306, 3022, 2867, 1691, 1584, 1521, 1233, 749	424.25 $[M+H]^+$ Purity: 99.71 %
294	1		131-133 °C	3326, 3016, 2938, 1693, 1582, 1516, 815, 749	438.26 $[M+H]^+$ Purity: 99.81 %
295	2	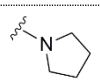	158-160 °C	3281, 3175, 3102, 3025, 2963, 2930, 1653, 745	438.21 $[M+H]^+$ Purity: ~100 %

Compd	n	NHR^1R^2	M.P.	IR characteristic peaks (cm^{-1})	LCMS data
296	2		173-175 °C	3018, 2974, 2931, 2799, 1683, 1537, 817,747	452.21 $[M+H]^+$ Purity: ~100 %
297	3		179-181 °C	3294, 3023, 2960, 2874, 2791, 1657, 1523, 818, 745	452.21 $[M+H]^+$ Purity: 99.05 %
298	3		173-175 °C	3296, 3023, 2928, 1657, 1523, 1409, 858, 745	466.21 $[M+H]^+$ Purity: 99.88 %

The ^{1}H-NMR spectrum of compound (**293**) showed a singlet at δ 9.76 for one amide proton (-NH_nCO). A singlet at δ 8.37 for one proton (ArH_e), a doublet at δ 8.17 for one proton (ArH_a) and multiplet at δ 7.19-7.72 for eleven protons (Ar$H_{b\text{-}d,f\text{-}i,}$ vinylic-$H_{j,k}$) confirmed a total of eleven aromatic protons and two vinylic protons in the structure. It showed a singlet at δ 3.25 for two proton (-$COCH_{2/o}$), a multiplet at δ 2.56-2.61 for four protons (-$NCH_{2/p}$), and a multiplet at δ 1.69-1.81 for four protons (-$NCH_2CH_{2/q}$). A quartet appeared at δ 4.43 for two protons (-$NCH_{2/l}CH_3$) and a triplet appeared at δ 1.31 for three protons (-$NCH_2CH_{3/m}$) confirming the presence of *N*-ethyl group. The ^{13}C-NMR spectrum showed peak at δ 169.00 due to C=O carbon of the amide. The aromatic and vinylic carbons appeared at δ 140.33, 139.66, 138.15, 133.32, 128.85, 128.61, 126.85, 126.34, 125.69, 125.01, 123.03, 122.71, 120.87, 120.10, 119.38, 118.78, 109.78 and 109.73 whereas the aliphatic carbons appeared at δ 59.97, 54.20, 37.53, 23.95 and 14.21.

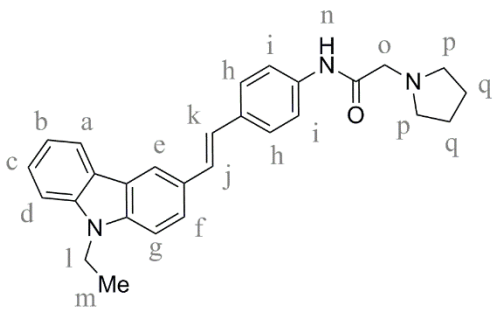

(293)

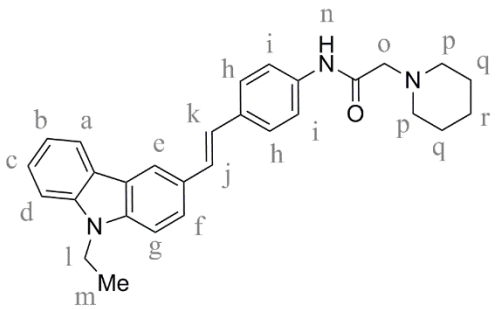

(294)

The ^{1}H-NMR spectrum of compound (**294**) showed a singlet at δ 9.72 for one amide proton (-NH_nCO). A doublet at δ 8.37 for one proton (ArH_e), a doublet at δ 8.17 for one proton (ArH_a) and multiplet at δ 7.19-7.71 for eleven protons (Ar$H_{b\text{-}d,f\text{-}i,}$ vinylic-$H_{j,k}$) confirmed a total of eleven aromatic protons and two vinylic protons in the structure. It showed a singlet at δ 3.07 for two protons

(-$COCH_{2/o}$), a multiplet at δ 2.46-2.52 for four protons (-$NCH_{2/p}$), a multiplet at δ 1.54-1.60 for four protons (-$NCH_2CH_{2/q}$), and a multiplet at δ 1.37-1.42 for two protons (-$CH_{2/r}$). A quartet appeared at δ 4.43 for two protons (-$NCH_{2/l}CH_3$) and a triplet appeared at δ 1.32 for three protons (-$NCH_2CH_{3/m}$) confirming the presence of *N*-ethyl group. The ^{13}C-NMR spectrum showed peak at δ 170.57 due to C=O carbon of the amide. The aromatic and vinylic carbons appeared at δ 140.43, 139.65, 138.77, 133.01, 128.88, 128.46, 126.94, 126.33, 125.74, 124.99, 123.04, 122.71, 120.88, 119.66, 119.38, 118.77, 109.77 and 109.71 whereas the aliphatic carbons appeared at δ 53.88, 52.04, 37.52, 36.64, 23.65 and 14.20.

The ^{1}H-NMR spectrum of compound (**295**) showed a singlet at δ 10.14 for one amide proton (-NH_nCO). A singlet at δ 8.36 for one proton (ArH_e), a doublet at δ 8.17 for one proton (ArH_a) and multiplet at δ 7.18-7.72 for eleven protons ($ArH_{b\text{-}d,f\text{-}i,}$ vinylic-$H_{j,k}$) confirmed a total of eleven aromatic protons and two vinylic protons in structure. It showed a triplet at δ 2.71 for two protons (-$COCH_{2/o}$), a multiplet at δ 2.46-2.50 for six protons (-$NCH_{2/p,q}$) and a multiplet at δ 1.66-1.69 for four protons (-$NCH_2CH_{2/r}$). A quartet appeared at δ 4.43 for two protons (-$NCH_{2/l}CH_3$) and a triplet appeared at δ 1.31 for three protons (-$NCH_2CH_{3/m}$) confirming the presence of *N*-ethyl group. The ^{13}C-NMR spectrum showed peak at δ 171.59 due to C=O carbon of the amide. The aromatic and vinylic carbons appeared at δ 140.43, 139.64, 138.87, 132.90, 128.89, 128.40, 126.90, 126.33, 125.76, 124.99, 123.03, 122.71, 120.88, 119.65, 119.37, 118.75, 109.78 and 109.72 whereas the aliphatic carbons appeared at δ 53.88, 52.04, 37.52, 36.64, 23.65, 14.20. Single crystal X-ray diffraction analysis confirmed that the *trans* configuration of compound (**288**) was maintained during the course of the reaction and the final compound (**295**) was obtained as *trans* isomer (**Figure 4.20**).

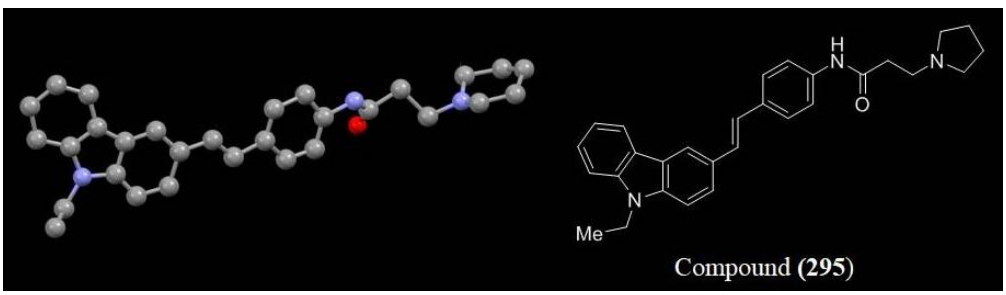

Figure 4.20. Single crystal X-ray diffraction analysis of compound (**295**)

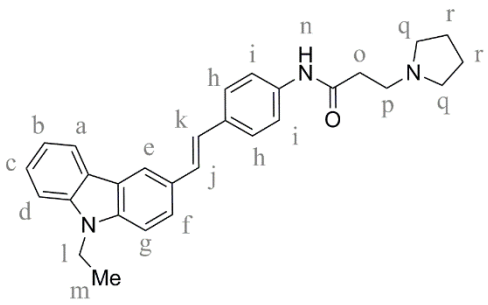

(295)

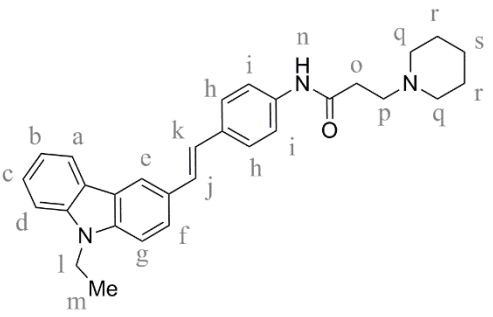

(296)

The ^{1}H-NMR spectrum of compound (**296**) showed a singlet at δ 10.24 for one amide proton (-N*H*$_{n}$CO). A singlet at δ 8.36 for one proton (Ar*H*$_{e}$), a doublet at δ 8.17 for one proton (Ar*H*$_{a}$) and multiplet at δ 7.18-7.72 for eleven protons (Ar*H*$_{b\text{-}d,f\text{-}i,}$ vinylic-*H*$_{j,k}$) confirmed a total of eleven aromatic protons and two vinylic protons in the structure. It showed a triplet at δ 2.60 for two proton (-COCH$_{2/o}$), a multiplet at δ 2.37-2.40 for four protons (-NC*H*$_{2/p,q}$) and a multiplet at δ 1.52-1.49 for four protons (-NCH$_2$C*H*$_{2/r}$), a multiplet at δ 1.36-1.41 for two protons (-C*H*$_{2/s}$). A quartet appeared at δ 4.44 for two protons (-NC*H*$_{2/l}$CH$_3$) and a triplet appeared at δ 1.32 for three protons (-NCH$_2$C*H*$_{3/m}$) confirming the presence of *N*-ethyl group. The ^{13}C-NMR spectrum showed peak at δ 170.70 due to C=O carbon of the amide. The aromatic and vinylic carbons appeared at δ 140.43, 196.65, 138.73, 133.0, 128.8, 128.47, 126.96, 126.34, 125.73, 125.01, 123.03, 122.71, 120.88, 119.63, 119.37, 118.75, 109.78 and 109.72 whereas the aliphatic carbons appeared at δ 54.93, 54.13, 37.52, 34.57, 26.10, 24.48 and 14.21.

The ^{1}H-NMR spectrum of compound (**297**) showed singlet at δ 9.96 accounting for amide proton (-N*H*$_{n}$CO). A singlet at δ 8.36 for one proton (Ar*H*$_{e}$), a doublet at δ 8.17 for one proton (Ar*H*$_{a}$), a doublet of doublet at δ 7.71 for one proton (Ar*H*$_{f}$), multiplet at δ 7.18-7.63 for ten protons (Ar*H*$_{b\text{-}d,g\text{-}i,}$ vinylic-*H*$_{j,k}$) confirmed a total of eleven aromatic protons and two vinylic protons in the structure. It showed multiplets at δ 2.34-2.42 for eight protons (-COCH$_{2/o}$, -NC*H*$_{2/q,r}$), a multiplet at δ 1.73-1.77 for two protons (-NCH$_2$C*H*$_{2/p}$) and a multiplet at δ 1.65-1.68 for four protons (-NCH$_2$C*H*$_{2/s}$). A quartet appeared at δ 4.44 for two protons (-NC*H*$_{2/l}$CH$_3$) and a triplet appeared at δ 1.32 for three protons (-NCH$_2$C*H*$_{3/m}$) confirming the presence of *N*-ethyl group. The ^{13}C-NMR spectrum showed peak at δ 171.59 due to C=O carbon of the amide. The

aromatic and vinylic carbons appeared at δ 140.43, 139.64, 138.87, 132.90, 128.89, 128.40, 126.90, 126.33, 125.76, 124.99, 123.03, 122.71, 120.88, 119.65, 119.37, 118.75, 109.78 and 109.72 whereas the aliphatic carbons appeared at δ 55.63, 54.00, 37.52, 35.00, 24.85, 23.60 and 14.20.

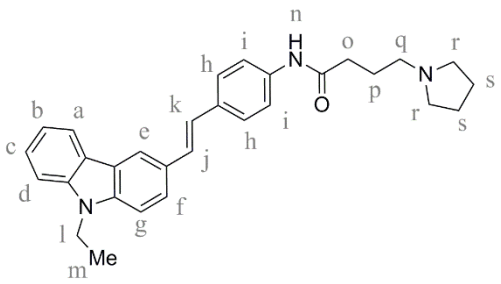

(297)

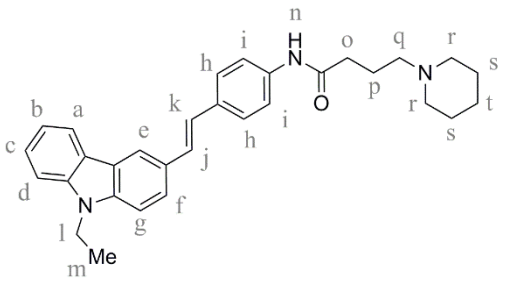

(298)

The ^{1}H-NMR spectrum of compound (**298**) showed singlet at δ 9.93 for one amide proton (-N*H*$_{n}$CO). A singlet at δ 8.36 for one proton (Ar*H*$_{e}$), a doublet at δ 8.17 for one proton (Ar*H*$_{a}$), a doublet of doublet at δ 7.71 for one proton (Ar*H*$_{f}$), multiplet at δ 7.18-7.63 for ten protons (Ar*H*$_{b\text{-}d,g\text{-}i,}$ vinylic-*H*$_{j,k}$) confirmed a total of eleven aromatic protons and two vinylic protons in the structure. It showed multiplet at δ 2.34-2.24 for eight proton (-COC*H*$_{2/o}$, -NC*H*$_{2/q,r}$), at δ 1.75-1.72 for two protons (-NCH$_2$C*H*$_{2/p}$), at δ 1.50-1.44 for four protons (-NCH$_2$C*H*$_{2/s}$) and at δ 1.36-1.33 for two protons (-C*H*$_{2/t}$). A quartet appeared at δ 4.44 for two protons (-NC*H*$_{2/l}$CH$_3$) and a triplet appeared at δ 1.31 for three protons (-NCH$_2$C*H*$_{3/m}$) confirming the presence of *N*-ethyl group. The ^{13}C-NMR spectrum showed peak at δ 171.61 due to C=O carbon of the amide. The aromatic and vinylic carbons appeared at δ 140.43, 139.64, 138.88, 132.87, 128.90, 128.39, 126.89, 126.34, 125.77, 124.99, 123.03, 122.71, 120.88, 119.65, 119.37, 118.74, 109.78 and 109.72 whereas the aliphatic carbons appeared at δ 58.54, 54.52, 37.52, 34.99, 26.08, 24.66, 22.85 and 14.21.

4.2.1.2.2.3. Synthesis of (*E*)-*N*-(4-(2-(9-ethyl-9*H*-carbazol-3-yl)vinyl) phenyl)aminoalkylureas (299-304)

Synthesis of urea derivatives (**299-304**) was carried out as presented in **Scheme 4.12**. Compound (**289**) was primarily reacted with *p*-nitrophenyl chloroformate in the presence of triethylamine in DCM:THF (1:1) followed by reaction with the respective aminoalkylamines to obtain the titled urea derivatives (**299-304**).[161]

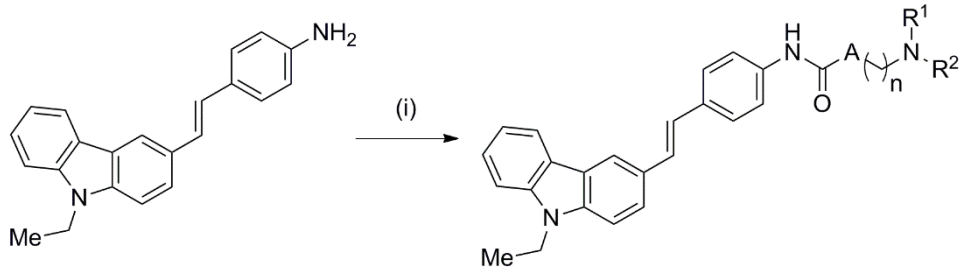

Compd.	A	n	NR^1R^2
299	--	0	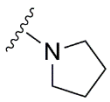
301	NH	2	
303	NH	3	

Compd.	A	n	NR^1R^2
300	--	0	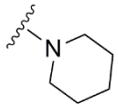
302	NH	2	
304	NH	3	

Scheme 4.12. Synthetic route for the synthesis of (*E*)-*N*-(4-(2-(9-ethyl-9*H*-carbazol-3-yl)vinyl)phenyl)aminoalkylureas (**299-304**). Reagents and conditions: (i) (a) *p*-nitro phenyl chloroformate, TEA, DCM:THF (1:1), 0 °C to RT; (b) pyrrolidine/ piperidine/ 1-pyrrolidinylalkylamines/1-piperidinylalkylamines, RT.

The IR spectra of (*E*)-*N*-(4-(2-(9-ethyl-9*H*-carbazol-3-yl)vinyl)phenyl) aminoalkylurea derivatives (**299-304**) showed peaks at ~1650 cm^{-1} (amide C=O stretching), and ~3300 cm^{-1} (amide N-H stretching), whereas the amine N-H stretching peaks got disappeared. The analytical data of the compounds (**299-304**) are mentioned in **Table.4.29**.

Table 4.29. Analytical data of (*E*)-*N*-(4-(2-(9-ethyl-9*H*-carbazol-3-yl)vinyl) phenyl)aminoalkylurea derivatives (299-304)

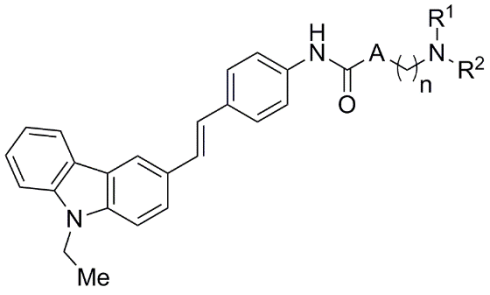

(299-304)

Compd	A	n	NR^1R^2	M.P.	IR characteristic peaks (cm^{-1})	LCMS data
299	-	0	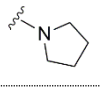	144-146 °C	3334, 3018, 2974, 1630, 1522, 1234, 965, 753	-
300	-	0		214-216 °C	3305, 3026, 2972, 2931, 1633, 1589, 1234, 746	-

Compd	A	n	NR^1R^2	M.P.	IR characteristic peaks (cm^{-1})	LCMS data
301	NH	1		>250 °C	3299, 3025, 2969, 2931, 1645, 1593, 1234, 743	453.16 $[M+H]^+$, Purity: ~100%
302	NH	1		213-216 °C	3307, 3023, 2962, 1641, 1581, 1237, 743	467.21 $[M+H]^+$, Purity: 99.88%
303	NH	2		215-217 °C	3322, 3022, 2982, 1634, 1588, 1235, 959, 745	467.21 $[M+H]^+$, Purity: 97.38%
304	NH	2		206-207 °C	3308, 3027, 2961, 1641, 1591, 1233, 959, 745	481.17 $[M+H]^+$, Purity: ~100%

The ^{1}H-NMR spectrum of compound (**299**) showed a doublet at δ 8.23 for one proton (ArH_e), a doublet at δ 8.15 for one proton (ArH_a), a doublet of doublet at δ 7.68 for one proton (ArH_f) and multiplet at δ 7.10-7.69 for ten protons (Ar$H_{b\text{-}d,g\text{-}i,}$ vinylic-$H_{j,k}$) confirmed a total of eleven aromatic protons and two vinylic protons in the structure. A singlet appeared at δ 6.28 for one proton (-NH_nCO). It showed a multiplet at δ 3.48-3.52 for four protons (-NC$H_{2/p}$) and a multiplet at δ 1.98-2.02 for two protons (-$NCH_2CH_{2/q}$). A quartet appeared at δ 4.39 for two protons (-NC$H_{2/l}CH_3$) and a triplet appeared at δ 1.46 for three protons (-$NCH_2CH_{3/m}$) confirming the presence of *N*-ethyl group. The ^{13}C-NMR spectrum showed peak at δ 155.25 due to C=O carbon of the urea. The aromatic and vinylic carbons appeared at δ 140.39, 131.58, 129.01, 127.68, 126.64, 126.37, 125.97, 124.92, 123.00, 122.66, 120.89, 120.11, 120.01, 119.38, 118.61, 109.76 and 109.68 whereas the aliphatic carbons appeared at δ 46.17, 37.51, 25.46 and 14.16. Its mass spectrum showed $[M+H]^+$ ion peak at 410.3 m/z.

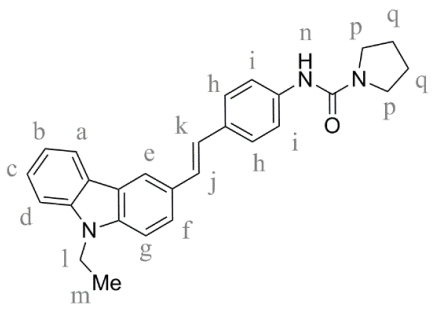

(299)

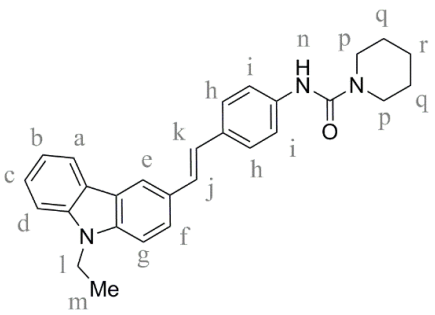

(300)

The ^{1}H-NMR spectrum of compound (**300**) showed a singlet at δ 8.24 for one proton (ArH_e), a doublet at δ 8.15 for one proton (ArH_a), a doublet of

doublet at δ 7.68 for one proton (ArH_{f}), multiplet at δ 7.10-7.52 for ten protons (Ar$H_{b\text{-}d,g\text{-}i,}$ vinylic-$H_{j,k}$) confirmed a total of eleven aromatic protons and two vinylic protons in the structure. A singlet appeared at δ 6.47 for one proton (-NH_{n}CO). It showed a multiplet at δ 3.49-3.51 for four protons (-NC$H_{2/p}$) and a multiplet at δ 1.64-1.70 for six protons (-$NCH_2C$$H_{2/q}$,-$CH_{2/r}$). A quartet appeared at δ 4.39 for two protons (-NC$H_{2/l}CH_3$) and a triplet appeared at δ 1.46 for three protons (-$NCH_2C$$H_{3/m}$) confirming the presence of *N*-ethyl group. The ^{13}C-NMR spectrum showed peak at δ 155.26 due to C=O carbon of the urea. The aromatic and vinylic carbons appeared at δ 140.41, 140.38, 139.55, 131.51, 129.05, 127.65, 126.61, 126.32, 126.00, 124.92, 123.02, 122.70, 120.87, 120.09, 119.35, 118.59, 109.76 and 109.70 whereas the aliphatic carbons appeared at δ 45.17, 37.51, 26.00, 24.58 and 14.20. Its mass spectrum showed $[M+H]^+$ ion peak at 424.3 m/z.

The ^{1}H-NMR spectrum of compound (**301**) showed a singlet at δ 8.73 accounting for one proton (–NH_{n}CONH). A singlet at δ 8.34 for one proton (ArH_{e}), a doublet at δ 8.17 for one proton (ArH_{a}), a doublet at δ 7.69 for one proton (ArH_{f}) and multiplet at δ 7.15-7.60 for ten protons (Ar$H_{b\text{-}d,g\text{-}i,}$ vinylic-$H_{j,k}$) confirmed a total of eleven aromatic protons and two vinylic protons in the structure. A triplet appeared at δ 6.15 for one proton (-NHCONH_{o}). It showed a multiplet at δ 3.20-3.24 for two protons (-NHC$H_{2/p}$), a multiplet at δ 2.43-2.49 for six protons (-$NCH_2C$$H_{2/q,r}$) and a multiplet at δ 1.66-1.72 for four protons (-$NCH_2C$$H_{2/s}$). A quartet appeared at δ 4.42 for two protons (-NC$H_{2/l}CH_3$) and a triplet at δ 1.31 for three protons (-$NCH_2C$$H_{3/m}$) confirming the presence of *N*-ethyl group. The ^{13}C-NMR spectrum showed peak at δ 155.64 due to C=O carbon of the urea. The aromatic and vinylic carbons appeared at δ 140.43, 139.60, 139.03, 132.00, 129.10, 127.94, 127.40, 127.03, 125.86, 124.98, 123.03, 122.71, 120.89, 119.37, 118.87, 118.68, 118.14 and 109.78 whereas the aliphatic carbons appeared at δ 55.83, 53.97, 38.06, 37.52, 23.61 and 14.02.

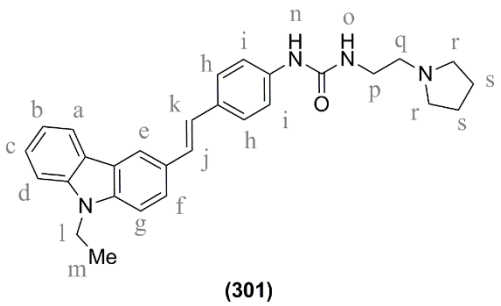

(301)

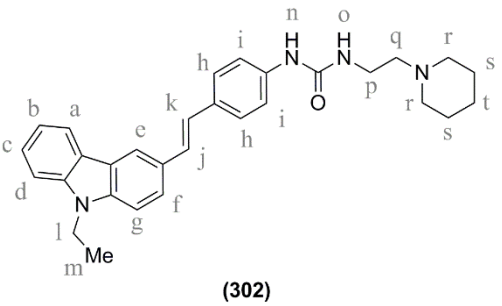

(302)

The ^{1}H-NMR spectrum of compound (**302**) showed a doublet at δ 8.22 for one proton (ArH_{e}), a doublet at δ 8.13 for one proton (ArH_{a}), a doublet of doublet at δ 7.67 for one proton (ArH_{f}) and multiplet at δ 7.10-7.54 for ten protons (Ar$H_{b\text{-}d,g\text{-}i,}$ vinylic-$H_{j,k}$) confirmed a total of eleven aromatic protons and two vinylic protons in the structure. A triplet appeared at δ 6.00 for one proton (–NHCONH_{o}). It showed a multiplet at δ 3.43-3.47 for two protons (–NHC$H_{2/p}$), a multiplet at δ 2.50-2.69 for six protons (-NCH$_2$C$H_{2/q,r}$) and a multiplet at δ 1.70-1.76 for four protons (-NCH$_2$C$H_{2/s}$) and a multiplet at δ 1.51-1.59 for two protons (-C$H_{2/t}$). A quartet appeared at δ 4.37 for two protons (-NC$H_{2/l}$CH$_3$) and triplet appeared at δ 1.45 for three protons (-NCH$_2$C$H_{3/m}$) confirming the presence of *N*-ethyl group. The ^{13}C-NMR spectrum showed peak at δ 155.54 due to C=O carbon of the urea. The aromatic and vinylic carbons appeared at δ 140.41, 140.19, 139.53, 131.02, 129.07, 127.41, 127.41, 126.31, 126.00, 124.90, 123.02, 122.71, 120.88, 119.34, 118.56, 118.18, 109.76 and 109.70, whereas the aliphatic carbons appeared at δ 58.60, 54.50, 37.51, 36.92, 26.01, 24.57 and 14.02.

The ^{1}H-NMR spectrum of compound (**303**) showed a singlet at δ 8.74 for one proton (–NH_{n}CONH). A doublet at δ 8.34 for one proton (ArH_{e}), a doublet at δ 8.17 for one proton (ArH_{a}), a doublet of doublet at δ 7.69 for one proton (ArH_{f}) and multiplet at δ 7.15-7.60 for ten protons (Ar$H_{b\text{-}d,g\text{-}i,}$ vinylic-$H_{j,k}$), confirmed a total of eleven aromatic protons and two vinylic protons in structure. A triplet appeared at δ 6.07 for one proton (–NHCONH_{o}). It showed multiplet at δ 3.17-3.22 for two protons (–NHC$H_{2/p}$), a multiplet at δ 2.33-2.36 for six protons (-NC$H_{2/r,s}$), a multiplet at δ 1.49-1.54 for four protons (-NCH$_2$C$H_{2/t}$) and a multiplet at δ 1.36-1.42 for two protons (-NCH$_2$CH$_2$C$H_{2/q}$). A quartet appeared at δ 4.44 for two protons (-NC$H_{2/l}$CH$_3$) and a triplet appeared

at δ 1.31 for three protons (-NCH$_2$C$H_{3/m}$) confirming the presence of *N*-ethyl group. The ^{13}C-NMR spectrum showed peak at δ 155.64 due to C=O carbon of the urea. The aromatic and vinylic carbons appeared at δ 140.41, 140.18, 139.58, 131.03, 129.07, 127.42, 127.01, 126.31, 126.00, 124.89, 123.02, 122.71, 120.87, 119.34, 118.57, 118.26, 109.75 and 109.69, whereas the aliphatic carbons appeared at δ 54.09, 53.75, 38.06, 37.51, 29.51, 23.56 and 14.20.

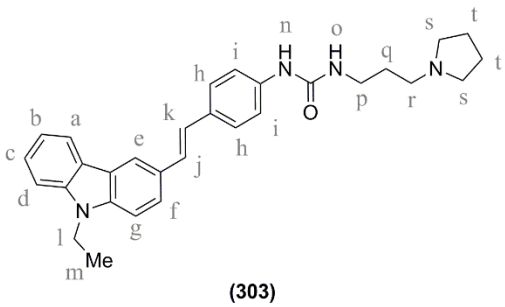

(303)

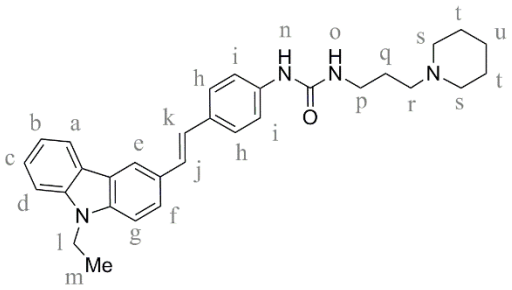

(304)

The ^{1}H-NMR spectrum of compound (**304**) showed a singlet at δ 8.53 accounting for one proton (–NH_nCONH). A doublet at δ 8.34 for one proton (ArH_e), a doublet at δ 8.17 for one proton (ArH_a), a doublet of doublet at δ 7.69 for one proton (ArH_f) and multiplet at δ 7.15-7.60 for ten protons (Ar$H_{b\text{-}d,g\text{-}i,}$ vinylic-$H_{j,k}$) confirmed a total of eleven aromatic protons and two vinylic protons in structure. A triplet appeared at δ 6.17 for one proton (-NHCONH_o). It showed a multiplet at δ 3.08-3.13 for two protons (-NHC$H_{2/p}$), a multiplet at δ 2.23-2.29 for six protons (-NC$H_{2/r,s}$), a multiplet at δ 1.55-1.59 for two protons (-NCH$_2$C$H_{2/q}$), a multiplet at δ 1.46-1.51 for four protons (-NCH$_2$C$H_{2/t}$) and a multiplet at δ 1.35-1.40 for two protons (-NCH$_2$CH$_2$C$H_{2/u}$). A quartet appeared at δ 4.43 for two protons (-NC$H_{2/l}$CH$_3$) and a triplet appeared at δ 1.31 for three protons (-NCH$_2$C$H_{3/m}$) confirming the presence of *N*-ethyl group. The ^{13}C-NMR spectrum showed peak at δ 155.64 due to C=O carbon of the urea. The aromatic and vinylic carbons appeared at δ 140.41, 140.19, 139.52, 131.03, 129.07, 127.41, 127.01, 126.30, 126.00, 124.88, 123.03, 122.71, 120.87, 119.34, 118.58, 118.28, 109.74 and 109.63 whereas the aliphatic carbons appeared at δ 56.64, 54.57, 38.09, 37.50, 27.52, 26.01, 24.62 and 14.19.

4.2.1.2.2.4. Synthesis of (*E*)-*N*-(4-(2-(9-ethyl-9*H*-carbazol-3-yl)vinyl) phenyl)aminoalkylthioureas (305-307)

Synthesis of (*E*)-*N*-(4-(2-(9-ethyl-9*H*-carbazol-3-yl)vinyl)phenyl) aminoalkylthiourea derivatives (**305-307**) was carried out as presented in **Scheme 4.13**. Compound (**289**) was reacted with thiocarbonyl diimidazole in the presence of triethylamine in DCM:THF (1:1), followed by reaction with the respective aminoalkylamines to obtain the titled thiourea derivatives (**305-307**).[164]

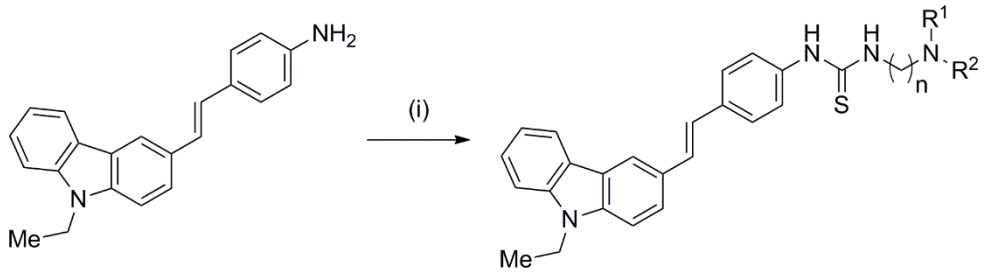

(289) **(305-307)**

Compd.	n	NR^1R^2	Compd.	n	NR^1R^2
305	2	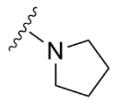	**306**	2	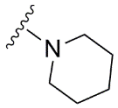
307	3				

Scheme 4.13. Synthetic route for the synthesis of compounds (**305-307**). Reagents and conditions: (i) (a) Thiocarbonyldiimidazole, DCM:THF (1:1), 0 °C to RT; (b) 1-pyrrolidinylalkylamines/1-piperidinylethylamine, RT.

The IR spectra of compounds (**305-307**) showed characteristic peaks at ~1235 cm^{-1} (thiourea C=S stretching), ~3250 cm^{-1} (N-H stretching), while the amine N-H stretching peaks disappeared. The analytical data of the compounds (**305-307**) are given in **Table 4.30**.

Table. 4.30. Analytical data of (*E*)-*N*-(4-(2-(9-ethyl-9*H*-carbazol-3-yl)vinyl) phenyl)aminoalkylthioureas (305-307)

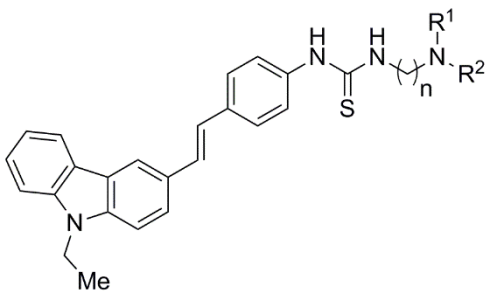

(305-307)

Compd	n	NHR^1R^2	M.P.	IR characteristic peaks (cm^{-1})	LCMS data
305	0		114-116 °C	3248, 3026, 2966, 1597, 1512, 1480, 1233, 1057, 961, 746	469.3 $[M+H]^+$ Purity: ~100 %
306	0		183-185 °C	3290, 3029, 2934, 1599, 1513, 1478, 1236, 961, 821, 750	483.4 $[M+H]^+$ Purity: ~100 %
307	1		188-190 °C	3186, 2967, 2871, 2816, 1594, 1524, 1236, 958, and 747	483.4 $[M+H]^+$ Purity: ~100 %

The ^{1}H-NMR spectrum of compound **(305)** showed a singlet at δ 9.71 for one proton (–NH_nCSNH). A doublet at δ 8.36 for one proton (ArH_e), a doublet at δ 8.17 for one proton (ArH_a), multiplet at δ 7.69-7.73 for one proton (ArH_f) and multiplet at δ 7.19-7.61 for ten protons (Ar$H_{b\text{-}d,g\text{-}i,}$ vinylic-$H_{j,k}$), confirmed a total of eleven aromatic protons and two vinylic protons in structure. It showed a multiplet at δ 3.54-3.61 for two proton (–NHC$H_{2/p}$), a triplet at δ 2.61 for two protons (-NC$H_{2/q}$), a multiplet at δ 2.47-2.51 for four protons (-NC$H_{2/r}$) and a multiplet at δ 1.67-1.74 for four protons (-$NCH_2CH_{2/s}$). A quartet appeared at δ 4.44 for two protons (-NC$H_{2/l}CH_3$) and a triplet appeared at δ 1.30 for three protons (-$NCH_2CH_{3/m}$) confirming the presence of *N*-ethyl group. In ^{13}C-NMR, the aromatic and vinylic carbons appeared at δ 139.96, 139.22, 133.43, 128.48, 128.32, 126.27, 125.90, 125.10, 124.62, 122.55, 122.23, 120.44, 118.94, 118.39, 109.35 and 109.30 whereas the aliphatic carbons appeared at δ 53.43, 42.90, 37.06, 23.20 and 13.77.

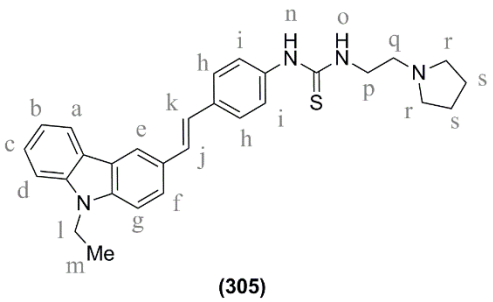

(305)

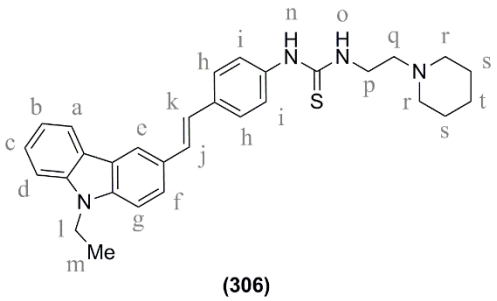

(306)

The ^{1}H-NMR spectrum of compound (**306**) showed a singlet at δ 9.72 accounting for one proton (–N*H*$_{n}$CSNH). A doublet at δ 8.37 for one proton (Ar*H*$_{e}$), a doublet at δ 8.17 for one proton (Ar*H*$_{a}$), multiplet at δ 7.71-7.73 for one proton (Ar*H*$_{f}$) and multiplet at δ 7.19-7.61 for ten protons (Ar*H*$_{b\text{-}d,g\text{-}i,}$ vinylic-*H*$_{j,k}$) confirmed a total of eleven aromatic protons and two vinylic protons in structure. It showed a multiplet at δ 3.52-3.58 for two protons (–NHC*H*$_{2/p}$), a triplet at δ 2.47 for two protons (-NC*H*$_{2/q}$), a multiplet at δ 2.33-2.38 for four protons (-NC*H*$_{2/r}$), a multiplet at δ 1.45-1.52 for four protons (-NCH$_2$C*H*$_{2/s}$) and a multiplet at δ 1.34-1.41 for two protons (-NC*H*$_{2/t}$). A quartet appeared at δ 4.44 for two protons (-NC*H*$_{2/l}$CH$_3$) and a triplet appeared at δ 1.30 for three protons (-NCH$_2$C*H*$_{3/m}$) confirming the presence of *N*-ethyl group. In ^{13}C-NMR, the aromatic and vinylic carbons appeared at δ 139.96, 139.24, 133.61, 128.59, 128.30, 126.41, 125.91, 125.06, 124.64, 122.85, 122.55, 122.23, 120.44, 118.95, 118.42, 109.35 and 109.30 whereas the aliphatic carbons appeared at δ 53.87, 41.20, 37.06, 25.63, 24.08, 13.76.

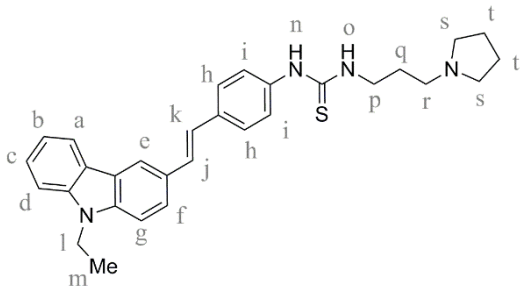

(307)

The ^{1}H-NMR spectrum of compound (**307**) showed a singlet at δ 9.55 for one proton (–N*H*$_{n}$CSNH). A doublet at δ 8.37 for one proton (Ar*H*$_{e}$), a doublet at δ 8.17 for one proton (Ar*H*$_{a}$), a multiplet at δ 7.96-8.00 for one proton (Ar*H*$_{f}$) and multiplet at δ 7.19-7.73 for ten protons (Ar*H*$_{b\text{-}d,g\text{-}i,}$ vinylic-*H*$_{j,k}$) confirmed a total of eleven aromatic protons and two vinylic protons in the structure. It showed a multiplet at δ 3.51-3.55 for two proton (–NHC*H*$_{2/p}$), a

multiplet at δ 2.37-2.45 for six protons (-NC$H_{2/r,s}$), a multiplet at δ 1.66-1.75 for two protons (-$NCH_2CH_{2/q}$) and a multiplet at δ 1.55-1.59 for four protons (-$NCH_2CH_{2/t}$). A quartet appeared at δ 4.44 for two protons (-NC$H_{2/l}CH_3$) and a triplet appeared at δ 1.32 for three protons (-$NCH_2CH_{3/m}$) confirming the presence of *N*-ethyl group. The ^{13}C-NMR spectrum showed peak at δ 179.90 due to C=S carbon of the urea. The aromatic and vinylic carbons appeared at δ 139.96, 139.24, 133.69, 128.60, 128.29, 126.40, 125.04, 124.64, 123.09, 122.55, 122.23, 120.44, 118.95, 118.42, 109.35 and 109.30 whereas the aliphatic carbons appeared at δ 53.59, 37.06, 27.34, 23.03 and 13.77.

All the above synthesized carbazole-based stilbene derivatives (**275-286** and **293-307**) were obtained as *trans*-isomers. Efforts were also made to synthesize the *cis*-isomers but all our attempts failed as a mixture of both the geometric isomers only could be obtained as the reaction products. It was also attempted to separate both the isomers from the crude product using chromatographic techniques, but unfortunately, the cis isomer was getting converted to the trans isomer during processing. Hence all our attempts to obtain the desired *cis* isomer failed.

4.2.1.3. Biological evaluation of the synthesized compounds

All the synthesized carbazole-based stilbene derivatives (**275-286** and **293-307**) were evaluated for their multifactorial anti-AD activities, including cholinesterase inhibitory activity, $A\beta_{1-42}$ aggregation inhibitory activity, anti-oxidant activity, metal chelation activity which are discussed under the following subheadings:

4.2.1.3.1. *In vitro* cholinesterase inhibition studies,

4.2.1.3.2. Self-mediated $A\beta_{1-42}$ aggregation inhibition study,

4.2.1.3.3. Antioxidant activity (DPPH radical scavenging activity),

4.2.1.3.4. Metal chelation study.

4.2.1.3.1. *In vitro* cholinesterase inhibition studies

The potential of the synthesized compounds to inhibit ChEs was evaluated *in vitro* by Ellman's assay, as reported by our group earlier.[115-117] The obtained IC_{50} values of the compounds for both AChE and BuChE enzymes and their selectivity indices (SI) are summarized in **Table 4.31**. All the compounds

(**275-286**) offered IC_{50} values in the range of 1.84-6.63 μM for AChE and 1.02-5.01 μM for BuChE as shown in **Table 4.31**.

It was observed that changing the length of the carbon chain affected the inhibitory activity. A comparative analysis of the inhibitory potential of compounds (**276**, **278** and **280**) having a piperidine ring, revealed that compound (**280**, n = 4) showed good AChE inhibitory activity (IC_{50} value of 1.84 μM) while compound (**278**, n = 3) and compound (**276**, n = 2) showed slightly less AChE inhibitory activities (IC_{50} values of 2.91 and 3.00 μM, respectively) **(Table 4.31**). A similar activity pattern was also observed for the compounds (**275**, **276** and **277**). Among these, compound (**276**, n = 2) showed better BuChE inhibition (IC_{50} value of 1.40 μM) in comparison to other amide-based derivatives.

When the pyrrolidinyl (compound **281**) and piperidinyl (compound **282**) moieties were attached directly (n = 0, **Table 4.31**) to form urea derivatives, the inhibitory activities against both the enzymes decreased notably. Due to direct attachment, these compounds lost their basic centers, which are seemingly indispensable for cation-π interaction with Trp84 of AChE. Compounds (**281**and **282**) showed inhibitory activities (AChE; IC_{50} = 6.63 μM and 5.99 μM, respectively and BuChE; IC_{50} = 4.48 μM and 5.01 μM, respectively). There was no significant change observed in inhibitory activities when the amide linkers (compounds **277-280**) were substituted with urea linkers (compounds **283**, **284**) (**Table 4.31**).

Shifting the chain from the carbazole (ring A, **Figure 4.16**) to phenyl ring (ring B) preserved the ChEs inhibitory activities (**Table 4.32**). A comparative analysis of the inhibitory potential of compounds (**293**, **295** and **297**) having a pyrrolidine ring, revealed that compound (**295**, n = 2) showed the best AChE and BuChE inhibitory activities (IC_{50} values of 2.36 μM and 1.46 μM, respectively) while compound (**293**, n = 1) and compound (**295**, n = 3) showed slightly lesser AChE and BuChE inhibitory activities. A similar activity pattern was also observed for the compounds (**294**, **296**, and **298**). Among these, compound (**296**, n = 2) showed good AChE and BuChE inhibitory activities (IC_{50} values of 2.25 μM and 1.74 μM, respectively).

Table 4.31. *In vitro* inhibition of AChE and BuChE, and selectivity indices (SI) of compounds (275-286)

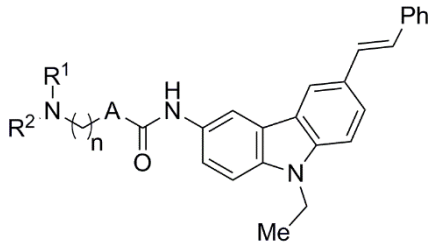

(275-286)

Compd	A	n	R^1R^2N	IC_{50} ± SEM (µM)		SI[c]
				AChE[a]	BuChE[b]	
275	-	2		3.00 ± 0.52	1.53 ± 0.31	0.51
276	-	2		4.69 ± 0.25	1.40 ± 0.22	0.29
277	-	3		2.91 ± 0.14	1.51 ± 0.35	0.52
278	-	3		3.54 ± 0.56	2.56 ± 0.29	0.72
279	-	4		2.63 ± 0.31	3.17 ± 0.43	1.20
280	-	4		1.84 ± 0.27	2.51 ± 0.19	1.36
281	-	-		6.63 ± 0.54	4.48 ± 0.15	0.67
282	-	-		5.99 ± 0.07	5.01 ± 1.02	0.83
283	-NH	2		2.65 ± 0.32	1.70 ± 0.18	0.64
284	-NH	2	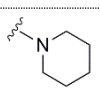	3.79 ± 0.41	1.99 ± 0.21	0.52
285	-NH	3		4.54 ± 0.52	3.19 ± 0.35	0.70
286	-NH	3	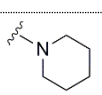	3.57 ± 0.29	1.02 ± 0.18	0.28
Tacrine				0.056 ± 0.01	0.008 ± 0.00	0.14
Donepezil				0.023 ± 0.01	1.87 ± 0.08	81.3

[a]AChE from human erythrocytes; IC_{50}, 50% inhibitory concentration (means ± SEM of three experiments), [b]BuChE from equine serum, [c]Selectivity Index = IC_{50} (BuChE)/IC_{50} (AChE).

Table 4.32. *In vitro* inhibition of AChE and BuChE, and selectivity indices (SI) of compounds (293-307)

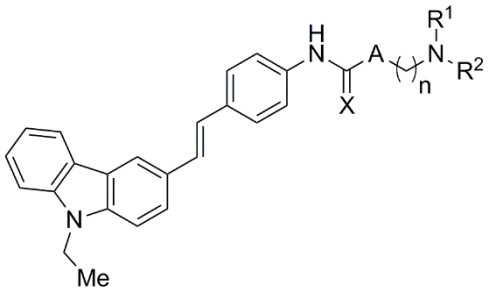

(293-307)

Compd	X	A	n	R^1R^2N	IC_{50} ± SEM (µM)		SI[c]
					AChE[a]	BuChE[b]	
293	O	-	1		2.98 ± 0.78	2.49 ± 0.65	0.84
294	O	-	1		3.52 ± 0.87	2.72 ± 0.98	0.79
295	O	-	2		2.36 ± 0.20	1.46 ± 0.42	0.62
296	O	-	2	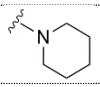	2.25 ± 0.31	1.74 ± 0.19	0.77
297	O	-	3		4.77 ± 0.61	4.76 ± 1.03	0.99
298	O	-	3	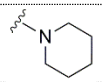	3.29 ± 1.09	2.11 ± 0.69	0.64
299	O	-	-		16.22 ± 1.03	11.65 ± 0.51	0.68
300	O	-	-		12.37 ± 0.87	8.58 ± 1.02	0.69
301	O	-NH	2		4.71 ± 1.05	2.32 ± 0.97	0.49
302	O	-NH	2	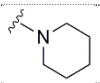	3.13 ± 0.71	1.20 ± 0.57	0.38
303	O	-NH	3	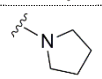	3.04 ± 0.43	1.92 ± 0.25	0.63
304	O	-NH	3		2.94 ± 0.98	1.98 ± 0.84	0.67
305	S	-NH	2	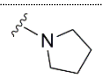	2.64 ± 0.41	1.29 ± 0.10	0.49
306	S	-NH	2		3.41 ± 0.25	1.72 ± 0.25	0.50
307	S	-NH	3		3.19 ± 0.34	1.32 ± 0.17	0.41

[a]AChE from human erythrocytes; IC_{50}, 50% inhibitory concentration (means ± SEM of three experiments). [b]BuChE from equine serum. [c]Selectivity Index = IC_{50} (BuChE)/IC_{50} (AChE).

All the urea derivatives (**299-304**) showed good ChEs inhibition except for compounds (**299** and **300**, n = 0) in which the heterocyclic amines were directly attached to form urea derivatives. Compounds (**299** and **300**) showed moderate inhibitory activities (AChE; IC_{50} = 16.22 μM and 12.37 μM, respectively and BuChE; IC_{50} = 11.65 μM and 8.58 μM, respectively). There was no significant change observed in AChE inhibitory activities when the amide linkers (compounds **297** and **298**) were substituted with urea linkers (compounds **301** and **302**), whereas the BuChE inhibitory activity was observed to be increased by two folds. All the thiourea derivatives (**305-307**) showed the best ChEs inhibitory activities amongst all the derivatives. Amongst them, compound (**305**) conferred the best AChE and BuChE inhibitory activities (n = 2, IC_{50} value of 2.64 μM and 1.29 μM, respectively).

4.2.1.3.2. Self-mediated $A\beta_{1-42}$ aggregation inhibition study

Aβ peptides present in the extracellular amyloid plaques are produced by sequential cleavage of APP by β- and γ-secretases. $A\beta_{1-40}$ and $A\beta_{1-42}$ are the two main isoforms of Aβ peptides present in the plaques. $A\beta_{1-40}$ is the predominant product in the proteolytic cleavage, whereas $A\beta_{1-42}$ is more fibrillogenic in nature. So, $A\beta_{1-42}$ was chosen to study the Aβ aggregation inhibition. The potential of the compounds to inhibit self-mediated $A\beta_{1-42}$ aggregation was assessed using Thioflavin T (ThT) fluorescence assay.[165] Curcumin was used as a positive control in this assay. Percentage inhibitions of self-mediated $A\beta_{1-42}$ aggregation of all the tested compounds at 25 μM concentrations are listed in **Table 4.33** and **Table 4.34**. All the tested compounds showed good $A\beta_{1-42}$ aggregation inhibition ranging from 38.9 to 55.79 % except for compounds (**281** and **282**). Amongst them, compound (**302**) showed the best $A\beta_{1-42}$ aggregation inhibition (55.79 %) at 25 μM concentration.

Table 4.33. Aβ_{1-42} aggregation inhibitory and DPPH radical scavenging activity of the compounds (275-286)

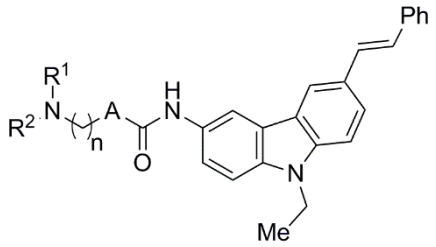

(275-286)

Compd	A	n	R^1R^2N	Aβ_{1-42} aggregation Inhibition (%) at 50 µM conc.	RP of DPPH IC_{50} ± SEM (µM) or % inhibition at 100 µM
275	-	2		42.72 ± 0.31	144.61 ± 2.32 (35.46 %)
276	-	2		52.08 ± 0.64	135.42 ± 2.05 (39.31 %)
277	-	3		53.92 ± 0.28	145.02 ± 3.61 (36.15 %)
278	-	3		49.88 ± 0.15	122.41 ± 3.20 (41.63 %)
279	-	4		46.72 ± 0.33	134.63 ± 1.29 (38.11 %)
280	-	4		48.09 ± 0.54	138.18 ± 1.53 (36.97 %)
281	-	-		17.58 ± 0.42	> 500 (7.38 %)
282	-	-		21.55 ± 0.62	> 500 (4.62 %)
283	-NH	2		52.29 ± 0.42	104.28 ± 3.87 (48.94 %)
284	-NH	2		50.08 ± 0.42	110.42 ± 2.62 (47.54 %)
285	-NH	3		54.94 ± 0.42	123.62 ± 3.53 (42.49 %)
286	-NH	3		54.35 ± 0.42	118.58 ± 3.20 (45.62 %)
Tacrine				nd	> 500
Donepezil				nd	> 500
Curcumin				20.43 ± 0.72 µM (IC_{50})	nd
Ascorbic acid				nd	13.9 ± 1.8

Table 4.34. Aβ_{1-42} aggregation inhibitory and DPPH radical scavenging activity of the compounds (293-307)

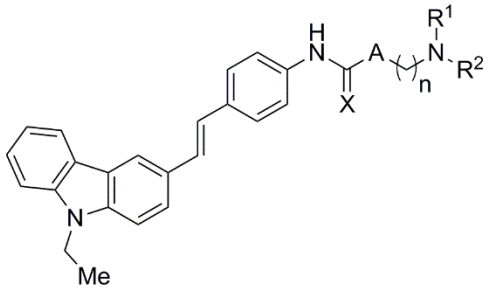

(293-307)

Compd	X	A	n	R^1R^2N	Aβ_{1-42} aggregation Inhibition (%) at 25 µM conc.	RP of DPPH IC_{50} ± SEM (µM) or % inhibition at 100 µM
293	O	-	1		51.14 ± 0.31	132.42 ± 1.17 (42.34 %)
294	O	-	1		45.17 ± 0.64	146.28 ± 3.21 (35.46 %)
295	O	-	2		54.27 ± 0.28	189.10 ± 2.26 (30.15 %)
296	O	-	2		51.92 ± 0.15	178.51 ± 3.66 (25.81 %)
297	O	-	3		53.08 ± 0.33	126.43 ± 2.27 (41.34 %)
298	O	-	3		49.78 ± 0.54	118.58 ± 1.12 (42.91 %)
299	O	-	-		42.84 ± 0.82	> 500 (4.65 %)
300	O	-	-		44.15 ± 0.67	> 500 (5.27 %)
301	O	-NH	2		38.90 ± 0.42	161.45 ± 1.46 (13.67 %)
302	O	-NH	2		55.79 ± 0.42	97.36 ± 1.46 (51.19 %)
303	O	-NH	3		53.86 ± 0.42	106.01 ± 1.39 (45.95 %)
304	O	-NH	3		54.06 ± 0.42	134.70 ± 1.17 (41.98 %)
305	S	-NH	2		51.29 ± 0.42	86.13 ± 1.23 (72.36 %)
306	S	-NH	2		53.24 ± 0.42	91.72 ± 3.43 (66.36 %)
307	S	-NH	3		53.29 ± 0.42	90.33 ± 1.20 (70.36 %)

4.2.1.3.3. Antioxidant Activity (DPPH radical scavenging activity)

The antioxidant activity of the compound was evaluated by its ability to reduce DPPH· radical (purple) to DPPHH (yellow) and the corresponding radical-scavenging potential was assessed by the decrease in the absorbance at 517 nm.[120] Ascorbic acid was employed as a positive control in this assay. All the test compounds displayed moderate free radical scavenging activity (**Table 4.33** and **Table 4.34**). Amongst the thiourea derivatives (compounds **305**, **306** and **307**) showed moderate free radical scavenging activity (IC_{50} values 86.13 μM, 91.72 μM and 90.33 μM, respectively) compared to ascorbic acid (IC_{50} value of 13.9 μM) whereas tacrine and donepezil (IC_{50} values > 500 μM) were found to be devoid of significant free radical scavenging activity at this concentration.

4.2.1.3.4. Metal Chelation study

The high levels and deregulation of biometal ions, such as Cu^{2+}, Zn^{2+}, and Fe^{2+} are closely involved in the pathogenesis of AD.[166] Thus, the potential of compounds to form chelates with these biometals present in the brain of AD patients is adding a feather in the cap of ideal MTDLs to treat AD patients.

The ability of the test compounds to chelate biometals was assessed using UV-vis spectroscopy assay.[165] 8-Hydroxyquinoline (8-HQ) was selected as a positive control (**Figure 4.21**). The results demonstrated that when $CuSO_4$ was added to the solutions of compound (**305**), the maximum absorption at 343 nm decreased dramatically, indicating the formation of ligand-Cu^{2+} complexes (**Figure 4.21**). There were only vague changes in the position and value of absorbance when $FeSO_4$, $FeCl_3$, $ZnCl_2$ or $AlCl_3$ were added into the solutions of the test compounds, suggesting that the test compound had poor chelation abilities for Fe^{2+}, Fe^{3+}, Zn^{2+}, and Al^{3+}. The test compounds were also assessed for their binding property to other biologically significant metals, such as Mg^{2+}, Ca^{2+} wherein compound (**305**) exhibited very poor binding to these metals.

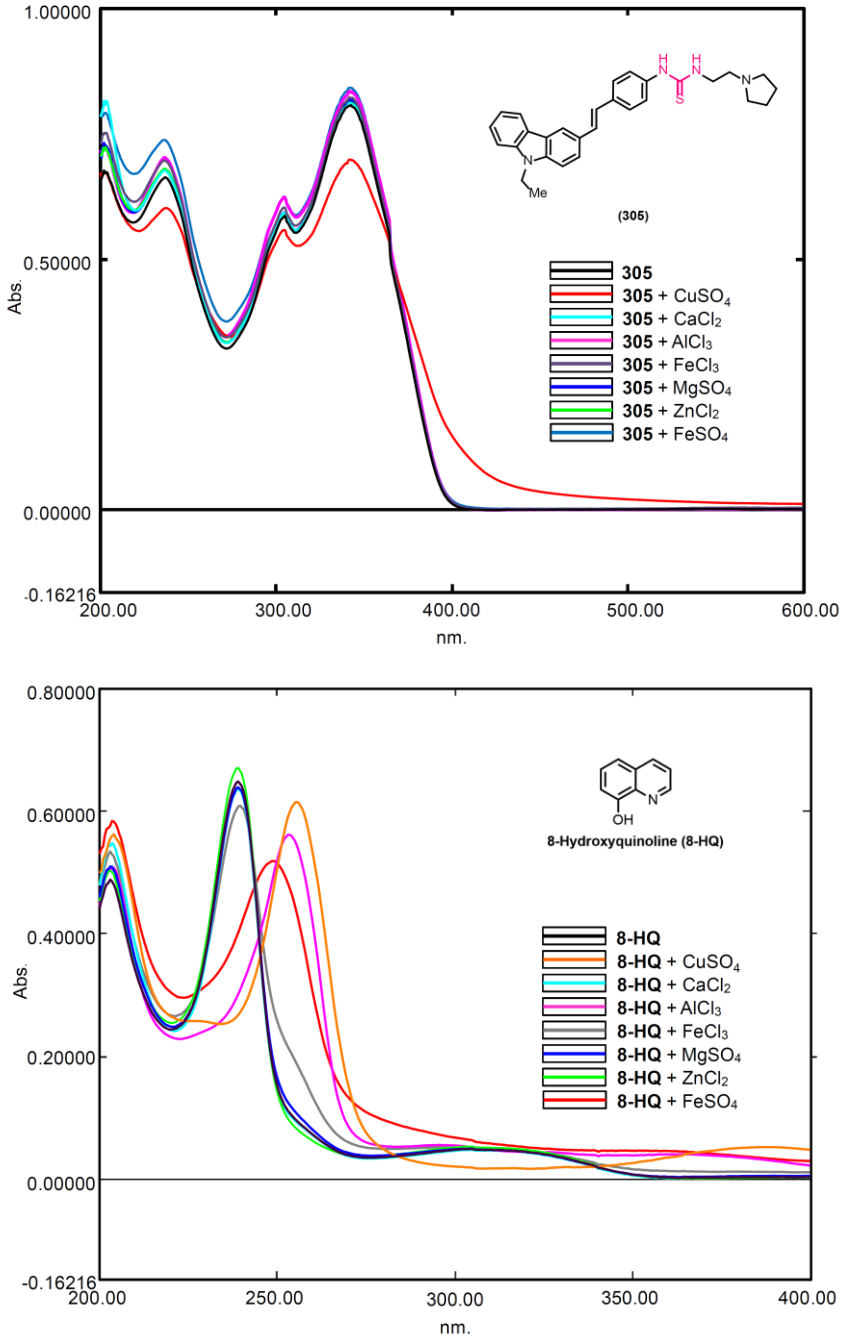

Figure 4.21. Metal chelation study of compound (**305**) and HQ. UV-vis spectra of (**A**) compound (**305**) and (**B**) HQ (25 µM) alone and in the presence of $CuSO_4$ (25 µM), $ZnCl_2$ (25 µM), $FeSO_4$ (25 µM), $FeCl_3$ (25 µM), $AlCl_3$ (25 µM) $MgSO_4$ (25 µM) and $CaCl_2$ (25 µM) in methanol at room temperature

The above results evinced that the target compound (**305**) could selectively chelate Cu^{2+}. This high specificity for a metal ion is of prime importance in the design of a metal chelator to avoid chaotic binding to other critical biometal ions, the depletion of which can lead to allied side effects.

4.2.1.4. Computational studies of the most promising compound

Computational studies of the most promising compound (**305**) were performed to understand the binding mode of the compound with the target proteins and to predict *in silico* ADMET properties of the compound (**305**) and discussed under the following subheads:

4.2.1.4.1. Docking studies of compound (**305**) with target proteins and

4.2.1.4.2. Prediction of virtual physicochemical and pharmacokinetics parameters of compound (**305**).

4.2.1.4.1. Docking studies of compound (305) with target proteins

To understand the molecular interactions and binding mode of the most active compound (**305**) with the ChEs, docking studies were carried out with the active sites of *Tc*AChE (PDB code: 2CKM) and *h*BuChE (PDB code: 4BDS).[132] In the docking study of **305** with AChE, the pyrrolidinylethyl thiourea part of the scaffold was observed interacting with the CAS of the active site gorge, whereas the *N*-ethyl carbazole moiety of the scaffold was found to be interacting with receptor active site at PAS of the gorge (**Figure 4.22**).

At PAS, aromatic carbazole exhibited very strong π-π interactions with Tyr70 and Tyr334 (*h*AChE: Tyr72 and Tyr341). Phenyl spacer used of compound (**305**) was observed to be stabilized comfortably in the active site of the enzyme by forming hydrophobic interactions with aromatic amino acids Tyr116, Phe330 and Phe331 (*h*AChE: Tyr119, Tyr337 and Phe338). Stability to the ligand-receptor complex in CAS is mainly observed because of hydrogen bonding, cation-π interaction and salt bridge. The -NH of thiourea interacted with Tyr130 (*h*AChE: Tyr133) by forming a stable hydrogen bond. In addition to this, at physiological *p*H, the protonated nitrogen of pyrrolidine moiety exhibited strong cation-π interaction with Trp84 (*h*AChE: Trp86) along with a hydrogen bonding and salt bridge interaction with Glu199 (*h*AChE: Glu202).

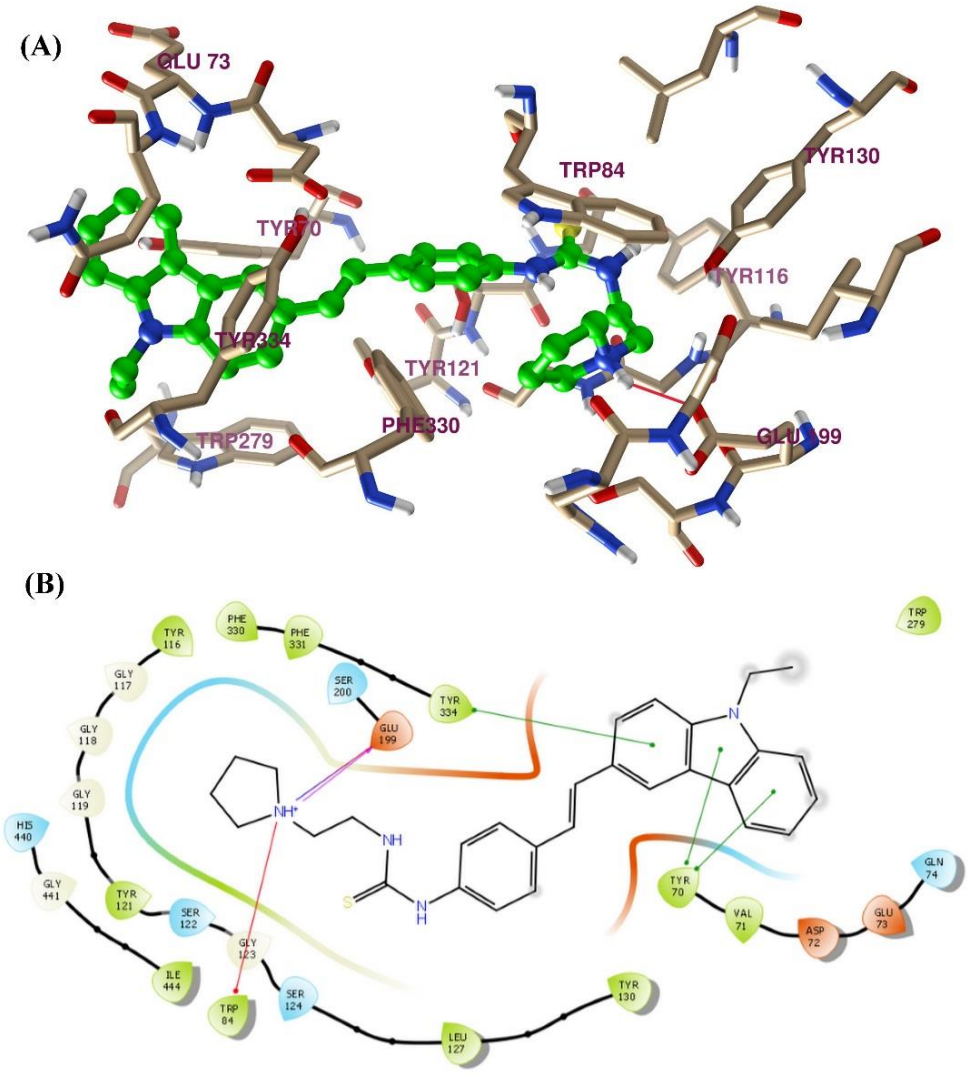

Figure 4.22. Docking model of compound (**305**) with *Tc*AChE (PDB ID: 2CKM). (A) Binding mode of **305** in the active site of *Tc*AChE. (B) Ligand interaction diagram of **305** with *Tc*AChE.

The binding mode of **305** with the BuChE enzyme indicated that it also occupied a large catalytic cavity of BuChE (**Figure 4.23**). Carbazole ring was found to be stabilized in the hydrophobic pocket of nonpolar amino acids Ala277, Val280, Pro285 and Leu286. The phenyl ring in the spacer stabilized the ligand-receptor complex by forming stable π-π interaction with Tyr332. The hydrogen bonding between the -NH of thiourea and Tyr332 imparted stability to the ligand-receptor complex. Further stability to this complex was also provided by the protonated nitrogen of pyrrolidine by forming cation-π interaction with Trp82.

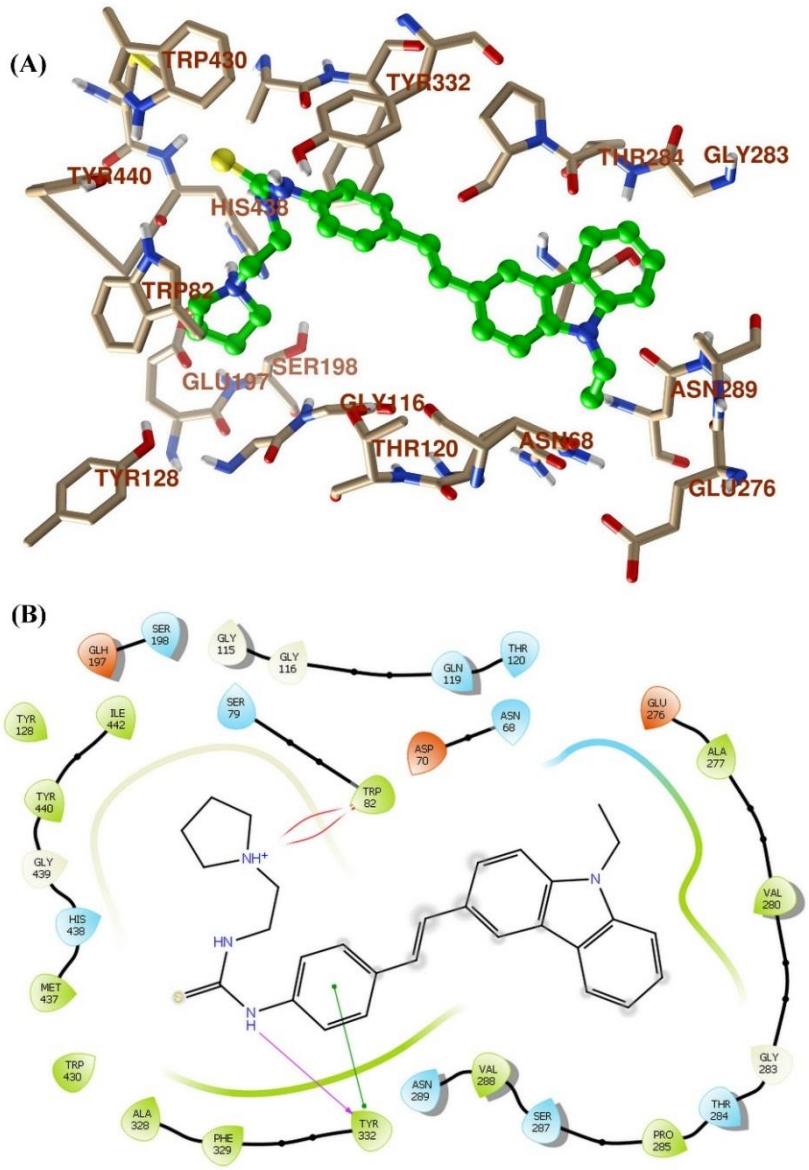

Figure 4.23. Docking model of compound (**305**) with *h*BuChE (PDB ID: 4BDS). (A) Binding mode of **305** in the active site of *h*BuChE. (B) Ligand interaction diagram of **305** with *h*BuChE.

To understand the binding interaction of compound (**305**) with $A\beta_{1\text{-}42}$, a blind docking study was performed using the X-ray crystal structure of human $A\beta_{1\text{-}42}$ (PDB code: 1IYT).[84] In this study, the most stable ligand-receptor complex showed promising interactions (**Figure 4.24**). Compound (**305**) was observed to be aligned with the chain of $A\beta_{1\text{-}42}$. The carbazole ring formed a stable π-π interaction with Phe19, whereas both the -NH of thiourea were observed to be interacting strongly with Asp7 by hydrogen bonding. Further the protonated nitrogen of pyrrolidine established the stable salt bridge interactions

with Asp7 and Glu11. Along with this interaction, ligand-receptor stability was further supported by the hydrogen bonding of the nitrogen of pyrrolidine with Asp7 residue.

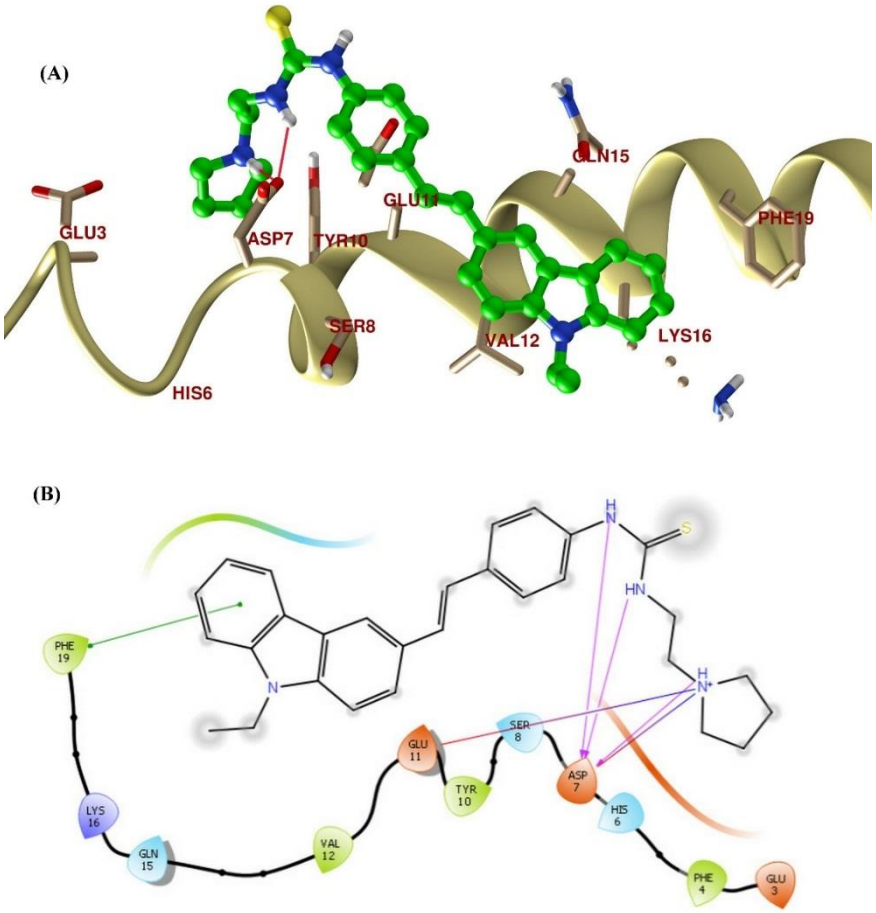

Figure 4.24. Docking model of compound (**305**) with $A\beta_{1-42}$ (PDB code 1IYT): (A) Binding mode of **305** with $A\beta_{1-42}$. The possible hydrogen bonding between compound (**305**) and Asp7 residue is shown by the red line (B) Ligand interaction diagram of **305** with *h*BuChE.

4.2.1.4.2. Prediction of virtual physicochemical and pharmacokinetics parameters

The virtual physicochemical and pharmacokinetic parameters like Lipinski's parameters, NRB, PSA, QPPCaco, QPMDCK, CNS, QPlogBB, QPlogKhsa were predicted for compound (**305**) with QikProp module[136] (**Table-4.35**).

Table 4.35. Predicted ADMET Parameters of Compound (305) and Donepezil[a]

Parameter	Limit	Compd (305)	Donepezil
MW	130-725	468.659	379.498
HBA	2-20	4.5	5.5
HBD	0-6	2	0
NRB	0-8	8	6
QPlogP$_{o/w}$	-2 to 6.5	7.002	4.242
PSA	7 to 200	38.55	46.234
Volume	500-2000	1571.159	1248.451
ReFG	0-2	0	0
SASA	300 to 1000	878.316	681.675
Rule of Five (violation)	0-1	1	0
CNS	-	1	1
QPMDCK	-	1284.443	589.289
QPlogBB	-3 to 1.2	0.219	0.223
QPPCaco	-	1235.258	1070.771
QPlogKhSa	-1.5 to 1.5	1.58	0.516
QPlogS	-6.5 to 0.5	-8.12	-4.059
% HOA	0-100	100	100
#star	0-5	4	0

[a]MW: molecular weight, HBA: hydrogen-bond acceptor atoms, HBD: hydrogen-bond donor atoms, NRB: number of rotatable bonds, QPlogP$_{o/w}$: Predicted octanol/water partition coefficient, PSA: polar surface area, #rtvFG: number of reactive functional groups; SASA: total solvent accessible surface area, CNS: predicted central nervous system activity on a -2 (inactive) to +2 (active) scale, QPMDCK: Predicted apparent MDCK cell permeability in nm/s, QPlogBB: brain/blood partition coefficient, QPPCaco: Caco-2 cell permeability in nm/s, QPlogKhsa: binding to human serum albumin, QPlogS: predicted aqueous solubility, % HOA: human oral absorption on 0–100% scale, #star: number of parameters with values that fall outside the 95% range of similar values for known drugs.

Compound (**305**) follows all the Lipinski's rule-of-five parameters[137] in the given acceptable ranges except QPlogPo/w (value > 5). Compound (**305**) violates only one limit of the Lipinski's rule-of-five, making it a promising lead for further development. The NRB and TPSA are the two key parameters introduced by Veber as discussed earlier.[138] Compound (**305**) possesses eight rotatable bonds and TPSA value of 38.55 $Å^2$. QPCaco-2 value relates with oral absorption of a drug. It shows apparent gut-blood barrier permeability. Values above 500 predict high oral absorption which is attained for compound (**305**). Good oral bioavailability of compounds (**305**) is also supported by the predicted human oral absorption percent (% HOA) value. Brain/blood partition coefficient (QPlogBB), CNS, *n*-octanol-water partition coefficient ($QPlogP_{o/w}$), and apparent MDCK cell permeability (QPPMDCK) predict the ability of the compound to cross the BBB. Compound (**305**) is predicted to be CNS active as it possesses a CNS value of 1 and QPlogBB value of 0.219. QPPMDCK value predicts apparent MDCK cell permeability in nm/s. It is recognized as a good mimic for the BBB. A QPPMDCK value higher than 25 is viewed as good, and the compound (**305**) has shown considerably high values. The QPlogKhsa value predicts the binding of compound with human serum albumin. Compound (**305**) showed slightly higher value than the recommended value of QPlogKhsa. #star shows the number of parameters with values that fall outside the 95% range of similar values for known drugs. Larger number of #stars suggests that the compound would prove to be less druglike than the one with fewer #stars. Value of #star for compound (**305**) suggests its druglikeness. Further, a compound having the tertiary nitrogen-containing moiety, which is a common feature in many CNS active drugs, exhibits a higher degree of brain permeation.[140] As shown, the compound (**305**) is predicted to have a good pharmacokinetic profile, which would strengthen its biological significance.

4.2.2. Carbazole-based azahelicene derivatives

The work carried out under this heading has been further divided into 4 subheadings i.e. designing aspect, chemical studies, biological studies, and computational studies as mentioned below:

4.2.2.1. Designing of carbazole based azahelicene derivatives as anti-AD agents,

4.2.2.2. Synthesis and characterization of the envisaged azahelicenes,

4.2.2.3. Biological evaluation of synthesized compounds as anti-AD agents and

4.2.2.4. Computational studies of the promising compound.

4.2.2.1. Designing of carbazole-based azahelicene derivatives as anti-AD agents

Helicenes are defined as ortho-fused polycyclic aromatic compounds having at least five ortho-condensed rings arranged in such a way that the molecules become helical in shape.[167] These helical molecules attract the attention of the researchers due to their unique structural, optical and spectral properties. Self-mediated Aβ aggregation inhibition is one of the strategies to confront the AD. The role of π-stacking in Aβ aggregate formation suggests that any ligand that can inhibit the π-stacking interactions may be a good candidate for the treatment of AD. Helicenes have high π electron density which might be useful for the inhibition of π-stacking in Aβ aggregate formation.

Carbazole, an important nitrogen containing heterocycle widely present in many phytochemicals has large array of biological activities associated with AD as discussed previously. So, keeping the above points in mind we merged these two moieties i.e. carbazole and helicene into one scaffold i.e. azahelicene with the hope to obtain the beneficial effects of both the moieties. We have previously reported substituted triazinoindole derivatives as anti-AD agents, in which the pyrrolidine and piperidine moieties showed an indispensable role in the cholinesterase inhibitory activity. Here we designed a series of carbazole based azahelicene derivatives in which the heterocyclic amines were linked to the designed scaffold using suitable linkers endowed with additional anti-AD properties (**Figure 4.25**).

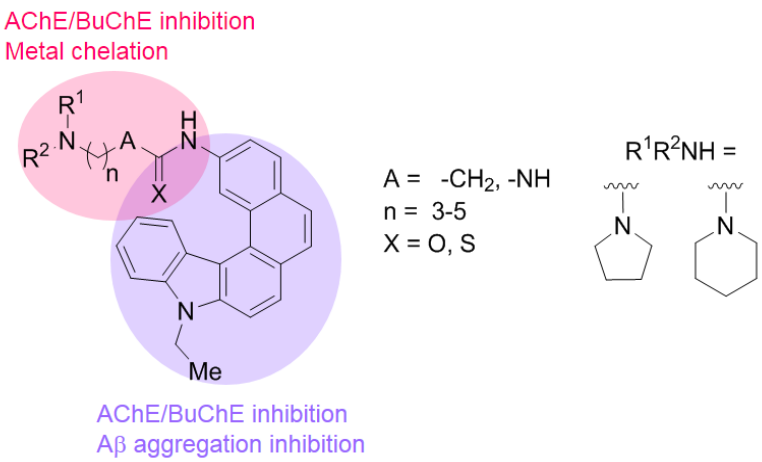

Figure 4.25. Designing aspects of novel azahelicene derivative.

4.2.2.2. Synthesis and characterization of the envisaged azahelicene

The envisaged azahelicene derivatives were synthesized from commercially available carbazole as depicted in **Scheme 4.14-4.17**. The synthetic work has been divided into four subheadings as mentioned below:

4.2.2.2.1. Synthesis of a key intermediate 9-ethyl-9*H*-naphtho[2,1-*c*] carbazol-2-amine (**312**),

4.2.2.2.2. Synthesis of 1-(9-ethyl-9*H*-naphtho[2,1-*c*]carbazol-2-yl) aminoalkylamides (**316-321**),

4.2.2.2.3. Synthesis of 1-(9-ethyl-9*H*-naphtho[2,1-*c*]carbazol-2-yl) aminoalkylureas (**322-327**),

4.2.2.2.4. Synthesis of 1-(9-ethyl-9*H*-naphtho[2,1-*c*]carbazol-2-yl) aminoalkylthioureas (**328**, **329**).

4.2.2.2.1. Synthesis of a key intermediate 9-ethyl-9*H*-naphtho[2,1-*c*] carbazol-2-amine (312)

Synthesis of a key intermediate 9-ethyl-9*H*-naphtho[2,1-*c*]carbazol-2-amine (**312**) was synthesized from carbazole as depicted in **Scheme 4.14**. 9-Ethyl-9*H*-carbazole-3-carbaldehyde (**268**) was synthesized from carbazole as discussed previously in **Scheme 4.7**.

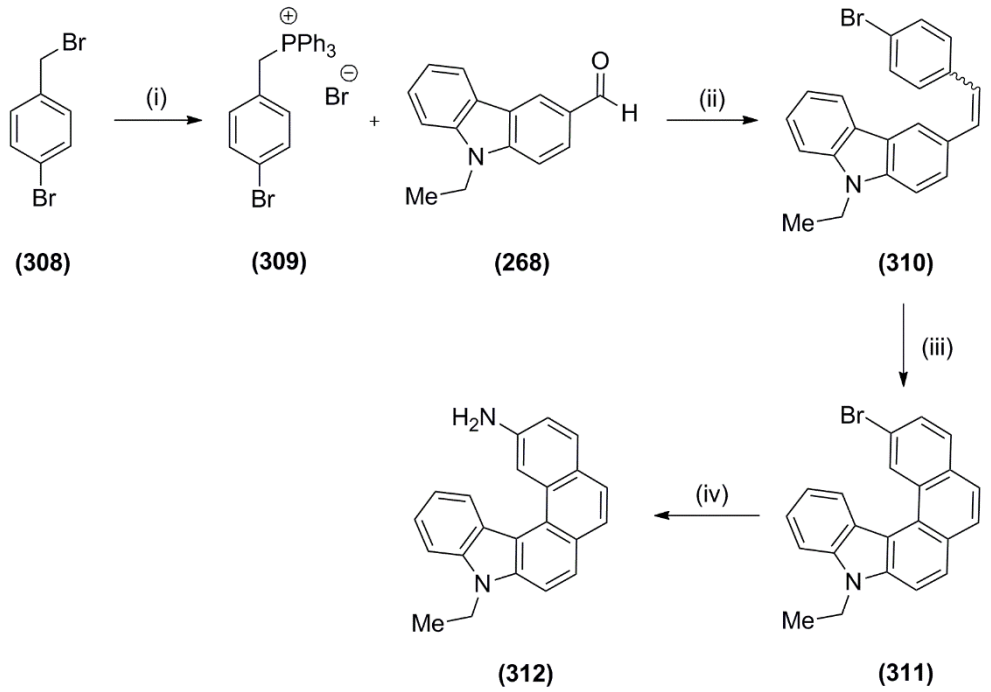

Scheme 4.14. Synthetic route for the synthesis of a key amine intermediate (**312**)**.** Reagents and conditions: (i) Triphenylphosphine, toluene, 100 ºC; (ii) aqueous NaOH soln., $CHCl_3$; (iii) I_2, THF, toluene, HPMV lamp; (iv) $TMSN_3$, 2-aminoethanol, Cu, dioxane, 95 ºC.

Wittig reagent i.e. 4-bromobenzyltriphenylphosphonium bromide (**309**) was synthesized by reaction of 4-bromobenzyl bromine (**308**) with triphenylphosphine in toluene at 100 ºC for 6-7 hrs. After complete consumption of the starting material, white precipitates of the Wittig reagent so obtained were filtered, washed with *n*-hexane, dried and used in Wittig reaction without further purification.[168] Wittig reaction of 9-ethyl-9*H*-carbazole-3-carbaldehyde (**268**) with 4-bromobenzyltriphenylphosphonium bromide (**309**) in the presence of aqueous sodium hydroxide in chloroform gave a mixture of *cis* and *trans* 3-(4-bromostyryl)-9-ethyl-9H-carbazole (**310**).[168]

Photodehydrocyclization of this 3-(4-bromostyryl)-9-ethyl-9*H*-carbazole isomeric mixture (**310**) with a catalytic amount of iodine in toluene under high-pressure mercury vapor lamp (HPMV) irradiation gave cyclized product i.e. 2-bromo-9-ethyl-9*H*-naphtho[2,1-*c*]carbazole.[169] In presence of light, the *trans* isomer was firstly converted to *cis* isomer, and this *cis* isomer was photocyclized to dihydro-intermediate which was unstable and not isolated. This dihydro-intermediate got oxidized by iodine to 2-bromo-9-ethyl-9*H*-

naphtho[2,1-*c*]carbazole. THF was used to scavenge the co-product hydrogen iodide produced during the oxidation of dihydro-intermediate by iodine. This photodehydrocyclization was performed in dilute solution as high concentrations lead to formation of a [2+2] cycloaddition product.

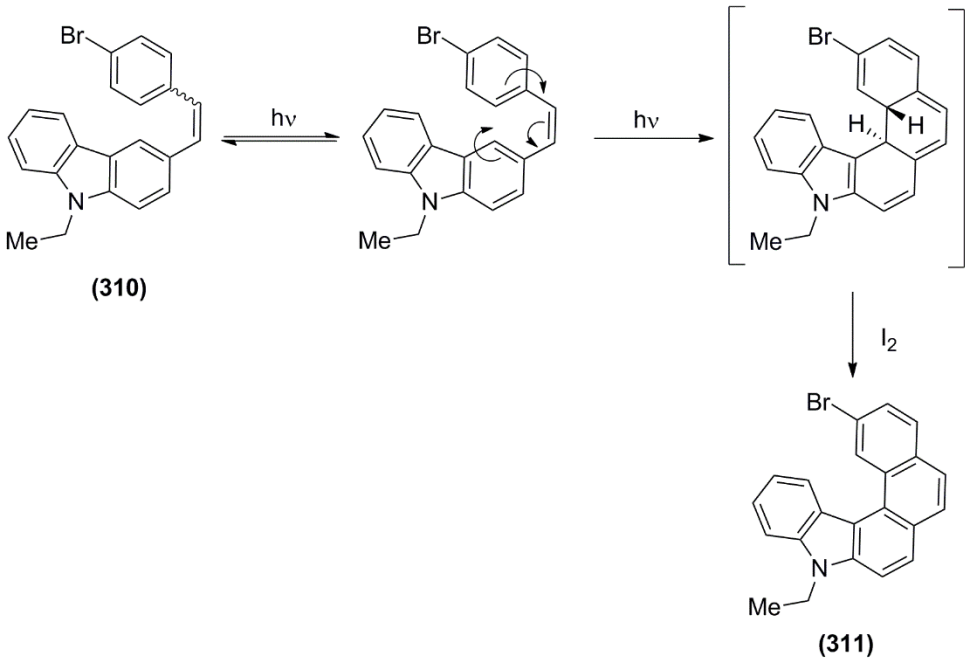

Figure 4.26. Mechanism of photodehydrocyclization for synthesis of azahelicene (**311**).

The IR spectrum of compound (**311**) showed peaks at 3042 cm^{-1} (aromatic C-H stretching), 2968 cm^{-1} and 2928 cm^{-1} (aliphatic C-H stretching), and at 1582 cm^{-1} and 1511 cm^{-1} (aromatic C=C stretching). The ^{1}H-NMR spectrum of compound (**311**) showed a doublet at δ 9.60 for one proton (ArH_k), a doublet at δ 8.82 for one proton (ArH_a) and multiplet at δ 7.95-7.28 for nine protons (ArH_{b-j}) confirming a total of eleven aromatic protons in the structure. A quartet appeared at δ 4.58 for two protons (-NC$H_{2/l}$CH$_3$) and a triplet appeared at δ 1.55 for three protons (-NCH$_2$C$H_{3/m}$) confirming the presence of *N*-ethyl group. Its mass spectrum showed $[M]^+$ molecular ion peak and $[M+2]^+$ ion peak at 374.17 and 376.15 m/z, respectively.

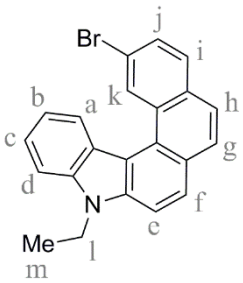

(311)

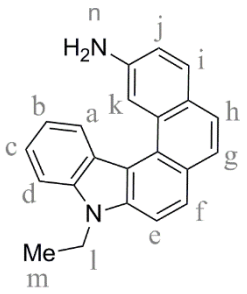

(312)

9-Ethyl-9*H*-naphtho[2,1-*c*]carbazol-2-amine (**312**) was synthesized from 2-bromo-9-ethyl-9*H*-naphtho[2,1-*c*]carbazole (**311**) by reacting it with trimethylsilylazide ($TMSN_3$) in the presence of ethanolamine and copper in 1,4-dioxane at 90 ºC for 24 hrs.[170] The crude product was purified by column chromatography. Its IR spectrum showed peaks at 3417 cm^{-1} and 3307 cm^{-1} (primary N-H stretching), 3042 cm^{-1} (aromatic C-H stretching), 2973 cm^{-1} (aliphatic C-H stretching), 1622 cm^{-1}, 1331 cm^{-1} (C-N stretching) and 1600 cm^{-1} (N-H bending). The ^{1}H-NMR spectrum of compound (**312**) showed a doublet at δ 8.84 for one proton (ArH_a), a doublet at δ 8.65 for one proton (ArH_k), a doublet at δ 7.87 for one proton (ArH_f), a doublet at δ 7.79 for one proton (ArH_i), multiplet at δ 7.52-7.69 for four protons (Ar$H_{d,e,g,h}$), a multiplet at δ 7.48-7.51 for one proton (ArH_b), a multiplet at δ 7.24-7.28 for one proton (ArH_c), a doublet of doublet at δ 7.08 for one proton (ArH_j) confirming a total of eleven aromatic protons in the structure. It showed a broad singlet at δ 3.95 accounting for two protons (-N$H_{2/n}$). A quartet appeared at δ 4.55 for two protons (-NC$H_{2/l}$$CH_3$) and a triplet appeared at δ 1.52 for three protons (-$NCH_2C$$H_{3/m}$) confirming the presence of *N*-ethyl group. Its mass spectrum showed $[M+H]^+$ ion peak at 311.33 m/z.

4.2.2.2.2. Synthesis of 1-(9-ethyl-9*H*-naphtho[2,1-*c*]carbazol-2-yl)amino alkylamides (316-321)

Syntheses of 1-(9-ethyl-9*H*-naphtho[2,1-*c*]carbazol-2-yl)aminoalkyl amide derivatives (**316-321**) were carried out from the key amine intermediate (**312**) in two steps as depicted in **Scheme 4.15**. In the first step, acylation of compound (**312**) was carried out by reacting it with the respective acid halides to obtain amide intermediates (**313-315**).

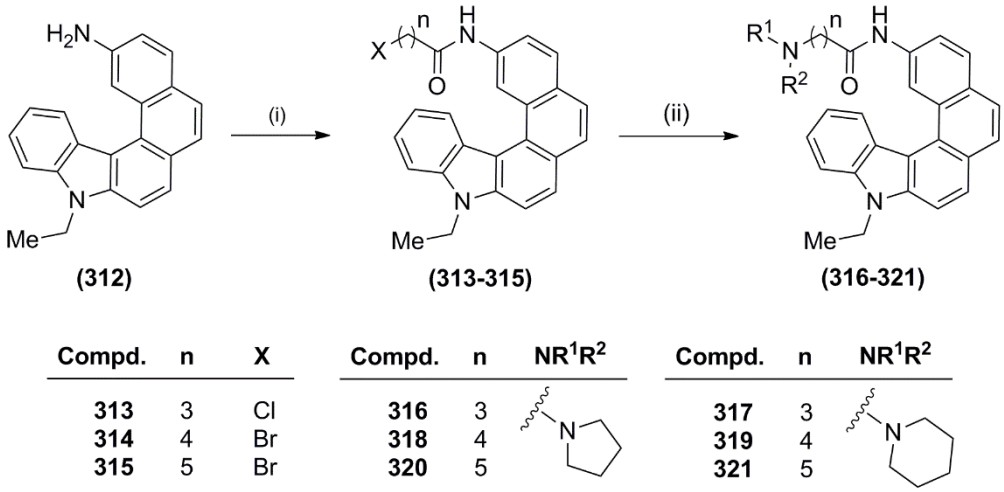

Compd.	n	X	Compd.	n	NR^1R^2	Compd.	n	NR^1R^2
313	3	Cl	**316**	3		**317**	3	
314	4	Br	**318**	4		**319**	4	
315	5	Br	**320**	5		**321**	5	

Scheme 4.15. Synthetic route for the synthesis of compound **(316-321).** Reagents and conditions: (i) Acid chloride, K_2CO_3, acetone; (ii) NHR^1R^2, THF, reflux.

The IR spectra of amide intermediates (**313-315**) showed peaks at ~1660 cm^{-1}(amide C=O stretching) and ~3290 cm^{-1}(amide N-H stretching) while the amine N-H stretching peaks disappeared. The analytical data of the intermediates (**313-315**) are mentioned in **Table. 4.36**.

Table 4.36. Analytical data of amide intermediates (313-315)

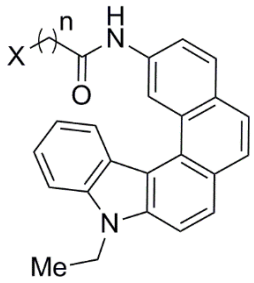

(313-315)

Compd	n	X	M.P.	MS	Characteristic IR peaks (cm^{-1})
313	3	-Cl	105-107 °C.	415 $[M]^+$, 417 $[M+2]^+$	3281, 3043, 2970, 2930,2861, 1660, 1641, 1328, 1153, 746
314	4	-Br	112-114 °C.	473 $[M]^+$, 475 $[M+2]^+$	3294, 3042, 2965, 1658, 1326, 1155, 835, 744
315	5	-Br	125-127 °C.	487 $[M]^+$ 489 $[M+2]^+$	3299, 3043, 2970, 1661, 1329, 1154, 836, 746

These amide intermediates (**313-315**) in second step, were reacted with the respective alicyclic amines i.e. pyrrolidine and piperidine to obtain the titled compounds (**316-321**) which were purified by crystallization. The IR spectra of

compounds (**316-321**) showed peaks at ~3250 cm^{-1} (amide N-H stretching), 3040 cm^{-1} (aromatic C-H stretching), 2930 cm^{-1} (aliphatic C-H stretching) and at ~1660 cm^{-1} (amide C=O stretching). The analytical data for 1-(9-ethyl-9*H*-naphtho[2,1-*c*]carbazol-2-yl)aminoalkylamide derivatives (**316-321**) have been shown in **Table 4.37**.

Table 4.37. Analytical data for 1-(9-ethyl-9*H*-naphtho[2,1-*c*]carbazol-2-yl) aminoalkylamide derivatives (316-321)

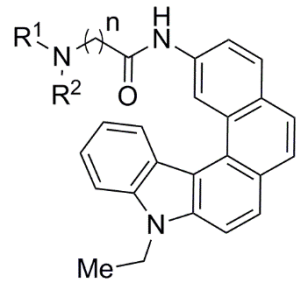

(316-321)

Compd	n	NR^1R^2	M.P.	IR characteristic peaks (cm^{-1})	HPLC data
316	3		96-98 °C	3272, 3043, 2930, 1649, 1587, 1549, 1303, 821, 752	Purity: 98.8 %, t_R = 4.11 min
317	3		98-100 °C	3293, 3042, 2931, 1665, 1612, 1586, 1326, 838, 742	Purity: 98.9 %, t_R = 4.02 min
318	4		161-163 °C	3234, 3041, 2932, 1661, 1610, 1579, 1323, 837, 742	Purity: 99.5 %, t_R = 4.14 min
319	4		141-143 °C	3235, 3041, 2931, 1662, 1584, 1508, 1322, 836, 742	Purity: 98.1 %, t_R = 4.05 min
320	5		102-104 °C	3225, 3043, 2930, 2863, 1664, 1573, 1327, 839, 745	Purity: 98.9 %, t_R = 4.20 min
321	5		163-165 °C	3222, 3044, 2930, 1663, 1611, 1572, 1328, 838, 744	Purity: 97.6 %, t_R = 4.52 min

The ^{1}H-NMR spectrum of compound (**316**) showed a singlet at δ 9.65 for one amide proton (-NH_nCO). A singlet at δ 9.36 for one proton (ArH_k), a doublet at δ 8.90 for one proton (ArH_a), a doublet at δ 8.08 for one proton (ArH_j), multiplet at δ 7.52-7.98 for seven protons (Ar$H_{b,d-i}$) and a multiplet at δ 7.29-7.33 for one proton (ArH_c) confirmed a total of eleven aromatic protons in the structure. It showed a multiplet at δ 2.80-2.83 for six proton (-NC$H_{2/q,r}$), a multiplet at δ 2.68-2.72 for two protons (-NHCOC$H_{2/o}$) and a multiplet at δ 1.82-1.84 for six protons (-NCH$_2$C$H_{2/p,s}$). A quartet appeared at δ 4.59 for two

protons (-NC$H_{2/l}$CH$_3$) and a triplet appeared at δ 1.55 for three protons (-NCH$_2$C$H_{3/m}$) confirming the presence of *N*-ethyl group. Its mass spectrum showed $[M+H]^+$ ion peak at 450 m/z.

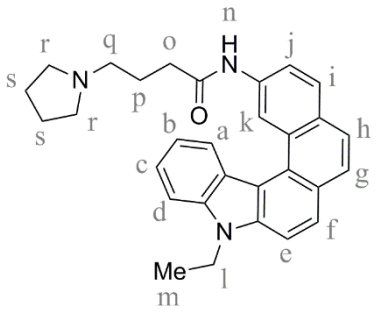

(316)

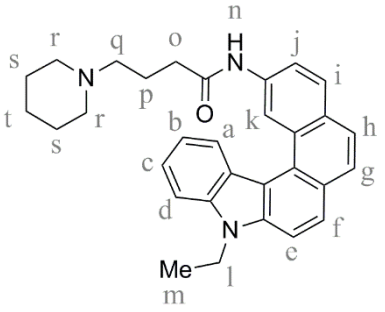

(317)

The ^{1}H-NMR spectrum of compound (**317**) showed a singlet at δ 9.21 for one proton (ArH_k), a doublet at δ 8.90 for one proton (ArH_a), a doublet at δ 8.13 for one proton (ArH_j), multiplet at δ 7.53-7.99 for seven protons (Ar$H_{b,d-i}$) and a multiplet at δ 7.29-7.33 for one proton (ArH_c) confirming a total of eleven aromatic protons in the structure. It showed a quartet at δ 4.60 for two protons (-NC$H_{2/l}$CH$_3$), a multiplet at δ 2.55-2.58 for two protons (-NHCOC$H_{2/o}$), a multiplet at δ 2.41-2.49 for six protons (-NC$H_{2/q,r}$), a multiplet at δ 1.95-2.00 for two protons (-C$H_{2/p}$) and multiplet at δ 1.36-1.58 for nine protons (-NCH$_2$C$H_{2/s}$, -NCH$_2$C$H_{3/m}$, -C$H_{2/t}$). Its mass spectrum showed $[M+H]^+$ ion peak at 464 m/z.

The ^{1}H-NMR spectrum of compound (**318**) showed a singlet at δ 10.22 for amide proton (-NH_nCO). A singlet at δ 9.55 for one proton (ArH_k), a doublet at δ 8.72 for one proton (ArH_a), a multiplet at δ 8.00-8.02 for one proton (ArH_j), multiplets at δ 7.74-7.88 for four protons (ArH_{d-i}), a multiplet at δ 7.51-7.55 for one protons (ArH_b), multiplet at δ 7.21-7.24 for one proton (ArH_c) confirmed a total of eleven aromatic protons in the structure. It showed a multiplet at δ 2.61-2.90 for six protons (-NC$H_{2/r,s}$), a multiplet at δ 2.42-2.45 for two protons (-NHCOC$H_{2/o}$), a multiplet at δ 1.77-1.82 for four protons (-NCH$_2$C$H_{2/t}$) and a multiplet at δ 1.60-1.71 for four protons (-C$H_{2/p,q}$). A quartet appeared at δ 4.68 for two protons (-NC$H_{2/l}$CH$_3$) and triplet appeared at δ 1.41 for three protons (-NCH$_2$C$H_{3/m}$) confirming the presence of *N*-ethyl group. Its mass spectrum showed $[M+H]^+$ ion peak at 464.01 m/z.

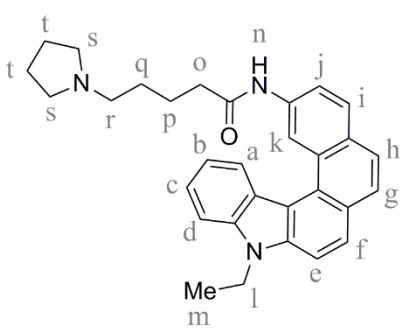

(318)

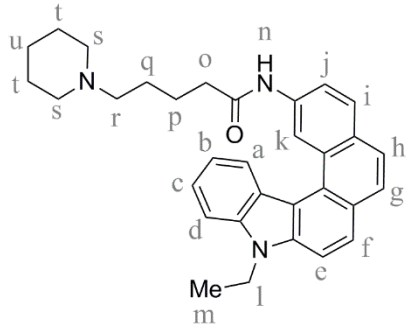

(319)

The ^{1}H-NMR spectrum of compound (**319**) showed a singlet at δ 9.27 for one proton (ArH_k), a doublet at δ 8.87 for one proton (ArH_a), a multiplet at δ 8.11-8.13 for one proton (ArH_j), multiplet at δ 7.54-7.98 for seven protons (Ar$H_{b,d-i}$) and multiplet at δ 7.30-7.33 for one proton (ArH_c) confirming a total of eleven aromatic protons in the structure. It showed a multiplet at δ 2.45-2.54 for six protons (-NC$H_{2/r,s}$), a multiplet at δ 2.13-2.24 for two protons (-NHCOC$H_{2/o}$), a multiplet at δ 1.78-1.90 for two protons (-C$H_{2/p}$), a multiplet at δ 1.62-1.77 for six protons (-NCH$_2$C$H_{2/q,t}$) and a multiplet at δ 1.41-1.51 for two protons (-C$H_{2/u}$). A quartet appeared at δ 4.59 for two protons (-NC$H_{2/l}$CH$_3$) and a triplet appeared at δ 1.56 for three protons (-NCH$_2$C$H_{3/m}$) confirming the presence of *N*-ethyl group. Its mass spectrum showed $[M+H]^+$ ion peak at 478.03 m/z.

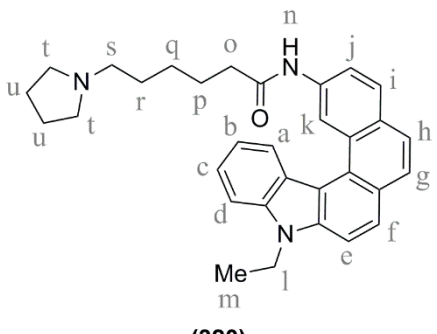

(320)

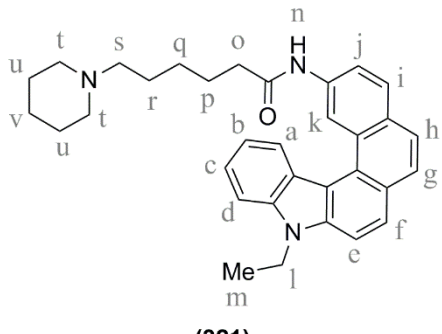

(321)

The ^{1}H-NMR spectrum of compound (**320**) showed a singlet at δ 10.19 for amide proton (-NH_nCO). A singlet at δ 9.55 for one proton (Ar*H*), a doublet at δ 8.85 for one proton (Ar*H*), multiplets at δ 7.22-8.24 nine protons (Ar*H*), confirmed a total of eleven aromatic protons in the structure. It showed a multiplet at δ 4.68-4.71 for two protons (-NC$H_{2/l}$CH$_3$), a multiplet at δ 2.41-2.79 for eight protons (6H, -NC$H_{2/s,t}$, 2H, -NHCOC$H_{2/o}$), a multiplet at δ 1.25–2.07

for thirteen protons (6H, -$NCH_2CH_{2/r,u}$, 4H, -$COCH_2CH_{2/p}CH_{2/q}$, 3H, -$NCH_2CH_{3/m}$). Its mass spectrum showed $[M+H]^+$ ion peak at 478.03 m/z.

The ^{1}H-NMR spectrum of compound (**321**) showed a singlet at δ 10.17 for amide proton (-NH_nCO). A singlet at δ 9.54 for one proton (ArH_k), a doublet at δ 8.81 for one proton (ArH_a), multiplets at δ 7.96-8.06 and at δ 7.74-7.88 for seven protons (ArH_{d-j}), a multiplet at δ 7.51-7.55 for one proton (ArH_b) and a multiplet at δ 7.19-7.23 for one proton (ArH_c) confirmed a total of eleven aromatic protons in structure. It showed a quartet at δ 4.68 for two protons (-$NCH_{2/l}CH_3$), a multiplet at δ 2.49-2.54 for two protons (-$NHCOCH_{2/o}$), a multiplet at δ 2.32–2.47 for six protons (-$NCH_{2/s,t}$), a multiplet at δ 1.61-1.71 for two protons (-$CH_{2/p}$), a multiplet at δ 1.45-1.59 for six protons (-$NCH_2CH_{2/r,u}$) and multiplet at δ 1.32-1.44 for seven protons (-$NCH_2CH_{3/l,}$ -$CH_{2/q,v}$). Its mass spectrum showed $[M+H]^+$ ion peak at 492 m/z.

4.2.2.2.3. Synthesis of 1-(9-ethyl-9*H*-naphtho[2,1-*c*]carbazol-2-yl)amino alkylureas (322-327)

Synthesis of 1-(9-ethyl-9*H*-naphtho[2,1-*c*]carbazol-2-yl)aminoalkyl urea derivatives (**322-327**) was carried out as presented in **Scheme 4.16**. Compound (**312**) was reacted with *p*-nitrophenyl chloroformate in the presence of triethylamine in DCM:THF (1:1), followed by reaction with respective aminoalkylamines to get the titled urea derivatives (**322-327**).[161]

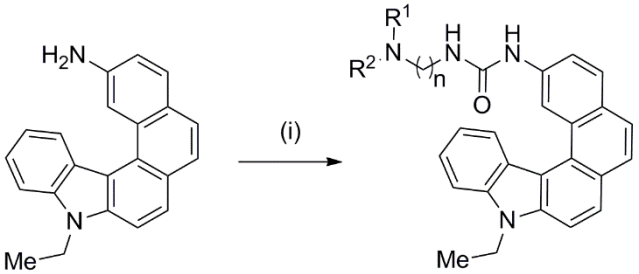

(312) (322-327)

Compd.	n	NR^1R^2	Compd.	n	NR^1R^2
322	2	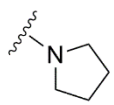	**323**	2	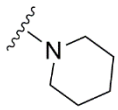
324	3		**325**	3	
326	4		**327**	4	

Scheme 4.16. Synthetic route for the synthesis of compounds (**322-327**)**.** Reagents and conditions: (i) (a) *p*-Nitrophenyl chloroformate, TEA, DCM:THF (1:1), 0 °C to RT; (b) pyrrolidine/piperidine/aminoalkylamines, RT.

The IR spectra of compounds (**322-327**) showed peaks at ~1675 cm^{-1} (amide C=O stretching) and ~3300 cm^{-1} (amide N-H stretching), whereas the amine N-H stretching peaks were missing. The analytical data of the compounds (**322-327**) are presented in **Table.4.38**.

Table 4.38. Analytical data of 1-(9-ethyl-9*H*-naphtho[2,1-*c*]carbazol-2-yl) aminoalkylureas (322-327)

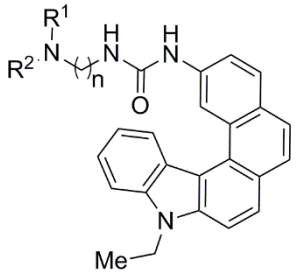

(322-327)

Compd	n	NR^1R^2	M.P.	IR characteristic peaks (cm^{-1})	HPLC data
322	2		173-175 °C	3305, 3046, 2930, 1694, 1652, 1592, 1323, 837, 743	Purity: 98.6 %, t_R = 3.82 min
323	2		191-193 °C	3317, 3044, 2932, 1691, 1649, 1592, 1323, 837, 744	Purity: 99.1 %, t_R = 4.31 min
324	3		105-107 °C	3302, 3044, 2963, 1658, 1327, 1237, 837, 745	Purity: 98.7 %, t_R = 3.91 min
325	3		99-101 °C	3297, 3045, 2930, 1658, 1572, 1325, 1236, 836,745	Purity: 98.1 %, t_R = 4.42 min
326	4		117-119 °C	3305, 3046, 2961, 1647, 1554, 1307, 1236, 827, 751	Purity: 99.2 %, t_R = 3.72 min
327	4		127-129 °C	3289, 3045, 2931, 1658, 1556, 1327, 1236, 836, 744;	Purity: 98.3 %, t_R = 4.02 min

The ^{1}H-NMR spectrum of compound (**322**) showed a singlet at δ 9.06 for one proton (ArH_k), a doublet at δ 8.83 for one proton (ArH_a) and multiplet at δ 7.27-7.98 for nine protons (ArH_{b-j}) confirming a total of eleven aromatic protons in structure. A broad singlet appeared at δ 5.52 for one proton (-NHCONH_o). It showed a multiplet at δ 3.38-3.42 for six protons (-NHC$H_{2/p}$), a triplet at δ 2.68 for two protons (-NC$H_{2/q}$), a multiplet at δ 2.51-2.58 for four protons (-NC$H_{2/r}$) and a multiplet at δ 1.61-1.70 for six protons (-$NCH_2CH_{2/s}$). A quartet appeared at δ 4.56 for two protons (-NC$H_{2/l}CH_3$) and a triplet appeared

at δ 1.54 for three protons (-NCH$_2$C$H_{3/m}$) confirming the presence of *N*-ethyl group. Its mass spectrum showed $[M+H]^+$ ion peak at 451 m/z.

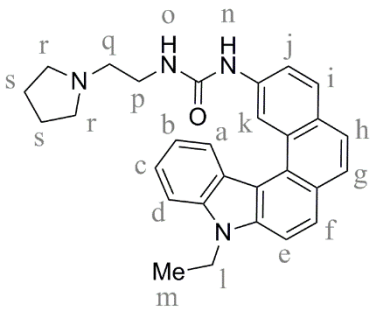

(322)

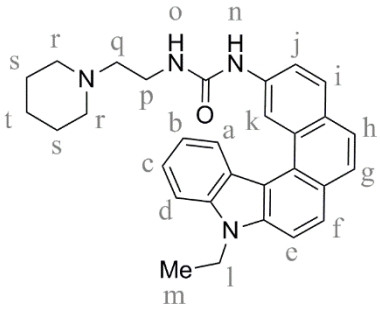

(323)

The ^{1}H-NMR spectrum of compound (**323**) showed a singlet at δ 9.11 for one proton (ArH_k), a doublet at δ 8.83 for one proton (ArH_a) and multiplet at δ 7.27-7.97 for nine protons (ArH_{b-j}) confirming to a total of eleven aromatic protons in structure. A triplet appeared at δ 5.60 for one proton (-NHCONH_o). It showed a multiplet at δ 3.35-3.39 for two protons (-NHC$H_{2/p}$), a triplet at δ 2.46 for two protons (-NC$H_{2/q}$), a multiplet at δ 2.34-2.38 for four protons (-NC$H_{2/r}$), a multiplet at δ 1.87-1.91 for four protons (-NCH$_2$C$H_{2/s}$) and a multiplet at δ 1.32-1.36 for four protons (-C$H_{2/t}$). A quartet appeared at δ 4.56 for two protons (-NC$H_{2/l}$CH$_3$) and a triplet appeared at δ 1.54 for three protons (-NCH$_2$C$H_{3/m}$) confirming the presence of *N*-ethyl group. Its mass spectrum showed $[M+H]^+$ ion peak at 465.03 m/z.

The ^{1}H-NMR spectrum of compound (**324**) showed a singlet at δ 9.12 for one proton (ArH_k), a doublet at δ 8.84 for one proton (ArH_a), multiplet at δ 7.27-7.97 for nine protons (ArH_{b-j}) confirming a total of eleven aromatic protons in structure. A broad singlet appeared at δ 5.95 for one proton (–NHCONH_o). It showed a multiplet at δ 3.42-3.45 for two proton (-NHC$H_{2/p}$), a triplet at δ 3.45 for two protons (-NC$H_{2/s}$), a multiplet at δ 2.39-2.42 for four protons (-NC$H_{2/t}$) and a multiplet at δ 1.70-1.74 for six protons (-NCH$_2$C$H_{2/u}$). A quartet appeared at δ 4.58 for two protons (-NC$H_{2/l}$CH$_3$) and triplet appeared at δ 1.55 for three protons (-NCH$_2$C$H_{3/m}$) confirming the presence of *N*-ethyl group. Its mass spectrum showed $[M+H]^+$ ion peak at 465.03 m/z.

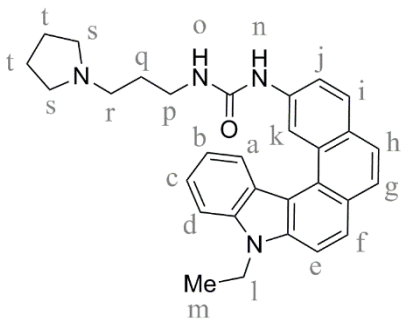

(324)

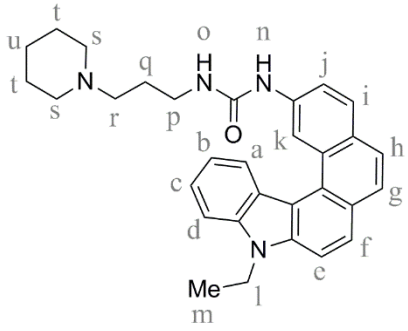

(325)

The ^{1}H-NMR spectrum of compound (**325**) showed a singlet at δ 9.13 for one proton (ArH_k), a doublet at δ 8.83 for one proton (ArH_a), multiplet at δ 7.26-7.96 for nine protons (Ar$H_{b\text{-}j}$) confirming a total of eleven aromatic protons in the structure. A broad singlet appeared at δ 6.24 for one proton (–NHCONH_o). It showed a multiplet at δ 3.33-3.39 for two protons (-NHC$H_{2/p}$), a multiplet at δ 2.40-2.43 for two protons (-NC$H_{2/r}$), a multiplet at δ 2.22-2.32 for four protons (-NC$H_{2/s}$), a multiplet at δ 1.90-2.00 for six protons (-NCH$_2$C$H_{2/q,t}$) and multiplet at δ 1.24-2.38 for two protons (-C$H_{2/u}$). A quartet appeared at δ 4.55 for two protons (-NC$H_{2/l}$CH$_3$) and triplet appeared at δ 1.35 for three protons (-NCH$_2$C$H_{3/m}$) confirming the presence of *N*-ethyl group. Its mass spectrum showed $[M+H]^+$ ion peak at 479.02 m/z.

The ^{1}H-NMR spectrum of compound (**326**) showed a doublet at δ 9.13 for one proton (ArH_k), a multiplet at δ 8.70-8.73 for two protons (-NH_nCONH, ArH_a), multiplet at δ 7.50-8.00 for seven protons (Ar$H_{d\text{-}j}$), a multiplet at δ 7.50-7.55 for one proton (ArH_b) and a multiplet at δ 7.22-7.26 for one proton (ArH_c) confirming a total of eleven aromatic protons in the structure. A triplet appeared at δ 6.25 for one proton (–NHCONH_o). It showed a quartet at δ 4.67 for two protons (-NC$H_{2/l}$CH$_3$), a multiplet at δ 3.10–3.15 for two protons (-NHCONHC$H_{2/p}$), a multiplet at δ 2.53-2.62 for two protons (-NC$H_{2/s}$), a multiplet at δ 2.30-2.40 for four protons (-NC$H_{2/t}$), a multiplet at δ 1.46-1.50 for six protons (-NCH$_2$C$H_{2/r,u}$) and multiplet at δ 1.36-1.42 for five protons (-NCH$_2$C$H_{3/m}$, -C$H_{2/q}$). Its mass spectrum showed $[M+H]^+$ ion peak at 479.03 m/z.

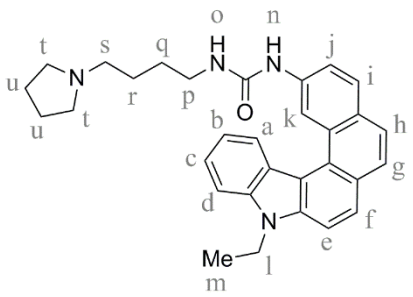

(326)

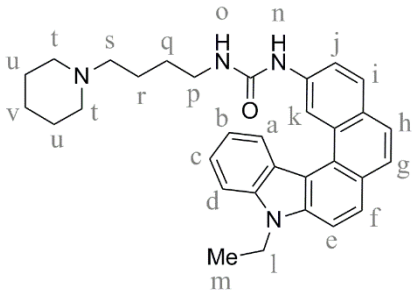

(327)

The ^{1}H-NMR spectrum of compound (**327**) showed a singlet at δ 9.06 for one proton (ArH_k), a doublet at δ 8.80 for one proton (ArH_a), multiplet at δ 7.04-7.94 for nine protons (Ar$H_{b\text{-}j}$) confirming a total of eleven aromatic protons in the structure. A broad singlet appeared at δ 5.70 for one proton (-NHCONH_o). It showed a quartet appeared at δ 4.55 for two protons (-NC$H_{2/l}$CH$_3$), a multiplet at δ 3.25-3.28 for two proton (-NHC$H_{2/p}$), a multiplet at δ 2.38-2.43 for four protons (-NC$H_{2/t}$), a multiplet at δ 2.29-2.33 for two protons (-NC$H_{2/s}$), a multiplet at δ 1.90-1.95 for six protons (-NCH$_2$C$H_{2/r,u}$), a multiplet at δ 1.53-1.59 for five protons (-C$H_{2/q}$, -NCH$_2$C$H_{3/m}$) and a multiplet at δ 1.39-1.44 for two protons (-C$H_{2/v}$). Its mass spectrum showed $[M+H]^+$ ion peak at 493.10 m/z.

4.2.2.2.4. Synthesis of 1-(9-ethyl-9*H*-naphtho[2,1-*c*]carbazol-2-yl)amino propylthioureas (328, 329)

Synthesis of 1-(9-ethyl-9*H*-naphtho[2,1-*c*]carbazol-2-yl)aminopropyl thiourea derivatives (**328, 329**) was carried out as presented in **Scheme 4.17**. Compound (**312**) was reacted with thiocarbonyldiimidazole in the presence of triethylamine in DCM:THF (1:1), followed by reaction with the respective aminoalkylamines to obtain the titled thiourea derivatives (**328, 329**).[164]

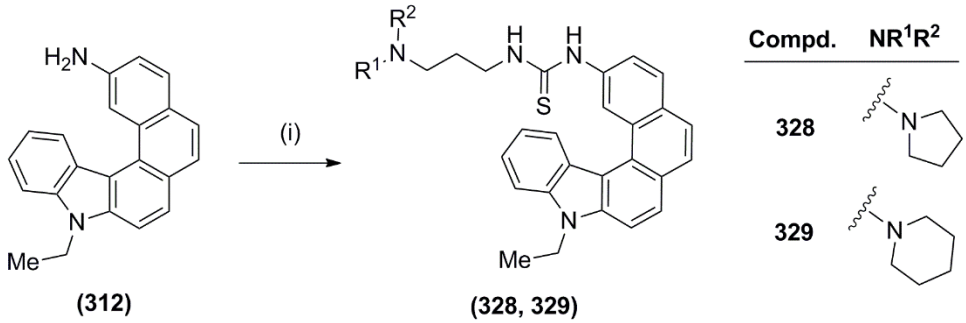

(312) (328, 329)

Scheme 4.17. Synthetic route for the synthesis of the compounds (**328, 329**). Reagents and conditions: (i) (a) Thiocarbonyldiimidazole, DCM:THF (1:1), 0 °C to RT; (b) 3-aminopropylamines, RT.

The IR spectra of the compounds (**328, 329**) showed characteristic peaks at ~1235 cm^{-1} (thiourea C=S stretching) and ~3150 cm^{-1} (N-H stretching), whereas the amine N-H stretching peaks were absent. The analytical data of the compounds (**328, 329**) are mentioned in **Table 4.39**.

Table 4.39. Analytical data of 1-(9-ethyl-9*H*-naphtho[2,1-*c*]carbazol-2-yl) aminoalkylthiourea derivatives (328, 329)

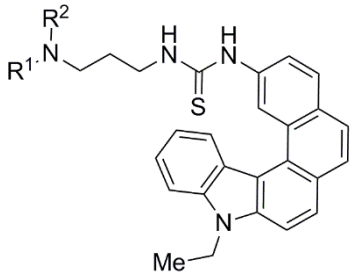

(328, 329)

Compd	NR^1R^2	M.P.	IR characteristic peaks (cm^{-1})	HPLC data
328		199-201 °C	3171, 3042, 2692, 2868, 1586, 1526, 1328, 1239, 837, 750	Purity: 99.0 %, t_R = 3.78 min
329	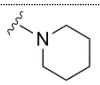	148-151 °C	3136, 3043, 2930, 1583, 1328, 1245, 838, 750	Purity: 98.3 %, t_R = 4.11 min

The ^{1}H-NMR spectrum of compound (**328**) showed a singlet at δ 9.73 for one proton (–NH_nCSNH). A doublet appeared at δ 9.06 for one proton (ArH_e), a multiplet at δ 8.62-8.70 for one proton (ArH_a) and multiplet at δ 7.17-8.00 for ten protons (Ar$H_{b\text{-}d,g\text{-}i}$, -NHCSN$H_o$) confirming a total of eleven aromatic protons in the structure. It showed a quartet at δ 4.63 for two protons (-NC$H_{2/l}$$CH_3$), a multiplet at δ 3.48-3.55 for two protons (-NHCONHC$H_{2/p}$), a multiplet at δ 2.27-2.37 for two protons (-NC$H_{2/r}$), a multiplet at δ 2.12-2.26 for four protons (-NC$H_{2/s}$), a multiplet at δ 1.60-1.62 for two protons (-NCH_2C$H_{2/q}$) and a multiplet at δ 1.34-1.38 for seven protons (-NCH_2C$H_{3/m}$, -C$H_{2/t}$). In deuterium exchange spectrum, peaks at δ 9.73 and at δ 7.87-8.00 for -NH of thiourea group disappeared, while the other peaks remained as such as mentioned above. Its mass spectrum showed $[M+H]^+$ ion peak at 481 m/z. Single crystal X-ray diffraction analysis also confirmed the structure of the compound **(328)** (**Figure 4.20**).

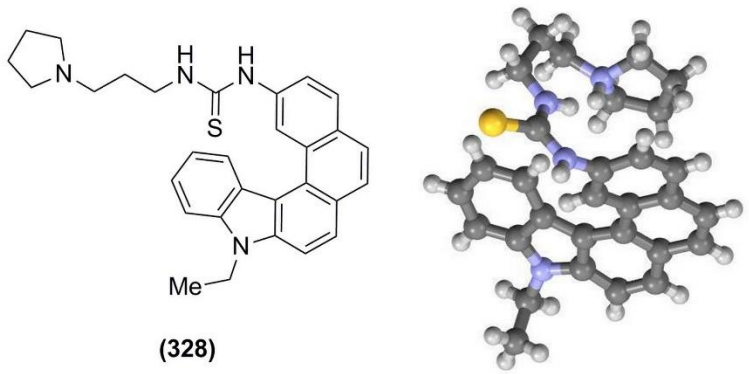

(328)

Figure 4.20. Single crystal X-ray diffraction analysis of compound (**328**)

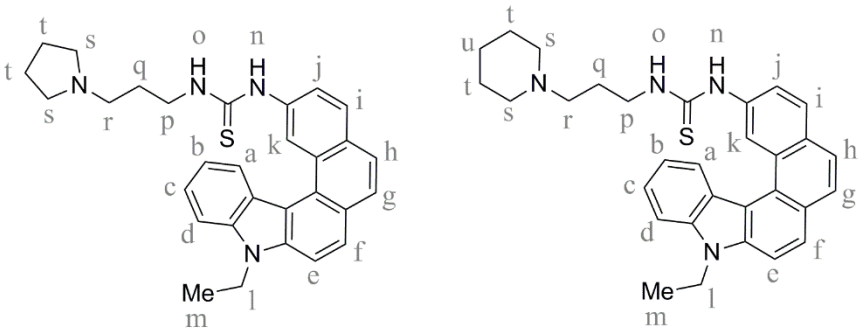

(328) (329)

The ^{1}H-NMR spectrum of compound (**329**) showed a singlet at δ 9.74 for one proton (-NH_{n}CSNH). A singlet appeared at δ 9.07 for one proton (ArH_{e}), a doublet at δ 8.67 for one proton (ArH_{a}), and multiplet at δ 7.17-8.00 for ten protons (Ar$H_{b\text{-}d,g\text{-}i}$, -NHCSN$H_{o}$) confirming a total of eleven aromatic protons. It showed a quartet at δ 4.63 for two protons (-NC$H_{2/l}$CH$_3$), a multiplet at δ 3.42–3.48 for two protons (-NHCONHC$H_{2/p}$), a multiplet at δ 2.15-2.19 for six protons (-NC$H_{2/r,s}$), a multiplet at δ 1.59-1.62 for two protons (-NCH$_2$C$H_{2/q}$), a triplet at δ 1.35 for three protons (-NCH$_2$C$H_{3/m}$) and a multiplet at δ 1.20-1.33 for six protons (–C$H_{2/t,u}$). Its mass spectrum showed $[M+H]^+$ ion peak at 495 m/z.

4.2.2.3. Biological evaluation of the synthesized compounds (316-329) as anti-AD agents

All the synthesized azahelicene derivatives (**316-329**) were evaluated for their multifactorial anti-AD activities, including cholinesterase inhibitory activity, Aβ_{1-42} aggregation inhibitory activity as discussed under the following subheadings:

4.2.2.3.1. *In vitro* cholinesterase inhibition studies,

4.2.2.3.2. Self-mediated $A\beta_{1-42}$ aggregation inhibition study,

4.2.2.3.3. Metal chelation study.

4.2.2.3.1. *In vitro* cholinesterase inhibition studies

The potential of the synthesized compounds to inhibit ChEs was evaluated *in vitro* by Ellman's assay, as reported earlier.[115-117] The obtained IC_{50} values of the compounds for both the AChE and BuChE enzymes and their selectivity indices (SI) are summarized in **Table 4.40**. As shown in **Table 4.40**, all the compounds (**316-329**) offered IC_{50} values in the range of 1.76-4.95 μM for AChE and 0.54-1.58 μM for BuChE.

It was observed that changing the length of the carbon chain affected inhibitory activity. A comparative analysis of the inhibitory potential of compounds (**316**, **318** and **320**) having a pyrrolidine ring, revealed that compound (**320**, n = 5) showed the best AChE and BuChE inhibitory activities (IC_{50} value of 2.09 μM and 1.27 μM, respectively) while compound (**316**, n = 3) and compound (**318**, n = 4) showed slightly lesser AChE and BuChE inhibitory activities. A similar activity pattern was also observed for the compounds (**317**, **319** and **321**). Among these, compound (**321**, n = 5) showed better AChE and BuChE inhibitory activities (IC_{50} value of 1.76 μM and 1.03 μM, respectively). Among them, compounds having piperidine ring exhibited higher potency compared to the compounds with pyrrolidine ring.

There was no significant change observed in AChE inhibitory activities when the amide linkers (compounds **320**, **321**) were substituted with urea linkers (compounds **324**, **325**) whereas the BuChE inhibitory activity got increased significantly. Among these urea derivatives, compounds (**324** and **325**) showed good AChE inhibitory (n = 3, IC_{50} value of 3.50 μM and 2.02 μM, respectively) and significant BuChE inhibitory (IC_{50} value of 0.61 μM and 0.56 μM, respectively) activities.

Similar ChEs inhibition was observed when the urea moiety in compounds (**324** and **325**) was replaced with thiourea moiety in compounds (**328** and **329**). Both the compounds (**328** and **329**) showed good ChE inhibitory (n = 3, IC_{50} value of 3.61 μM and 1.89 μM, respectively) and significant BuChE inhibitory (IC_{50} value of 0.57 μM and 0.54 μM, respectively) activities.

Table 4.40. *In vitro* inhibition of AChE and BuChE, and selectivity indices (SI) of compounds (316-329)

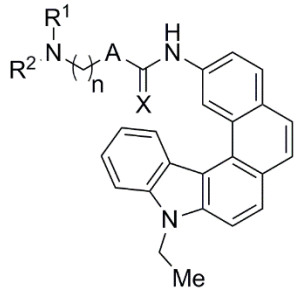

(316-329)

Compd	X	A	n	NR^1R^2	IC_{50} ± SEM (µM)		SI[c]
					AChE[a]	BuChE[b]	
316	O	-	3		4.27 ± 0.24	1.08 ± 0.18	0.25
317	O	-	3		2.05 ± 0.41	1.42 ± 0.32	0.69
318	O	-	4		3.54 ± 0.18	1.58 ± 0.27	0.45
319	O	-	4	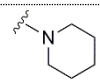	2.34 ± 0.25	1.33 ± 0.32	0.57
320	O	-	5	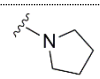	2.09 ± 0.41	1.27 ± 0.30	0.61
321	O	-	5	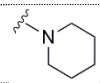	1.76 ± 0.19	1.03 ± 0.15	0.58
322	O	-NH	2		4.95 ± 0.73	1.01 ± 0.21	0.20
323	O	-NH	2		2.74 ± 0.87	0.76 ± 0.13	0.28
324	O	-NH	3		3.50 ± 0.28	0.61 ± 0.10	0.17
325	O	-NH	3		2.02 ± 0.11	0.56 ± 0.07	0.28
326	O	-NH	4	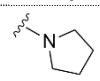	2.32 ± 0.26	0.71 ± 0.15	0.31
327	O	-NH	4	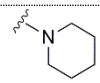	1.82 ± 0.17	0.65 ± 0.09	0.67
328	S	-NH	3	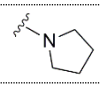	3.61 ± 0.28	0.57 ± 0.08	0.36
329	S	-NH	3		1.89 ± 0.25	0.54 ± 0.12	0.29

[a] AChE from human erythrocytes; IC_{50}, 50% inhibitory concentration (means ± SEM of three experiments), [b]BuChE from equine serum, [c]Selectivity Index = IC_{50} (BuChE)/IC_{50} (AChE).

4.2.2.3.2. Self-mediated Aβ$_{1–42}$ aggregation inhibition study

The potential of the compounds to inhibit the self-mediated Aβ$_{1-42}$ aggregation was assessed using Thioflavin T (ThT) fluorescence assay.[165] The percentage inhibition of self-mediated Aβ$_{1-42}$ aggregation of all the tested compounds at 25 μM concentrations is listed in **Table 4.41**.

Table 4.41 Self-induced A*β*$_{1-42}$ aggregation inhibitory activity of the compounds (316-329)

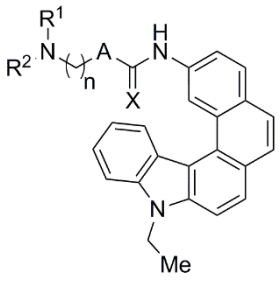

(316-329)

Compd	X	A	n	R^1R^2N	A*β*$_{1-42}$ aggregation Inhibition (%) at 25 μM conc.
316	O	-	3		49.60 ± 0.29
317	O	-	3		59.93 ± 0.44
318	O	-	4		53.07 ± 0.47
319	O	-	4		52.58 ± 0.19
320	O	-	5		61.23 ± 0.44
321	O	-	5		59.71 ± 0.41
322	O	-NH	2		59.90 ± 0.53
323	O	-NH	2		62.20 ± 0.33
324	O	-NH	3		62.23 ± 0.45
325	O	-NH	3		65.44 ± 0.31
326	O	-NH	4		62.74 ± 0.67
327	O	-NH	4		67.93 ± 0.54
328	S	-NH	3		62.93 ± 0.33
329	S	-NH	3		64.65 ± 0.28

All the tested compounds showed good $A\beta_{1-42}$ aggregation inhibition ranging from 53.07 to 67.93 %. Amongst them, compound (**327**) showed the highest $A\beta_{1-42}$ aggregation inhibition (67.93 %) at 25 µM concentration.

4.2.2.3.3. Metal Chelation study

The ability of the test compounds to chelate biometals was assessed using UV-vis spectroscopy assay.[165] The results were shown in **Figure 4.26**. 8-Hydroxyquinoline (8-HQ) was used as a positive control as shown in **Figure 4.21**.

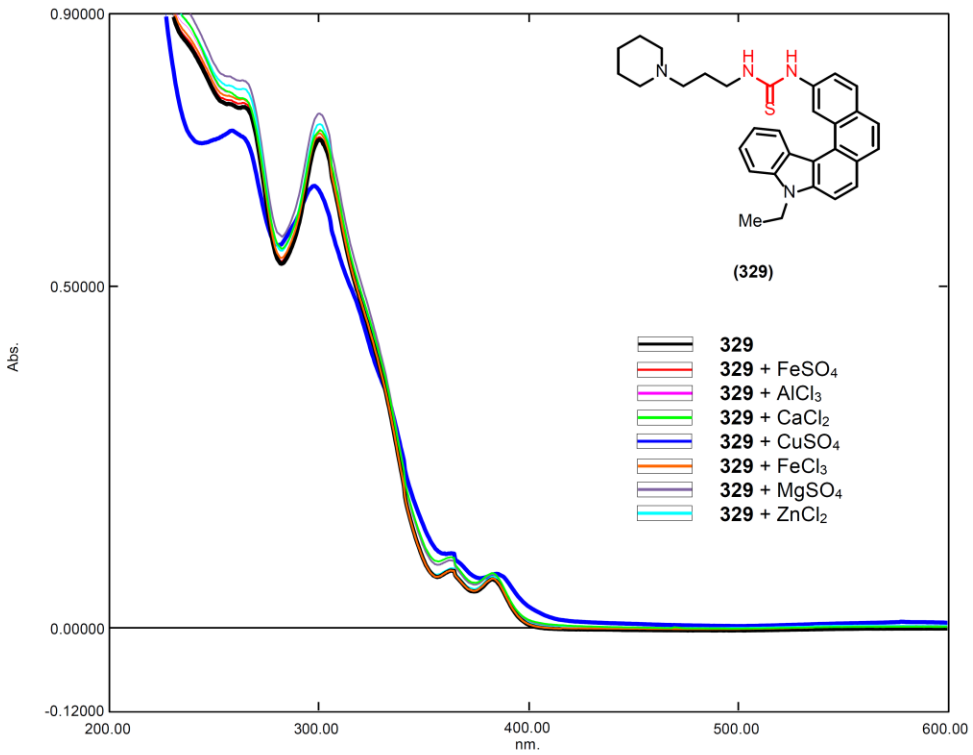

Figure 4.26. Metal chelation study of compound (**329**). UV-vis spectra of compound (**329**) (25 µM) alone and in the presence of $CuSO_4$ (25 µM), $ZnCl_2$ (25 µM), $FeSO_4$ (25 µM), $FeCl_3$ (25 µM), $AlCl_3$ (25 µM), $MgSO_4$ (25 µM) and $CaCl_2$ (25 µM) in methanol at room temperature

The results demonstrated that when $CuSO_4$ was added to the solutions of compound (**329**), the maximum absorption decreased dramatically, indicating the formation of ligand-Cu^{2+} complexes (**Figure 4.26**). There were only vague changes in the position and value of absorbance when $FeSO_4$, $FeCl_3$, $ZnCl_2$ or $AlCl_3$ were added into the solutions of the test compounds, suggesting that the test compound had poor chelation abilities for Fe^{2+}, Fe^{3+}, Zn^{2+}, and Al^{3+}. The

test compounds were also assessed for their binding property to other biologically significant metals, such as Mg^{2+}, Ca^{2+} wherein compound (**329**) exhibited very poor binding to these metals.

The above results evinced that the target compound (**329**) could selectively chelate Cu^{2+}. This high specificity for a metal ion is of prime importance in the design of a metal chelator to avoid chaotic binding to other critical biometal ions, the depletion of which can lead to allied side effects.

4.2.2.4. Computational studies of the most promising compound (329)

Computational studies of the most promising compound (**329**) was performed to understand the binding mode of the compound with the target proteins and to predict the *in silico* ADMET properties of the compound (**329**) as discussed under the following subheadings:

4.2.2.4.1. Docking studies of compound (**329**) with target proteins and

4.2.2.4.2. Prediction of virtual physicochemical and pharmacokinetics parameters of compound (**329**)

4.2.2.4.1. Docking studies of compound (329) with target proteins

To understand the molecular interactions and binding mode of the most active compound (**329**) with the AChE, docking studies were carried out with the active sites of *Tc*AChE (PDB code: 2CKM) and hBuChE (PDB code:4BDS).[132] In the docking study of **329** with AChE, the aromatic carbazole was observed to be stabilized comfortably in the active site of the enzyme by forming hydrophobic interactions with aromatic amino acids Trp84 and Phe330 (*h*AChE: Trp86, and Phe337). At physiological *p*H, the protonated nitrogen of the piperidine moiety exhibited strong cation-π interaction with Trp279 (*h*AChE: Trp287) (**Figure 4.26**). Molecular interactions of the compound (**329**) with these two amino acids (Trp84 and Trp279) were considered to be responsible to offer strong inhibitory effect by the dual binding site inhibitors.

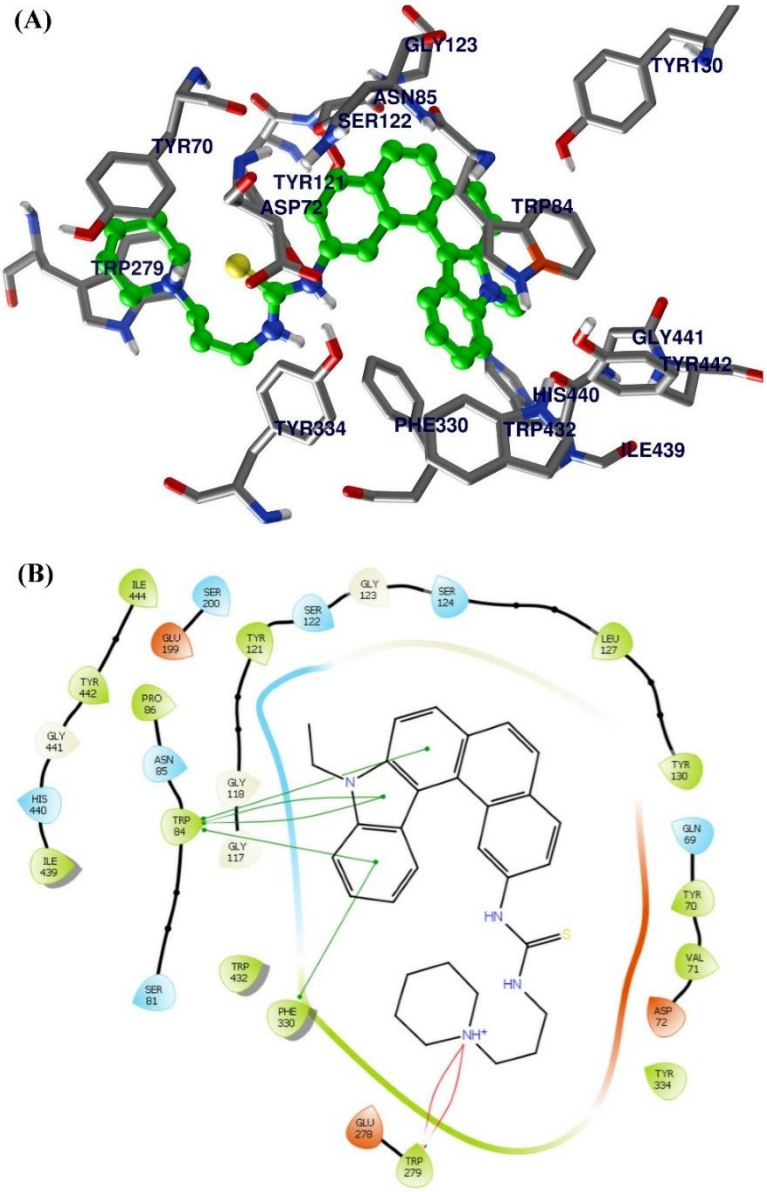

Figure 4.26. Docking model of compound (**329**) with *Tc*AChE (PDB ID: 2CKM). (A) Binding mode of **329** in the active site of *Tc*AChE. (B) Ligand interaction diagram of **329** with *Tc*AChE.

The binding mode of **329** with the BuChE receptor revealed that it also occupied a large catalytic cavity of the BuChE. The phenyl ring of azahelicene scaffold was observed to be in the active site of the enzyme by forming stable π-π interaction with Tyr332. Further stability to this complex was also provided by the protonated nitrogen of piperidine by forming cation-π interaction with Gly115 (**Figure 4.27**).

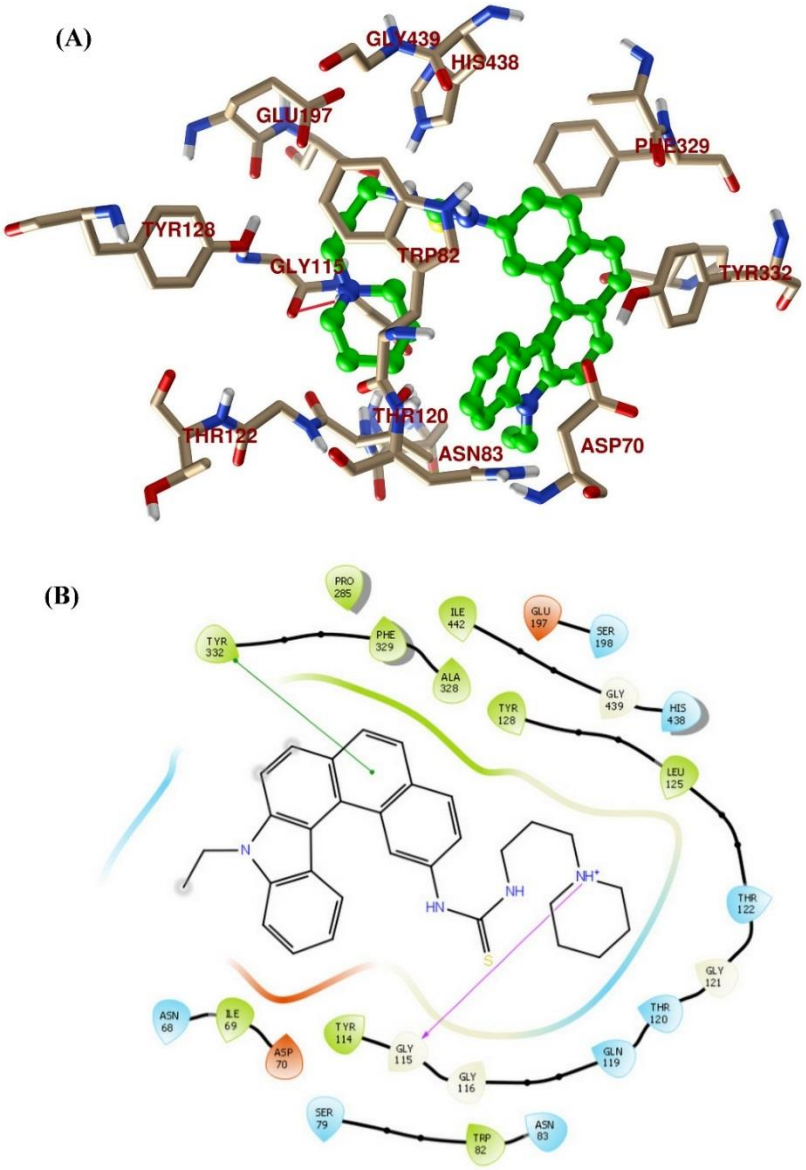

Figure 4.27. Docking model of compound (**329**) with BuChE (PDB ID: 4BDS): (A) Binding mode of **329** in the active site of BuChE. (B) Ligand interaction diagram of **329** with BuChE.

The binding mode of compound (**329**) with human $A\beta_{1\text{-}42}$ (PDB code: 1IYT)[84] is represented in Figure **4.28**. The azahelicene formed a stable π-π interaction with Phe19. Two -NH groups of thiourea was observed to be interacting strongly with Gln15 by hydrogen bonding. Further the protonated N of piperidine established the stable salt bridge interactions with Glu11.

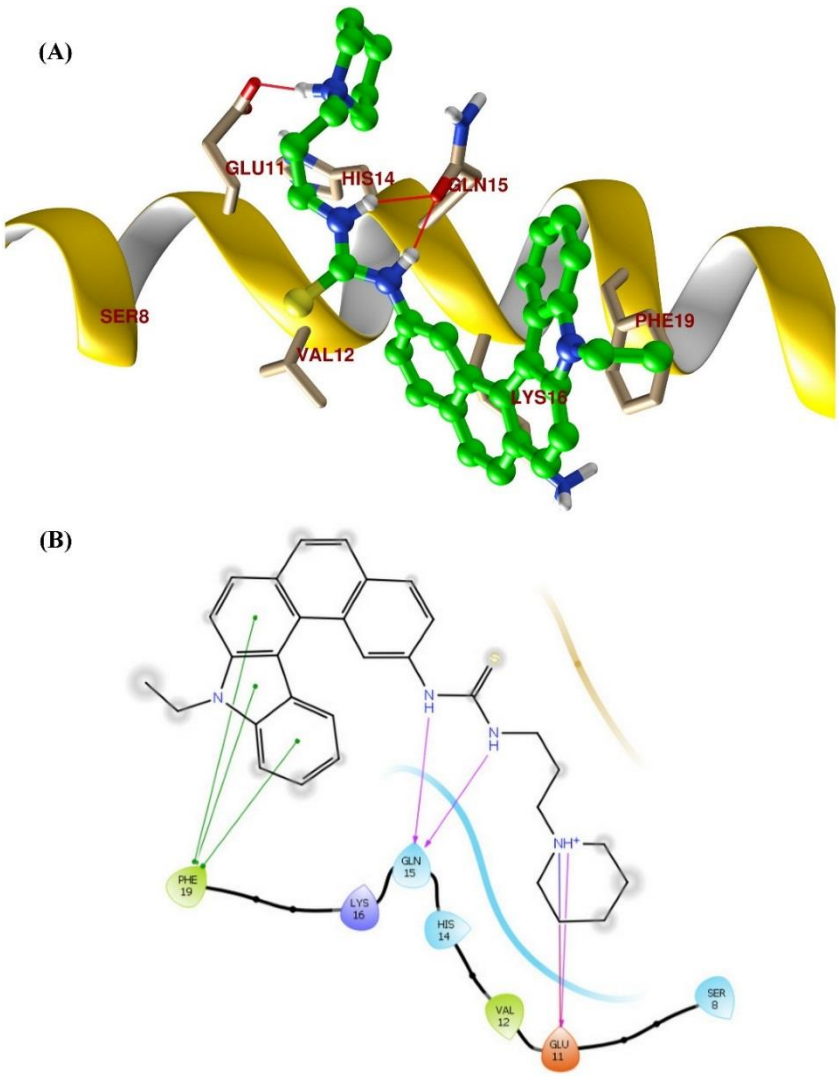

Figure 4.28. Docking model of compound (**329**) with $A\beta_{1-42}$ (PDB code 1IYT). (A) Binding mode of **329** in the active site of BuChE. The possible hydrogen bonding between compound (**329**) and Gln15 and Glu11 residues is shown by the red line. (B) Ligand interaction diagram of **329** with BuChE.

4.2.2.4.2. Prediction of virtual physicochemical and pharmacokinetics parameters of compound (329)

The virtual physicochemical and pharmacokinetic parameters like Lipinski's parameters, NRB, PSA, QPPCaco, QPPMDCK, CNS, QPlogBB, QPlogKhsa were predicted for compound (**329**) with QikProp module[136] (**Table-4.42**).

Table 4.42. Predicted ADMET Parameters of Compound (329) and Donepezil[a]

Parameter	Limit	Compd (329)	Donepezil
MW	130-725	494.696	379.498
HBA	2-20	4.5	5.5
HBD	0-6	2	0
NRB	0-8	6	6
QPlogP$_{o/w}$	-2 to 6.5	7.14	4.242
PSA	7 to 200	39.886	46.234
Volume	500-2000	1603.651	1248.451
ReFG	0-2	0	0
SASA	300 to 1000	874.77	681.675
Rule of Five (violation)	0-1	1	0
CNS	-	1	1
QPPMDCK	-	1238.148	589.289
QPlogBB	-3 to 1.2	0.33	0.223
QPPCaco	-	1186.375	1070.771
QPlogKhSa	-1.5 to 1.5	1.761	0.516
QPlogS	-6.5 to 0.5	-8.384	-4.059
% HOA	0-100	100	100
#star	0-5	3	0

[a]MW: molecular weight, HBA: hydrogen-bond acceptor atoms, HBD: hydrogen-bond donor atoms, NRB: number of rotatable bonds, QPlogP$_{o/w}$: Predicted octanol/water partition coefficient, PSA: polar surface area, #rtvFG: number of reactive functional groups; SASA: total solvent accessible surface area, CNS: predicted central nervous system activity on a -2 (inactive) to +2 (active) scale, QPPMDCK: Predicted apparent MDCK cell permeability in nm/s, QPlogBB: brain/blood partition coefficient, QPPCaco: Caco-2 cell permeability in nm/s, QPlogKhsa: binding to human serum albumin, QPlogS: predicted aqueous solubility, % HOA: human oral absorption on 0–100 % scale, #star: number of parameters with values that fall outside the 95 % range of similar values for known drugs.

Compound (**329**) obeys all the Lipinski's rule-of-five[137] parameters in given acceptable ranges except for $QPlogP_{o/w}$ (value > 5). Compound (**329**) violates only one limit of the Lipinski's rule-of-five, molding it a promising lead molecule. The NRB and TPSA are the two key parameters introduced by Veber as discussed earlier.[138] Compound (**329**) possesses six rotatable bonds and TPSA value of 39.886 $Å^2$. QPCaco-2 value co-relates with oral absorption of a drug. It shows the apparent gut-blood barrier permeability. Values above 500 predict high oral absorption which is attained for compound (**329**). Good oral bioavailability of compounds (**329**) is also supported by the predicted human oral absorption percent (% HOA) value. Brain/blood partition coefficient (QPlogBB), CNS, *n*-octanol-water partition coefficient ($QPlogP_{o/w}$), and apparent MDCK cell permeability (QPPMDCK) predict the ability of the compound to cross the BBB. Compound (**329**) is predicted to be CNS active as it possesses a CNS value of 1 and QPlogBB value of 0.33. QPPMDCK value is predicted apparent MDCK cell permeability in nm/s. It is recognized as a good mimic for the BBB. A QPPMDCK value higher than 25 is viewed as good, and the compound (**329**) has shown considerably high values. The QPlogKhsa value predicts the binding of a compound with human serum albumin. The compound (**329**) showed slightly higher value than the recommended values of QPlogKhsa. #Star shows the number of parameters with values that fall outside the 95% range of similar values for known drugs. Larger number of #stars suggests that the compound is less druglike than the compound with few #stars. Values of #star for compound (**329**) suggests its druglikeness. As shown, the compound (**329**) is predicted to have a good pharmacokinetic profile, which would strengthen its biological significance.